Development of a System Level Post Prognostics Reasoner for FRP turbine blades

PhD Thesis

Javier Contreras Lopez

Naval Architechture, Oceanic and Marine Energy

University of Strathclyde, Glasgow

Supervisors:

Athanasios Kolios

Feargal Brennan

April 27, 2024

This thesis is the result of the author's original research. It has been composed by the author and has not been previously submitted for examination which has led to the award of a degree.

Signed: 

Date: April 27, 2024

Abstract

The surge in offshore wind energy amplifies the urgency to optimise O&M lifecycle costs, a pivotal endeavor for bolstering affordability. These costs are anticipated to constitute a significant portion of overall lifecycle expenditures. A crucial strategy in achieving these cost reductions involves transitioning from traditional maintenance models, such as calendar-based repairs, to more sophisticated approaches like Predictive Maintenance.

This paradigm shift poses a formidable challenge, as uncertainties related to damage propagation, weather dynamics, and maintenance planning exert considerable pressure on O&M practitioners. The objective of this thesis is to delineate steps illustrating the design of an autonomous decision-making system for wind turbine blades. The initial phase involves identifying the most consequential failure modes through a comprehensive Failure Modes, Effects and Criticality Analysis (FMECA). Subsequently, a degradation function is proposed for a primary failure mode, namely leading edge erosion, furnishing the groundwork for approaching the O&M optimisation challenge.

In the progression toward an autonomous system, an essential tool is introduced to facilitate the selection of baseline calendar-based maintenance strategies for leading edge erosion at the wind farm level. This tool serves as a precursor to the ultimate design of a RL-based autonomous decision-making agent, incorporating prognostics information specifically for leading edge erosion. The obtained results showcase the efficacy of the proposed agent, demonstrating a noteworthy reduction in expected costs ranging from 12% to 21% when compared to condition-based maintenance. Furthermore, the agent contributes to a diminished risk of blade failure, highlighting the promising impact of autonomous decision-making in the realm of wind turbine O&M.

Contents

List of Figures

List of Tables

Nomenclature

α	Parameter controlling sampling probability
$\bar{g}(t_k)$	Average reliability at time t_k
$\bar{G}$	Average reliability over lifetime
β	Parameter for the calculation of sampling weights
γ	Discount factor
μ	Average
π	Policy
π^*	Optimal policy
σ	Standard deviation
A	Action
C	Weight vector update frequency
C_1, C_2	Coating behaviour parameters
C_{aero}	Aerodynamic losses
C_{dt}	Downtime costs
C_{om}	Maintenance costs
d	Damage

Nomenclature

d	LEE damage
D_{ins}	Estimated damage obtained through inspection
D_{max}	Estimated maximum LEE damage
E	Energy produced
$g(X)$	Performance function
G	Return
H	Accumulated rain impingement to erosion failure
h	Accumulated rain impingement
H_s	Significant wave height
h_s	Significant wave height
I	Rain intensity
M	Calendar month
M	Experience replay buffer
m_a	Maintenance access cost
m_b	Maintenance booking cost
m_e	Maintenance execution cost
N	Experience replay buffer's size
$P(u, d)$	Turbine power
p	Damage threshold
p	Sampling probability
P_1, P_2, P_3	Maintenance success probabilities

Nomenclature

$q^*(s, a)$	Optimal value function
$q_\pi(s, a)$	Action-value function
R	Reward
S	State
T	Month of operation
t_{td}	Time to decommissioning
t_{tm}	Time from last maintenance
u	Wind speed
v	Local rotor speed
W	Average wind speed
w	Set of weights of the behaviour network
w^-	Set of weights of the target network
w_s	Sampling weights

List of abbreviations

AEP	Annual Energy Production
AoA	Angle of Attack
ANN	Artificial Neural Network
ANNs	Artificial Neural Networks
BEM	Blade Element Momentum
CBM	Condition-Based Maintenance
CFD	Computational Fluid Dynamics
CFRP	Carbon-Fiber-Reinforced Polymer
CPS	Cyber-Physical Structures
DQN	Deep Q Networks
EoL	End of Life
FMECA	Failure Mode, Effect and Criticality Analysis
FPN	Fuzzy Petri Nets
FRP	Fiber-Reinforced Polymer
FSI	Fluid-Structure Interaction
HLV	Heavy Lift Vessel

I&M	Inspection & Maintenance
iPHM	Intelligent PHM
LCOE	Levelised Cost of Energy
LEE	Leading Edge Erosion
LEP	Leading Edge Protection
MCS	Monte Carlo Simulation
MDP	Markov Decision Process
NLP	Non-linear Programming
NREL	National Renewable Energy Laboratory
O&M	Operation & Maintenance
OWTs	Offshore Wind Turbines
PdM	Predictive Maintenance
PHM	Prognostics and Health Management
PMCs	Polymer-Matrix Composites
PN	Petri Nets
PNs	Petri Nets
PPNs	Plausible Petri Nets
PvM	Preventive Maintenance
PWAS	Piezoelectric Wafer Active Sensors
PoF	Probability of Failure
RL	Reinforcement Learning

ROI	Return On Investment
RUL	Remaining Useful Life
SCADA	Supervisory Control and Data Acquisition
SDGs	Sustainable Development Goals
SHM	Structural Health Monitoring
SPIFT	Single Point Impact Fatigue Tester
UV	Ultraviolet
WARER	Whirling Arm Rain Erosion Test Rig

Preface/Acknowledgements

I would like to begin by gratefully acknowledging the European Union's Horizon 2020 research and innovation programme that have funded my research under the ENHAnCE project (Marie Skłodowska-Curie grant agreement No 859957). I would like to thank the management team of ENHAnCE, Professor Manuel Chiachío and María Megía, for putting together such an enriching experience for all the ENHANcE Early Stage Researchers.

I would like to give a special mention to my supervisors, Professor Athanasios Kolios and Professor Feargal Brennan, for their patience, guidance and support offered throughout this journey.

This special achievement would have not been possible without the love and support of my family. The love and positiveness of my wife, Olenka, and the new star of our family, our son Mateo, have given me the determination that I needed for the completion of this task. My parents, Javier and Rafaela, for supporting me in every step of my education, and my brother Sergio, for being a true inspiration in life. I feel grateful for having all of you in my life.

Chapter 0. Preface/Acknowledgements

Research output

The list of publications, which have served to shape the main chapters of this thesis, is shown below:

- Paper A: "*A cross-sectoral review of the current and potential maintenance strategies for composite structures*". SN Applied Sciences, 2022. Authors: Javier Contreras Lopez, Juan Chiachio, Ali Saleh, Manuel Chiachio and Athanasios Kolios. [83].
- Paper B: "*Risk-based maintenance strategy selection for wind turbine composite blades*". Energy reports, 2022. Authors: Javier Contreras Lopez, Athanasios Kolios. [239]
- Paper C: "*A wind turbine blade leading edge rain erosion computational framework*". Renewable Energy, 2023. Authors: Javier Contreras Lopez, Athanasios Kolios, Lin Wang, Manuel Chiachio. [240]
- Paper D: "*Reliability-based leading edge erosion maintenance strategy selection framework*". Accepted for publication at Applied Energy. Authors: Javier Contreras Lopez, Athanasios Kolios, Lin Wang, Manuel Chiachio, Nikolay Dimitrov.
- Paper E: "*An autonomous decision-making agent for offshore wind turbine blades under leading edge erosion*". [*Accepted for publication*] - Renewable Energy. Authors: Javier Contreras Lopez, Athanasios Kolios.

The methods and outcomes of these papers have been included in this thesis as I have been the main contributor to them. In all of the papers used in the thesis, my contribution has been the following: conceptualisation/ideation, methodology, analysis

and software development (when required) and conclusions. The appreciated support of the coauthors was primarily in the areas of research guidance, methodological discussions and guidance on responding to the comments of the reviewers to improve the quality of the manuscripts.

Chapter 1

Introduction

1.1 Background

In recent decades, the global energy landscape has witnessed a remarkable shift towards sustainable and renewable sources. One of the most prominent contributors to this transition is the rise of wind energy, with offshore wind energy emerging as a key player in harnessing the vast potential of wind resources. This paradigm shift has been fueled by the increasing demand for clean energy solutions and the need to reduce reliance on conventional fossil fuels.

However, the integration and expansion of offshore wind energy come with a set of distinctive challenges. Notably, the logistical intricacies associated with offshore installations and the substantial increase in the size of turbines pose formidable obstacles to the industry's seamless growth. As wind turbines evolve to harness more energy from the wind, the complexity of their designs and the logistics involved in installation and maintenance become critical areas demanding thorough investigation.

A significant aspect contributing to the overall lifecycle costs of offshore wind turbines is the Operation and Maintenance (O&M) phase, which accounts for approximately 30% of the total life cycle costs [256, 393]. Surprisingly, O&M costs for offshore installations can range from 2 to 5 times those incurred for onshore wind turbines [16]. This discrepancy is attributed to the harsh marine environment, increased maintenance complexity, and the need for specialized equipment and personnel.

Moreover, the structural integrity of offshore wind turbines, particularly the composite materials forming the blades, faces intricate challenges. The complex damage modes experienced by these materials necessitate an in-depth understanding to develop effective maintenance strategies and optimise the overall turbine performance.

In light of these challenges, there is a pressing need for advanced decision support tools. These tools can play a pivotal role in mitigating O&M costs, enhancing the reliability of offshore wind turbines, and ultimately making them more economically viable. By leveraging cutting-edge technologies and data analytics, decision support tools aim to streamline maintenance processes, predict potential failures, and optimise resource allocation.

This thesis delves into the multifaceted landscape of offshore wind energy, examining the challenges posed by logistics, turbine size, and intricate damage modes in composite materials. Through a comprehensive analysis of the composite damage modes and the intricacies of turbine blade O&M activities, the research aims to provide insights that contribute to the development of decision support tools for the O&M of wind turbine blades. These tools are envisioned to play a crucial role in reducing costs, increasing affordability, and ensuring the long-term sustainability of offshore wind energy.

1.2 Structure of the thesis

The structure of the presented thesis does not follow the classical approach, instead it is composed by a collection of papers produced during the PhD, which have been peer-reviewed prior to the incorporation to this thesis. Chapters 2 to 6 are largely based on the papers published or submitted to the journals stated in Research Output section. These Chapters include a section named Chapter Contribution that highlights the specific contribution of the Chapter to the thesis and references the paper which constitutes its base. Moreover, the contribution of the author of the thesis to the paper is stated in this Section.

This thesis is structured as follows: this chapter will first of all introduce the research question and the motivation behind this thesis. It will also give a high level approach of the steps followed in this research.

Chapter 2 presents an extensive literature review of the benefits and limitations in the use of composite structures in safety critical applications. Moreover, the structural health monitoring (SHM) techniques and the maintenance strategies used for these structures are discussed.

Chapter 3 delves into the failure modes of wind turbine blades. It provides a failure mode effect and criticality analysis (FMECA) of this part to evaluate the criticality of the different failure modes identified for this component.

Chapter 4 provides a computational framework for one of the most critical failure modes of the blades, Leading Edge Erosion (LEE). This framework considers the aerodynamic effects of LEE and provides a tool to evaluate its progression throughout the operational life of the turbine.

Chapter 5 presents a tool to evaluate the risk of different candidate maintenance policies for LEE and make informed decisions for baseline maintenance scheduling at wind farm level.

Chapter 6 provides the definition of the autonomous decision-making agent for LEE. This agent makes use of the computational framework defined in Chapter 4 and a reinforcement learning (RL) agent to recommend O&M actions based on the estimated damage state of the blade.

Chapter 7 presents a discussion about the findings of the thesis, the application of the methods used, and the usability of the different frameworks and tools proposed in the chapters of this document.

Finally, Chapter 8 presents the conclusions that can be drawn from the research performed, discussion of the findings, the key advantages and limitations of the methodologies presented and the opportunities that arise from this research to potential future work.

1.3 Research question and objectives

The aim of the research is to provide insight into the following research question: *"How an autonomous decision-making system to support O&M for wind turbine blades based on prognostics can be designed?"*

To answer this primary research question, a rational analysis of wind turbine blade failure modes must be first performed. Once done, the top O&M cost contributors need to be analysed to identify the key parameters in their evolution and propose a degradation function. The definition of the degradation function unveils the possibility of framing the problem as a Partially Observable Markov Decision Process (POMDP) and the training of the autonomous decision-making system. Having stated this, this thesis will be broken down into 5 research objectives:

1. *Assemble a state-of-the-art literature review of current maintenance methods for wind turbine blades.*
2. *Identify the most critical failure modes of a wind turbine blade.*
3. *Provide a degradation function for one fo the most critical failure modes, LEE, to evaluate O&M policies.*
4. *Provide a risk-based tool to evaluate baseline calendar-based LEE maintenance scheduling policies.*
5. *Design an autonomous decision-making system for the blade's O&M.*

These questions are answered throughout each of the chapter of this thesis and map onto Chapters 2, 3, 4, 5 and 6, respectively. The beginning of each chapter will present the research question to be answered and the research performed. The conclusions of all the research objectives will then be joined in the context of the primary research question in the final chapter.

1.4 Novelty of Research

The novelty of the research embodied in this thesis stems from the following principles:

1. A risk-priority ranking of the most critical failure modes of a turbine blade provided through a Failure Mode and Effects Analysis at sub-component level.

2. The development of a novel framework to estimate blade LEE progression and evaluate wind turbine Annual Energy Production (AEP) considering weather uncertainty.

3. The proposal of a methodology to design baseline calendar-based maintenance strategies for LEE at wind farm level.

4. The design and proposal of a autonomous decision-making system for offshore wind turbine blades O&M optimisation.

1.5 Approach to research

There are several steps in the journey to provide autonomous decisions for wind turbine blade O&M optimisation. The methodologies followed are thoroughly described in Chapters 2, 3, 4, 5 and 6. Figure 1.1 provides a high-level view of the sequence of this research followed towards answering the primary research question of the thesis.

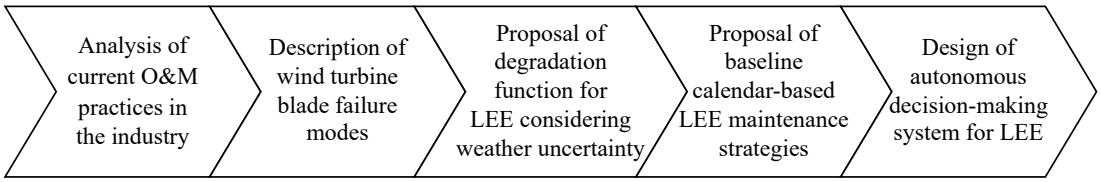

Figure 1.1: Research steps

To answer the primary research question, the current O&M practices and maintenance models for safety critical composite structures were first reviewed in Chapter 2. Following this, in Chapter 3, the wind turbine blade component was analysed through an FMECA to identify critical failure modes to represent in the simulations and target with the O&M activities. Then, a degradation model for one of the most risk-critical failure modes, LEE, is presented in Chapter 4. This model has been used first to tune calendar-based maintenance intervals and provide baseline maintenance strategies for this failure mode in Chapter 5. In Chapter 6, an autonomous decision-support agent based on reinforcement learning techniques is proposed. This agent makes use of the proposed LEE computational framework for the estimation of LEE degradation. Chap-

ter 7 presents a discussion of the findings of the thesis, the application of the methods used, and the usability of the different frameworks and tools proposed in the chapters of this work. Finally, Chapter 8 presents the conclusions derived from the research and highlights the key advantages, limitations and opportunities arising from this research.

Chapter 2

Maintenance strategies in composite structures: the potential of PHM

Chapter contribution

The use of fiber-reinforced polymer composite structures has increased during the last decade due to several factors. Among them, their superior strength-to-weight ratio and fatigue capacity stand up. These materials experience complex failure modes that depend on several parameters such as the types of fibres, resin, composition and layup of the laminate. Moreover, they can develop barely visible impact damage than can develop without being detectable by visual inspection. The combination of these two factors difficult the greater spreading of the use of these materials in many safety-critical applications.

This chapter aims to accomplish the following research objective: *Assemble a state-of-the-art literature review of current maintenance methods for wind turbine blades.*

The contributions of this chapter to the thesis are as follows:

- Provide an overview of the use of composite materials for wind turbine blades.
- Show the current limitations to the growth the use of composite materials in the

wind industry are.

- Convey what inspection and SHM techniques are currently available and what their applicability and limitations are.
- Provide insight into the potential benefits of the application of PHM to wind turbine blades and analyse the current maintenance techniques used and their limitations.

The published peer reviewed journal article Contreras Lopez, Javier, et al. "*A cross-sectoral review of the current and potential maintenance strategies for composite structures*" SN Applied Sciences 4.6 (2022) was authored by myself as part of my research completed under the direction and consultation of my supervisor, Professor Athanasios Kolios, and my coauthors. The published article is incorporated in this chapter and forms part of the comprehensive literature review presented.

2.1 Introduction

The commitment towards global sustainable development was signed by all United Nations Member States in 2015 and resulted in the 2030 Agenda for Sustainable Development[1]. This agreement is based on 17 Sustainable Development Goals (SDGs) which target the most critical issues that we need to face as a society. Fiber-reinforced polymer (FRP) composite materials are high-efficiency and high-durability lightweight materials that have the potential to positively impact several SDGs driving a change towards sustainability. Notwithstanding, a paradigm shift in the use of these advanced materials by the different industries is challenged by several issues, among which the following stand out: uncertainty about long-term damage behaviour and reliability [74], inadequacy or absence of design standards in several industries, lack of technological demonstrators [210], unreliable manufacturing [124], shortage of long-term durability data [165,367], high material costs [200], and recyclability issues [190,217]. These issues mainly derive from an immature knowledge about the optimal monitoring and maintenance strategies throughout the lifetime of these materials within a healthy balance

[1] https://sdgs.un.org/goals

between safety and cost for safety-critical applications. Hence, the use of composite materials by the different industries is still dissimilar, depending on their attitude towards risk and their expectancy about the use of composites.

These reasons call for cross-sectoral research and development approaches to overcome the constraints of each of the industries with the knowledge and experience of the others. The more profound knowledge and technology development of the aerospace industry in the use of composite structures along with the extensive experience of lower risk industries such as the automotive and wind energy can be utilised in favour of less developed industries such as the civil and naval. In general, we can envisage that the (open) data and knowledge provided by the more advanced industries will boost the adoption of composites materials by increasing the confidence of the stakeholders of different industries to design, produce, manage and utilise composite structures. However, finding common grounds and knowledge to overcome the particularities of each type of industry is a significant challenge, which, to the authors' best knowledge, has not been tackled before in the open literature. This work represents a first step in this direction.

In particular, this chapter provides a cross-sectoral overview of the potential and limitations of different maintenance technologies and operation strategies for thin-walled composite structures through the analysis of their role in four key industries, namely: aerospace, wind energy, civil and naval. These industries are currently employing FRP materials in their applications [208], and accrue a high percentage, between 50-60%, of the total use of carbon-fiber-reinforced polymers [450]. To this end, a cross-sectoral maturity analysis is firstly provided by means of a *maturity index* which measures and ranks the position of the refereed industries in the use of composites. Next, the possibilities brought about by the recent advances in Structural Health Monitoring (SHM) across industries are investigated in application to the inspection and monitoring of composite structures. Finally, an overview about the different maintenance strategies suitable for composite structures and their impact across the industries is analysed. In essence, this research has revealed that, although relevant developments have been carried out in the field of SHM [143, 147, 161, 328, 333, 442] and more re-

cently in the field of Prognostics and Health Management (PHM) in application to composite structures [71, 86, 93, 242, 308], these have not yet been translated into optimised and predictive maintenance strategies. In this context, the development of predictive maintenance strategies for composite structures assisted by PHM technologies and Physics-Enhanced Artificial Intelligence methods have been concluded as a key element to boost the adoption of composites across industries by reducing the uncertainty surrounding their future performance and reliability [121]. This predictability allows inspection and maintenance strategies to be tailored for a particular structure, which, in turn, translates into an extended lifetime and therefore increased sustainability. In this context of sustainability, evidence is shown here through a quantitative analysis that composites across the different industries can significantly contribute to two important SDGs, in particular, SDG 7 (*Affordable and Clean Energy*) and SDG 9 (*Industry, Innovation and Infrastructure*).

The rest of the chapter is structured as follows. First, Section 2.2 identifies the current use and limitations of plate-like composite structures within the aforementioned industries and presents innovative technologies and approaches being currently explored. Following this, Section 2.3 reviews the current developments on SHM in application to composite structures along with its use and limitations as per the different industries. After the introduction of SHM, Section 2.4 provides a brief description of the different existing maintenance strategies and their characteristics along with an analysis of the impact of maintenance on whole life cycle costs of composite structures in the context of these industries. Later, Section 2.5 builds on the necessary steps towards intelligent PHM (iPHM) and the constraints to be overcome to integrate all the information to produce Cyber-Physical Structures (CPS). Finally, Section 2.6 briefly summarises the findings and conclusions of the chapter.

2.2 Overview of the main technological applications of composite structures – Use and limitations

In this section, the degree of maturity and the main applications of composite structures are reviewed within the context of four key industries: aerospace, wind, civil construction, and naval.

2.2.1 Aerospace industry

Since its early days, this industry has pushed the technological limits of materials due to the harsh environment to which they are exposed. The aerospace industry adopts strict requirements for structures [251], such as very high reliability (even higher in civil aviation applications), mechanical and chemical durability, aerodynamic performance, multi-role applications, stealth, and all-weather operation. Traditionally, these requirements were partially met by the use of advanced metallic alloys; however, these are heavier and prone to corrosion. Thus, composites have achieved an important role in aerospace due to their high strength-to-weight and stiffness-to-weight ratios, greater fatigue and corrosion resistance, and ability to tailor stiffness and strength to specific design loads [251]. This allowed the expansion of application cases of composites structures over military and civil aircraft, helicopters, satellites, launch vehicles, etc. [8, 329, 376].

Indeed, the use of FRP composites in aircraft has increased since 1970 and has reached around 50% of its total mass in some cases (e.g., the Boeing 787 structure) [281]. Initially, composite materials were used as secondary structures to provide weight savings, although nowadays they are increasingly being used for primary plate-like structures [107]. The early development of composite structures in aviation was specially notorious in small fighter aircraft, achieving weight content of composites above 20% for F/A-18E/F, Rafale, F-22 and Gripen models produced during the decades of the 1970s to 1990s [376], as depicted in Figure 2.1a. It is noticeable that this development has seen a maximum participation of composites in the military aircraft with content above 50% by weight in the Eurofighter [119]. Regarding the application in the civil

aviation, the available data from reference aircraft manufacturers such as Boeing and Airbus show a slower adoption of composites use with a rampant tendency since the last two decades, as shown in Figure 2.1b. In fact, in the last years, these manufacturers have taken a great shift passing from composite participation in weight around 12% and 25% in their B777 and A380, respectively, to more than 50% in their latest B787 and A350.

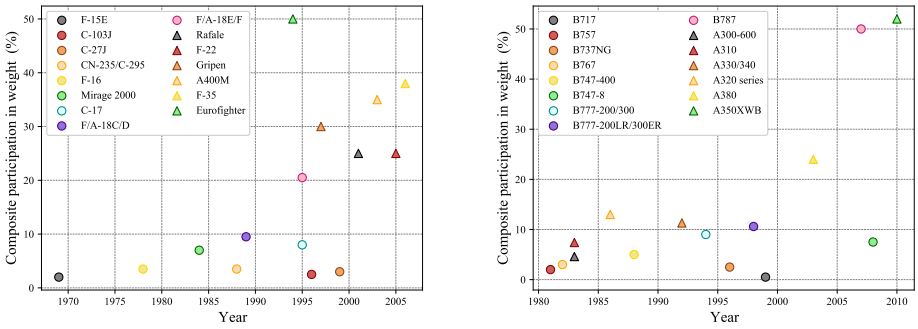

(a) Military sector (b) Civil aviation sector

Figure 2.1: Aircraft's composite participation in weight [376].

These weight reductions translate into fuel savings which, apart from the monetary savings for operators, directly impact SDG 12 (*Responsible Consumption and Production*). In fact, despite the initial manufacturing emissions being higher for hybrid composites and carbon-fiber-reinforced polymers (CFRP) than for classical aluminium and steel solutions, the whole-life CO_2 emissions during operation are lower, and break-even times range from 60 to 320 flight hours [344].

Besides, despite the positive experience and maturity of the production market, there are still some concerns with the use of composites in plate-like structures in the aerospace industry. Some researchers point to the severity and conservatism of the current airworthiness regulations [110] as limitation towards an efficient use of composite structures thus leading to over-conservative and oversized structures [329]. In addition to this, the need for clear guidance in the operation and maintenance of composite structures by their operators has been highlighted in works like [410]. Another concern with the use of composite materials is their lack of ductility during

the fracture process. Brittle micro-cracks and delamination cracks [400], which are difficult to detect visually, appear and progress during operation due to fatigue [399], impact [380], and lighting strikes [18,134], leading to an uncertainty increase about their mechanical performance. In recent years, different solutions have emerged to partially solve the latter drawbacks through the use of hybrid and advanced composites [7, 411] although they typically imply a reduction of the strength-to-weight and stiffness-to-weight ratios.

2.2.2 Wind industry

Despite the fact that the first steps of electric power generation from wind date from the late 19^{th} century, it was in the 1970s when the production of wind turbines experienced a rampant increase. Initially, classical materials such as steel were used for turbine blades, like the one manufactured by the U.S. company S.Morgan-Smith in 1941 experiencing failure after a few hundred hours of intermittent operation. This induced the need for a transition to high-performance blade materials such as composites, despite the reduced knowledge about these tailored materials at that time. Moreover, in response to the 1973 oil crisis, NASA started a program in 1975 to develop wind turbines [317] with composites as primary blade materials based on the knowledge gained from the application to the aerospace industry. Since then, the production of wind turbines has experienced an unceasing increase which still continues nowadays.

The growth of this tendency has been accelerated during the last decades since the world is moving towards greater utilisation of renewable energy due to its environmental and economical advantages. Indeed, the wind is one of the most efficient renewable energy resources for its numerous advantages [111], and today it is becoming strongly cost competitive in relation to other power generation methods [183]. This efficiency explains how fast the wind industry is growing worldwide. For example, the EU goal is to increase the use of renewable energy to 27% of the total energy generation by 2030 and to cut greenhouse emissions by 80-95% by the year 2050 [85]. China has experienced an increase of 27% in the growth rate of the electricity generated from wind between 2016 and 2017 [89]. The United States set a target to increase the electricity

generated from wind to 20% of the total electricity generated [435]. Figure 2.2 depicts the tendency and growth of installed wind capacity by region from 2011 until 2020, which reveals an increase of worldwide installed capacity from 220,019 MW in 2011 to 733,276 MW in 2020 [185]. Moreover, there are expectations of future growth for electricity generated from wind and solar photovoltaics, which will probably continue to expand reaching 29% of the market share in 2021 from 28% in 2020 [185]. These trends indicate an increasing need for composite materials mostly applied in turbine blades.

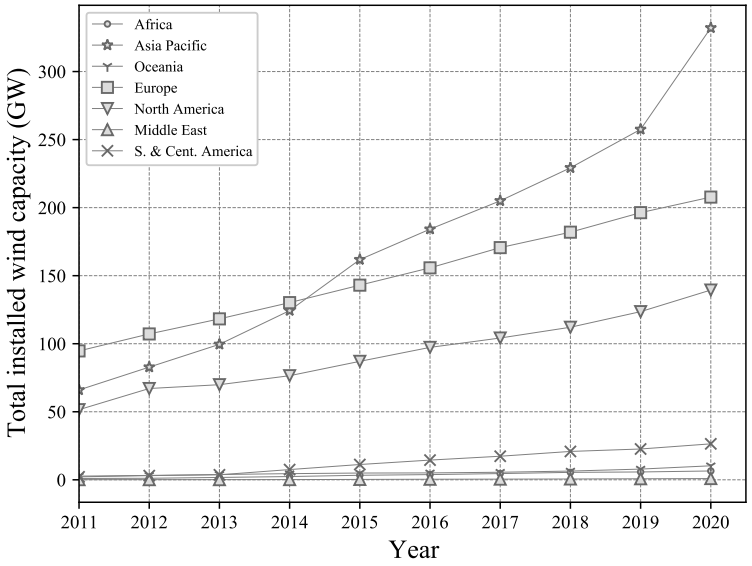

Figure 2.2: Evolution of wind energy capacity by region. Data taken from [185].

Typically, laminates used on wind turbine blades (refer to Figure 2.3 for a cross-section schematic view) are made of e-glass fibers and thermoset matrices, such as epoxy, polyester, or vinylesther, with fiber content of about 75% in weight. Notwithstanding, the increasing demand for larger wind turbine blades driven by offshore applications has opened up the possibilities of carbon fibers to provide greater strength and stiffness-to-weight ratios, thus improving their resistance to gravitational loads and fatigue life [117].

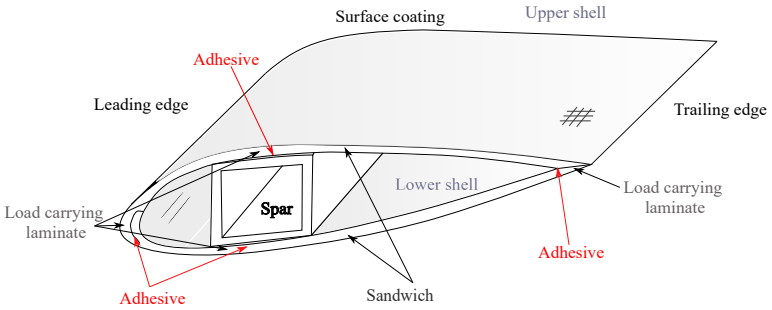

Figure 2.3: Typical turbine blade cross-section.

Irrespective of the recent advances in manufacturing for large size blades of different composite materials [44], there are still some unveiling challenges with the use of composites in the wind industry, with the most important being damage detection, location and identification [108,163,361], long-term reliability under damage [363], and remaining useful life prognosis [64, 226]. There is a long perception that the current design safety factors are too high; arguably as a consequence of the aforementioned challenges, among others. Further improvements and developments in those could help to reduce the Levelised Cost Of Energy (LCOE) [268].

In particular, with regards to damage diagnostics, SHM has shown promising results using different techniques (see for example [62,273,325,343,416]). Similarly, there have been some attempts to provide fatigue damage and erosion modelling [112,166,304,449], damage progression [444] and prognosis [153,365]. Even though the feasibility of these approaches seems encouraging, the experiments were predominantly conducted in controlled laboratory environments using simplified loading and damage scenarios. Therefore, the long-term and reliable performance of these systems in real operating conditions remain to be proven [153]. Notwithstanding, some research groups such as the Sandia National Laboratories have developed several projects such as the Continuous Reliability Enhancement for Wind (CREW) database [176] that aims to provide data-driven tools for the industry to self-assess the performance of wind turbines and adapt the operation and maintenance accordingly. Other studies focus on the fatigue behaviour of wind turbine blades under real conditions [5, 249, 250].

The opportunities for availability and revenue improvement that SHM and predic-

tive maintenance can bring to the industry are analysed in detail in Sections 2.3 and 2.4.2, respectively.

2.2.3 Civil construction industry

For around two hundred years until today, steel and concrete have dominated the civil construction industry. For several decades, this industry has been reluctant to incorporate composite materials for primary structures except for certain applications [261] and pilot projects, with the most relevant ones shown in Tables 2.2, 2.3 and Figure 2.4. Composite materials have unique properties that make them appealing to the civil industry [157, 178, 200], in particular their superior resistance to corrosion in aggressive environments along with their high strength-to-weight ratio ([198, 241, 272]) and high fatigue capacity (mainly for CFRP [336]). Also, composites provide important weight reductions as compared to traditional materials which would enable new architectural designs [38], easier and faster building procedures [198,241], extended lifetime [187], and therefore, improved sustainability [445]. However, irrespective of their potential, there are important reasons that are limiting the adoption of composites by this industry, amongst which the following are identified as the major ones: (1) lack of standards and design codes [360], (2) high material costs [420], (3) lack of experience and conservationism of the industry [330].

In regards to the lack of regulatory design codes, the NIST (the US National Institute of Standards and Technology) has recently warned about the lack of design codes and standards as one of the barriers against the adoption of composites in sustainable infrastructure [360]. Yet, the US Congress passed the Composite Standards Act in August 2020 that will publish guidelines and standards for using composites in infrastructure applications [141]. In Europe, there are plans to create such a *FRP Design Eurocode* [80], as stated in a recent report from the European Commission [17]. In the meantime, some European countries have developed their own guidelines, with the most relevant ones being summarised in Table 2.1.

Table 2.1: Published composite design guidelines.

Document	Details
EUROCOMP	Structural Design of Polymer Composites (Design Code and Handbook, Finland, France, Sweden, UK, 1996);
CUR 96	Fiber Reinforced Polymers in Civil Load Bearing Structures (Dutch Recommendation, 2003);
BD90/05	Design of FRP Bridges and Highway Structures (The Highways Agency, Scottish Executive, Welsh Assembly Government, the Department for Regional Development, Northern Ireland, May 2005);
DIBt	Medienliste 40 für Behälter, Auffangvorrichtungen und Rohre aus Kunststoff, Berlin (Germany, May 2005);
CNR-DT 205/2007	Guide for the Design and Construction of Structures made of Pultruded FRP elements (Italian National Research Council, October 2008);
ACMA	Pre–Standard for Load and Resistance Factor Design of Pultruded Fiber Polymer Structures (American Composites Manufacturer Association, November 2010);
DIN 13121	Structural Polymer Components for Building and Construction (Germany, August 2010);
BÜV	Tragende Kunststoff Bauteile im Bauwesen [TKB] – Richtlinie für Entwurf, Bemessung und Konstruktion (Germany, 2010).

In regards to the high material costs in comparison with traditional materials such as concrete and steel, this is a long-standing claimed issue by the construction industry that becomes exacerbated by the massive material utilisation in this industry. A shift from the initial-construction-cost viewpoint to a holistic lifecycle approach considering the higher durability of composite materials in a circular economy context would help; however, these lifecycle methods are still not widely adopted in civil engineering practice [63, 187]. Notwithstanding, the development of efficient manufacturing techniques such as pultrusion [391] and filament winding [22] among others [113, 235], along with the need for strengthening and rehabilitation of existing structures [178], have opened up opportunities for composite materials in the construction sector [28]. In particular, the repair and strengthening of ageing structures using FRP materials is arguably the most promising application of composites in civil engineering up to date, as revealed by the extensive literature in this area (see for example the following reviews papers [6, 272, 285]).

Table 2.2: List of pedestrian composite bridges.

Location	**Year**	**Type**	**Details and notes**
Kolding, Denmark	1997	100% GFRP	40 m long and 3.2 m wide, 15 years of operation without any damage [17, 125].
Svendborg, Denmark	2009	pultruded GFRP deck	40 m long and 3.2 m wide, installed in just two hours [17, 398].
Esbjerg, Denmark	2012	steel beams adhesively bonded to pultruded GFRP deck	18 m long and 3 m wide [17].
Grosseto, Italy	2004	GFRP pultruded profile	27 m long, installed in an archeological area [17].
Harderwijk, Netherland	2013	100% GFRP made by vacuum infusion technology	22 m long and 6.3 m wide [17, 419].
Rotterdam, Netherlands	2013	GFRP sandwish inside VARTM made core	62 park bridges with lengths ranging between 1.5 m and 4.5 m [17, 422].
University of Salerno, Italy	2014	GFRP pultruded I-beam with GFRP sandwich panels deck	148 m long and 37 m main span [17].
Floriadeburg, Netherland	2012	Steel beams covered with GFRP pultruded deck	127.5 m long and 6 m wide, designed to carry heavy vehicles (12t weight) [17].
Nørre Aaby, Denmark	2007	100% pultruded Glass FRP (GFRP)	23 m long, installed in just two hours, it replaces an old RC bridge that is 20 times heavier [17, 127].
Moscow, Russia	2008	FRP profiles moulded by infusion	22.6 m long and 2.8 m wide, the first bridge made of composite moulded by vacuum infusion [17].

Finally, as for the lack of experience and conservationism in the construction industry, the knowledge gained during decades (even centuries) about the use of traditional materials makes the adoption of new materials a difficult and competitive task. However, this barrier could be expected to diminish as long as new evidence and pilot applications of FRP composites become available. In general, most of FRP applications in civil engineering structures including the aforementioned pilot projects are relatively new, and therefore, the longer the service life of these structures, the more useful information can be collected. This will contribute to reducing the uncertainty about the long-term reliability of composites and therefore boost the application of composites in the civil engineering sector.

Figure 2.4: Applications of composite material in bridges. (a-j) pedestrian bridges. (k-p) road bridges. locations: Kolding, Denmark (a), Svendborg, Denmark (b), Esbjerg, Denmark (c), Grosseto, Italy (d), Harderwijk, Netherland (e), Rotterdam, Netherlands (f), University of Salerno, Italy (g), Floriadeburg, Netherland (h), Nørre Aaby, Denmark (i), Moscow, Russia (j), Delft, Netherlands (k), Karrebæksminde, Denmark (l), Utrecht, Netherlands (m), Klipphausen, Germany (n), Oxfordshire, UK (o), Lancashire, UK (p). Source of photographs: [17].

Table 2.3: List of road composite bridges.

Location	Year	Type	Details
Oxfordshire, UK	2002	100% GFRP and CFRP pultruded profiles	The first composite public road bridge, no damage found when inspecting it after 12 years of service life [51, 461].
Klipphausen, Germany	2002	100% GFRP	The first GFRP road bridge in Germany [17, 126].
Utrecht, Netherlands	2013	Hybrid GFRP-steel bridge made with VARTM injection	142 m long and 6.5 m wide, composite deck carry Eurocode traffic loads and all the horizontal loads [184].
Karrebæksminde, Denmark	2011	pultruded GFRP deck	100% pedestrian and cycle bridge was hung on the side to increase capacity, the first Danish road bridge made with a composite deck [17, 390].
Delft, Netherlands	2014	Vacuum infused GFRP sandwish structures with steel members	34 m long and 12 m wide [460].
Lancashire, UK	2006	GFRP pultruded profile	52 m long, Carry up to 400 KN weight [17, 22, 299].

2.2.4 Naval Shipbuilding industry

Steel and aluminium alloys have been the traditional materials massively used by the naval industry for decades. The use of composites started in the US NAVY between the mid-1940s and 1960s in the shape of non-critical structures and predominantly in small boats [255]. Slightly later, the Royal Navy and the French Navy started to make use of composites as structural material mainly for their acoustic transparency (*stealth*) [182, 403]. For this reason, composites started as preferred materials in minehunting ships in the 1970s [375]. Since those military applications, and mostly during the last few decades, the use of FRP in naval shipbuilding has grown significantly, although there are authors pointing out that the full potential of these materials is yet to be realised in this industry [138].

Three main benefits drive the interest in the use of FRP in this industry, namely weight reduction, good fatigue resistance, and high durability in the marine environment [61]. The weight reduction due to the greater strength-to-weight ratio directly translates into increased payload, range, hydrodynamic performance, greenhouse-gas emissions savings, and durability [138, 375]. Some authors have reported that expected

weight reduction with FRP could reach up to 30% and could result in fuel consumption savings up to 15% ([138]), which directly impacts SDG 12. As a drawback, moisture absorption degrades the FRP by reducing tensile and bending strengths [434]. Notwithstanding, this type of damage is less severe than the experienced by metals (e.g., corrosion [283, 378, 447]) and repairs are easier and less expensive [150, 447], providing FRP an overall better suitability for the marine environment. Even the lower stiffness of e-glass FRP can favour areas with high local stress concentrations where the structures are prone to suffer fatigue cracking such as deckhouses [318].

Thus, considering the positive balance provided by FRPs, there is a natural tendency to favouring their wider application, but still for small/sport vessels or for non-structural components [279, 354]. As with other industries, these reasons are predominantly centred on the shortage of knowledge and lack of reliable data about FRP performance in the marine environment [279]. The lack of knowledge poses to all stages of the production of the structure, starting from its design, following by its validation, and ending with its manufacturing. With regards to the design stage, there is a lack of design codes and reference models to optimise the designs of large complex vessels ([279]). To overcome this problem, the traditional approach has been to increase the safety factors in the design [96, 120], which results in diluting the weight-saving benefits of FRP. In the verification stage, Safety Of Life At Sea (SOLAS) regulations did not contemplate the use of a material other than steel until 2002. After 2002, FRP composites can be considered structural materials but the verification process has been reported as long, expensive, and with a significant level of uncertainty to get the final approval [137]; in fact, this reduces the motivation of designers to use composite materials. Finally, there is a lack of open databases to estimate the cost of fabricating naval structures with composites and a lack of high-quality and low-cost manufacturing processes for massive composite structures. In this context, the European Union has recently funded two research projects to address the lack of knowledge that is limiting the expansion of FRP, namely, RAMSSES and fiberShip [210]. These projects aim at providing the tools, data, and demonstrators of FRP vessels to overcome the code and knowledge constraints mentioned and familiarise the stakeholders of the industry with

the requirements and processes of FRP structures.

2.2.5 Cross-sectoral maturity overview of composites and contribution to SDGs

As shown before, the different industries have unequal experience and track record in the use of composite materials. To quantify this observation, a maturity index m is proposed here to measure and rank the relative position of these industries in regards to the use of composites. Three contributing factors ranging from 1 to 5 have been considered in this index: the relative participation of composites in structures suitable for these materials (Participation P); the time since the first standards or regulations of the use of composites were released (Standards S); and the equivalent number of publications during the last 40 years in the field of composite structures applied to the industry (equivalent number of Publications Pu_{eq}), where Pu_{eq} is computed as:

$$Pu_{eq} = \frac{\sum_{i=1981}^{2020} n_i(2021 - i)}{40} \tag{2.1}$$

with n_i being the number of composite publications at year i. Table 2.4 summarises the aforementioned factors and the criteria used to assign the different scores.

Table 2.4: Score values for maturity factors.

Factor	**Description**	**Score**				
		5	4	3	2	1
Participation	Relative participation of composites in the industry	Very high	High	Medium	Low	Very low / Non-existent
Standards	Time since first standards were published	More than 20 years	Between 10 and 20 years	Between 5 and 10 years	Less than 5 years	Non-existent
Publications	Equivalent number of publications in 40 years	Greater than 7,000	Between 5,000 and 7,000	Between 3,000 and 5,000	Between 1,000 and 3,000	Below 1,000

Finally, the maturity index, m for each industry is calculated as $m = (P+S+Pu_{eq})/15$

and the results are shown in Table 2.5.

These results reveal that, according to the proposed index, the aerospace industry has achieved the greatest maturity followed by the wind industry, which is the one with the highest rate of participation of composites. On the contrary, results show a gap between the aforementioned industries and the civil and naval industries in the use of composites, with the naval being the worst positioned industry in the use of composites.

Table 2.5: Maturity factor values by industry.

Industry	**Participation**	**Standards**	**Publications**	**Maturity**
Aerospace	3	5	5	0.867
Wind	5	4	1	0.667
Civil	2	1	2	0.333
Naval	1	1	1	0.200

Apart from the maturity, the contribution of the use of composite materials across industries in the achievement of the SDGs is presented next. To this end, the 17 SDGs (described in Table A.1 in Appendix A.1) are considered by the achievement indicators of their corresponding targets [418]. These indicators are assigned a unitary value if composites directly contribute towards their achievement and 0 otherwise. The analysis for each of the industries is presented in Appendix A.1, specifically in Tables A.2 to A.4. The results are summarised using polar bar charts in Figure 2.5. These results show that a wider use of composite structures across the different industries can significantly contribute to SDGs 7 (*Affordable and Clean Energy*) and 9 (*Industry, Innovation and Infrastructure*). Besides, to a lower extent, composites have a positive impact on SDGs 11 (*Sustainable cities and communities*) and 12 (*Responsible consumption and production*), with the remaining SDGs being minimally affected by composites (unitary indices equal to or lower than 0.25).

In contrast, there are a few concerning issues that need to be addressed to reduce the potential negative impact of the use of composite materials: the recyclability of composite materials after decommissioning; the rampant increase in the extraction of raw materials for the production of constituent materials (matrix, fibers); and the

higher demand of energy for the manufacturing of FRPs as compared to traditional materials. These issues have captured the attention of the research community as seen in a number of recent publications [21, 47, 149, 189, 233, 445] and constitute impacting research challenges to address in a near future.

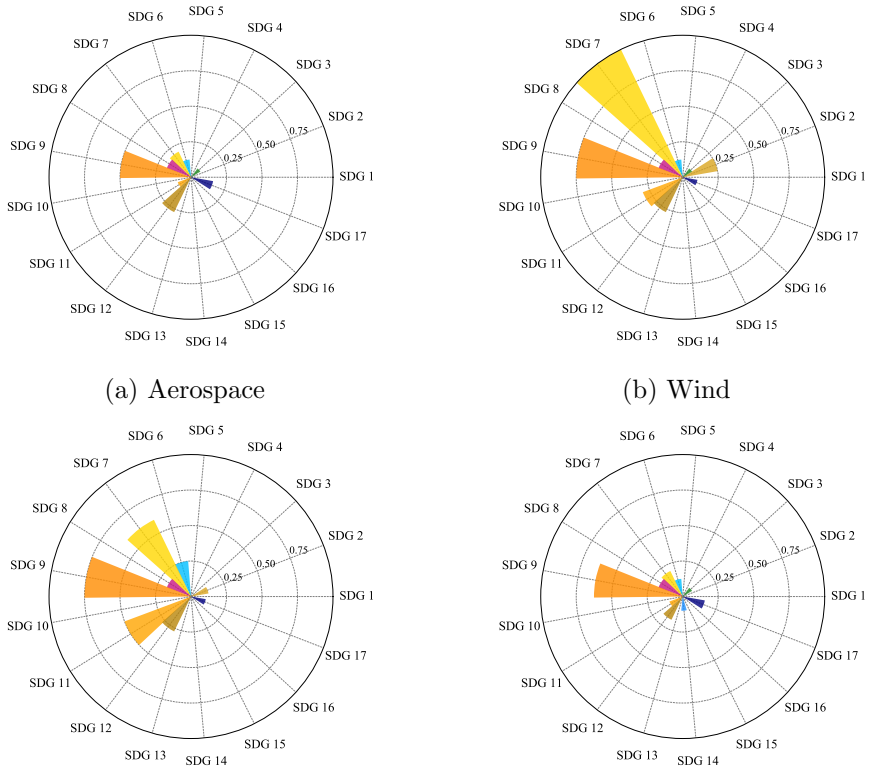

(a) Aerospace (b) Wind

(c) Civil (d) Naval

Figure 2.5: Schematic view of the analysis of contribution of composite materials towards the achievement of the SDGs.

2.3 Health Monitoring of FRP composites across industries

The long-term reliability and the complexity of the inspection and maintenance of thin-walled composite structures have emerged as barriers to the expansion of these materials among different industries. In this context, the SHM technology has the potential to overcome these barriers as it enables a quasi-real-time data acquisition by attaching

sensors to the structure or even by incorporating them into their internal structure [264, 328]. This data provides the basic information for damage prognostics and predictive maintenance [121]. Table 2.6 provides a synoptic view of the most established SHM sensing techniques for composite structures across industries, including their advantages and limitations. In the following, the role of SHM technology and its connection with CBM is discussed for the industries considered in this study.

2.3.1 Aerospace industry

As with the use of composites, military aircraft has pioneered the use of SHM. It was in the late 1950s when the UK Royal Air Force started using a device based on accelerometers to evaluate the in-flight loads experienced in fighter airplanes [40]. Since then, the interest of the aeronautic industry in non-destructive testing (NDT) and SHM (both civil and military) has steadily grown [412]. At the same time, the literature on this topic has seen a rampant development and a number of new sensing techniques and damage identification methods have been proposed during the last few decades. Rocha et al. [328] provides a recent review of the literature on SHM in aerospace composites. They conclude that the adequacy of the selection of an SHM system lies in a set of multidisciplinary factors such as the specificity of the structure, shape, size, constituent materials, expected damage location and type, and maintenance. In Towsyfyan et al. [412], a comprehensive review of the capabilities and limitations of certificated NDT technologies for aerospace composite structures is provided.

As evident from the literature, there is a general consensus about SHM as an effective technology for optimised condition-based maintenance. In fact, the main manufacturers of the aviation industry have identified the potential benefits of SHM predominantly in the field of maintenance [395, 408]. In this industry, damage detection, primarily based on visual inspection, takes a considerable part of the maintenance budget. Indeed, access to inspection areas is one of the major drivers of maintenance costs for aircraft. A clear example is provided by Cawley [59], which reports that Boeing calculated that out of the 25,000 hours required for corrosion inspection for a 747-400 aircraft, 21,000 hours were spent gaining access to the inspection areas (over 80% of

Table 2.6: List of structural health monitoring techniques used in fiber reinforced polymers.

SHM Technique	A/P	Detectable Damages	Advantages	Limitations	References
Acoustic emission	P	Impacts, micro-cracks, cracks, delaminations	Highly sensitive to damage and its location	Requires knowledge about the attenuation of the component to produce accurate results and is sensitive to background noise	[45, 98, 142, 334]
Guided waves	A	Impacts, micro-cracks, delaminations, cracks, debonding	Low signal attenuation, highly sensitive to damage, can be integrated inside thin members	Experiences difficulties in complex structural components	[56, 76, 161, 379]
Acousto-ultrasonic	A/P	Delaminations, cracks, debonding	Sensitive to both surface and subsurface discontinuities	Requires calibration of the system and knowledge to analyse and interpret the data, presents difficulties in evaluation of irregular materials and further research on disbond detection	[216, 277, 335, 421]
Digital image correlation	A	Cracks, debonding	Sensors (cameras) do not need wiring and can cover large areas	Unable to identify internal small damage	[48, 58, 188, 312]
Electromechanical impedance spectroscopy	A	fiber cracks, delamination, cracks, debonding	Uses short wavelength and can detect small and incipient cracks	Can only detect damage relatively close to the sensors	[151, 315, 353]
Electrical impedance tomography	A	fiber cracks, delaminations, cracks	Low cost of sensors	Attenuated in depth, only feasible for shallow damage	[441, 455]
Strain monitoring	P	Impacts, delamination, cracks	Easy to integrate within the structure and mature technology	Needs a considerable number of sensors to identify damage since detection range is low	[97, 199, 429]
Vibration monitoring	A/P	Cracks and large debonding	Sensors can be easily integrated within the structure, reliable and mature technology	Low resolution, can only detect the presence of large damage and experiences problems with environmental disturbances and measurement errors	[206, 275, 311, 465]
Comparative vacuum monitoring	A	Cracks, debonding	Sensors can be discretely placed along the structure	Not reliable for internal damage	[394]
Infrared thermography	A/P	Debonding, cracks and delamination	Cameras can cover large areas of the structure	Is affected by environmental temperatures and material thermal conductivity	[15, 370, 382]

A/P: Active/Passive monitoring

the inspection time). These figures make clear the industry's interest in SHM. Another driver for SHM as enabling technology for advanced maintenance is life extension of existing aeroplanes that are close to their nominal end-of-life. SHM provides valuable information about the actual degree of damage that can be used for informed life-extension decision-making. [415].

Despite the aforementioned benefits of SHM and the feasibility of their use in composite structures, there are also concerns that limit their use in the aerospace industry (and to some extent in other industries). The first concern is about the reliability of the damage detection, location, and quantification of damage for in-service real structures. Most of the current progress about SHM in aerospace composites has been carried out in coupons, plates, and scaled structures under laboratory conditions [71, 87, 436]. However, irrespective of some insightful progress on in-situ damage monitoring technologies [114, 243], there is still much uncertainty about the performance of on-board SHM technology during long periods of time and against harsh and changing environmental conditions. In this sense, Unmanned Aerial Vehicles (UAV) are seen as an interesting opportunity to test SHM systems in real conditions while reducing economic and safety risks [12, 77]. Secondly, there is a lack of publicly available data for SHM developers to work with. The research community would highly benefit from the use of open datasets to build robust models for damage detection, quantification and prognosis, and therefore increasing the reliability of the systems. Thirdly, there is uncertainty surrounding how SHM systems can deal with patched or bolted repairs. In this context, the SHM system shall be able to evaluate and monitor the repaired condition of the structure so that the system has the same reliability as the original structure; otherwise, the main advantage of SHM (reducing inspection costs) will be jeopardised. Finally, there is a need for a publicly available demonstrator project investigating the whole SHM process for composite structures. A direct comparison of the whole life cycle costs of the application of SHM against the current inspection strategies would help close the existing gap between academic research and industrial needs in SHM.

2.3.2 Wind industry

In the wind industry, the turbine blades along with the gearbox and electrical generators, have been identified as the turbine components with the highest failure rates [234,405]. Moreover, the damage in the blades is regarded as one of the most expensive and difficult to detect among the potential failures of the turbine and has the potential to act as a precursor of secondary damages in other parts of the turbine [236]. Thus, deploying SHM technology on turbine blades will translate in maintenance optimisation and fewer operation costs for the entire system [352]. A variety of damage types have been identified as susceptible to appear in composite blades during their lifetime [108,384]; these are, damage in the adhesive layer between the skin and flanges of the spar (debonding); damage in the adhesive layer between the top and bottom skins along the leading or trailing edge (debonding); damage in sandwich panels between the face and the core (debonding); delamination caused by tensional or buckling load; fiber failure in tension; laminate failure in compression; buckling of the skin (debonding); and cracks in the gelcoat or debonding of the gelcoat from the skin. Among them, delamination and adhesive joint failures are reported as the most usual ones [363]. A number of SHM techniques have appeared in the literature dealing with one or more of the damages mentioned above [442], including vibration analysis [194, 297, 406], strain monitoring [34, 160], acoustic emission [211, 439], ultrasonic detection [148, 362] and infrared thermography [180]. Several authors [108, 254] have provided recent literature surveys about the state-of-the-art damage detection techniques for turbine blades. Of the existing techniques, acoustic emission and strain monitoring have demonstrated efficiency on damage detection in real case scenarios [352,407], whilst Lamb-wave monitoring is recently being explored for its efficiency in damage location in large thin-walled composite structures [50,397].

In practice, there are commercially available monitoring systems for the drive train and gearbox components using information from Supervisory Control and Data Acquisition (SCADA) along with other vibration control systems [92]. However, the monitoring of the blades is still in its infancy although an increasing research effort is reported in the literature with sound solutions [99, 108, 254, 383, 406, 442]. The exis-

tence of data already available registered through the SCADA system has encouraged some researchers to further explore the data so as to find meaningful features for the blades [104, 292, 451]. Nonetheless, an effective blade damage detection and evaluation need dedicated blade SHM systems [254]. Indeed, a dedicated SHM system for the blades opens up the possibilities of blade pitch control (*derating*) as a way of no-growth control of existing damage or lifetime extension [154]. In addition, it has been reported to provide a more balanced and stable load for the rotating parts of the drive train and gearbox and thus extending their lifetime [42].

As a general comment, current SHM systems for wind turbine blades are able to provide data in controlled environments and meaningful damage indicators [262]. Notwithstanding, there is no proof of the systems performing during long time periods and under harsh-condition environments. How the system is going to react to uncertain and harsh environments remains unknown and conform one of the technological challenges of this industry. A non-durable SHM system will end up adding more maintenance costs and downtime on its own.

2.3.3 Civil construction industry

Generally, civil engineering structures are designed for long service life periods, about 100 years, and they usually require minimum maintenance throughout a significant part of their service life. In this context, the structural asset management strategy followed by this industry has been oriented to reactive maintenance mainly [231]. Notwithstanding, an increasing amount of structures are nowadays reaching their nominal lifetime and the use of SHM is gaining attention as a rational tool to support a reliable and cost-efficient life extension [230]. Life extension reduces the environmental impact of decommissioning and constructing a replacing structure and, therefore, it can be considered as a sustainable development strategy [215].

After damage has been detected and evaluated (e.g., corrosion in concrete structures), structural retrofitting is the natural step towards the life extension of the damaged component. In this regard, FRP composite materials have proven efficiency for retrofitting or rehabilitation of civil engineering structures [6,33,109,316], as explained

before. Notwithstanding, a key challenge that still remains open is the long-term reliability assessment of the retrofitted structure [227], to which dedicated SHM and PHM solutions are needed [6, 109, 324].

The literature about SHM in FRP structures for the civil industry is still very limited and mainly focused on the vibration analysis and the performance monitoring of FRP bridges. In [282], state-of-the-art SHM technologies in some demonstration FRP bridge projects in Canada are reported. Guan and Karbhari [158] provide a framework for a web-based SHM of an FRP composite bridge based on the vibration analysis and modal identification along with its variation throughout time considering the degradation of the structure. Following this, the same authors presented an application of this framework for the Kings Stormwater Channel Composite Bridge [159]. Separately, Mikołaj et al. [271] investigated the rheological effects of long-term loading on an FRP bridge using SHM. According to their study, no rheological effects were found for a 3-month test load. Long-term degradation was studied in [371], where the performance of the first all-composite bridge in Poland was controlled for 8 months finding no relevant degradation of the structural behaviour.

As a general comment, SHM has the potential to contribute to overcoming some of the main barriers posed in this industry to the extensive use of FRP composites; however, the literature on this topic is still limited and this potential is not fully exploited.

2.3.4 Naval Shipbuilding industry

It is well known that the environmental impact of ship failures is massive, perdurable in time, and especially difficult to revert. Each year, around a hundred large ships end up sinking according to Allianz's Safety and Shipping Review [10] being ship hull damage among the top five causes of sinking. The predominant types of structural issues of ships made of traditional metal materials are related to corrosion and fatigue cracking. Currently, the ship's design life cycle is estimated at around 30 years over which the reliability of the structure should be maintained. The current practice in structural health assessment of ships is the deployment of NDT when the ship is dry-docked. The approach followed, unless there is an existing and known flaw in the ship, consists of

the inspection of strategic areas of the hull to determine the thickness of the plate and extrapolate the corrosion rate to other parts of the ship; inspecting the complete hull including its welds would be impractical, time-consuming and expensive [195].

As with other industries, SHM in naval ships can provide insightful information regarding the actual condition of the structure and the loads that the structure is supporting. This translates into optimal design, maintenance and operation of the structures and uncertainty reduction in fatigue-life prediction [274]. The SHM approaches predominantly followed in naval vessels are vibration analysis [70,327] and wave propagation analysis [195]. Passive systems (e.g., acoustic emission) instead of active systems (e.g., guided waves) have been reported as more practical for at-sea implementations since they require less energy and infrastructure to work [331].

Despite the existence of some SHM systems deployed on metallic hulls, they represent a tiny proportion that does not allow the potential of this technology to be fully explored. One of the reasons why SHM has not been intensively used in naval vessels is the difficulty to deal with the size and shape complexity of their structural systems [122, 331]. Thus, there is a clear space for this technology to be further developed in this industry and demonstrate its potential for reliability and serviceability increase and maintenance cost savings [197, 368, 396].

As explained before, FRP structures are currently limited to small vessels and therefore, the application of SHM is practically nonexistent. Even though corrosion is not expected to be such a relevant issue for FRP vessels, degradation due to water ingress and fatigue need further exploration in practice. The latter could constitute a rich research and application area in the context of SHM; however, to the best of the authors' knowledge, SHM in FRP hulls has been mostly limited to the study of small components and connections, as reported in [175, 228, 264, 396].

2.3.5 Cross-sectoral SHM overview

Whilst the studied industries present different levels of expertise in the use of SHM in composites, the wide range of sensing technologies and their development level increases the likelihood of its effective application. In terms of experience in the use

of SHM solutions, the aerospace industry has been using it for longer in military and civil aircraft. The military sector, more prone to innovation due to lower certification constraints, provides a real testing environment for SHM solutions. In this sense, these military SHM solutions are being used to gain knowledge and transfer similar solutions to the civil sector. In the case of the wind industry, most existing SHM solutions are installed in components different from the blade, such as the drivetrain or the bearings. This industry is currently more reliant on visual inspection and further NDT in case of detecting any issue on the blade rather than on the use of SHM solutions. In contrast, the civil industry has adopted on-board SHM for singular and critical structures, typically based on vibrations (accelerometers) to detect changes in the native response of the structure. Considering the dimensions of the civil structures, SHM technology is being used to detect large damages on metal or concrete structures. Finally, the naval industry shows less experience in the use of SHM and is currently reliant on the visual inspection of hotspots of the hull of the boat while dry-docked to detect damage. The literature does not show evidence that this industry will adopt SHM technology in the near future at a rate similar to the other analysed industries.

Some common concerns across industries are related to the reliability, optimisation and absence of open data for the further development and deployment of SHM systems. The higher initial costs and the difficulty of access to the structure in some of the industries such as the aerospace, wind or naval, have directed the spotlight onto their reliability. They shall be designed so that an additional burden is not posed on the maintenance of the structure and the limited experience in their long-time application is seen as a potential risk for their deployment. Separately, the added weight of sensors and wiring could dilute the potential benefits of their use, primarily in the case of the aerospace industry. Whilst one of the principal arguments in favour of the transition to composite materials is the positive environmental effects of weight reduction, the higher complexity and evolution of non-visible damage types in these materials require a more profound knowledge of the state of the structure. Finding a balance to provide effective damage detection, location and quantification with the increase of weight caused by the addition of sensors requires a careful study of the structure. This issue feeds back into

the absence of data with which developers could optimise and compare the results of different SHM system solutions, creating a complicated environment for the integration of these systems within the structures.

2.4 Maintenance of composite structures across industries

Long-term reliability and durability have been highlighted among the most relevant factors that drive the industry towards the use of composites in their structures. Maintenance is directly related to both of them, and its impact can be decisive enough to condition the design of the structure and the materials used. In this section, the impact of maintenance and its relation with composite structures of some of the most relevant industries using composite structures will be analysed.

2.4.1 Overview of existing maintenance strategies

In general terms, there are four broad categories of maintenance strategies currently in use by the industry. These categories evolved throughout time starting from the less efficient ones, Corrective Maintenance (CM) and Preventive Maintenance (PvM) to the more efficient and technological ones, Condition-Based Maintenance (CBM) and Predictive Maintenance (PdM) [462]. The selection of the most suitable type of maintenance for a given application is non-trivial and has been studied by many authors. For instance, Zhu et al. [456] presented and compared different maintenance strategies (CM, PvM and PdM) for wind turbine blades based on the necessary leading time to prepare and perform maintenance actions and the associated costs of these. This study showed that inspection costs may greatly influence the choice of the most cost-efficient maintenance policy. Also, Chen et al. [68] presented a comparison of different maintenance strategies (PvM, hybrid CBM combining scheduled inspections and continuous monitoring, and pure CBM) for aircraft made of composite parts. Their findings show that the hybrid CBM strategy, which could resemble the current way in which CBM is applied in the aerospace industry, is the most expensive maintenance strategy, and that this could be related to the reluctance to use SHM in the sector.

Additionally, Florian and Sørensen [130] studied the cost implications of optimising the inspection intervals for PvM considering debonding damage of wind turbine blades. PvM costs were found lower than those for CM for most of the range of inspection intervals considered.

The most basic maintenance strategy, CM, also known as run-to-fail maintenance, has as fundamental principle not to interfere until the failure of the system. Its main disadvantage is the risk of sudden failure leading to unscheduled maintenance and the structure being out of service during unpredictable time. This results in significant unforeseen costs that include those related to production, downtime, and inventory since workers should be always prepared with spare parts for a sudden failure. Besides, it may lead to more severe damage modes resulting in higher repairing costs. In contrast, the advantage of CM is that it does not require strong planning due to its simplicity, so it makes sense for non-safety-critical assets only when the repair and downtime costs are less than the operating costs using other maintenance types. In essence, CM would be suitable for composite or any type of structure; however, it is acceptable for non-critical and lightly loaded structures only [161].

As a more advanced maintenance concept, researchers and industry started to focus on PvM in the 1960s [260]. PvM is also known as time-based or scheduled maintenance because it is performed periodically based on a prespecified schedule [49]. The main advantage of PvM over CM is the scheduled planning, therefore, eliminating the unforeseen costs of the run-to-fail strategy. It also reduces maintenance time by preparing beforehand the required parts, supplies, and manpower. In addition, it enhances the safety level with respect to CM since failure is prevented by routine inspection and maintenance activities [431]. On the other hand, an important disadvantage of PvM is that it is scheduled based on previous experience, which, depending on the case, can be reduced or even biased [401]. In practice, this uncertainty translates into unnecessary maintenance actions to keep failure risk to an acceptable level. For example, matrix micro-cracks, as the first sign of fatigue in composites, tend to accumulate sharply at the beginning of the fatigue life of the structure. Thus, inspections should ideally be unevenly distributed to properly track this damage mode, instead of inspections at

periodic intervals. Furthermore, the actual maintenance costs depend on the degradation level when performing maintenance and the duration of the required maintenance action; both of them are time-varying variables [204] whereas PvM is performed periodically ignoring this variability. These limitations, among others, make PvM unsuitable for composite structures where degradation evolves in a highly nonlinear fashion. A sample of the relevance of adjusting inspection and maintenance intervals is a comprehensive study on the reduction of operation and maintenance costs for wind turbine blades through the optimisation of these intervals based on the maintenance cost by Yi and Sørensen [443]. Another example is provided in [191], where the inspection interval for an FRP aircraft wing is optimised and compared with the MSG-3 PvM planning philosophy (the classical maintenance planning approach for aircraft), providing a quantitative procedure to optimise the inspection and maintenance of civil aircraft.

In this context, the development of SHM enabled monitoring continuously or as needed opened the doors to CBM, in which maintenance is applied based on the actual degradation condition of the structure. CBM was introduced around 1975 [23–27] and it is defined as the maintenance triggered by the evidence of the current state of the system exceeding a predefined threshold. With CBM, unnecessary inspections can be avoided thereby reducing unnecessary downtime and costs. However, defining the proper threshold for maintenance requires accurate knowledge in order to guarantee a healthy balance between safety and cost under different (and uncertain) conditions [309]. In addition, performing maintenance based on the knowledge of the current damage state only could result in unscheduled maintenance activities leading to higher running costs due to the lack of anticipation. An example of the importance of the definition of an optimum maintenance threshold was provided by Zhang and Chen [448], who developed an optimised CBM policy for wind turbine blades based on a fatigue crack growth model including imperfect repairs in which the crack length repair threshold was tuned.

To overcome the drawbacks of CBM, more attention is recently moving toward PdM. Both CBM and PdM rely on monitoring the state of the system through SHM,

but they differ in the way maintenance is planned. In CBM, the maintenance decision is made depending on the current damage state, so there might not be enough time before the maintenance threshold is reached. Whereas in the case of PdM, the decision is planned not only based on the current damage state, but also on an anticipation of the future degradation of the system. The prediction of the RUL of the structure is therefore central to allowing a dynamic adaptation of the maintenance planning in advance. An example of the potential of PdM was provided by Griffith et al. [155], where the optimisation of wind turbine blades O&M strategies based on SHM and PHM was studied. The inclusion of smart operation modes during high wind periods to increase fatigue life and contain damage progression was explored showing promising O&M cost reduction.

In summary, the literature provides evidence showing that the criticality safety of some applications such as aerospace, along with the current state of maturity of SHM for large structures, pose a barrier in the adoption of innovative and optimised maintenance strategies, being PvM and CBM the most frequently used in FRP structures currently. In the aerospace sector, the requirements for maintenance and reliability are notably strict and these are limiting the full potential of PdM. Notwithstanding, considering the high inspection costs of this industry, the situation could change in the future with the development of SHM and the acquired knowledge using composite structures [68]. In contrast, the wind industry has the potential to evolve rapidly into the adoption of PdM given the lower risk of unexpected failures and the numerous opportunities highlighted in the sector for life cost reduction. To the authors' best knowledge, the research in the remaining industries covered in this review is very limited due to the immaturity of the use of composite structures in those, as explained in Section 2.2.

2.4.2 Impact of maintenance in whole-life cycle costs

There are many examples in the literature showing evidence about the impact of maintenance on the life-cycle cost of industrial and physical assets. See for example [20, 78, 323, 340, 437], to cite but a few. The same applies to composite structures; however, the literature on this field is still incipient. In the following sections, this

literature is reviewed across the industries considered in this work.

Aerospace industry

Worldwide air traffic has been continuously growing during the past years with an annual average of 4.6% and it is expected to double in 15 years [221]. With this growth in the aviation industry, some authors have foreseen that by 2050 the amount of accumulated aircraft composites waste will reach 500,000 tons [224]. Besides, the uncertainty about the long-term reliability of composite materials [74] along with their faster fatigue damage accumulation rate (in relation to metals) may speed up the formation of composite wastes from this industry. Optimising maintenance and inspection strategies can help extend the service life of composite aerostructures considerably by controlling and slowing down deterioration. This aspect has been treated in the aerospace literature but for materials different from composites. For example, Guo et al. [162] provided several examples of military aircraft like the Canadian CF-188 [280], the Australian F-111C [162], and the American F-4 and B-52 fleets [43] that are operating beyond their nominal lifespan by virtue of intensive maintenance. However, frequent inspections may require disassembly and reassembly of the parts, which, in composites, it may result in an increased probability of damage [144]. Also, frequent inspections can result in delays, which in turn lead to additional operating costs that can reach up to 78 $/min [84, 224]. A proof of this is the development of Boeing's B787, in which the inclusion of maintenance costs and aeroplane availability among the evaluated factors in the design stage has resulted in a composite participation of over 50% in weight [39]. This shift in the design has proven to be effective, resulting in a number of damage occurrences equal to or lower than those for an equivalent metal structure [123].

Also, it is estimated that $5 million dollars can be saved during the lifetime of an aircraft by reducing the downtime and maintenance costs using SHM with CBM [103], but the installation of permanent sensors can cause an additional load to the aircraft. Dong and Kim [103] found that it will require 10,000 PWAS (piezoelectric wafer active sensors) to cover the fuselage areas of a Boeing 737, and this can lead to an extra 1000 lbs load which will result in losing the savings from maintenance

and downtime. This illustrates the necessity of lightweight and long-range sensors for SHM in aerospace. Composites provide a good alternative in this context since FBG sensors can be directly embedded inside the material from the manufacturing stage [414] requiring no additional cabling and reducing the weight with respect to a traditional PWAS solution. Another equally important action is the optimal positioning of the sensors thus reducing the number of sensors (and therefore the weight, cable length, etc.) to a minimum with enhanced detectability [295]. Approaches related to this topic are based on either the value of information [179, 349], cost-benefit analysis [52, 209], or a combination of both.

Wind industry

The growing trend in the wind industry, as depicted in Section 2.2.2, is accompanied by the increase in wind turbine size that has led to a rise in FRP utilisation in the bigger blades. The majority of the structural components of the wind turbine can be easily recycled except the composite blades since the recycling of composite materials is still difficult with the current technology [190]. Only considering the wind industry, the amount of composite waste is expected to increase rapidly and reach around 483,000 tons of accumulated CFRP by 2050 [224]. To address this problem, Jensen and Skelton explored the possibility of using composite waste in a circular economy context by using different alternatives (reusing/repurposing, recycling and recovering); notwithstanding, they note that the experience in reusing wind turbine composite materials in new applications such as bridges, fibres in concrete, playground, urban furniture, etc. is very little [190]. Their reuse for public infrastructure presents the main difficulty of verifying its state and strength whilst recycling and recovering technologies are not ready for all composite materials. In this context, elongating the lifespan of turbine blades can be considered the only feasible choice today to postpone and control the future explosion of composite waste, thus, offering the opportunity and time for finding better recycling solutions for this problem. Besides, life extension can increase the ratio of the energy generated per waste produced, increases the Return On Investment (ROI) and decreases the LCOE [245]. Utilising SHM/CBM systems to continuously

assess the health of the structure can be an efficient way to extend the service life of the wind turbine when accompanied by an evaluation of the factors that influence O&M costs and the critical failure modes of the system [245]. Griffith et al. [155] found that monitoring the health of the blade to regulate the load and power generation can help in elongating its fatigue life by 300%. Besnard et al. [31] considered different strategies of inspection and online condition monitoring and the result was different optimal maintenance schedules with different life-cycle costs for each of the strategies. In regards to the offshore wind turbines, the impact of one or another maintenance strategy on life-cycle costs is even more accentuated, especially when considering end-of-life scenarios and the possibility of life extension [186, 323]. In offshore wind farms, the operation and maintenance costs are predicted to be about 30% of the total life cycle costs [129], and this can vary from two to five times the land-based costs [284]. This makes the energy costs of offshore turbines larger than land-based ones [377]. These costs can be reduced by using SHM technology and proactive maintenance in a profitable way taking into account the state of the structure, and this can also lead to an increase in the overall profit and availability of the turbine [155].

Civil construction industry

As stated in Section 2.2.3, the main drawback of the massive adoption of FRP materials in civil engineering construction is the high material costs, which can represent up to a 50% increase when compared to traditional solutions in the case of bridges [9]. Therefore, a key to the success and expansion of these materials in the construction industry will be the accurate prediction of the life cycle costs of the composite structures. Indeed, the choice of the wrong maintenance strategy can further increase the cost of these structures by incrementing unnecessary inspection and maintenance costs [94]. In this sense, the adoption of CBM strategies using state-of-the-art "on-board" SHM techniques seems a suitable approach in this direction. Orcesi and Frangopol [294] developed a generic approach to include the effects of SHM in the life cycle costs and to optimise the maintenance strategies based on monitoring data. In their study, the knowledge about the criticality and occurrence of the failure modes and the integration

of SHM data were highlighted as the challenges for decision-making requiring further analysis for O&M cost reduction. Zhao et al. [454] performed a life cycle assessment comparing traditional concrete-filled steel tubular columns with several options including concrete and FRP from an economic and environmental perspective considering PvM maintenance. The results revealed that, considering uncertainties, the traditional approach using steel and concrete is likely to be more economically and environmentally efficient. It is important to note that different parts, loading scenarios and maintenance policies can result in different life cycle analysis outcomes and that the optimised solution for a specific structure may be a combination of traditional and composite material parts and different maintenance strategies.

Naval shipbuilding industry

As stated in Section 2.2, the use of FRP composites as primary structural materials in shipbuilding is still limited in spite of their potential [61]. Accordingly, to the best of the authors' knowledge, there are no references in the literature investigating the impact of FRP composites in life cycle cost reduction, service life and sustainability in the naval shipbuilding industry. However, several papers in the literature presented generic methodological approaches for ship maintenance optimisation that could be extended in the case of marine composite structures. For example, Liu et al. [237] integrated risk and maintenance cost reduction and increase in availability to optimise the repair actions that help in extending the ship's service life. Garbatov et al. developed a risk-based framework for maintenance optimisation from the design stage and for updating future maintenance plans while satisfying safety transportation requirements [136]. Dong and Frangopol [105] developed an approach for maintenance optimisation and optimal inspection scheduling while minimising the life cycle costs and risk of failure. They formally found that an optimum inspection and maintenance plan can reduce the risk of prolonged exposure of the structure to corrosion and fatigue. In summary, a high impact would be expected from a massive application of FRP composites in the naval industry with life-cycle cost reduction being prominent; however, this needs to be confirmed by more research and new applications.

2.5 Discussion

As previously discussed in Section 2.4, most inspection and maintenance approaches currently adopted by the composite industry are based on preventive/corrective maintenance methodologies with maintenance activities being scheduled in planned calendars. These approaches can be seen as economically and managerially efficient in the short term; however, they heavily penalise the serviceability and availability, and therefore, the life cycle cost and sustainability of the composite structures in the longer term when compared with predictive maintenance. The need for continuously reducing the costly and possibly unsafe maintenance and inspection cycle of key composite structures, like those from aircraft and turbine blades, requires *ad-hoc*, on-board, yet intelligent systems, able to efficiently transfer data to knowledge [457] and knowledge to decision-making as a paradigm shift towards the *Maintenance 4.0*. The latter is aligned with Goal 9 (*Industries, Innovation and Infrastructure*) of the United Nations' SDGs [276], which enforces a radical new vision for structural asset management leading to more predictable, sustainable, and resilient assets. In such a context, these obsolete asset management solutions can be replaced by predictive maintenance, where decisions are taken based on the actual and predicted state of health of the structures.

Among the potential needs to successfully materialise the PdM paradigm in composite structures, we can highlight two key technology enablers, namely the PHM and CPS technology. The following subsections revise these two technology enablers in the context of composite structures and provide critical perspective and discussion about desirable research needs towards the aforementioned objective.

2.5.1 Intelligent Prognostics and Health Management (iPHM)

Prognostics is the science of predicting the remaining useful life (RUL) of physical assets (e.g., a turbine blade) given the information about the current degree of damage of the asset, the load history, and the anticipated future load and environmental conditions [146]. Technically speaking, PHM is a natural extension of SHM where the focus is not only on detecting, isolating and sizing a fault mode, but also on predicting the remaining

time before the failure occurs with quantified uncertainty, which is further used for rational and anticipated PdM decision-making [121]. From a practical viewpoint, it is a continuous process of update-predict-reassess which requires periodical measurement updates to increasingly improve the predictions of the RUL.

In application to composite structures, RUL predictions are subject to significant uncertainty that comes not only from uncertain inputs (upcoming loads, environmental conditions, material's voids, etc.) but also from the lack of knowledge about the physics of the damage process. This uncertainty, and the associated computational complexity of the prediction problem, is exacerbated when dealing with large-scale thin-walled composite structures under real operating conditions using noisy, sparse or missing SHM data [145]. This is mainly the reason explaining why probability-based frameworks have been preferred for prognostics in composites, rather than deterministic or point-valued RUL estimations. Damage prognostics for structural applications have been recently explored by several researchers [87, 93]. In the current literature, available damage prognostics approaches for composites are capable of only capturing some (but few) of the specific damage modes such as micro-crack propagation, delamination, etc., which are only representative of some of the potential deterioration patterns of a full-scale composite structure [71, 75, 86, 114, 243]. Moreover, the vast majority of PHM research to date deals with predicting the RUL of structural coupons or small structural parts and generally under laboratory-controlled damage conditions. Thus, there is a clear research opportunity to effectively deploy iPHM methods in real-world composite structures subject to realistic load and environmental conditions.

At this standpoint, it is important to remark that a keystone to deal with the abovementioned achievement relies on the availability of an effective sensing system to obtain real-time online data about the structural health state. Indeed, as previously specified in Section 2.3, ultrasonic guided waves and acoustic emission have exhibited strong potential as SHM solutions for detecting damage signatures in composite structures [114, 243, 436]. However, to the best knowledge of the authors, available SHM systems in composites still lack integrated, yet long-term reliable solutions adequate for working under operational conditions. Thus, there is a fundamental technological

and scientific issue that still remains open, which is to effectively integrate these SHM sensors on-board a composite structure properly working in operational (loading and environmental) conditions in the long-term.

The latter requires a deeper understanding of the sensing technology capable to cover a wider range of damage signatures (as no single sensor type can cover all), and most importantly, technology development for effective manufacturing methods which enable sensor network integration with minimal or no affection to the structural response of the composite. The aforementioned challenges imply a need for the development of novel manufacturing methods to render smart composite materials [171,342], which include robust, accurate and minimally invasive embedded systems for on-board, continuous, yet reliable monitoring.

Finally, we remark that the energy supply of on-board installed sensors and communication nodes supposes a major concern for efficiently deploying PHM solutions in composite structures. Energy harvesting methods are today a major research topic within the composites field providing suitable solutions mostly for structures subjected to dynamical excitation [46, 91, 118, 358, 464]. This, together with the development of low-consume sensors, might shed light on making on-board long-term embedded SHM systems feasible.

2.5.2 Structural composites as cyber-physical structures

The concept of CPS is at the core of AI and its related disciplines, like the Internet-of-Things (IoT) and robotics. CPS integrate physical assets with embedded sensing, processing, communication, and networking capabilities, whereby cyber and structural components form a collaborative integration transforming the monitored structure from being a physical asset to a cyber-physical entity [212].

Recent works [404, 459] propose that CPS can result in autonomous self-managed systems with diagnostics, prognostics, and decision-making capabilities using online SHM and PHM information. Indeed, the anticipation of CPS to structural damage can be granted by self-adaptiveness of operational decisions (e.g. go / no go for inspection) based on PHM predictions. Through self-adaptation, the predicted information

is updated to dynamically accommodate health state changes and provide autonomous maintenance decisions, therefore increasing the system efficiency and making it more resilient to the new conditions.

However, important research breakthroughs are needed for CPS to be directly applied to composites structures. Apart from scaling up the PHM techniques under demanding real conditions, as previously discussed in the last subsection, a key challenge still lies in formulating system-level mathematical tools to represent and simulate the dynamics of the CPS entity. The latter implies the development of expert system models capable of integrating SHM data, PHM predictions (whether model-based or data-based), and expert knowledge with system-level I&M non-linearities[2]. There are some available system-level modelling paradigms in the literature to mathematically represent expert systems [4, 300], like for example Hybrid automatas, Mixed logical dynamical models, Piecewise affine models, Petri Nets and max-min-plus-scaling systems [90, 172, 246, 313].

Among the aforementioned approaches, Petri nets (PN) [314] are typically regarded as powerful modelling tools for expert systems due to their ability to account for resource availability, concurrency, and synchronisation, which are common aspects that underline the majority of the aforementioned system-level non-linearities. Moreover, new PN variants like the fuzzy Petri nets (FPN) [67, 238, 319], Possibilistic Petri nets [54, 223], and Plausible Petri nets (PPNs) [73] have appeared in the literature to account and react to uncertain information (e.g. from sensors, experts, etc.), which are of special interest of CPS of composites due to the unavoidable presence of uncertainty in the damage predictions. Particularly, the recently formulated PPNs have demonstrated good results as self-adaptive expert-level models using off-line degradation data and expert knowledge [73], and might constitute a useful tool to mathematically represent the dynamics of cyber-physical composite structures at system-level.

It is important to note that, in a literature search, one can realise that the idea to integrate expert systems with other technologies is as old as AI, and this trend still continues in the new generation of expert systems [321, 322]. Particularly, expert

[2]System-level I&M non-linearities are understood here as artificial I&M actions and other human-based events that influence the "natural" damage and ageing progression of the composite structure.

systems applied as decision support tools for structural damage assessment date back earlier than the boost of the SHM technology [212], but not as cyber-physical systems.

Nowadays, the cyber-physical technology is being superseded by the *digital twin* concept [152] which combines interactive knowledge-based and geometrical virtual (digital) models with their physical counterparts within an IoT-based sensing environment [425], typically using cloud-computing and data intelligence. Within the context of composite structures, a desirable scenario would be so that PHM predictions and damage models were integrated within a system-level virtualisation that can be updated using data from the physical twin (namely the IoT-based monitored composite structure) to enable optimal dynamic task allocation, operations sharing, and PdM decision-making.

The latter is the so-called Level-5 Digital Twin technology and, together with new efficient-lightweight PHM and learning algorithms that can do on-board edge or cloud computing [404], constitute a potentially fruitful research direction to enable efficient and reliable I&M strategies in composite structures.

2.6 Concluding remarks

The use of FRP composites in thin-walled structures for safety-critical applications has seen a notable rise over the last few decades, especially in the aerospace and wind industries with evidence of reliability, durability, life cycle cost reduction and sustainability. Other industries such as the civil and naval have not seen such a rampant increase so far presumably due to the uncertainty about the long-term performance, the lack of technological demonstrators, and the absence of codes and standards.

To overcome this, the development of policies and codes regulating the design with composites along with a cross-sectoral knowledge transfer among industries could be the levers that unlock a greater use of these high-efficiency materials. Moreover, while still relatively immature for industrial application, converting composite structures into cyber-physical structures seems promising to promote the transition into predictive and optimised inspection and maintenance strategies and overcome the long-term performance uncertainty of FRP structures.

For the case of wind turbines, typically the laminates applied to the blades consist of e-glass fibers and thermoset matrices like epoxy, polyester, or vinylester, with a fiber content of approximately 75% by weight. The growing need for larger wind turbine blades, particularly in offshore applications, has prompted the exploration of carbon fibers to enhance strength and stiffness-to-weight ratios. This, in turn, enhances resistance to gravitational loads and improves fatigue life.

The utilisation of composite materials in the wind industry is associated with various challenges. Primary concerns include uncertainties regarding failure modes, challenges in monitoring damage progression during operational use, and reliability issues in the manufacturing process of large composite components.

In practical situations, the effectiveness of damage detection has been established through acoustic emission and strain monitoring. Additionally, there is a current exploration of Lamb-wave monitoring for its potential in pinpointing damage locations in large composite structures. The implementation of monitoring systems for drive train and gearbox components, utilising data from SCADA and other vibration control systems, has become a reality. Nevertheless, blade monitoring is still in its early stages, although a growing body of research in the literature is providing promising solutions.

Present SHM systems for wind turbine blades can furnish data under controlled conditions, offering meaningful damage indicators. However, the performance of these systems over extended durations and in challenging environmental conditions lacks substantiated evidence. The response of these systems to uncertain and harsh environments remains uncertain, posing a technological challenge within the industry. A non-durable SHM system has the potential to increase maintenance costs and downtime, ultimately counteracting its intended purpose.

Presently, the predominant approach to wind turbine maintenance relies on visual and tap test inspections. As discussed in this chapter, this method has limitations, particularly in detecting subtle impact damage that may go unnoticed. Implementing SHM or CBM systems for continuous structural assessment proves to be an effective strategy for prolonging the service life of wind turbines. This approach is most beneficial when coupled with an analysis of factors influencing O&M costs and critical failure

modes of the system.

In the realm of offshore wind farms, it is anticipated that operation and maintenance costs will constitute approximately 30% of the total life cycle costs. Moreover, these costs can be two to five times higher than their land-based counterparts, rendering energy costs for offshore turbines higher. Integrating SHM technology and adopting a proactive maintenance approach through PHM can contribute significantly to cost reduction by considering the structural condition. Furthermore, this approach has the potential to enhance overall profitability and turbine availability.

Chapter 3

Failure mode, effect and criticality analysis of wind turbine blades

Chapter contribution

This chapter aims to accomplish the following research objective: *Identify the most critical failure modes of a wind turbine blade.*

The contributions of this chapter are detailed below:

- Identify the most critical subcomponents of the blade.
- Provide insight into the failure modes to prioritise for O&M purposes.

The published peer reviewed journal article Contreras Lopez, Javier and Kolios, Athanasios "*Risk-based maintenance strategy selection for wind turbine composite blades*" Energy Reports 8 (2022) was authored by myself as part of my research completed under the direction and consultation of my supervisor, Professor Athanasios Kolios. The published article is incorporated in this chapter and forms part of the wind turbine blade failure mode identification presented in this Chapter.

3.1 Introduction

As highlighted in Chapter 2.6, the difficulties to predict and monitor damage in wind turbine blades requires the design of careful inspection and maintenance strategies for them. On this regard, the different failure modes of the blade need to be identified and ranked to provide cost effective solutions that could help improve current maintenance practices. In this sense, several offshore wind turbine life costs analyses have revealed that operation and maintenance (O&M) costs can represent up to more than 30% of the total costs of wind turbines throughout their life [256,393]. Furthermore, turbine blades along with the gearbox and electrical generators have been identified as the components with the greater failure rates of the turbines [234, 405]. In contrast with gearboxes, electrical generators and other components, where the use of condition monitoring is much more mature and is currently implemented in some turbines [35,100,258,286,359], the blades are rarely instrumented and their inspections and maintenance are usually calendar-based which creates an opportunity for improvement on their reliability and life extension by switching to condition-based types of maintenance [202, 257]. As presented in Chapter 2.6 the knowledge around failure modes of composite materials is limited and the uncertainty about its material properties, potential manufacturing defects and damage during installation require a careful understanding of the more critical failure modes, causes and effects.

To determine which failure modes are more relevant and drive the reliability of the blades, a systematic analysis is provided in this chapter by means of a comprehensive Failure Modes, Effects and Criticality Analysis (FMECA). In this analysis, the severity and occurrence of each of the failure modes is considered so as to define a criticality number (CN). Based on the resulting CN, risks will be prioritised to study the implementation of improved maintenance and inspection strategies. The types of maintenance under consideration are shown in Figure 3.1. Conceptually, there is a big difference from corrective maintenance or statistics-based preventive maintenance to condition-based maintenance based on non-destructive testing or sensor data. As opposed to corrective and statistics-based preventive maintenance, condition-based

maintenance requires a deep knowledge of the failure mode under study.

Later, the current maintenance strategy usually applied for the failure modes is be indicated. Following this, the feasibility of detection of each failure mode along with the feature or features and structural health monitoring (SHM) techniques used for its detection will be explored among the existing literature. Finally, the maintenance decision framework proposed in [203] will be used toward the development of a risk policy to determine a feasible maintenance strategy for each of the blade failure modes above a considerable risk threshold to enhance the current practice and impact in the overall reliability of the blade. This study will also serve as a guide for the main failure modes to be included in wind turbine blade O&M modelling for an effective representation of the physical system. In contrast with existing risk analysis of wind turbine components where the criticality of different components is presented, this study analyses in detail the failure modes at component level for the blades, providing a detailed vision of the nature and effects of the failure modes and a risk policy for the selection of the optimal inspection and maintenance strategy. Transitioning from predetermined or corrective maintenance to condition-based maintenance can report an increased availability of the assets if properly performed [205]. Therefore, this study provides the natural step forward to commence the implementation of practices to increase the reliability of wind turbines and could be used by wind farm operators and other stakeholders as a guide for other components (tower, generator, drivetrain, ...).

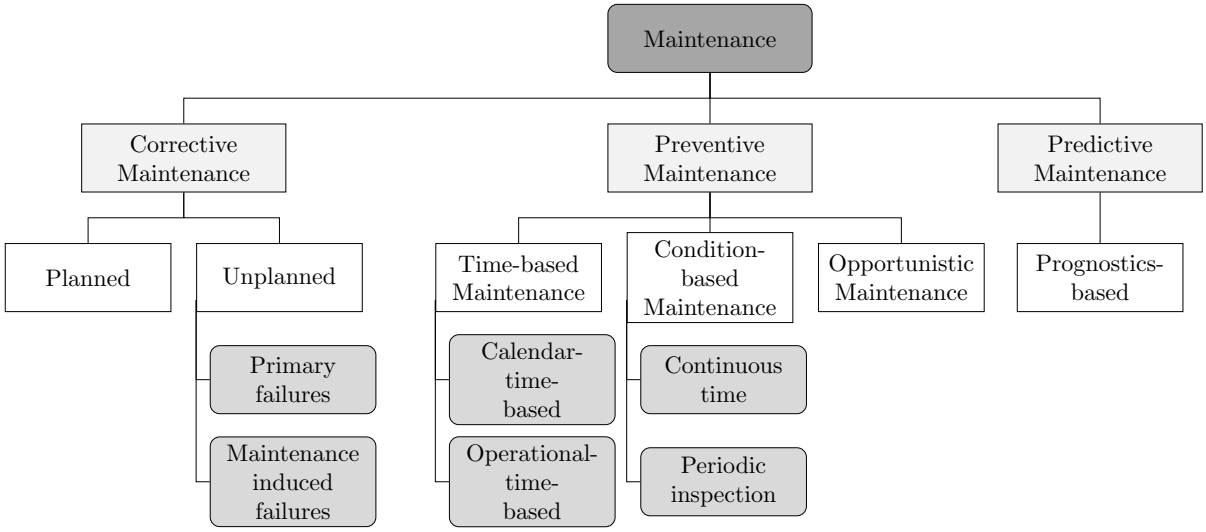

Figure 3.1: Types of maintenance. Adapted from [203].

3.2 Literature review

When facing the problem of increasing the reliability of a system, the concept of risk is widely used in the prioritisation of components and failure modes. It is defined in ISO 31000 [387] as *the effect of uncertainty on objectives*. A concept closely related to risk in O&M management is criticality. Both concepts combine the likelihood of an undesired event happening with the severity of its consequences (usually environmental, economic and safety), being the criticality used to provide a prioritisation of failure modes within a system [389]. Among the existing qualitative and quantitative methods to prioritise failure modes of systems presented in the ISO 31000 series of standards [386, 387], the Failure Mode and Effect Analysis (FMEA) and its extension, the Failure Mode Effects and Criticality Analysis (FMECA) that incorporates the analysis of the criticality of the failure modes of the system, have been extensively applied in the operation of physical assets in particular. Risk prioritisation studies such as the one provided in this chapter call for qualitative or semi-quantitative approaches in the absence of a significant amount of date. In this sense, the FMECA has been selected as the method for this study to overcome the lack of data with the data required to individually characterise the identified failure modes. In the future, the application of quantitative

methods like the ones proposed in ISO 2394 [388] will improve informed O&M decision-making for wind turbine blades. A comprehensive review of the different risk and reliability-based analysis can be found in [225]. The IEC 60812 standard [81] describes in a comprehensive way the steps for the application of the FMEA and the FMECA. The strength of these methods comes from its versatility to accommodate quantitative and qualitative data, and therefore the combination of physics-based and data-based knowledge, while preserving a logical and structured approach.

During the last decade, there have been several risk assessment studies considering the complete wind turbine [14, 95, 102, 229, 245, 247, 298, 347, 356, 357]. Considering the different environments to which wind turbines are exposed, the comparison of failure modes between onshore and offshore wind turbines was studied in [356], showing that risk and cost increase for offshore turbines while the risk rank of components is fairly consistent. In [229], a two-stage FMECA considering 13 components including the blades is presented in which blades are the most relevant component in terms of a combination of cost and risk priority. In [247], a FMEA and a failure mode maintenance analysis are presented in which six components, including the blades, are also analysed. Arabian-Hoseynabadi et al. [14] performed a FMEA of the wind turbine and compared it with reliability field data and suggested further analysis at the component level. Scheu et al. [347] performed an analysis based on an in-depth FMECA study in which 337 failure modes were identified and analysed by experts. Additionally, the potential benefit of deploying monitoring systems was assessed for the critical failure modes. Separately, Luengo and Kolios [245] reviewed the main failure modes of wind turbines found in the literature to provide a view on end of life scenarios for different components.

Notwithstanding the proliferation of different risk and reliability analysis of wind turbines, to the best of the authors' knowledge, the existing studies are focused on the identification and prioritisation of wind turbine components without the detail required to propose individual monitoring techniques and maintenance strategies for the most critical failure modes. This additional step is essential for the implementation of improvements in the system. Table 3.1 summarises some of the studies found in the literature in which the blades or rotor were studied. In order to challenge the

current maintenance practice, a detailed risk assessment at component level is deemed necessary. Thus, understanding and evaluating the impact of each of the failure modes of wind turbine blades is the first step toward the implementation of new practices for reliability improvement of this component.

Table 3.1: Risk and reliability studies including wind turbine blades in the literature.

Reference	**Blade included**	**Number of blade failure modes**	**Failure modes**
[14]	Yes	4	Mechanical rupture, fracture, detachment, fatigue
[229]	Yes	3	Blade cracks, delamination, gear teeth slip (rotor)
[247]	Yes	2	Crack in blade, gear teeth slip (rotor)
[347]	Yes	19	Cracks, delaminations, debonding, top coat damage, lightning damage
[245]	Yes	12	Cracks, delaminations, surface wear, increased surface roughness, fatigue, lightning strikes, high vibrations, flapwise fatigue damage, unsteady blades air loads, blade fracture, unsteady performance, corrosion
[357]	Yes	7	Abnormal vibration, blade surface roughness, bird crash, ice-forming, hurricane, earthquake, wrong materials

3.3 Developing a risk-based maintenance strategy selection policy

The stakeholders of the industry are seeking important cost reductions in the maintenance of wind energy assets. In this sense, the analysis of the reliability of the different components and the selection of the optimum maintenance strategy or combination of maintenance strategies are not trivial problems. Developing a risk policy and, therefore, assigning thresholds to target failure modes is a critical task to bring down these costs. In contrast with much more mature industries such as the automotive or offshore Oil&Gas which have developed standardised risk policies based on accumulated knowledge and data, the wind industry and, in particular the offshore wind industry, are in need of more studies.

In this study, the scope of the FMECA will be the blade, and it will be broken down into the following components as seen in Figure 3.2 (upper and bottom shell, spar, root, and the leading and trailing edges). The first step of the analysis is the

identification of the failure modes, which are the manners in which failures can occur. Secondly, the effects or consequences of the failures will be presented. Furthermore, the causes initiating them and the failure mechanisms that are developed toward the failure will also be identified.

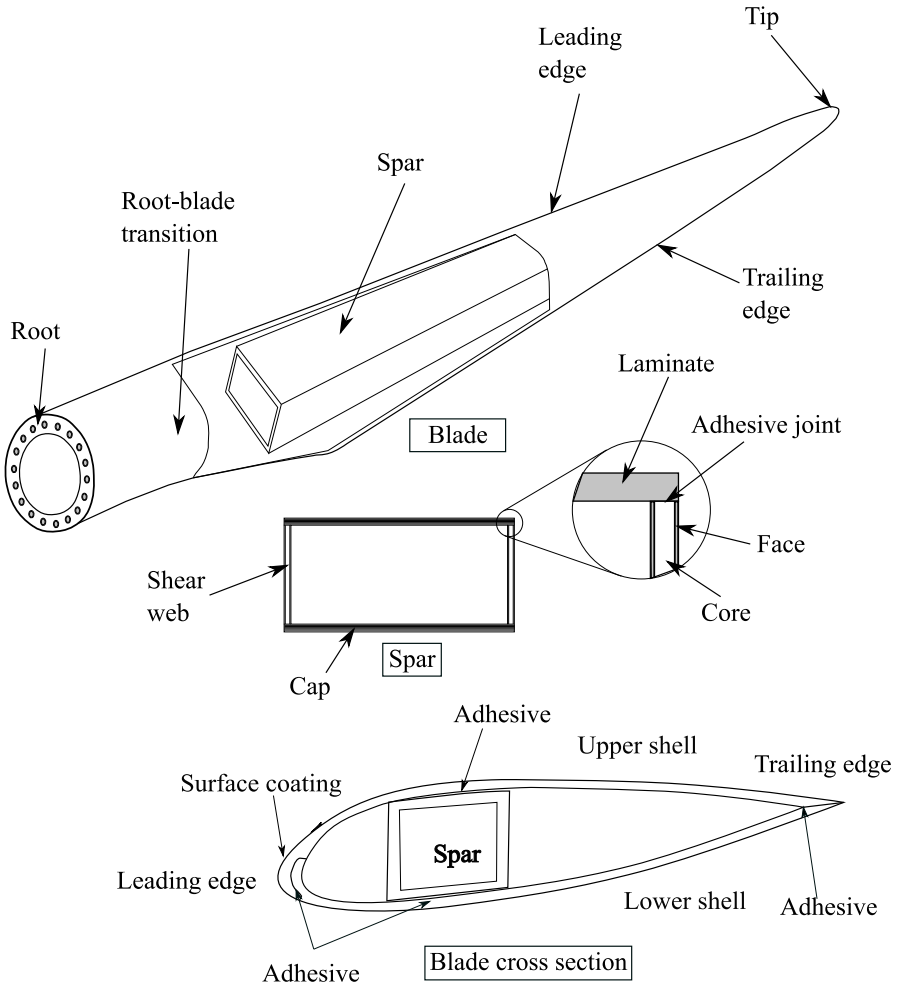

Figure 3.2: Wind turbine blade components.

The criticality will be assessed using a 2-parameter approach that will define the criticality number (CN). The CN will be computed as follows:

$$CN = S \cdot O \tag{3.1}$$

where S is the Severity (relative ranking of potential or actual consequences of a failure)

and O is the Occurrence (relative likelihood of the occurrence of a failure) factor. The range of values considered for these factors spans from 1 to 5 according to the criteria shown in Tables 3.2 and 3.3. The values of Occurrence have been set in agreement with the studies shown in Table 3.1 and expert elicitation. Separately, the values of Severity, have been chosen considering the economic and structural implications of the development of the failure mode. As defined for this work, occurrence and severity factors have equal weight toward the criticality of the failure mode. The values for the resulting criticality range from 1 for the less critical mode to 25 for the most critical. The criticality domain has been divided into four categories (low, moderate, high and extreme) as shown in the matrix of Figure 3.4 and described in Table 3.4. The guidelines presented in [13] have been carefully considered as to provide a risk matrix with sufficient resolution and to balance ratings so that negatively correlated frequency and severity values of the identified failure modes can provide insightful criticality numbers. The approach used for this study is in line with recent relevant papers in the same field, such as [347] and [203]. While other studies include a third factor called Beta factor or detectability, which represents the conditional probability of the failure end effect to materialise given that the failure mode has occurred, only Severity and Occurrence have been considered to use the risk matrix as an approach for risk visualisation and acceptance. This practice is widely used in industry through relevant standards and risk policies. In this study, failure modes with a criticality of high or above will be prioritised to propose monitoring and maintenance strategies for the reduction of their criticality owing to the potential of their consequences in the operation of the asset and the risk of producing economic and or environmental losses of entity.

Table 3.2: Severity factor categorisation.

Category	**Description**	**Factor**
Negligible	Unidentifiable or only cosmetic damage	1
Minor	Damage not causing interference with the normal operation of the wind turbine	2
Moderate	Damage having slight consequences to the operation of the turbine but not causing service disruptions	3
Major	Damage interfering with the operation of the wind turbine and causing service disruptions	4
Catastrophic	Failure of the system	5

Table 3.3: Occurrence factor categorisation.

Category	**Description**	**Factor**
Rare	Remote possibility of failure	1
Unlikely	Relatively few failures	2
Possible	Occasional failures	3
Likely	Repeated failures	4
Almost certain	Almost inevitable failure	5

Table 3.4: Description of Criticality Categories.

Category	**Description**	**Range**
Extreme	Failure modes causing great economic/environmental losses due to a high severity and or likely occurrence. Failure of the system or need for emergency stop.	15-25
High	Failure modes that could produce some economic losses, with a lower likelihood. Major disruption of operation or need for preventive stop.	8-14
Moderate	Failure modes affecting the normal operation of the turbine. Reduced power output, or increased vibration.	4-7
Low	Minor failure modes having a low or negligible effect on the operation of the asset. Even when very frequent, the operation of the turbine is not affected.	1-3

After the classification of failure modes according to the proposed CN, this study provides a systematic framework for maintenance strategy selection following the decision tree in Figure 3.3. The proposed maintenance strategies are corrective maintenance, preventive planned maintenance (time-based), preventive condition-based maintenance and predictive condition-based maintenance. The maintenance strategy selection starts with the FMECA of the blade and the determination of the criticality thresh-

old to consider so as to increase the efficiency of the improvements to be implemented. For non-priority failure modes, the corrective maintenance shall be enough since the failure is not so relevant in terms of risk. For those failure modes above the threshold, the feasibility of the monitoring is key to opt for condition-based (either predictive or preventive) or preventive or corrective maintenance. Condition-based maintenance has the advantage of considering the current state of the system. Choosing a predictive maintenance strategy requires the instrumentation of the blade [257] and the ability to provide reliable estimations on the future evolution of the failure mode under consideration, which is receiving attention from the research community as shown in [72], while preventive maintenance requires an optimised inspection interval to increase efficiency. For those failure modes that are not able to be monitored, preventive planned maintenance shall be used, when technically and economically feasible, and corrective maintenance otherwise. Finally, if the corrective maintenance is not acceptable due to economic, environmental, safety or other implications, improvements are required to reduce the risk of the failure mode (for example design modifications, improvement of materials or modification of operation).

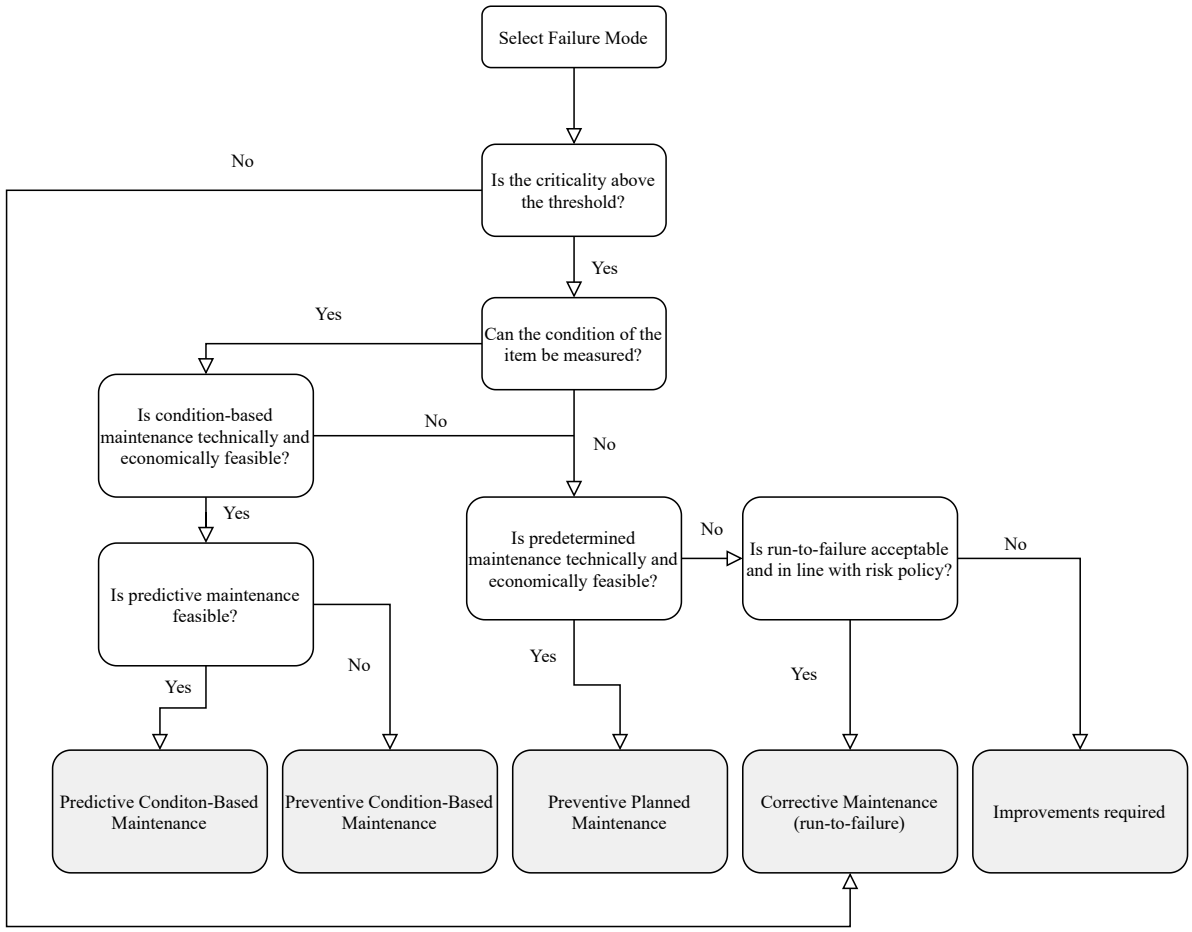

Figure 3.3: Maintenance decision tree. Adapted from [203].

3.4 Risk identification and criticality assessment

The identification of risks was performed in consultation with industry experts, of which, its distribution among the different components of the blade is shown in Table 3.5 and the causes divided in four categories (design, manufacturing, installation and operation) shown in Table 3.6. A total of 62 failure modes have been identified, being the spar and the upper and lower shells the components with the higher number of failure modes identified, with a total of 20, 11 and 11, respectively.

Table 3.5: Identified risks from the FMECA.

Failure mode	**LE**	**LS**	**R**	**S**	**T**	**TE**	**US**	**Grand Total**
Adhesive joint failure (debonding)	3					3		6
Blade rupturing, blade burnout, wire melting. (Lightning)					1			1
Buckling						1		1
Cracks	1	2		5		1	3	12
Cracks in the gelcoat		1						1
Debonding				2				2
Debonding (laminate to core)		1		1			1	3
Delamination		2		5			2	9
Erosion of leading edge protection (LEP)	3							3
Failure of root-hub connection			3					3
Ice accumulation	1							1
Intralaminar fracture (matrix cracking - microcracks)		3		6			3	12
Receptor vaporization, surface scorching, surface blotching, surface delamination (lightning)					1			1
Skin/adhesive debonding		1					1	2
Surface cracking, surface tearing (lightning)					1			1
Surface stripping, receptor loss (lightning)					1			1
Water ingress		1		1			1	3
Grand Total	**8**	**11**	**3**	**20**	**4**	**5**	**11**	**62**

LE: Leading edge LS: Lower shell R: Root S: Spar T: Tip TE: Trailing Edge US: Upper Shell

Table 3.6: Count of failure modes by cause.

Cause	**Count of failure modes**
Design	23
Installation	6
Manufacturing	22
Operation	11
Grand Total	62

The spar is the part of the blade having the mission of the structural integrity of the blade and, therefore, its failure modes can evolve until the complete failure of the blade requiring its complete replacement if not maintained in time. The spar is composed of the caps, responsible for the bearing of the flapwise bending loads of the blade, which are the predominant loads; and the shear webs, designed to withstand

shear loading and edgewise bending. The failure modes present in this part follow the usual damage progression of composite materials (intralaminar cracking - delamination - crack formation), with the severity of each of those failure modes growing with damage growth [164]. The occurrence of these failure modes provokes effects increasing in severity that include the following: reduction of energy production, increase of dislocations of the blade under operation, rise of stress on the laminates, critical dislocation of the blade (tower hit) and collapse of the blade. The initiation of these failure modes is usually related to defects present in the manufacturing process and fatigue damage accumulated throughout the life of the blade [11]. Additionally, the disbond of the cap-shear web connection and the water ingress constitute failure modes as well and can contribute to the structural performance degradation of the blade.

The upper and lower shells of the blade provide the aerodynamic design of the blade to maximize lift for energy production and minimise drag. The sandwich panels that conform the shells are coated with a gelcoat providing superior smoothness of the surface and wear protection. The shells are affected by the erosion effects of the rain and the abrasive particles carried in the air. Additional failure modes affecting the shells are related to damage in the sandwich panels forming them (interlaminar cracking, delamination, cracks and debonding between the laminate and the core). The effects of these failure modes are primarily related to a loss of energy production and the modification of the aerodynamic loading that can initiate damage in the spar.

The upper and lower shells are joined together in the leading and trailing edges by means of adhesives. The failure of the adhesive is one of the main failure modes of these parts. The leading edge is more prone to suffer erosion due to the incidence of the flow and is one of the most common failure modes of the blades. The blades located in frost-prone environments are usually equipped with deicing systems to avoid the accumulation of ice on the blade and the failure of these systems increases the mass of the blade and can provoke structural damage and rotor imbalance. Separately, the degradation of the trailing edge can result in the local buckling of the shells.

There are two regions of the blade that are affected by singular failure modes, the root and the tip of the blade. The root of the blade provides the connection of the

blade with the hub, and can experience failure modes due to manufacturing defects in the machining of the holes and the assembly of the blade to the hub. The failure modes affecting the root have critical consequences, since the failure of the connection of the blade to the hub can result in the detachment of the blade. Separately, even though the blade has a lightning protection system incorporated, it is sometimes not able to fully protect the blade against lightning strikes and could potentially result in different degrees of damage varying from simple receptor damage that is fixed by a simple replacement to more severe damage modes (surface scorching, surface blotching, delamination, surface cracking, surface tearing and blade rupturing) that could even require the replacement of the whole blade.

Severity \ Occurrence	1 Rare	2 Unlikely	3 Possible	4 Likely	5 Almost Certain
5 Catastrophic	5 Moderate	10 High	15 Extreme	20 Extreme	25 Extreme
4 Major	4 Moderate	8 High	12 High	16 Extreme	20 Extreme
3 Moderate	3 Low	6 Moderate	9 High	12 High	15 Extreme
2 Minor	2 Low	2 Low	6 Moderate	8 High	10 High
1 Negligible	1 Low	2 Low	3 Low	4 Moderate	5 Moderate

Figure 3.4: Criticality matrix

In light of the failure modes identified, the recent literature regarding damage detection and monitoring of wind turbine blades has been explored to assess the current feasibility of applying condition-based maintenance strategies, as shown in Table 3.7. This table summarises the feature and the monitoring techniques used for the different damage modes covered in this study to shed some light on the potential improvements that could be implemented. In terms of available non-destructive testing or monitoring techniques for the blades, thermography, acoustic emission, ultrasonic guided waves, digital image correlation, optical techniques and vibration analysis are the most used in the literature. The applicability of the different techniques depends on factors such

as the accessibility of the damaged component, the detectable size of damage, the type of failure mode and the possibility of embedding or attaching a sensor on the structure or needing to perform the inspection with an external device. The features and monitoring techniques identified are linked with the relevant failure modes as to identify the feasibility of continuous monitoring and propose the most adequate maintenance strategy following the decision chart proposed in Tables 3.8, B.1, B.2 and B.3.

Table 3.7: Damage monitoring references in the literature.

Reference	**Feature**	**Monitored damage**	**Technique**
[135]	Temperature distribution	Delamination, impact, cracks	Thermography
[181]	Temperature distribution	Delamination, surface damage	Thermography
[106]	Strain fields	Cracks	Strain gauges
[148]	Guided wave amplitude	Delamination in laminates and sandwich parts.	Ultrasonic guided waves.
[381]	Signal amplitude	Delamination, cracks	Acoustic emission
[69]	Temperature distribution, strain fields	Delamination in spar cap, adhesive joint debond, trailing edge buckling.	Thermography, DIC
[305]	Standing wave energy	Trailing edge, leading edge, spar debonding, Delaminations	Ultrasonic guided waves
[372]	Power curve, tower lateral oscillation acceleration	Ice formation detection	Vibration analysis, power curve analysis
[222]	Strain and displacement fields	Crack, debonding, delamination	3D DIC
[310]	FBG reflectivity - strain	Trailing edge debonding and cracking	Optical (FBG)
[438]	Strain and displacement fields	Crack, debonding, delamination	3D DIC
[296]	Natural frequency, damping ratio, mode shapes and curvatures, accelerations	Crack	Vibration analysis
[211]	AE power and spectral features	Debonding	Acoustic emission
[160]	Strain	Debonding and delamination	Optical (FBG)
[170]	Strain and displacement fields	Trailing edge disbond and buckling	Optical (FBG)
[156]	Modal shape, frequencies	Trailing edge disbond	Vibration analysis
[453]	AE power and amplitude	Cracks	Acoustic emission
[345]	Group wave propagation velocity, energy and amplitude of the wave	Sandwich debonding	Ultrasonic guided waves
[402]	AE energy, AE amplitude	Matrix cracking, fibre breaking, matrix-fibre debonding	Acoustic emission
[332]	Time of flight	Delamination	Acoustic emission
[439]	Amplitude, decay, energy, peak frequency	Matrix cracking, matrix fibre debonding, fibre breakage	Acoustic emission
[259]	Wind speed - rotational speed, Wind speed - power	Lightning strike detection	SCADA data analysis
[361]	Image analysis aided by deep-learning	Erosion, cracking and lightning	Deep learning
[430]	Image analysis	Anomaly detection	Deep learning
[207]	Current	Lightning impact location	Fibre optic sensor
[413]	Natural frequency, damping ratio	Ice formation detection	Vibration analysis
[364]	Peak magnitude, group phase velocity	Ice formation detection	Ultrasonic guided waves
[428]	Amplitude, group phase velocity	Ice formation detection	Ultrasonic guided waves
[339]	Temperature distribution	Cracks, delamination, dirt, erosion	Thermography
[417]	Statistical vibration features	Leading edge and trailing edge cracks	Vibration
[307]	Frequency response functions	Delaminations	Lamb wave propagation
[306]	Time of flight	Delaminations	Ultrasonic guided waves

AE: Acoustic emission DIC: Digital Image Correlation FBG: Fibre Bragg grating SCADA: Supervisory control and data acquisition

3.5 Results & discussion

The results of the FMECA are presented in Tables 3.8, B.1, B.2 and B.3. Figure 3.5 presents a summary of the criticality assessment by blade component based on the FMECA results, so the sum of criticality adds to 1 (or 100%). The results are presented subdividing the total criticality of those failure modes with extreme, high, moderate or low values. No extreme values (CN over 20) have been found in the identified failure modes. This assessment reveals the spar and the leading edge to be the components concentrating the highest criticality (38.2% and 16.9%, respectively) (see Figure 3.5). In this sense, leading edge erosion is one of the issues that has captured the attention of the industry due to the loss of production occasioned and the acceleration of degradation of other components of the blade. The structural mission of the spar makes it vital for the performance of the system and is also reflected in the criticality distribution. The blade subcomponent criticality assessment is a relevant result that provides guidance to concentrate design improvement, quality control or maintenance efforts on specific parts of the blade, increasing the efficiency of the actions. In this line, the decision tree presented in Figure 3.3 provides a systematic way for selecting the most appropriate maintenance strategy for each failure mode.

Table 3.8: FMECA analysis (Failure modes 1 to 31).

ID	Subcomponent Level 1	Subcomponent Level 2	Subcomponent Level 3	Failure mode	Effects	Cause	Cause detail	O	S	CN	Criticality level
LE1	Leading edge	Bondline		Adhesive joint failure (Debonding)	Reduction of aerodynamic efficiency, production losses, separation of the shell, rotor imbalance	Manufacturing	Defective application of adhesive	1	4	4	Moderate
LE2	Leading edge	Bondline		Adhesive joint failure (Debonding)	Reduction of aerodynamic efficiency, production losses, separation of the shell, rotor imbalance	Installation	Damage or overstress of adhesive during handling of the blade	2	4	8	High
LE3	Leading edge	Bondline		Adhesive joint failure (Debonding)	Reduction of aerodynamic efficiency, production losses, separation of the shell	Design	Underestimation of environmental loads and conditions	1	4	4	Moderate
LE4	Leading edge	Skin		Erosion of LEP	Reduction of aerodynamic efficiency, production losses, damage to laminates	Design	Underestimation of wear effects	4	3	12	High
LE5	Leading edge	Skin		Erosion of LEP	Reduction of aerodynamic efficiency, production losses, damage to laminates	Operation	Exposure to UV, rain, insects, salt spray and particle erosion	4	3	12	High
LE6	Leading edge	Skin		Erosion of LEP	Reduction of aerodynamic efficiency, production losses, damage to laminates	Manufacturing	Incorrect curing/application of top coating	3	3	9	High
LE7	Leading edge			Cracks	Exposition of adhesive joint, water ingress	Operation	Excessive loading, fatigue loading	1	3	3	Low
LE8	Leading edge			Ice accumulation	Reduction of aerodynamic efficiency, rotor imbalance, production losses, increase of weight	Operation	Failure of de-icing systems	1	2	2	Low
TE9	Trailing edge	Bondline		Adhesive joint failure (Debonding)	Reduction of aerodynamic efficiency, production losses, separation of the shell	Manufacturing	Defective application of adhesive	1	4	4	Moderate
TE10	Trailing edge	Bondline		Adhesive joint failure (Debonding)	Reduction of aerodynamic efficiency, production losses, separation of the shell, rotor imbalance	Installation	Damage or overstress of adhesive during handling of the blade	2	4	8	High
TE11	Trailing edge	Bondline		Adhesive joint failure (Debonding)	Reduction of aerodynamic efficiency, production losses, separation of the shell	Design	Underestimation of environmental loads and conditions	2	4	8	High
TE12	Trailing edge			Buckling	Collapse of the blade	Design	Underestimation of environmental loads and conditions	1	5	5	Moderate
TE13	Trailing edge			Cracks	Reduction of aerodynamic efficiency, production losses, increase of stress concentration	Design	Underestimation of fatigue loading	2	3	6	Moderate
T14	Tip			Blade rupturing, blade burnout, wire melting (lightning)	Catastrophic damage	Design	Insufficient lightning protection	1	5	5	Moderate
T15	Tip			Surface cracking, Surface tearing (lightning)	Serious damage requiring immediate repair	Design	Insufficient lightning protection	2	4	8	High
T16	Tip			Surface stripping, receptor loss (lightning)	Surface stripping, receptor loss (normal damage)	Design	Insufficient lightning protection	3	3	9	High
T17	Tip			Receptor vaporisation, surface scorching, surface blotching surface delamination (Lightning)	Receptor vaporisation, surface scorching, surface blotching surface delamination (minor damage)	Design	Insufficient lightning protection	4	2	8	High
R18	Root	Root-hub connection		Failure of root-hub connection	Increase of tension, vibrations of the blade, critical damage of the blade, detachment of blade	Design	Underestimation of environmental/operational loads	1	5	5	Moderate
R19	Root	Root-hub connection		Failure of root-hub connection	Increase of tension, vibrations of the blade, critical damage of the blade, detachment of blade	Manufacturing	Damage to the blade during the machining of the holes	1	5	5	Moderate
R20	Root	Root-hub connection		Failure of root-hub connection	Increase of tension, vibrations of the blade, critical damage of the blade, detachment of blade	Installation	Incorrect pretension applied to the bolts	2	5	10	High
US21	Upper shell	Skin	Gelcoat	Cracks	Increase of water ingress to sandwich and laminates, degradation of properties, loss of stiffness and strength	Design	Insufficient environmental and impact protection	1	1	1	Low
US22	Upper shell	Skin	Skin-laminate interphase	Skin/adhesive debonding	Exposure of laminates to environment, increase of degradation of sandwich composites, reduction of aerodynamic efficiency	Manufacturing	Incorrect application of adhesive	1	2	2	Low
US23	Upper shell	Sandwich	Core	Water ingress	Increase of weight, degradation of stiffness and strength	Design	Degradation of gelcoat exposing laminate and sandwich layers	2	1	2	Low
US24	Upper shell	Sandwich	Laminate-core interphase	Debonding (Laminate to core)	Increase of stress, reduction of stiffness of the sandwich	Manufacturing	Damage during manufacturing, incorrect application of adhesives	2	2	4	Moderate
US25	Upper shell	Sandwich	Laminate	Delamination	Increase of stress concentration, reduction of stiffness, reduction of power	Manufacturing	Voids during manufacturing	2	2	4	Moderate
US26	Upper shell	Sandwich	Laminate	Delamination	Increase of stress concentration, reduction of stiffness, reduction of power	Design	Failure in the design, underestimation of loads	2	2	4	Moderate
US27	Upper shell	Sandwich	Laminate	Intralaminar fracture (matrix cracking - microcracks)	Increase of stress concentration, reduction of stiffness, damage progress to delamination	Manufacturing	Voids in the laminate, fibre misalignment, wrinkles in the fibres	3	1	3	Low
US28	Upper shell	Sandwich	Laminate	Intralaminar fracture (matrix cracking - microcracks)	Increase of stress concentration, reduction of stiffness, damage progress to delamination	Installation	Damage in coating with tools, transportation, and assembly	3	1	3	Low
US29	Upper shell	Sandwich	Laminate	Intralaminar fracture (matrix cracking - microcracks)	Increase of stress concentration, reduction of stiffness, damage progress to delamination	Operation	Incorrect operation resulting in loads not covered by design	3	1	3	Low
US30	Upper shell	Sandwich	Laminate	Cracks	Increase of stress concentration, reduction of stiffness, reduction of power	Design	Underestimation of loads	1	2	2	Low
US31	Upper shell	Sandwich	Laminate	Cracks	Increase of stress concentration, reduction of stiffness, reduction of power	Manufacturing	Voids during manufacturing	1	2	2	Low

O:Occurrence S:Severity CN:Criticality number LEP: Leading edge protection AE: Acoustic emission FBG: Fibre Bragg grating

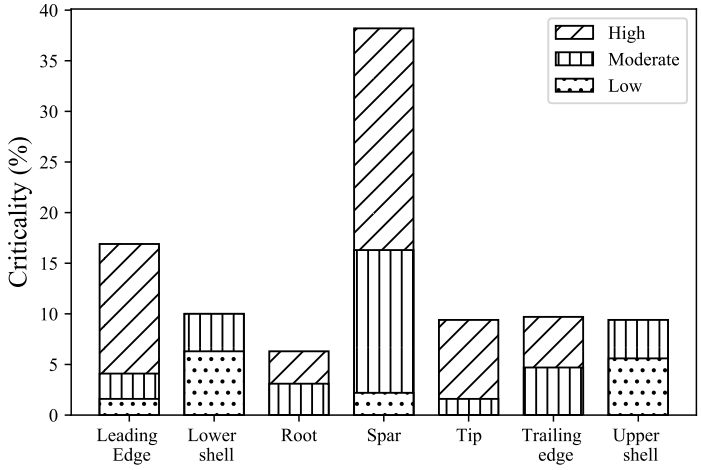

Figure 3.5: Criticality by blade component.

The top failure modes of the blade according to this study (refer to Table 3.9), include the erosion of leading edge protection due to an underestimation in the design stage and the usual operation of the wind turbine, the failure of root-hub connection due to an incorrect pretension applied to the bolts, lightning damage of the blades fostered by an insufficient lightning protection system in the design, the adhesive joint failures of the leading and trailing edges and the crack formation and delamination of the members of the spar.

Table 3.9: Failure modes with high criticality.

ID	Failure mode	Effects	Cause	Cause detail	Failure mechanism	O	S	CN	Criticality level
LE4	Erosion of LEP	Reduction of aerodynamic efficiency, production losses, damage to laminates	Design	Underestimation of wear effects	Wear of coating, loss of mass of the blade	4	3	12	High
LE5	Erosion of LEP	Reduction of aerodynamic efficiency, production losses, damage to laminates	Operation	Exposure to UV, rain, insects, salt spray and particle erosion	Wear of coating, loss of mass of the blade	4	3	12	High
R20	Failure of root-hub connection	Increase of tension, vibrations of the blade, critical damage of the blade, detachment of blade	Installation	Incorrect pretension applied to the bolts	Damage progression in the surroundings of the bolts until critical damage of the blade	2	5	10	High
S51	Cracks	Increase of stress concentration, reduction of stiffness, failure of the blade	Operation	Misoperation, increase of loads	Crack formation, failure of the blade	2	5	10	High
S52	Cracks	Increase of stress concentration, reduction of stiffness, failure of the blade	Design	Underestimation of loads	Crack formation, failure of the blade	2	5	10	High
S53	Cracks	Increase of stress concentration, reduction of stiffness, failure of the blade	Manufacturing	Voids during manufacturing	Crack formation, failure of the blade	2	5	10	High
LE6	Erosion of LEP	Reduction of aerodynamic efficiency, production losses, damage to laminates	Manufacturing	Incorrect curing/application of top coating	Wear of coating, loss of mass of the blade	3	3	9	High
T16	Surface stripping, receptor loss (lightning)	Surface stripping, receptor loss, normal damage	Design	Insufficient lightning protection	Strike of lightning	3	3	9	High
LE2	Adhesive joint failure (debonding)	Reduction of aerodynamic efficiency, production losses, separation of the shell, rotor imbalance	Installation	Damage or overstress of adhesive during handling of the blade	Overstress of the interphase (peeling stresses), separation of shells	2	4	8	High
TE10	Adhesive joint failure (debonding)	Reduction of aerodynamic efficiency, production losses, separation of the shell, rotor imbalance	Installation	Damage or overstress of adhesive during handling of the blade	Overstress of the interphase (peeling stresses)	2	4	8	High
TE11	Adhesive joint failure (Debonding)	Reduction of aerodynamic efficiency, production losses, separation of the shell	Design	Underestimation of environmental loads and conditions	Overstress of the interphase (peeling stresses)	2	4	8	High
T15	Surface cracking, Surface tearing (lightning)	Serious damage requiring immediate repair	Design	Insufficient lightning protection	Strike of lightning	2	4	8	High
T17	Receptor vaporization, surface scorching, surface blotching and surface delamination (lightning)	Minor damage	Design	Insufficient lightning protection	Strike of lightning	2	4	8	High
S45	Delamination (Caps)	Increase of stress concentration, reduction of stiffness, progress to crack formation	Manufacturing	Voids during manufacturing	Delamination will progress until cracks join and the cross section cannot withstand existing loads	2	4	8	High
S46	Delamination (Caps)	Increase of stress concentration, reduction of stiffness, progress to crack formation	Design	Failure in the design, underestimation of loads	Intralaminar fractures progressing and evolving into delamination, damage propagation until failure	2	4	8	High
S47	Delamination (Caps)	Increase of stress concentration, reduction of stiffness, progress to crack formation	Operation	Incorrect operation, increase of loads	Intralaminar fractures progressing and evolving into delamination, damage propagation until failure	2	4	8	High
S54	Delamination (Shear webs)	Increase of stress concentration, reduction of stiffness, progress to crack formation	Manufacturing	Voids during manufacturing	Delamination will progress until cracks join and the cross section cannot withstand existing loads	2	4	8	High
S55	Delamination (Shear webs)	Increase of stress concentration, reduction of stiffness, progress to crack formation	Design	Failure in the design, underestimation of loads	Intralaminar fractures progressing and evolving into delamination, damage propagation until failure	2	4	8	High

O: Occurrence S: Severity CN: Criticality number LEP: Leading edge protection

Leading edge erosion is known to produce annual energy production losses of around 5% after the first few years of operation and has the potential to reach 20-25% if unmaintained [341]. Considering this, the design of durable protective coatings and the identification of the optimum maintenance strategy is of vital importance to reduce operational costs. In this sense, the constant collection and analysis of data can provide good deterioration estimates to find optimum maintenance opportunities. The root-hub connection is also a critical part of the blade since the machining of the holes, the handling and the assembling of the blade are delicate operations and small defects and damage can grow into catastrophic failures since this is the only load path for the blade to transmit loads to the foundations of the turbine. Even though the in-place repair of this connection is usually unfeasible, the early detection of this damage mode can help plan the disassembly and protection of the blade to avoid catastrophic failures. The formation and development of cracks in the spar have the difficulty of progressing

unnoticeably for visual inspection techniques under the shells of the blade. Therefore, the advantage of monitoring this part is the reduction of unexpected critical failures of the blade. The debonding of the leading and trailing edges is a failure mode that will reduce the output of energy converted from the wind turbine and potentially produce rotor imbalance and increase the loads onto the blade. Being able to identify the length of the debonding is key to control its growth and plan its maintenance accordingly. Separately, lightning strike impact detection and location can also be helpful in terms of evaluating if inspection or maintenance may be necessary and could avoid the action of unnecessary inspections.

The reduction of the Levelised Cost of Energy (LCOE) has been achieved during the last decades, at least partially, with an increase in the size of the turbine and the blades [266, 369]. The constant evolution and increase in size of the blades require an understanding of how size and weight increase impact the criticality of the identified failure modes. Overall, the increase in size and the offshore environment to which the turbines are exposed have resulted in a decrease in reliability [60]. In this sense, the levels of stress occasioned by aerodynamic loads can be kept from an excessive growth by increasing the section of the spar, which results in an increase of the mass of the blade, and by the application of both active (primarily based on pitch control) [42, 79, 154, 326] and passive [41, 65] load control strategies. Load control strategies may thrive in importance even at the expense of energy production as maintenance costs are higher for offshore wind turbines. The increase of mass of the blade will lead to a rise in the stress, occasioned by the increase in the gravitational and inertial loads. Therefore, the role of both fatigue and extreme damage will grow in importance and those failure modes originated during operation will see their likelihood of occurrence increased and some new failure modes may appear. It is important to note that some fatigue-produced damage is originated from existing manufacturing defects [253] and thus, improvement in quality of the manufacturing will also reduce the initiation of these failure modes. Waiting times for weather windows represent a high percentage of these costs, and damage control along with an efficient planning can help to their reduction. Thus, using smart operation control modes can contribute to an overall LCOE reduction if

the state of the blade can be known, which grants SHM an additional importance.

3.6 Conclusion

In this study, a risk-based maintenance strategy selection for wind turbine composite blades was presented. First, the failure modes of the wind turbine blade were identified by means of an FMECA considering their likelihood of occurrence and the severity to determine their criticality. Later, the feasibility of monitoring the identified failure modes was explored in the literature. Finally, a maintenance decision tree was presented and applied to determine the preferred maintenance strategy of the prioritised failure modes providing a systematic way of choosing maintenance strategies for the critical failure modes of the blade.

The FMECA of a wind turbine blade identified the leading edge erosion, root-hub connection damage, spar caps and web damage, lightning strike damage, and the debonding of leading and trailing edges to be the most critical failure modes of the blade. This study has shown that detecting and/or monitoring these failure modes can be feasible as shown by the literature. Notwithstanding, the optimal placement of sensors, the tuning of inspection intervals and dealing with all the information obtained to take operation and maintenance decisions are non-trivial problems to be solved to unleash cost reductions for enhanced wind energy production.

Chapter 4

A degradation model for leading edge erosion

Chapter contribution

Leading edge erosion has been revealed as one of the most critical failure modes of the blade. In the absence of available data, a degradation model for its evolution can provide a tool to estimate its effects.

This chapter aims to accomplish the following research objective: *Provide a degradation function for one fo the most critical failure modes, LEE, to evaluate O&M policies.*

The contributions of this chapter are detailed below:

- Provide a degradation model to account for the LEE progression and estimate its effects in annual energy production.

The published peer reviewed journal article Contreras Lopez, Javier et al. "*A wind turbine blade leading edge rain erosion computational framework*" Renewable Energy 203 (2023) was authored by myself as part of my research completed under the direction and consultation of my supervisor, Professor Athanasios Kolios, and my coauthors. The published article is incorporated in this chapter and forms part of the definition of the leading edge erosion degradation framework.

4.1 Introduction

As shown in Chapter 3.6, the study of the most critical failure modes of wind turbine blades revealed leading edge erosion as one of the most prominent, as derived from Figure 4.1. The high velocities experienced by the sections of the leading edge close to the tip increases the criticality of this failure mode. Blade leading edge erosion is a phenomenon that is produced due to many factors: environmental degradation due to temperature, moisture, UV radiation and fatigue degradation of the edge protective coating due to rain, and hail or wind-borne debris impacting the blade during its rotation, to cite but the most important. Additionally, its initiation may be favoured by manufacturing defects in the application of the leading edge protection systems or impacts during the handling of the blade in the transport and construction phase. The erosion produces the detachment of fragments of the coating from the blade and also modify the airfoil geometry, which alter the performance of the blade in many aspects: aerodynamically, acoustically, and if left unattended, structurally.

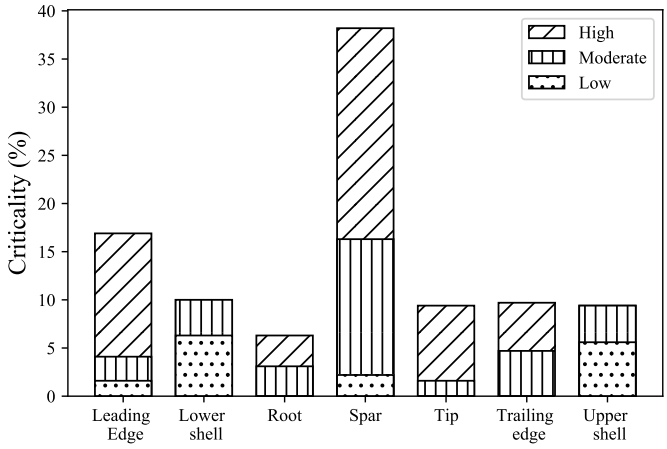

Figure 4.1: Criticality by blade component. Source: [82].

The effects of this erosion progress from turbine power degradation to potential damage to the skin laminates of the shell, evolving into more severe damage types such as delamination and the failure of the joint between shells. The power degradation of the blade is just a result of the modification of the aerodynamic properties of the

affected sections, which produce a reduction of lift and an increase in drag [139]. This power degradation occasions annual energy production (AEP) losses, the range of which is not yet clear due to the high uncertainty in the degradation process, the coating material characteristics, and the airfoil aerodynamic performance, among others. A comprehensive overview of the leading edge erosion is provided in [270, 374].

In terms of airfoil aerodynamic performance, Gaudern et al. [139] studied the lift and drag variation of different airfoils at different erosion stages using wind tunnel tests. Their results showed a lift reduction about 3-10 % for both airfoils, which increased with the erosion progression. In a similar manner, Sareen et al. [341] carried out a comprehensive wind tunnel test study for the DU 96-W-180 airfoil for different erosion levels with lift reductions in the range of 5-15% and an AEP loss between 3 and 23%. Schramm et al. [351] opted for a numerical approach using 2D computational fluid dynamics (CFD) to determine the behaviour of wind turbines with eroded blades. Airfoil polars were generated using CFD which were further employed to obtain wind turbine loads and power curves by the blade element momentum (BEM) theory. The referred study reported AEP losses of about 8%.

In a first effort to better understand the relation between erosion models and their mechanical effects on the turbines blades, Eisenberg et al. [112] made use of the rain erosion computational model developed by Springer [385] along with proprietary wind turbine historical observations to calibrate a model able to estimate rain mechanical erosion. Besides, a BEM code was applied, along with eroded aerodynamic data from [341] to evaluate AEP losses with results around a 1.7% for turbines with a 50% time spent operating at rated power. More recently, [366] provided experimental and numerical CFD studies to evaluate the effects of the erosion degradation of airfoils. Similarly, Cappugi et al. [53] used an approach based on artificial neural networks (ANNs) using wind turbine and eroded blade data, along with CFD and BEM theory to provide power curves, loads, and AEP of turbines with eroded blades at different erosion levels. AEP losses between 2.2 and 4 % were reported for advanced erosion states. An uncertainty quantification on the effects of rain-induced erosion on AEP was performed by Papi et al. [302], where average AEP losses of up to a 1.5% were estimated.

Regarding active erosion protection systems, there are some works covered in the literature, like the one by Hasager et al. [167] who performed a lifetime assessment of leading edge protections for turbines in Danish Seas considering a Vestas V52 turbine using the kinetic energy and accumulated rain damage models. Their results show expected leading edge protection lifetimes between 2 and 13 years. Also, Bech et al. [29] studied the use of smart turbine control to reduce the rotation speed of the blades and diminish the effect of rain erosion in a Vestas V52 850kW wind turbine. In a different study, Hasager et al. [169] studied the expected AEP loss and leading edge lifetime of a number of sites in the North and Baltic sea. Lifetimes between less than 1 year and more than 25 were reported and a potential O&M cost reduction using an active erosion safe operation mode of around 70% compared to the normal operation of the turbine.

According to the authors' opinion, despite the efforts recently made to model the erosion influence on the aerodynamics and mechanical behaviour of a turbine blade (including its effects on AEP), the inherent uncertainty around this damage mode has not been considered in a proper manner. The lack of knowledge about the expected life of erosion protection coatings for particular site conditions implies a barrier for the application of such preventive methods. Moreover, the current state of the knowledge in the open literature calls for a framework to determine AEP loss with less uncertainty and to evaluate the need of corrections, if required, in terms of operation and/or maintenance for wind farm operators. This chapter provides an efficient framework to estimate the evolution of erosion degradation based on rain erosion test data considering weather uncertainty. Furthermore, it provides an estimate of the power losses occasioned by it and an estimation of the remaining useful life of the blade. The proposed framework can be employed to investigate the O&M costs of different leading edge protection solutions in the design stage for a particular site and for the latter O&M planning of an operative turbine with potential benefits in cost reductions in both stages.

The chapter is structured as follows: Section 4.2 provides some fundamentals about the process of leading edge erosion, its causes and effects, the typical erosion protection configurations found in wind turbine blades, and current testing procedures. Section

4.3 describes the proposed modelling framework for AEP degradation calculation. In Section 4.4, a case study for a 5MW NREL bottom-fixed offshore wind turbine using the proposed framework is presented. Finally, conclusions derived from the use of this framework are drawn in Section 4.5.

4.2 Fundamentals about leading edge erosion

Leading edge blade erosion is a phenomenon that has attracted the attention of both the research community and the industry during the latest decades [112, 166, 173, 196, 220, 341]. This attention has been accentuated by the increase in rotor diameter and power of the turbines. The elevated speeds experienced by the sections closer to the tip of the blade increase the impact energy of rain, hail, insects and other wind-borne particles. Most of the experimental studies have been focused on the damage occasioned by rain, but numerical studies considering the impact of general wind-borne particles can also be found in the literature [57, 128]. Rain-related erosion is thought to be more predominant in offshore wind farms, and so the effort has been more focused on this aspect.

In the case of rain erosion, most leading edge failures are believed to be developed due to fatigue of the coatings that take place due to accumulated impacts of rain droplets. The transient stress waves that are occasioned in the surroundings of the location of the droplet's impact accumulate fatigue cycles in the coating layers that, after some time, result in the loss of coating mass [373]. The rate of progression of this phenomenon is influenced by different factors: material properties, meteorological and wind turbine operating characteristics are among the ones highlighted as the most influential [112].

With regard to the materials used to protect against this phenomenon, a variety of leading edge protection configurations can be found in the literature [2, 88, 192, 267, 269]. Leading edge protection coatings can be applied through in-mould manufacturing during the manufacturing of the shells of the blade or a post-mould application in the leading edge erosion-prone areas of the blade. The configuration of the coating protection adopts different schemes, with the most basic consisting of 2-3 layers of

protective coating over a layer of filler, to more advanced configurations including a layer of primer between the coating and the filler. The usual configurations of the protection system are shown in Figure 4.2.

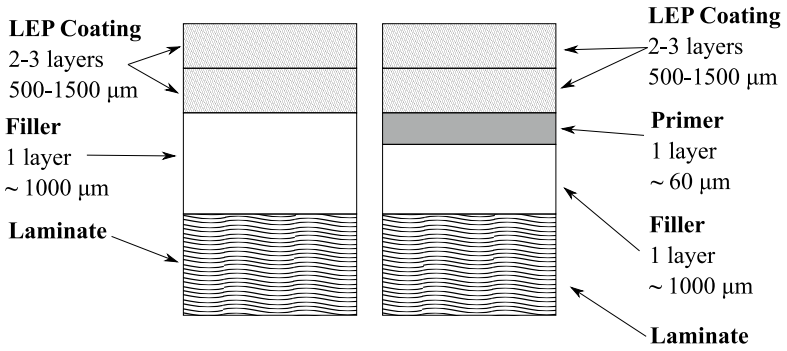

Figure 4.2: Typical leading edge protection configurations. Adapted from [88].

The evolution of impingement erosion has been discretised in different stages in the literature [36,112,341]. The first stage, known as the incubation period (Stage 0), where the fatigue limit of the coating has not been consumed, is characterised by no external signs of degradation or mass loss of the coating. After this, minor pits are formed in the LEP (leading edge protection) coating, with an increase in rugosity (Stage 1). This is followed by an increased mass loss stage, where minor flakes of the topcoat are removed and the filler can be intermittently seen below the topcoat (Stage 2). Then, the erosion progresses until the epoxy below the filler can be intermittently seen whilst the filler is not completely removed (Stage 3). The filler is then completely removed leaving the epoxy exposed, thus being this the final erosion stage of the coating, but having the risk of progressing to the laminate layers of the shell and creating delaminations and loss of mass of the sandwich panel (Stage 4). The effects of erosion have different implications through its progression and can affect the aerodynamic, acoustic, and structural behaviour of the blade.

Concerning the acoustic effects of the leading edge erosion, the emissions can be increased up to a 10% [218], which, in some cases, could be important for the negative environmental impact that this could produce. Also, the aerodynamic effects affect directly the power output of the turbine, producing a loss of power at below-rated wind speeds. This means that not only the turbine characteristics but also the rain

and wind characteristics of the site have an impact on the energy production losses of the blade.

Finally, the structural integrity of the blade is also compromised. The risk of cracks, fatigue damage and delamination grows as the erosion progresses through the protection layers and less impact energy is absorbed by them, until the laminate is exposed and the risk of structural damage is high. During the incubation period, there are no effects on the structural integrity of the blade, and only minimal to negligible effects can be observed on its aerodynamic performance. When the filler is exposed, the aerodynamic effects start growing in importance while the structural damage is still minor. Finally, when the epoxy is exposed, the structural integrity decays until maintenance of the leading edge is required to recover the integrity of the blade. Some guidance can be found in the literature published by Bladena [36] for the O&M actions related to leading edge erosion. The recommendation given in the referred work is to perform repairs within 6 months if the erosion reaches the laminate, and within 3 months if it reaches the second layer of the laminate to avoid compromising the structural integrity of the whole blade.

Rain erosion testing has been performed for several applications such as steam and gas turbines, cooling pipes of nuclear power plants, fan blades of aero engines, and wind turbines, with different impact speeds and droplet diameters. A summary of the different existing testing systems can be found in [115] and [452]. To evaluate the performance of erosion protection systems for wind turbine blades, the most common experimental testing arrangements are the stationary sample jet impacted by an interrupted jet or water jet slugs and the whirling arm testers [19]. While the stationary jet is a more simple arrangement and facilitates the sampling methods, using impact velocities higher than the terminal speed breaks the drops. Whirling arm testers produce the impact velocity by rotating the sample instead of accelerating the water droplet, which reduces the difficulties in producing high impact velocities but increases the difficulty in the sampling process. These tests aim to generate Wöhler-like curves with the impact speed versus the accumulated impacted water, time to failure, or specific impacts. In this study, data from whirling arm tests available in the literature will

be used to evaluate the effects of erosion degradation. Notwithstanding, these tests are argued to not reproduce the diversity of conditions experienced in the operation of turbine blades, which include intermittent rain, distributed raindrop sizes, and varying impact energy and droplet sizes. Some current research focused on these aspects are the studies of Bech et al. [30], who performed experimental tests to study the effect of drop size in rain erosion tests and lifetime prediction, or Verma et al. [423] who developed a probabilistic rainfall model to estimate the leading edge lifetime of coating systems in which the effects of rain intensity and droplet size are analysed. While rain erosion tests have been useful to comparatively analyse the performance of different protection systems, their application to lifetime analysis seems to be not so accurate for some researchers [66, 112].

4.3 Proposed modelling framework

The proposed framework is depicted in Figure 4.3. It starts with the generation of random rain and wind time series, which can be based on weather observations or ERA5 reanalysis data from the location of the turbine [174]. Additionally, aerodynamic performance polar curves of eroded airfoils are obtained. Alternatively, a full 3D CFD simulation of the blade can be performed. Notwithstanding, due to the computational cost of each simulations and the number of simulations needed to capture different states of degradation of the blade, the 2D approach was preferred. Also, the use of the BEM theory allows the integration of polar curves obtained numerically or experimentally in a more practical and efficient way. Figure 4.3 also indicates that using the modified polar curves, the operating power curves of different eroded states of the blades are calculated. Once this information is available, the synthetic weather data and the estimated aerodynamic performance of the airfoils are combined to calculate erosion and energy production at each timestep using the appropriate power curve representing the degraded state of the blade under the BEM theory.

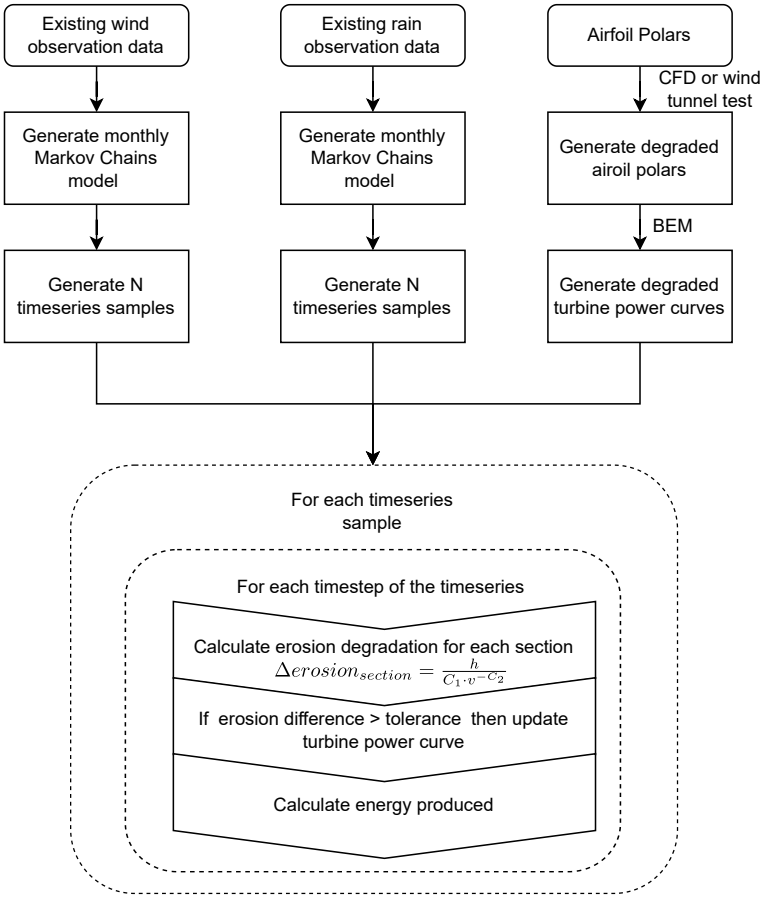

Figure 4.3: Computation framework.

4.3.1 Weather time series generation

Weather time series with high granularity and quality are typically difficult to obtain for a particular wind turbine location. A feasible alternative to obtain such weather data, which ranges between 20 and 25 years long, is the use of Markov chains [293] models to synthetically generate datasets while preserving the weather characteristics of the site. Therefore, random rain and wind scenarios can be generated to account for a probabilistic analysis of the erosion degradation of the blade. In this work, 10-minute average data for wind and rain are used. Wind and rain have been modelled as statistically independent variables. For wind data, a Markov probability transition matrix with 0.5 m/s bins has been calibrated using FINO1 [131] wind observation data. To avoid problems with the seasonality behaviour of wind, a different probability tran-

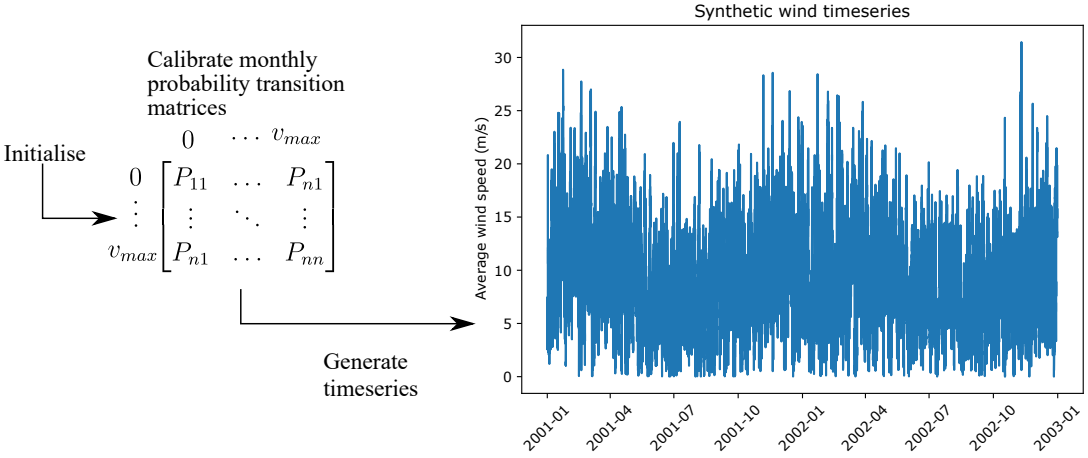

Figure 4.4: Synthetic wind data generation process. Subindex n refers to the number of bins in which wind speed is discretised.

sition matrix per month was considered, along with a general annual wind transition probability matrix, to avoid the wind speed falling in a range where there are no occurrences in a month. For clarity, the process is schematically illustrated in Figure 4.4. For the rain data, the shorter available data range called for the use of a different approach based on modelling rain intensity through monthly Weibull probability density functions, whereby Markov probability transition matrices with rain/no rain probability were obtained. While this approach results in unrealistic variability of rain intensities, it is assumed to not have a significant influence on the results of this study. The process is illustrated in Figure 4.5.

4.3.2 Airfoil performance estimation

CFD simulations are used for the estimation of the polar curves of the degraded airfoils. The Navier–Stokes CFD code from ANSYS FLUENT® is used in this work. The air flow has been modelled as incompressible and single-phase fluid. The pressure-based steady Reynolds-averaged Navier-Stokes (RANS) equations are solved in all cases, and the turbulence closure is accomplished utilising the Menter's two-equation $k-\omega$ shear stress transport (SST) model [263]. Polar curves are obtained at Reynolds numbers in the range $1 \cdot 10^6$ to $9 \cdot 10^6$ every $1 \cdot 10^6$ and in a range of angles of attack from $-20°$

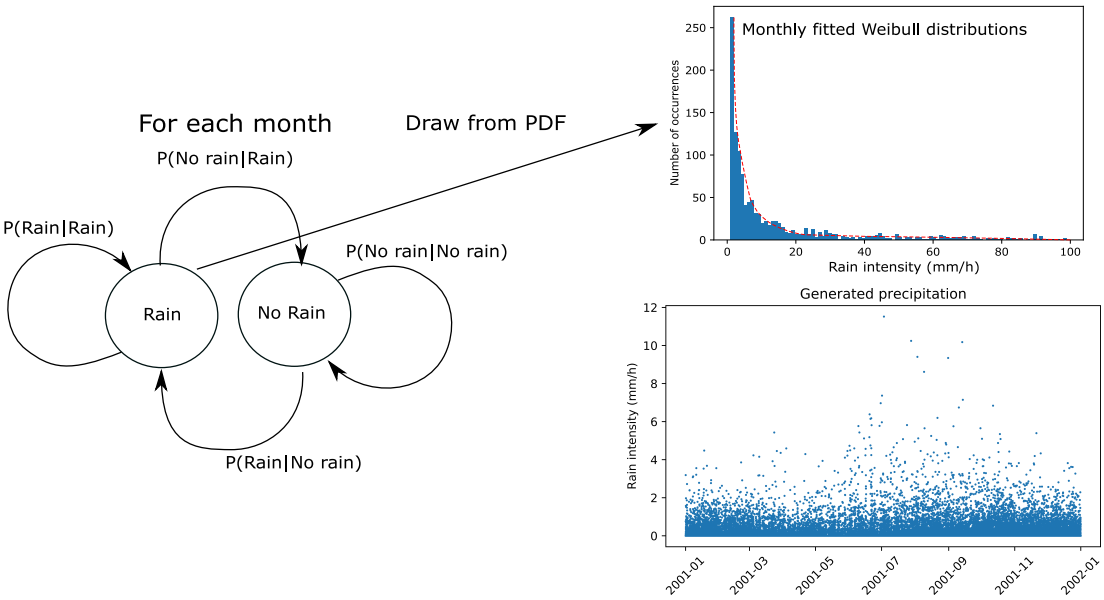

Figure 4.5: Synthetic wind data generation process.

to 20° every 1°. The degradation of the leading edge was modelled by adjusting the equivalent sand grain roughness height as proposed in [320] based on the stage 4 erosion parameters defined in [341]. The equivalent sand grain roughness height, k_s, was set to a value of $k_s/c = 0.0076$ for the final degraded state, where c is the chord of the airfoil. The roughness modification is applied in a length of a 10% of the chord in the top shell and a 13% in the bottom shell, to account for the blade increased erosion of the bottom shell during the pitching of the blade.

Finally, the resulting CFD-generated lift and drag curves were corrected for 3D stall effects and extrapolated for the whole -180° to +180° using the Viterna method [424] for their use in the BEM code OpenFAST [1].

4.3.3 Erosion degradation model

As previously mentioned in Section 4.1, there are different models to account for the erosion progression in the blades, where the most recent are based on a droplet impact model to establish stress states that consume the fatigue life of the coating. In most of the studies encountered in the literature, the analytical description of this phenomenon follows the model developed by George Springer [385], where the erosion resistance is

fitted to a curve based either on impact energy damage, specific impacts, accumulated rain under the rotor or impingement. Thus, the impingement model will be used here. The rain impingement, referred to here as h, can be calculated as follows:

$$h = \psi \cdot t \cdot v(r) \tag{4.1}$$

where t is the time, $v(r)$ the local rotor speed, and ψ, the volume concentration of rain in the air, which can be calculated as shown below:

$$\psi = I / v_{drop} \tag{4.2}$$

being I the rain intensity, and v_{drop} the droplet velocity at the rotor plane. The term v_{drop} can be obtained as the terminal velocity using the empirical relationship found in [385] and the droplet size being the median for the rain intensity distribution proposed in [32]. Experimental test data from whirling arm tests [19] is used to determine the number of impacts or accumulated energy of impact required to produce erosion in the material. These tests are performed at different speeds to provide a fit for the number of impacts causing fatigue damage. The fitting curve equation is described as follows:

$$H = C_1 \cdot v(r)^{-C_2} \tag{4.3}$$

where H is the accumulated rain impingement to erosion failure at local rotor velocity, and C_1, C_2 are material parameters calibrated using experimental test data. To evaluate the damage progression, linear damage accumulation using the Palmgren-Miner damage rule is assumed, as typically done to simplify damage accumulation for different amplitude fatigue damage [458]. Therefore, the erosion life consumption at timestep i, namely ΔD_i, will be computed as:

$$\Delta D_i = \frac{h_i}{C_1 \cdot v(r)_i^{-C_2}} \tag{4.4}$$

where h_i is the accumulated rain impingement, and $v(r)_i$ the local rotor speed at timestep i.

4.3.4 Calculation of degraded power curves

The calculation of the power curves has been performed with the BEM method using OpenFAST, running 200-second simulations of uniform wind fields at fixed intervals of wind speeds of 1 m/s from the cut-in to the cut-out wind turbine wind speeds. Airfoil sections are defined at the desired points of the blade at which the erosion is computed, whereas for the remaining control points, airfoil characteristics are averaged from the two closest stations. Note that enough simulation time is required to provide steady-state responses of the system and also to avoid transient disruptions of the results. These curves have been used to compute 10-min average energy production at each simulation timestep.

4.3.5 Erosion progression estimation

The estimation of erosion degradation has been computed according to a rain impingement accumulation fitted curve, as proposed in [167]. An incubation period of 30% of the total life has been assumed for the leading edge erosion protection system and, from that standpoint, linear degradation is assumed until the final erosion stage. Aerodynamic properties were obtained using CFD simulations with modifications of leading edge roughness and corrected for 3D stall, which could be substituted by wind tunnel test data, if available. For the 25-year meteorological time series required (precipitation and wind), observations from meteorological stations are required, otherwise ERA5 [174] data can be used to produce synthetic time series using Markov Chains with monthly fitted transition matrices. Leading edge erosion degradation shall be computed for, at least, the last third of the blade along with the time series. In this case, 10-min average wind speed and rain intensity data were used. The variability produced by using lower resolution data (i.e. 1-hour average data or 30-min average data) has not been studied here, and it is left as one of the desirable further works of this research. Eroded airfoil polar curves have been discretised in segments of 10% so that the 10% degraded curve is used for degradation ranges between 5% and 15%, the 20% for the range 15% to 25% and so on until the final degradation of the section.

4.4 Case study

To exemplify the use of the proposed framework, a case study is presented and analysed in the sections below.

4.4.1 Turbine and blade data

For this study, the 5 MW NREL wind turbine [193] has been chosen. The main characteristics of the turbine are shown in Table 4.1, where the airfoils used in the blade are shown in Table 4.2. In this case, only the erosion effect on the NACA64 airfoil was investigated due to the lower velocities experienced by the remaining airfoils of the blade. Leading edge erosion damage is more prone to appear on the outermost part of the blade due to the higher impact energy of the rain in those areas.

Table 4.1: 5 MW NREL Turbine data. Data extracted from [193].

Property	Value
Rated power	5 MW
Control	Variable speed, collective pitch
Drivetrain	High speed, multiple-stage gearbox
Rotor diameter	126 m
Hub height	90 m
Cut-In / Rated / Cut-out wind speed	3 m/s / 11.4 m/s / 25 m/s
Cut-in / Rated rotor speed	6.9 rpm, 12.1 rpm
Rated tip speed	80 m/s

Table 4.2: 5 MW NREL Blade Airfoil data. Data extracted from [193].

$Stationid$	$R(m)$	$Twist(°)$	$Chord(m)$	$Airfoil$
1	2.87	13.31	3.542	Cylinder
2	5.6	13.31	3.854	Cylinder
3	8.333	13.31	4.167	Cylinder
4	11.75	13.31	4.557	DU40 A17
5	15.85	11.48	4.652	DU35 A17
6	19.95	10.16	4.458	DU35 A17
7	24.05	9.1	4.249	DU30 A17
8	28.15	7.79	4.007	DU25 A17
9	32.25	6.54	3.748	DU25 A17
10	36.35	5.36	3.502	DU21 A17
11	40.45	4.18	3.256	DU21 A17
12	44.55	3.13	3.010	NACA64 A17
13	48.65	2.32	2.764	NACA64 A17
14	52.75	1.53	2.518	NACA64 A17
15	56.17	0.86	2.313	NACA64 A17
16	58.9	0.37	2.086	NACA64 A17
17	61.63	0.11	1.419	NACA64 A17

4.4.2 CFD setup

C-shaped structured mesh has been used for this analysis. Its structure and the boundary conditions used in the simulations are shown in Figure 4.6. To provide meaningful results, a mesh size independence study and a validation with published NACA64 A17 results has been performed, as is shown next.

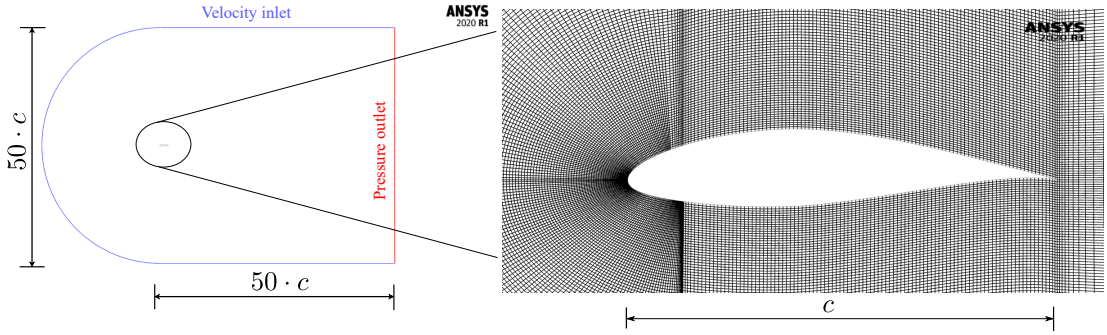

Figure 4.6: CFD setup.

Mesh size independence analysis

In this work, four different mesh sizes were explored, with a number of cells ranging from $3{\cdot}10^5$ to more than $1.2{\cdot}10^6$ for different angles of attack and Reynolds number of $6 \cdot 10^6$. The CFD simulation was solved utilising the Menter's two-equation $k-\omega$ shear stress transport (SST) model. The results, which are shown in Figure 4.7, show a close agreement of the lift coefficients for the two finer meshes ($1.2{\cdot}10^6$ and 615,00 cells, respectively) with maximum lift coefficient values as shown in the table of Figure 4.7. Considering the results presented and to reduce the computational effort of this case study, the second finer mesh (615,901 cells) was selected.

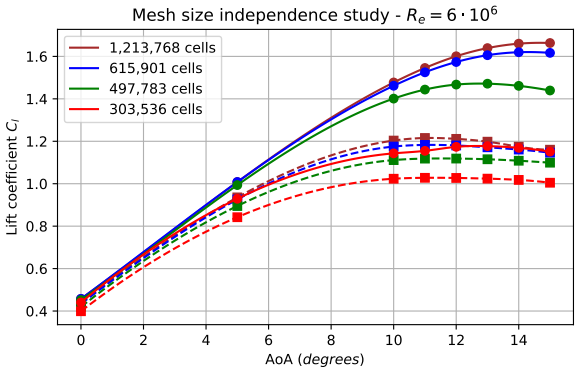

(a) Mesh size independence study (continuous and dashed lines represent the clean and eroded case respectively).

Cells	$C_{l,max}$(clean)	$C_{l,max}$(eroded)
1,213,768	1.6632	1.2154
615,901	1.6197	1.1828
497,783	1.4714	1.1186
303,536	1.1771	1.0278

(b) Mesh independence results.

Figure 4.7: Mesh independence study results.

Study of the influence of y^+

For the sake of efficiency, the effect of wall functions was investigated and solutions were compared for the cases of average y^+ values of approximately 1 and 87. The model with the greater value of y^+ makes use of wall functions to solve the flow within the boundary layer. The distribution of y^+ values along the chord is shown in Figure 4.8. Figure 4.9 shows the results of lift coefficient for different angles of attack and a $R_e = 6 \cdot 10^6$ for the studied models. The results show a good agreement for the lift of the airfoil in the linear and non-linear parts of the graph, with a slight overestimation

of lift by the model using a $y^+ \sim 87$. Considering the efficiency of both models, the model with the $y^+ \sim 87$ was chosen in this case.

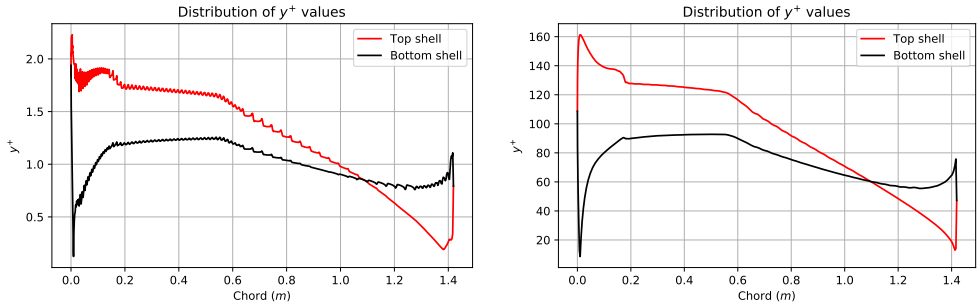

(a) Low y^+ mesh. (b) Large y^+ mesh (wall functions).

Figure 4.8: Distribution of y^+ value for the studied meshes.

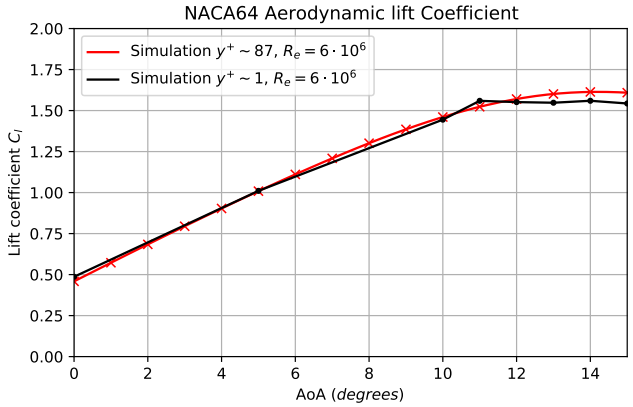

Figure 4.9: Lift results using different y^+ values.

Validation

To evaluate the accuracy of our CFD setup, simulation results were compared with NACA64 experimental aerodynamic coefficient results from [409] in Figure 4.10. Note that, in general, the simulation results show a good agreement in terms of the overall behaviour of the flow detachment around 12°-14°, and generally a fair agreement in terms of maximum lift coefficient. Note also that the lift values of the simulations are in close agreement with the experimental results for the range -5° to 5° of angle of attack (AoA), while the model tends to overestimate them for higher AoAs.

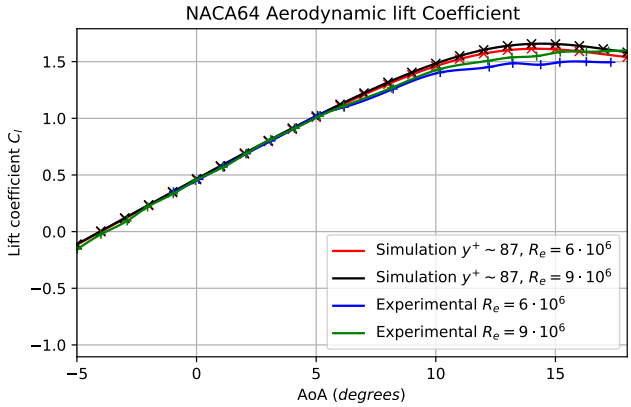

Figure 4.10: NACA64 CFD setup validation with experimental results from [409].

Baseline and eroded aerodynamic properties of the NACA64 airfoil were generated using Fluent Ansys following the procedure detailed in Section 4.3.2 and the CFD setup explained above. The resulting lift coefficients for the baseline and eroded profiles after their correction for 3D stall effects and extrapolation for the whole -180° to +180° range by the Viterna method, are shown in Figure 4.11.

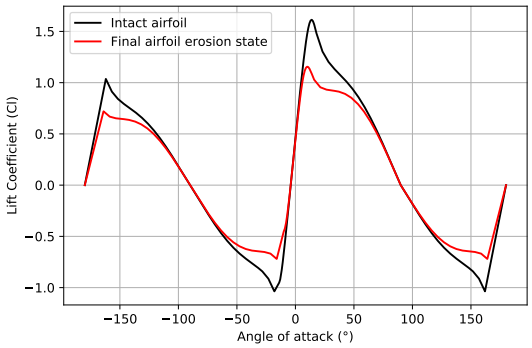

Figure 4.11: NACA64 CFD results extrapolated Polars $Re = 9 \cdot 10^6$ after 3D stall correction and extrapolation.

Moreover, Figure 4.12 shows a comparison between the baseline power curve of the wind turbine and a power curve considering the full degradation of sections 12 to 17 (from 45 to 62.5 meters from the root of the blade), which would simulate the final erosion state of the blade.

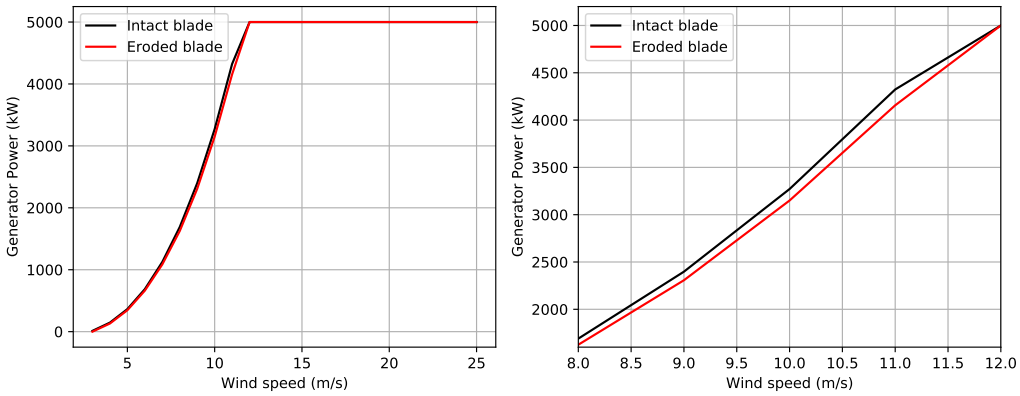

Figure 4.12: Turbine original vs degraded power curve. In the rightmost panel, the plot is zoomed in for the range 8 to 12 m/s of wind speed.

4.4.3 Weather data

In this work, the location of the turbine is assumed in the vicinity of FINO1 offshore measurement platform, sited 45 km north of the coast of the island of Borkum, Germany. Wind speed data was obtained from the FINO1 database and rain data from ERA5 reanalysis and used to calibrate the Markov Chains models as explained in Section 4.3.1. A hundred random 25-year wind and rain time series were generated. The average values of 10-min wind speed and rain intensity by month are shown in Figures 4.13 and 4.14.

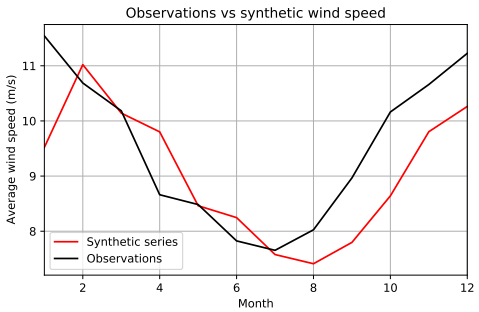

(a) Average monthly wind speed - Observed vs Synthetic data.

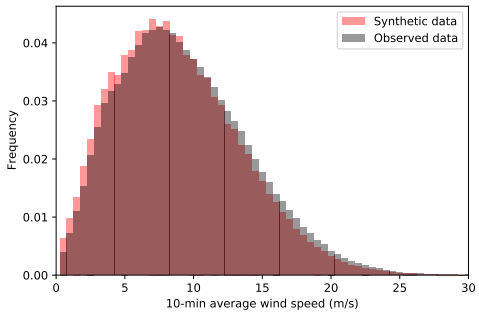

(b) Wind speed distribution - Observed vs Synthetic data.

Figure 4.13: Weather data used in the case study.

For the case of wind, the generation of time series follows the overall monthly shape

with a lag, producing a slight underestimate of the average wind speed (Figure 4.13a). The annual wind speed distribution of the observed and synthetically generated data are presented in Figure 4.13b. It can be seen that the distribution of the generated data is slightly shifted towards lower wind speeds; however, the overall shape is maintained. Separately, the synthetic rain generation time series process seems to provide a closer match with the average weather observations, even though there is also a slight underestimation of the average rain intensity for some months.

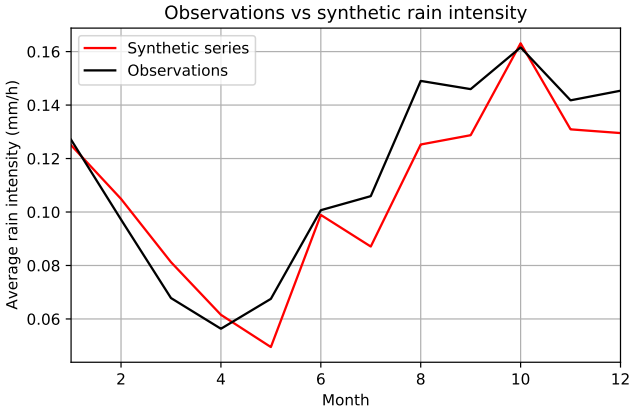

Figure 4.14: Average rain intensity - Observed vs Synthetic data.

4.4.4 Erosion leading edge protection configuration

Here, several erosion protection configurations are investigated. The different configurations are labelled as '*3Layer*', '*GS*', '*GC*', and '*GA*'. The '*GC*' and '*GA*' configurations are simpler, consisting only of a single layer of PU elastomeric coating, while '*3Layer*' and '*GS*' are more complex consisting of several coating layers and a filler. Their characteristic whirling arm test SN curves are shown in Figure 4.15.

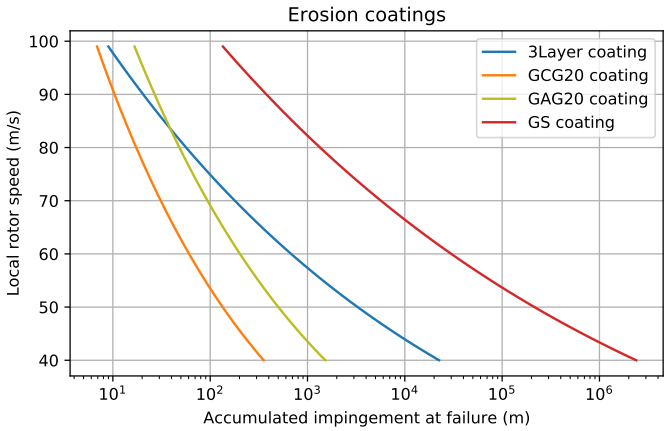

Figure 4.15: Whirling arm rain erosion test data. *3Layer*: 3-layer system estimated from [29] provided by PolyTech A/S, *GC*: 1-layer elastomeric PU coating from [192]. *GA*: Generic blade coating system supplied by Olsen Wings A/S from [192]. *GS*: 3-layer system including a pink filler and PU elastomeric coating from [192]. The term *G20* (3.5 mm droplets) refers to the type of needles used for the tests.

It is important to note that these curves represent the average behaviour of a number of tests, and that the variability shown by the different samples can represent a significant impact on the final service life of the erosion protection coating. This issue can be overcome with the use of inspection data, with which the model can be corrected and the behaviour of the actual erosion protection coating of the blade captured for better O&M optimisation.

4.4.5 Erosion degradation

The results of the progression of erosion degradation is shown in Figure 4.16. This figure represents the time at which the total degradation is reached for the sections at which the erosion degradation has been calculated. The results show that the leading edge coatings composed of 1-2 layers (namely, *GC* and *GA*) have a faster progression of the erosion front, reaching the erosion failure of the tip sections between years 2 and 4. The more advanced erosion protection configurations (*GS* and *3Layer*) revealed greater resistance. Note that the erosion protection coating configuration *3Layer* is consumed at the tip section before year 7, whereas *GS* is able to survive the complete lifetime of the turbine. With the progression of the erosion front, the laminate of the

leading edge shell starts deteriorating, thus the risk of leading edge splitting increases. These results are useful for leading edge erosion maintenance planning, being able to set maintenance targets based on specific damage thresholds.

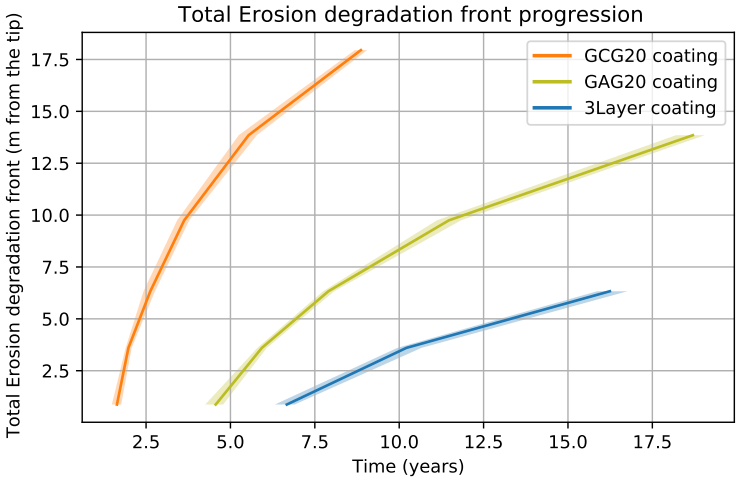

Figure 4.16: Erosion front progression for the different coatings analysed (*GCG20*, *GAG20* and *3Layer*). The shadowed areas represent the 2.5-97.5% probability bands.

4.4.6 Annual energy production results

The degradation along the blade has a direct impact on the aerodynamic behaviour of the aifoils, which translates into AEP losses. The results of the analysis are shown in Figure 4.17. The evolution of the AEP loss is presented into 2 phases: the incubation period and the deterioration phase. As mentioned before, during the incubation period, there are negligible effects on mass loss, aerodynamic performance, and AEP. Following the incubation period, LEP coatings start to deteriorate and the rate of increase of AEP loss is reduced throughout time in consequence of a reduction of damage with the reduction in local rotor velocity with the distance from the tip. The results reflect the complete failure of the leading edge erosion protection for sections 12 to 17 (17.5 meters from the tip) using the *GC* configuration by year 9; while *GA*, *3Layer* and *GS* are not completely consumed within the service life of the wind turbine (25 years). The maximum AEP degradation for the failure of the 17.5 meters of the leading edge protection for this site and turbine is between 1.5-1.75%. The *GC* configuration reaches

the maximum AEP loss by year 9, while *GA* and *3Layer* would reach an average AEP loss of 1.5% and 0.9% at year 25 respectively. Finally, *GS* would not see its incubation period consumed, experiencing no AEP erosion-related losses in the 25 years of operation.

Notice that an important point to note is that weather-related uncertainty in the loss of AEP with respect to leading edge erosion, can be quantified whereby probabilistic scenarios can be assessed. The referred uncertainty grows with time and, for the case of study presented here, accounts for an approximate value of 0.3% AEP at the most advanced erosion stages.

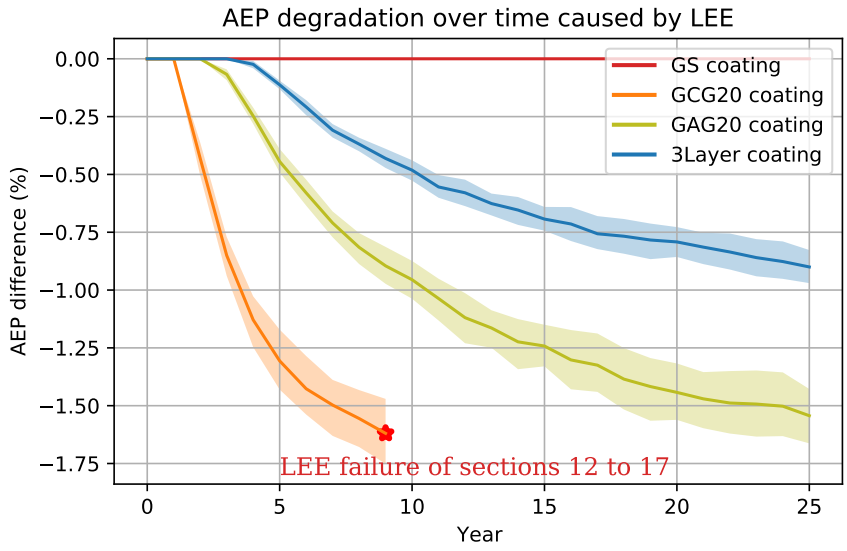

Figure 4.17: AEP degradation curve for blades using the coatings analysed (*GCG20*, *GAG20* and *3Layer*). The shadowed areas represent the 2.5-97.5%. probability bands.

4.5 Conclusion

An efficient leading edge erosion framework for AEP degradation erosion estimation has been presented and illustrated through a case study. The presented framework requires the aerodynamic curves of the pristine and eroded airfoils of, approximately, the outermost third of the blade (obtained through wind-tunnel tests or CFD simulations), weather (rain and wind) data of the site of study (based on on-site observations or other

sources such as ERA5 reanalysis data), and erosion protection coating survivability data (based on erosion tests such as whirling arm tests). Based on this and assuming linear damage accumulation of the rain impingement model and a BEM model, the erosion and AEP degradation throughout time can be estimated. Alternatively, the aerodynamic performance of the blade can be obtained considering 3D CFD simulations. Physical testing of weathered sections of the blade can improve the accuracy of the evaluation of the aerodynamic performance of eroded airfoils.

The case study using the 5MW NREL wind turbine located in the location of FINO1 weather station revealed the importance of designing an adequate LEP coating. For one of the LEP configurations, *GS*, the incubation period was not consumed, and no relevant AEP losses are expected. For the other configurations analysed, maximum AEP losses in the range of 0.9-1.75% have been obtained. The AEP loss for the total degradation of the blade, are in fair agreement with those reported by Eisenberg et al. [112] and Papi et al. [302]. The variability of results obtained from the use of different LEP configurations, the uncertainty of the behaviour of each sample in the rain erosion whirling arm test, and the unpredictability of the response of the LEP under local rotor velocities lower than those tested guide the requirements for the optimisation of O&M towards a model that can be dynamically updated with inspection data.

The interest of this framework relies on its capability to be applied in the development stage for O&M cost estimation, and in the operation phase for O&M planning. The variability of the erosion degradation behaviour of the sample from the whirling arm test to its actual conditions can be overcome by updating the parameters of the power-law with inspection or SHM data through bayesian updates [72]. Qualitative damage levels, which can be identified during blade inspections, can be mapped to erosion damage intervals and used to provide an estimate of the deterioration state of the blade at different sections that would serve to better capture the particular behaviour of the erosion process of the inspected blade and plan its maintenance accordingly; degradation caused by manufacturing defects can be also be corrected in the same way. This prognosis model can provide an estimation of the current power loss of the turbine due to this phenomenon and its expected evolution, providing a tool to actively plan

maintenance to avoid catastrophic failures of the blades and optimise the production of the wind turbine.

Chapter 5

A reliability-based framework for leading edge erosion baseline maintenance selection

Chapter contribution

This chapter aims to accomplish the following research objective: *Provide a risk-based tool to evaluate baseline calendar-based LEE maintenance scheduling policies.*

The contributions of this chapter are detailed below:

- Provide a framework to design calendar-based LEE maintenance strategies at wind farm level for offshore locations considering site-specific climatic conditions.

The published peer reviewed journal article Contreras Lopez, Javier et al. "*Reliability-based leading edge erosion maintenance strategy selection framework*" Applied Energy 358 (2024) was authored by myself as part of my research completed under the direction and consultation of my supervisor, Professor Athanasios Kolios, and my coauthors. The published article is incorporated in this chapter and forms part of the definition of a framework for baseline O&M decision-making at wind farm level for leading edge erosion.

5.1 Introduction

The interest for offshore wind has grown driven by the greater availability of space, the higher energy availability, and the lower social impact of the marine environment [244]. Some of the most important constraints to its growth are the high construction costs and the difficulties in the operation and maintenance (O&M) of the wind turbines, which can constitute a considerable percentage of their life cycle costs [219, 248].

To address the problem of life cycle cost reduction, a proper understanding the wind turbine failure modes and their implications in cost and risk is a key aspect. In this line, the blades are one of the components carrying the highest cost and of which the maintenance and potential replacement have important influence in terms of planning, logistics, cost, and unavailability of the turbine [348]. While other mechanical components of the turbine have more complex condition monitoring systems such as the drivetrain or the bearings, the blades are usually inspected using time-based schedules either visually or with the aid of drones to identify potential damage. The difficulty of scheduling these campaigns in geographical zones with harsh weather conditions and the implications of damage or failure that require blade removal necessitate careful consideration. The degradation model for leading edge erosion proposed in Chapter 4.5 opens the opportunity to improve maintenance scheduling for this failure mode.

Risk-based maintenance emerges as a potential solution to optimise maintenance planning. Nielsen and Sorensen [289] present an overview of the available risk-based planning methods for wind turbines in the literature. The same authors [287] also proposed a risk-based optimal planning method. The proposed approach considers the optimisation from the design stage, considering some candidate designs, to the final decommissioning of the turbine and bayesian updating to incorporate any available information that can improve the decision-making such as Structural Health Monitoring (SHM), inspection data or data from other turbines. Morato et al. [278] propose a combination of dynamic Bayesian networks with Partially Observable Markov Decision Processes (POMDPs) in a joint framework for optimal inspection and maintenance planning in problems dominated by structural reliability. This proposed framework is

compared with classic heuristics-based policies showing a better performance. Nielsen et al. [288] estimate the value of information of a vibration-based SHM system through bayesian networks and MCS using the computational framework proposed in [291]. Dimitrov [101] presented a risk-assessment for wind turbine blade damages observed during visual inspection demonstrated on LEE and trailing edge cracks.

Depending on the severity of LEE damage sustained, the repair process can encompass a wide range of techniques, from the application of coatings, tapes, or shields for minor damage, to filling and sealing techniques or resin injection for non-structural matrix cracks, small surface cracks, or delamination, to the use of composite laminate patching for structural damage. A classification of damage according to its severity is shown in Table 5.1. The time required for repair can vary greatly, and in certain cases, the disassembly of the blade may be needed if the damage is critical. Figure 5.1 shows an example of leading edge blade repair. The challenges associated with performing the repair without disassembly, coupled with the difficulties of accessibility, workforce safety, and weather-related constraints, present significant obstacles in the successful completion of wind turbine blade repair missions. Therefore, it is essential to carefully plan its maintenance to overcome these challenges and improve the efficiency and safety of wind turbine blades. There are guidelines in the literature, such as the provided by Bladena [36], that contain recommendations for operation and maintenance actions related to LEE. It is suggested that repairs should be done within 6 months if the erosion reaches the laminate and within 3 months if it reaches the second layer of the laminate to prevent compromising the structural integrity of the whole blade.

Table 5.1: Leading edge damage classification by severity [36].

Damage Type	Severity	Action recommended by [37]
LE discoloration, paint or bugs	1	No need for immediate action Continue normal turbine operation
Coat/paint damage, surface: Missing less than 10 cm^2	2	Repair only if other damages are to be repaired Continue normal turbine operation
Coat/paint damage, surface. Missing more than 10 cm^2 Damaged leading edge protection Damaged leading edge tape LE erosion, down to laminate	3	Repair within 6 months Continue normal turbine operation
LE erosion, down to laminate and first layer laminate	4	Repair within 3 months and monitor damage Continue normal turbine operation
LE erosion, through laminate / Open LE	5	Repair immediately Stop turbine operation

The problem of LEE on wind turbine blades is met with a diverse array of solutions. These include the use of protection tapes, protective coatings, and epoxy or polyurethane fillers. Protective coatings are relatively quick to install and may offer reliable protection but can also alter the original aerodynamics of the blade, potentially impacting Annual Energy Production (AEP). Epoxy and polyurethane fillers require a more labour-intensive application process and may be impacted by weather conditions such as temperature and relative humidity. On the other hand, tapes or sheets, which are easy to install and have fewer weather-related restrictions, may be a viable option. However, the lifetime of each solution and its cost-benefit and suitability for a specific site are not yet fully understood [133], as research on this topic is still ongoing.

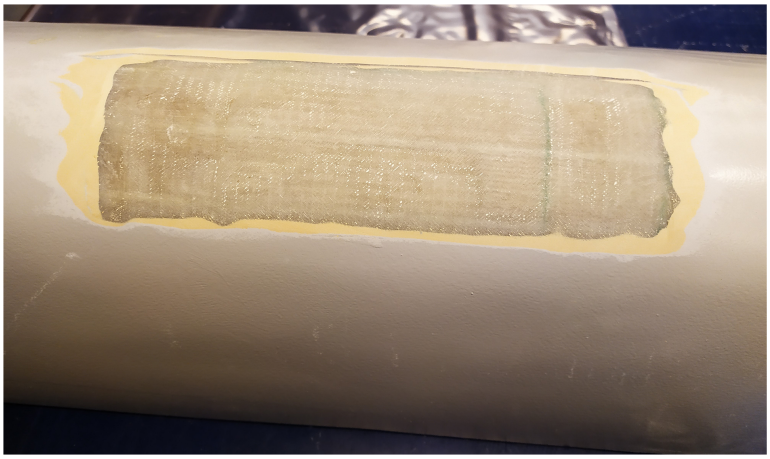

Figure 5.1: Repaired leading edge of the wind turbine blade (demonstration of composite repair by Danish Blade Service Aps). Source: [265].

The potential criticality of blade erosion-related failures [270], the difficulties to access offshore wind turbines for inspection and maintenance due to the harsh weather conditions of some regions and the uncertainty in the evolution of this failure mode increase the importance of adequate maintenance scheduling given that the miss of a maintenance opportunity window can lead to a late maintenance and suboptimal operation of the asset or even a catastrophic failure of the blade. In response to this, the present chapter aims to provide a framework for the maintenance planning of leading edge erosion of offshore wind turbine blades based on reliability and considering the uncertainty in weather, damage evolution and the success on the planning and execution of the maintenance missions. This framework can be of great use for baseline maintenance planning at wind farm level when the need to consider different failure modes and conditions for a number of failure modes and turbines can increase the complexity of the problem making it difficult to be scheduled efficiently.

Designing O&M policies for wind energy assets is a non-trivial task requiring a multi-level and site-specific approach. The first step is being able to obtain a good representation of the dynamics of high priority failure modes at low-level (component/subcomponent level), which is the foundation for an accurate description of the system. It is important that the low-level modelling is able to capture the most important sources of uncertainties (material and weather among others) related to each of the failure modes considered. For some offshore locations, the constraints and particularities of a site can widely modify the evolution of particular failure modes and the characteristics for optimal policies. The next step would be the joint analysis of the relevant failure modes of different components of the system. For this step to be performed, a description of the evolution of the failure modes considered by efficient surrogate models may be required for a computationally affordable simulation of different maintenance strategies. Finally, a reliability analysis of the system is to be performed in order to make risk-informed O&M strategy decisions for the asset that align with the tolerance to risk of the organisation managing the asset.

In this chapter, a framework for risk-based maintenance strategy selection for leading edge blade erosion is proposed. This method provides an approach for O&M opera-

tors to design baseline calendar-based site-specific maintenance strategies at wind farm level using rain test erosion experiment data. One of the novelties of this work is the consideration of uncertainty in weather and coating durability. A reliability function for this failure mode is proposed to obtain the probability of failure of the proposed maintenance policies. A pareto front plot is then drawn considering risk and cost metrics such as the accumulated Probability of Failure (PoF) at the end of the lifetime and median of O&M lifetime costs, respectively, to aid in the design of the policy.

The chapter is structured as follows. Section 5.2 provides a description of the methodology used, the definition of the reliability function and the stochastic variables considered for the reliability analysis. Section 5.3 presents all the assumptions considered in the O&M simulations. A case study demonstrating the use of the proposed framework and considering a 5-MW turbine is presented in Section 5.4. Finally, the conclusions of this study are presented in Section 5.5 and the potential of condition-based maintenance is also discussed.

5.2 Methodology

The proposed framework for risk-based maintenance strategy selection for leading edge blade erosion is presented here. The first step in the framework is the definition of the stochastic variables to consider in the study. In this case, model parameters governing the dynamics of the evolution of LEE and site-specific environmental parameters (namely, wind speed, u, and rain intensity, I) are considered as stochastic variables to analyse the reliability of the blade affected by leading edge erosion. Second, the definition of the LEE damage threshold for the reliability function defining the failure of the blade. Then, candidate O&M policies are simulated through MCS to obtain their lifetime cost distribution and Probability of Failure (PoF). Two type of policies are considered, namely policies based strictly on the calendar, labelled as *SM*, and others based on a maintenance interval or time between repairs, labelled as *TBR*. In this work, maintenance interval is defined as the time threshold over which a maintenance action is scheduled after a successful repair. For *SM* policies, maintenance is attempted once the planned maintenance month is reached until success. In the case of *TBR* policies,

a time interval from the last performed maintenance is defined. Once this interval is reached, maintenance actions attempted until weather constraints allow their completion. With the results of the simulations using the candidate policies, a Pareto front plot can be drawn in order to identify the policy that meets the requirements of a predefined maintenance strategy, providing a way to make risk-informed decisions. The suggested metrics for the Pareto plot are the median of the cost and the accumulated PoF at the end of life following a specific policy. Figure 5.2 provides a scheme to better clarify the main calculation steps of the proposed methodology.

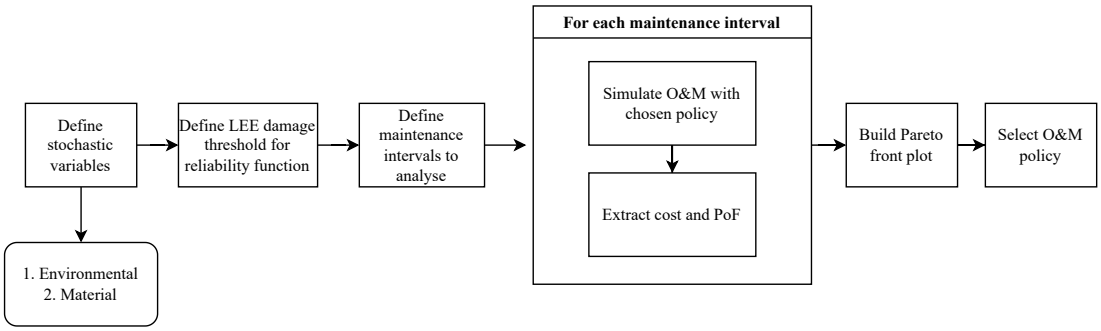

Figure 5.2: LEE risk-based O&M policy selection.

This study is focused on the leading edge erosion failure mode and will be the only one considered for the reliability-based maintenance optimisation. As commented above, this failure mode develops over time and requires timely maintenance to avoid the structural failure of the blade. For the reliability analysis, a performance function $g(X)$ is needed. In the case of leading edge erosion, the following performance function can be defined:

$$g(X,t) = p - d(X,t) \tag{5.1}$$

where p is the selected damage threshold, X the set of stochastic variables affecting erosion damage progression and $d(X,t)$ is the accumulated erosion damage at time t. Damage progression can be calculated as:

$$d(X,t) = \sum_{i=0}^{i=t} \frac{h_i}{H} \tag{5.2}$$

where h_i is the accumulated rain impingement h during time step i and H the accumulated rain impingement to erosion failure of the coating resulting from Whirling Arm Rain Erosion Test Rig (WARER) or Rain Erosion Tester (RET) tests, which is considered as the equivalent of damage severity 5 from Table 5.1. The accumulated rain impingement to erosion failure, H, can be obtained as:

$$H = C_1 \cdot v(r)^{-C_2} \tag{5.3}$$

being C_1, C_2 model parameters describing the durability of the system and calibrated using experimental WARER test data for a specific protection system.

The computation framework used in this study is taken from Chapter 4.5 and reproduced here under a concise and unifying notation, for clarity. A schematic of this framework is shown in Figure 5.3. To address the impact of uncertain site-specific weather conditions, the proposed methodology commences with the generation of stochastic wind and rain time series. These can be derived from either observed meteorological data or ERA5 reanalysis data for the precise location of the wind turbine [174]. In the absence of data, the aerodynamic effects of LEE can be estimated through 2D or 3D Computational Fluid Dynamics (CFD) simulations or experimental testing, such as wind tunnel experiments of eroded airfoils. Given the significant computational expense of each simulation, and the number of simulations necessary to capture the various stages of blade degradation, the 2D modelling approach is preferred in this study. The maximum expected aerodynamic losses for a severe degradation state can be estimated using the 2D CFD method on the different airfoils conforming the last third of the blade by adjusting the sand grain roughness height, k_s, to a value of $k_s/c = 0.0076$, where c is the chord of the airfoil, as proposed in [320]. Intermediate degradation states can be linearly interpolated considering the damage state of the section of interest. Moreover, the use of the Blade Element Momentum (BEM) theory enables the integration of numerically or experimentally obtained polar curves in a more practical and efficient manner, as shown in [213], given that different combinations of damage states along the blade can be considered in a more efficient way than a 3D CFD simulation. Once the aerodynamic efficiency of eroded airfoils has been estimated, the power production of

the wind turbine across different degrees of blade erosion can be computed. A number of calculation points are defined in the last third of the blade, which is the area more prone to LEE. For the calculation points defined, d is calculated at every time step. Lift values of the airfoils are linearly interpolated for discrete degradation states. In the current study, damage was discretised every 10% increase. The synthetic weather data and the estimated aerodynamic performance of airfoils are subsequently merged to estimate LEE degradation and energy production at each time step, using the appropriate power curve that represents the degraded state of the blade under the BEM theory.

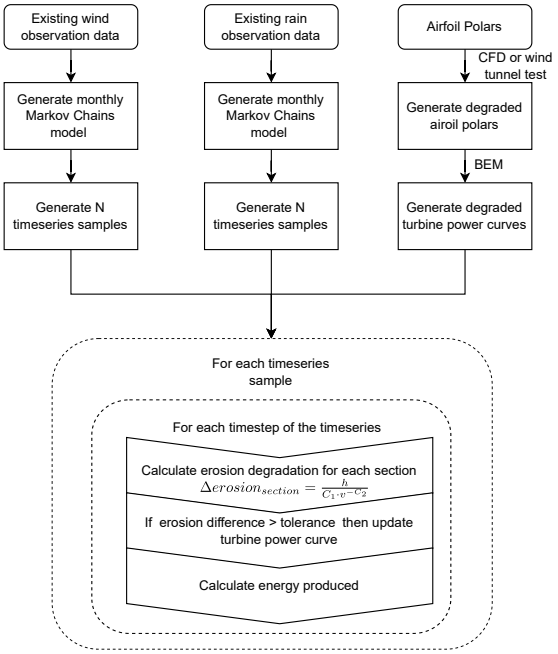

Figure 5.3: LEE calculation framework. Source: [240].

5.2.1 Limit States/Design Criteria

Linear degradation has been assumed for the LEE failure mode. In this study, damage, d, is defined in the interval [0,1]. The physical meaning attributed to different physical degradation states of the blade is shown in Figure 5.4. The intervals between different damage severity categories can be tuned using a thorough WARER test campaign or based on experience of operation data of turbine blades using similar coatings. This

categorisation is used to assign meaningful repair costs to the different degradation states. The evaluation of the performance function requires a careful selection of the abovementioned damage threshold, p. In this case, a value of 0.8 was chosen for the damage threshold representing the beginning of damage to the laminate (transition from severity 4 to severity 5), which requires a careful repair treatment to avoid the damage evolution that could develop into a catastrophic failure of the blade. Damage above this level could lead to difficult repairs of the blade requiring its disassembly or catastrophic failures leading to a large downtime. The failure of the blade is then considered when $g(X,t) \leq 0$. For the computation of the PoF this study assumes the failure of the blade from a specific time step t even if the blade is restored to a working condition $g(X) > 0$. The PoF is obtained by MCS and computed as:

$$PoF(t) = \frac{f(t)}{n} \tag{5.4}$$

where $f(t)$ is the number of failures at a given time step and n the number of simulations.

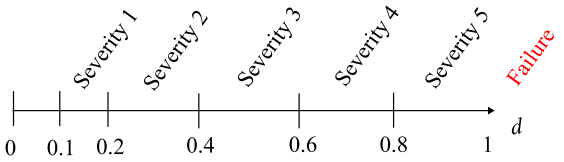

Figure 5.4: Damage, d, assigned to different damage severity categories.

5.2.2 Selection of stochastic variables

In this study, both parameters C_1 and C_2 describing the durability of the coatings and site-specific environmental parameters wind speed, u, and rain intensity, I are considered as stochastic variables to analyse the reliability of the blade affected by leading edge erosion.

Model parameters C_1 and C_2

This framework allows the consideration of the uncertainty in the results of experiments on the model parameters of the protection system. This approach overcomes the limita-

tions of relying solely on a deterministic value for the entire population, which may not accurately reflect the behaviour of each individual. By conducting experiments with varying drop sizes and rotation speeds, the uncertainty in the results can be taken into account for the maintenance of the blades, thereby preventing an unnecessary increase in maintenance costs and avoiding catastrophic failures. A proper definition of these parameters allows us to include test data using different testing conditions. To this end, confidence intervals can be defined with the number of tests performed on the coating and the fitting parameters C_1 and C_2. Figure 5.5 shows this approach for a specific coating defined in [192].

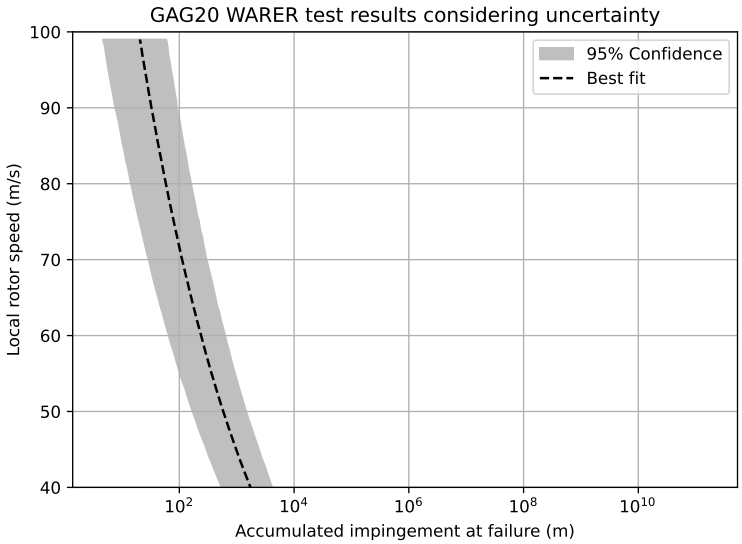

Figure 5.5: Accumulated impingement at failure for GAG20 coating.

Climatic variables

Acquiring high-granular and high-quality weather time-series data for a specific wind farm location over extended periods can be challenging and costly. To account for site-specific weather conditions, uncertainty in wind speed u and rain intensity I has been considered in this framework. Depending on the availability of data for the location, different approaches can be applied.

The solution proposed to generate synthetic wind speed datasets that mimic the weather patterns at the site of interest considers the use of Markov chain models [293].

The generated datasets must cover a period of 20 to 25 years, which encompasses the expected service life of the turbine. This study utilises 10-minute average data for wind speed and rain intensity. The wind data is modelled using a Markov probability transition matrix with 0.5 m/s bins, calibrated using FINO1 10-minute average wind speed observation data [131]. A finer discretisation would produce a distribution closer to the observations at the expense of a greater amount of data for the calibration of the transition probability matrices. The process can be summarised in the following steps:

1. Calibration of the generative model:
    (a) Binning the observations of wind speeds using the desired bin width monthly and annually.
    (b) Computing the transition probabilities by counting the number of wind speed transitions from each of the bins to the rest of the bins.
2. Generation of synthetic time series:
    (a) Initialise wind value from histogram of observations. The wind speed value is drawn from a uniform PDF within the limits of the drawn bin.
    (b) Drawing the next wind value bin using the transition probabilities of the current bin.
    (c) Next wind value is drawn from a uniform PDF within the limits of the current bin.
3. Postprocessing: The first year of the synthetic series can be removed to reduce the bias.

To account for the seasonal variation of average wind speeds, separate probability transition matrices for each month, in addition to a general annual wind transition probability matrix, are considered to ensure that wind speeds fall within observed ranges.

In the case of rain intensity an alternative approach is required given that the available data range was limited. The approach considered in this study is described here:

1. Using ERA5 reanalysis data, fit monthly probability density functions for rain intensity. In this case, Weibull PDFs were used.

2. From the reanalysis data, calibrate a simple Markov chain model considering 2 states (Raining and not raining) and the transition probabilities from each of them to the other states.

3. For data generation, every time step a rain state will be drawn. When the state is *raining*, the rain intensity will be drawn from the site-calibrated Weibull PDFs.

ERA5 reanalysis data can be obtained to fit monthly Weibull probability density functions of 10-min average rain intensity data. In addition, Markov probability transition matrices for rain/no rain probability can be generated. When combining these techniques, rain intensities are drawn for the monthly fitted density functions when the rain state is drawn from the Markov chains. While this approach may result in abrupt variations in rain intensities, it will not significantly affect the results of the study since the relative variation of rain intensity is assumed not to affect the degradation rate of the blade. In this study, wind and rain have been modelled as statistically independent variables.

5.3 O&M model assumptions

For the O&M simulations, the following assumptions were considered:

- Only the O&M costs of the blade due to LEE are considered as defined in Table 5.2 and obtained from [288] and [446].

- Operation of the turbine is assumed to start at the beginning of January.

- Imperfect repairs. After each repair, the true damage state of every calculation point, d, is set to a value drawn from a normal distribution $d \sim \mathcal{N}(\mu, \sigma^2)$ with

$\mu = 0.05$ an $\sigma = 0.001$ and truncated at the interval $[0, 1]$ to avoid values out of the defined interval for d.

- Imperfect inspection is considered. Inspected damage, D, follows a Gaussian distribution with $\mu = d$ and $\sigma = 0.1$, truncated at the interval $[0, 1]$ to avoid values out of the defined interval for D.

- If any of the calculation points of the blade reaches $d = 1$, the turbine will be preventively stopped until its repair/replacement. This study assumes that when the blade reaches that degradation step, other systems such as SCADA will produce alarms and the turbine will be preventively stopped.

- Energy cost of 50£/MWh is considered, which is in line with the Contracts for Difference (CfD) strike price signed for CfD4 in 2022 in the UK.

- Probabilistic definition of repair success discretised by month and trying to mimic the real O&M scheduling. The associated cost of a repair is a function of the damage and the month at which the repair is attempted. This is defined in Section 5.3.1.

- For calendar-based scheduled maintenance strategies (labelled as *SM*), repairs are attempted until success when the scheduled date arrives. In these policies, maintenance is planned for a specific calendar month (i.e. June) and is attempted until success irrespective of what the state of the blade is.

- For time between repair maintenance strategies, labelled as *TBR*, a time between successful repairs threshold is defined. Once the threshold is surpassed, repairs are attempted until weather constraints allow their completion.

- Energy production losses due to the reduced aerodynamic performance of the blade caused by erosion are considered following the calculation framework from [82].

- Energy production losses due to downtime and preventive stops are also considered.

5.3.1 Repair modelling

Repair costs have been discretised according to the erosion damage level of the blade. The costs considered are shown in Table 5.2.Repair costs are made of 3 factors:

$$C_m = m_b + m_a + m_e \tag{5.5}$$

Being m_b the booking cost for the logistics and staff required for the inspection/repair, m_a the access cost to the turbine and m_e the execution cost of the maintenance activity. The costs of maintenance activities depending on the severity of the damage are shown in Table 5.2.

Table 5.2: Repair costs per damage severity - 3 blades. Data obtained from [288] and [446].

Damage severity	m_b (£)	m_a (£)	m_e (£)
0 (Inspection)	1,600	1,000	3,200
1	2,000	1,000	4,000
2	2,000	1,000	4,000
3	3,000	1,000	6,000
4	5,000	1,000	36,000
5	0	250,000	3,500,000
6	0	250,000	5,000,000

In this study, the probabilities of repair success have been modelled in three steps. First, the probability of a given month having wind speed values below the constraints shown in Table 5.3, P_1. These constraints have been adopted from [290]. Second, the probability of the forecast weather to comply with a required weather window, P_2. Finally, the probability of the real weather to comply with a required weather window, P_3. These probabilities have been obtained through MCS for each month and damage severity. Weather time series have been built using the framework shown in [240]. Synthetic significant wave height, H_s, data has been created through a Artificial Neural Network (ANN) trained using FINO1 data. The chosen fully connected ANN architecture is composed of an input layer, a hidden layer of 4 neurons using the sigmoid activation function and the output layer. The ANN The parameters used for the ANN

are described here:

- $H_{s_{i-1}}$: Average significant wave height of the previous time step.
- $H_{s_{i-2}}$: Average significant wave height of 2 time steps ago.
- W_i: Current average wind speed.
- W_{i-1}: Average wind speed of previous time step.
- W_{i-2}: Average wind speed of 2 time steps ago.
- M_i: Month of time step i.

In order to verify the quality of the H_s generative model, it has been tested in an unseen dataset of 22,000 samples. The distribution of H_s for the synthetic data and observations and the calibration plot are shown in Figure 5.6 showing a good agreement and therefore a good potential for the generation of synthetic H_s time series for the location of the project.

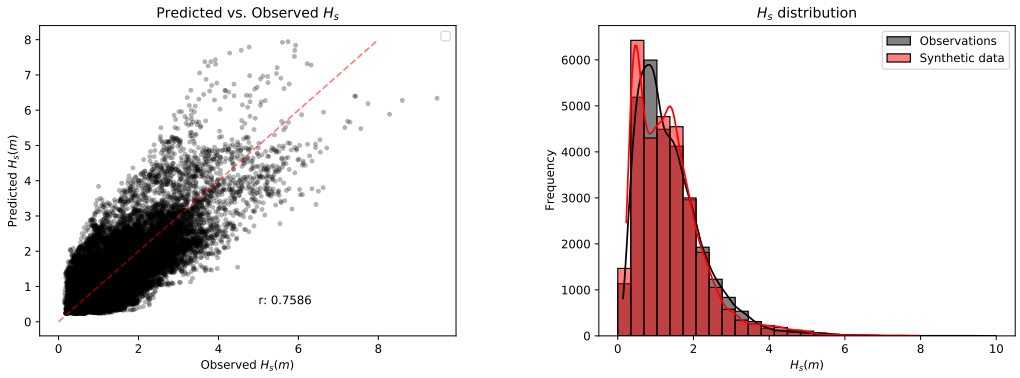

(a) Wind speed distribution - Observed vs Synthetic data.

(b) Distribution of H_s - Observed vs Synthetic data.

Figure 5.6: Weather data used in the case study.

A sample of the ANN outcome when compared with FINO1 data is shown in Figure 5.7. The weather restrictions parameters to comply for a successful weather window are significant wave height and 10-min average wind speed at hub height. It is assumed that for the case of P_3, the real weather deviates from the forecast with a growing

uncertainty. This has been modelled as a Gaussian distribution centred on the forecast value with a standard deviation that grows a 4% daily.

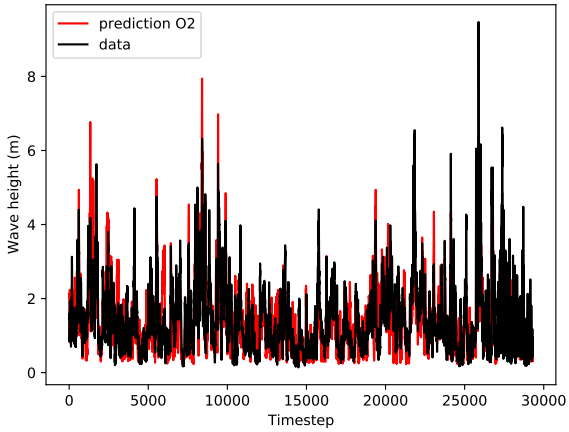

Figure 5.7: Sample H_s prediction.

The modelling of the repair success and the associated cost of each of the repair outcomes is depicted in Figure 5.8.

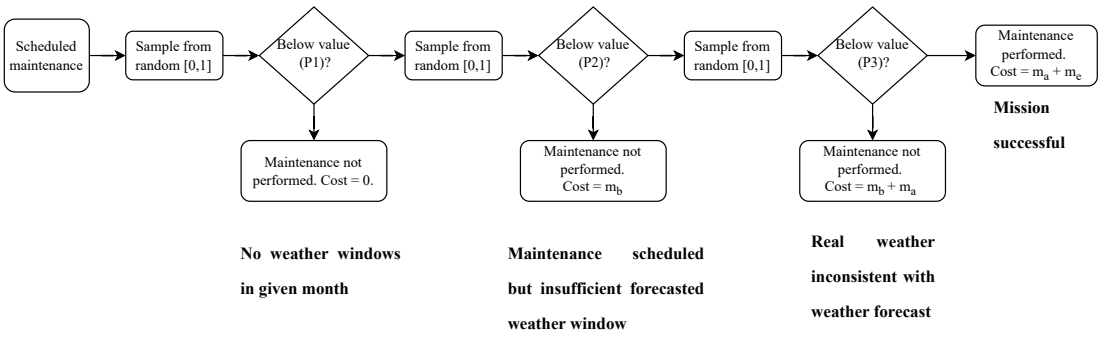

Figure 5.8: Repair modelling.

Repair success probability matrices P_1, P_2 and P_3 for the study case are shown in Section C.1.

5.3.2 Repair constraints

The repair constraints considered for the study are based on the weather restrictions assumed by [290] and summarised in Table 5.3.

Table 5.3: Weather repair constraints.

Damage category	Logistic requirements	Duration (h)	Max. significant wave height (m)	Max 10-min wind speed (m/s)
1: LE discoloration, paint or bugs	CTV, rope access	6	1.5	11
2: Coat/paint damage, surface: Missing less than 10 cm^2	CTV, rope access	15	1.5	11
3: Coat/paint damage, surface: Missing more than 10 cm^2 Damaged leading edge protection Damaged leading edge tape LE erosion, down to laminate	CTV, rope access	18	1.5	11
4: LE erosion, down to laminate and first layer laminate	CTV, crawler platform	40	1.5	12
5: LE erosion, through laminate / Open LE	HLV, blade disassembly	72	1.8	10
6: LE erosion, blade failure	HLV, blade disassembly	72	1.8	10

5.3.3 Cost model

The O&M cost for the simulations is calculated as follows:

$$C = C_l + C_m + C_d \tag{5.6}$$

where C_l is the the cost of the energy lost due to the degradation caused by the ageing of the turbine and the aerodynamic performance of LEE; C_m is the maintenance costs including the costs of booking, logistics and performance of the repair for all the maintenance activities performed on the blades; and C_d are the losses produced by the downtime of the turbine due to its preventive stop to avoid catastrophic failures or the repair of the blades.

5.4 Case study

To demonstrate the utility of this framework, a case study using an NREL 5-MW fixed-bottom wind turbine [193] located in the vicinity of FINO1 offshore measurement platform, sited 45 km north of the coast of the island of Borkum, Germany. Wind speed data was obtained from the FINO1 database and rain data from ERA5 reanalysis. Wind and rain synthetic data is shown in Figure 5.9.

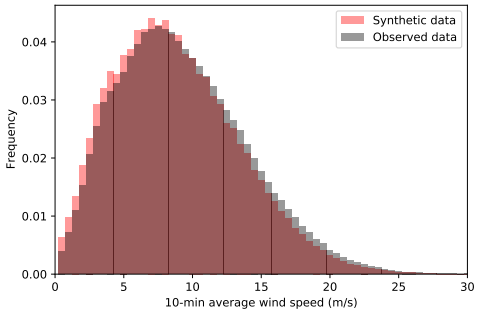

(a) Wind speed distribution - Observed vs Synthetic data.

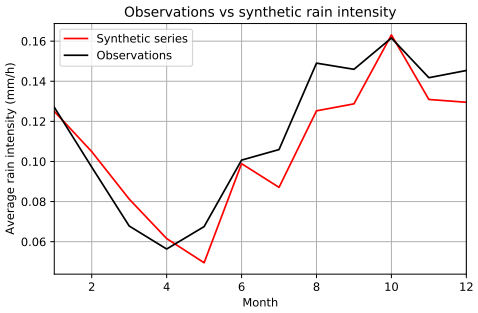

(b) Average rain intensity - Observed vs Synthetic data.

Figure 5.9: Weather data used in the case study.

The maximum effects of erosion considered for the calculations derived from 2D CFD simulations of pristine and eroded airfoils are shown in Figure 5.10. The degraded power curve represents an expected AEP loss for the site between 1.46% to 1.78% [240] with a LEE degradation of the last third of the blade. The coating of the blade considered for this study is a generic blade coating system supplied by Olsen Wings A/S from [192]. For each of the runs, C_1 and C_2 are drawn from normal distributions with mean and standard deviation as shown here: $C_1 \sim \mathcal{N}(1.45 \cdot 10^{11}, 0.05 \cdot 1.45 \cdot 10^{11})$ $C_2 \sim \mathcal{N}(4.98, 0.02{\cdot}4.98)$. These distributions for the model parameters are derived from the WARER test results using G20 needles, 3.5 mm droplet size, found in [192], and represent damage evolution rates in the range of others found in the literature [167,169]. The uncertainty in the behaviour for different droplet sizes in the WARER test was not considered in this case study.

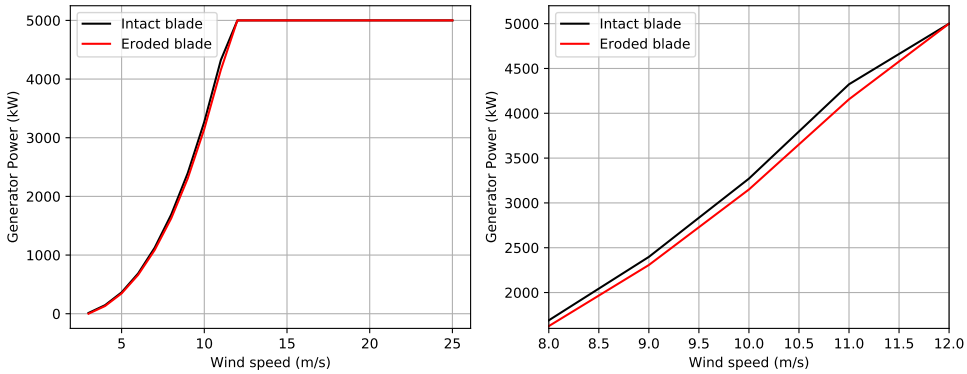

Figure 5.10: Wind turbine power curves for pristine and eroded states.

The maintenance strategies analysed for this case are divided in two types, calendar-based scheduled in the months of summer and time-between repairs. The analysed strategies are summarised in Table 5.4.

Table 5.4: Maintenance strategies analysed.

Label	Description
SM-12	Repairs every June (annually)
TBR-4	Repairs every 4 months
TBR-6	Repairs every 6 months
TBR-8	Repairs every 8 months
TBR-10	Repairs every 10 months
TBR-12	Repairs every 12 months
TBR-14	Repairs every 14 months

Every of the maintenance strategies was run for 50,000 simulations for the 25 years of the lifetime of the turbine. In the case of *TBR* maintenance strategies, the trigger for maintenance is the time since last repair. Once it is reached, the maintenance is attempted until being successful. For *SM* maintenance strategies, repairs are attempted once the scheduled calendar month arrives until the maintenance is executed successfully.

5.4.1 Reliability analysis

The reliability of the blade using the different maintenance strategies has been studied using Equation 5.1. The reliability and PoF over the life time of the turbine are shown in Figure 5.11. The PoF was calculated after running 50,000 independent simulations. The average reliability at time t_k, $\bar{g}(t_k)$, can be defined as follows:

$$\bar{g}(t_k) = \frac{1}{n}\sum_{i=1}^{n} g_i(X, t_k) \tag{5.7}$$

Similarly, the average reliability over the lifetime of the turbine, $\bar{G}$ can be defined as:

$$\bar{G} = \frac{1}{n \cdot T}\sum_{i=1}^{n}\sum_{t_k=T_0}^{T} g_i(x, t_k) \tag{5.8}$$

being T_0 and T the initial and final month of operation of the turbine, respectively.

In terms of reliability, it can be observed a first non-stationary phase in which failures having a lower time to failure than time to first maintenance appear and increase the accumulated PoF. After this phase, the rate of increase of PoF over time decreases until it is reduced to a small value. The accumulated PoF values at the end of the service life are summarised in Table 5.5. As expected, PoF increases with the increase in time between repairs. The lower repair success probability during winter months is noted by the difference in the PoF and $\bar{G}$ of maintenance strategies *SM-12* and *TBR-12* for which PoFs are 0.0850 and 0.1216 and average $\bar{G}$ of 0.5577 and 0.5360, respectively.

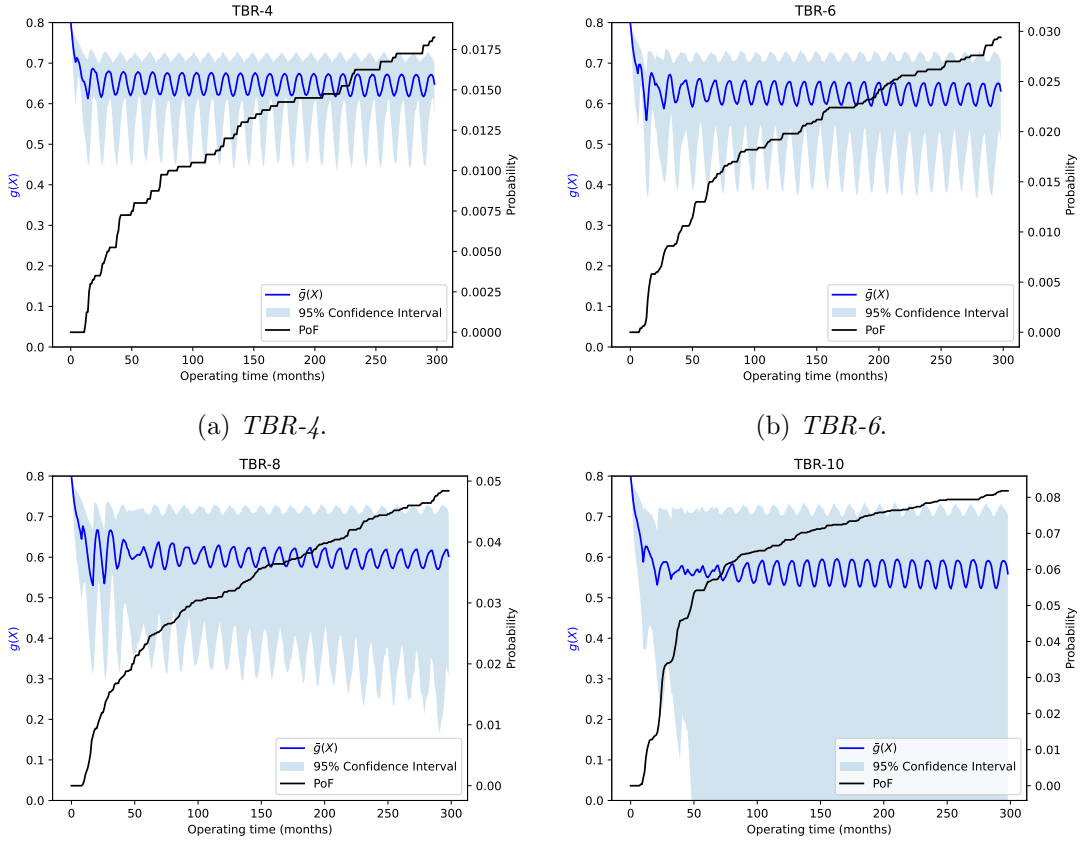

(a) *TBR-4*. (b) *TBR-6*.

(c) *TBR-8*. (d) *TBR-10*.

Figure 5.11: Reliability analysis. The left axis represents the reliability $g(x)$ of the LEP system, the right axis represents the cumulative probability of failure.

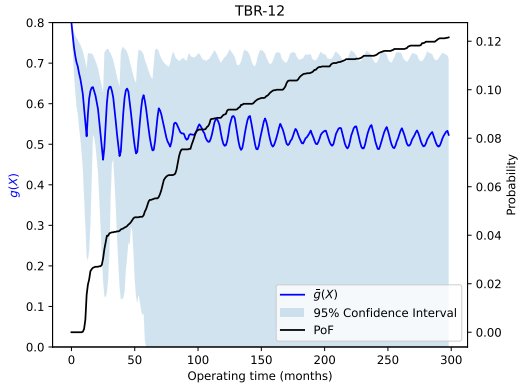

(e) *TBR-12*.

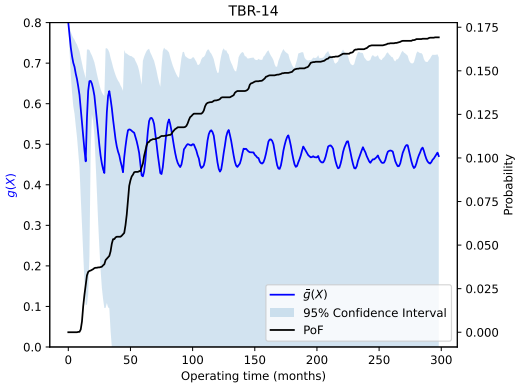

(f) *TBR-14*.

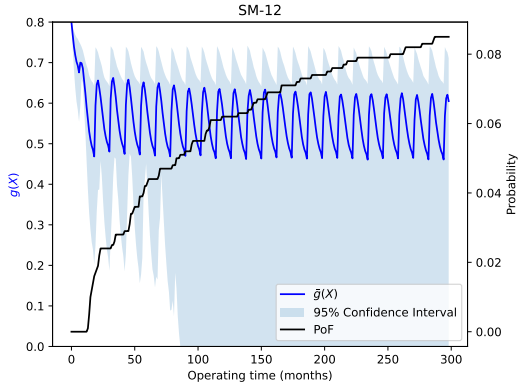

(g) *SM-12*.

Figure 5.11: Reliability analysis. The left axis represents the reliability $g(x)$ of the LEP system, the right axis represents the cumulative PoF.

Table 5.5: End of Life (EoL) reliability summary.

Label	PoF at EoL	$\bar{G}$
TBR-4	0.0183	0.6522
TBR-6	0.0294	0.6307
TBR-8	0.0484	0.6054
TBR-10	0.0818	0.5695
TBR-12	0.1216	0.5360
TBR-14	0.1692	0.4936
SM-12	0.0850	0.5577

5.4.2 Cost analysis

O&M costs for the maintenance strategies analysed have been obtained considering the ageing and erosion losses, downtime losses and maintenance costs. The total cost distributions are shown in Figure 5.12. This figure presents the effects of an increased number of maintenance activities, with an increase on the median of the cost and a reduction of its variance with the decrease of time between repairs. There is a trade-off between the probability of failure and the median of the O&M cost.

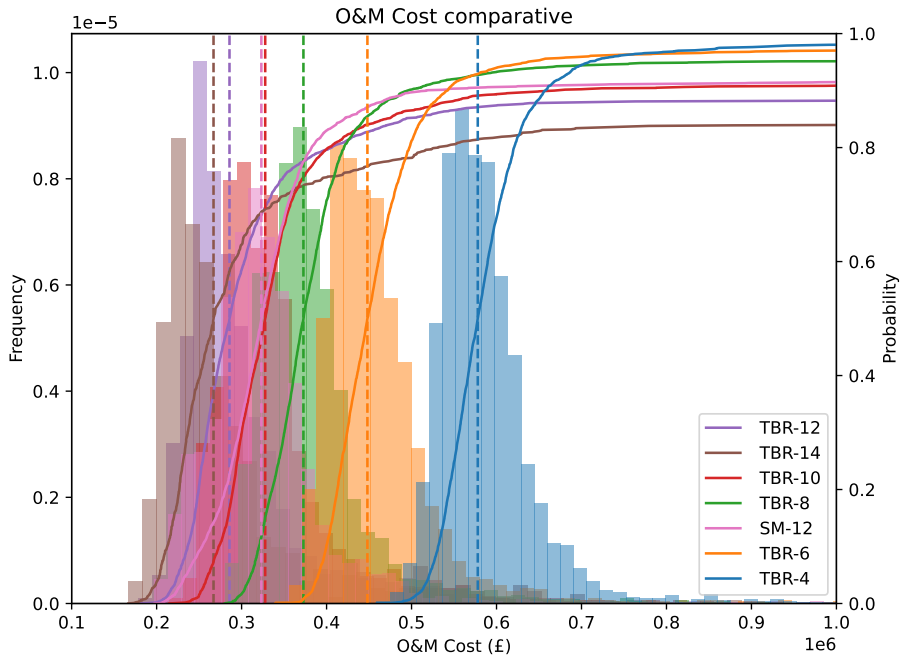

Figure 5.12: Total O&M cost distribution for analysed maintenance strategies. The left axis represents the frequency and the right axis the cumulative probability of occurrence. The dashed line represents the median of the O&M strategy. The cumulative probability of occurrence tends to 1, but the plot was truncated at 1M for a better visualisation of the distribution of the costs.

5.4.3 Pareto front analysis

A Pareto front analysis of the results obtained through the simulations is presented in Figure 5.13. In this case, the median and the PoF were chosen as representative values for the decision-making of this failure mode, although these metrics can be chosen as

per the organisation's requirements. This step is critical for a risk-informed decision-making. In this particular case, it can be noted that there is a trade-off between the median of the O&M cost and the PoF of the LEE. By analysing the different strategies, it can be observed that the relation of the increase in PoF and the decrease in median cost is non-costant. Once this information is ready, the most appropriate maintenance strategy according to the policy of the organisation operating the asset can be selected.

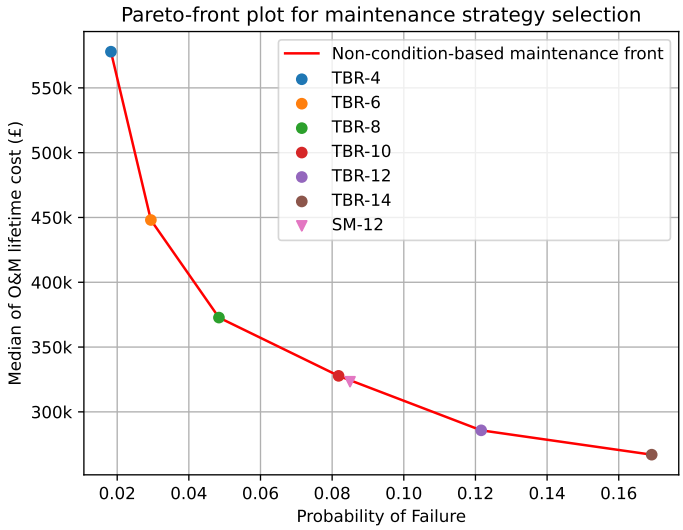

Figure 5.13: Pareto front plot - O&M decision-making.

5.5 Conclusions and further remarks

This section presents a framework for site-specific analysis and O&M policy selection of LEE damage for wind turbine blades. This approach can serve to study different maintenance strategies at the planning stage, anticipate the degradation rates of different coating solutions and plan inspections/maintenance at wind farm level. This framework is able to accommodate the uncertainty that lies in the coating behaviour and degradation dynamics, weather and maintenance success. The definition of a reliability function $g(x)$ allows for the quantification of the PoF of the chosen maintenance strategies. By selecting the appropriate cost metric and combining it with the probability of failure, a maintenance strategy can be chosen by adjusting the balance between

cost and PoF to meet the policy of the organisation in charge of the operation of the asset. While suboptimal policies are achieved by not considering the actual condition and material properties of the component of the turbine being operated, this can serve as a baseline for the O&M of the asset while policies based on inspection/SHM are deployed. The adoption of predictive maintenance techniques can be a complicated and costly task if not performed in a structured approach and counter-producing if not executed properly. Therefore, improvements in the O&M shall be deployed in a staged way and with the aid of preanalysis based on models of the assets and the environment. The detailed knowledge of the dynamics of the most risk-critical failure modes requires an exhaustive analysis of all the uncertainties surrounding it. Once this knowledge is acquired, different failure modes can be analysed and combined through the use of surrogate models to provide computationally affordable representations of the asset that allow the study of combined failure modes, such as proposed in [337]. Given the potential catastrophic failures that a high-risk O&M policy can produce, numerical models emerge as a key tool to unveil further O&M cost reductions. Condition-based maintenance is more common for other components of the turbine such as the drivetrain, for which advanced data-based predictive models are developed, not without the difficulty of dealing with different parameters, logging frequencies and equipment manufacturers. In the case of the blade, it is not yet clear for the industry what failure modes to monitor, for which a risk analysis at component level is highly important [239].

Given the highly dimensional state space that this problem entails, conditon-based maintenance design is not a trivial task. A promising strategy to extract insightful information is the use of Reinforcement Learning (RL) agents to try to discover and exploit interesting policies. While this technique requires a careful definition of the problem, reward function and parameters among others, the outcomes can be of great importance for the iteration towards optimal policies. A promising follow-up study would be the comparison of the proposed maintenance strategies with condition-based policies discovered through autonomous decision-making systems.

The framework introduced in this chapter serves as a valuable tool for comparing candidate strategies by considering both risk and cost metrics. It enables the evaluation

of the impact of different maintenance intervals, allowing for the definition of baseline strategies at the wind farm level during the initial planning stage. These baseline strategies can subsequently be refined and updated with condition-based approaches once the operational phase starts.

Furthermore, the presented framework equips O&M practitioners with a tool to juxtapose the cost against the PoF associated with candidate maintenance policies. This capability facilitates alignment with a global risk tolerance policy for the wind farm, ensuring that maintenance decisions are made in accordance with overarching risk management objectives.

The incorporation of this framework into the decision-making process enhances the strategic planning for wind farm maintenance, offering a systematic approach that considers both economic considerations and risk mitigation in the development and adaptation of maintenance strategies.

Chapter 6

An autonomous decision-making agent for offshore wind turbine blades under leading edge erosion

Chapter contribution

This chapter aims to accomplish the following research objective: *Design an autonomous decision-making system for blade's O&M.*

The contributions of this chapter are detailed below:

- Define the simulation environment for the O&M simulations.
- Design the autonomous system for the decision-making of O&M activities.

The submitted peer reviewed journal article Contreras Lopez, Javier and Kolios, Athanasios "*An autonomous decision-making agent for offshore wind turbine blades under leading edge erosion*" was authored by myself as part of my research completed under the direction and consultation of my supervisor, Professor Athanasios Kolios. The submitted article is incorporated in this chapter and forms part of the definition of a framework for baseline O&M decision-making at wind farm level for leading edge erosion.

6.1 Introduction

Despite the promising outlook for the offshore wind industry, several issues still need to be addressed to make this technology as competitive as its onshore counterpart. The O&M costs of OWTs are estimated to account for 25-30% of the total lifecycle costs [392]. Offshore maintenance activities are estimated to be five to ten times more expensive than those performed onshore [177, 355]. When combined with the required weather windows for maintenance activities, this can result in O&M costs that are double those of onshore turbines [16]. The combination of accessibility challenges and the lower reliability of large rotor turbines offshore turbines [60] creates a challenging scenario leading the operators to use preventive or reactive maintenance resulting in unnecessary O&M costs [427].

Given the challenges of maintenance planning, the use of decision support tools is vital for offshore wind farm operators, as discussed in Chapter 5.5. The limitations of calendar-based maintenance policies lie on the difficulty to provide cost-effective solutions when the dynamics of the evolution of the damage are uncertain. The tunning of the maintenance interval can be a complex task and end up producing repair activities with a higher frequency than needed or end in a catastrophic failure. Many efforts have recently been made to develop different tools to optimise one or many of the different existing maintenance methods: routine inspections, corrective maintenance, preventive maintenance, condition-based maintenance, predictive maintenance or opportunistic maintenance. Several different approaches have been used. These include methods such as Mixed Integer Programming (MIP), Non-linear Programming (NLP), stochastic models, Markov models, Petri Nets (PN) models, analytical models, fuzzy models, intelligent algorithmic models, and multi-objective models, to name a few. Regardless of the method used, scholars have targeted different levels for optimisation, ranging from individual components such as the tower, foundation, or drivetrain, to the entire turbine or wind farm. The objectives for optimisation include O&M costs, logistics costs, availability, reliability, and environmental impact. Some of the most recent publications are summarised here. Saleh et al. [338] proposed a PN model combined with RL

for the O&M of wind turbines. Elusakin et al. [116] developed a stochastic PN model for O&M planning of floating offshore wind turbines. Yan and Dunnet [440] studied the maintenance of OWTs under the PN paradigm and considering periodic maintenance, condition-based maintenance and reactive maintenance policies. Ge et al. [140] designed a maintenance planning optimisation algorithm based on MIP to minimise power generation losses on maintenance activities. Li et al. [232] proposed a multi-objective maintenance strategy optimisation framework at wind-farm level considering uncertainty in the maintenance performance. In [350], Schouten et al. introduce a single-component model for maintenance optimisation under time-varying costs that is applicable to offshore wind turbine maintenance. Aafif et al. [3] provides an optimal preventive maintenance strategy for a wind turbine gearbox based on its temperature. In [432], Yong and Qirong propose an optimisation maintenance scheme for the maintenance missions considering the time windows based on a hybrid ant colony algorithm. In [463], Zou and Kolios propose a framework to improve maintenance decision-making by quantifying the value of information of condition monitoring.

The modelling of the O&M of OWTs at turbine level or wind farm level requires a deep knowledge about the failure modes of the components that carry the highest weights in the maintenance activities. Damage is usually discretised in states and its progression represented with a probabilistic description of the transition between them. The calibration of these require the possession of considerable amounts of failure and maintenance data of the same or similar equipment in sites with similar weather conditions to provide good results. Alternatively, the use of detailed models, can provide with a numerical testing environment to obtain synthetic data. Higher level models require more computationally affordable damage descriptions that can mimic the real behaviour of damage degradation. Being the rotor one of the most critical components [239, 426] and LEE one of the failure modes carrying the higher criticality [168, 173, 196, 239], its O&M planning requires a careful analysis. Lifetime assessments of erosion protection systems can be found in the literature, such as the works performed by Hasager et al. [167, 169] and [29]. In [167], the lifetime assessment of leading edge protection systems of Vestas V52 turbines for sites in the Danish Seas was performed, finding ex-

pected lifetimes between 2 and 13 years. Also, in [169], for sites in the North and Baltic Sea, the expected lifetime of coatings was in the range of 1 to 25 years. Under this high uncertainty in coating lifetime and weather effects, there is a need for a decision support tool to improve the decision-making capability of wind farm operators. In this sense, the current study presents an autonomous decision-making RL agent to optimise OWT LEE O&M costs. The uncertainties in weather scenarios, maintenance performance and LEE protective coating behaviour are considered in this analysis. The proposed agent, once trained, can provide an action suggestion at any stage of the turbine service life. Also, the proposed agent can be retrained once real operation data becomes available improving its accuracy an providing further cost O&M cost reduction.

The remainder of this chapter is structured as follows: Section 6.2 presents the methodology used for the optimisation of the O&M planning. Section 6.3 provides the assumptions and considerations of the O&M model used in this study. Section 6.4 presents two case studies to evaluate the performance of the proposed decision-support agent. Section 6.5 offers a discussion about the benefits and limitations of the framework presented as well as some follow-up opportunities. Finally, Section 6.6 summarises the conclusions of the application of the proposed methodology.

6.2 Methodology

This section delineates the methodology employed in this study, which is divided into two subsections. The first subsection elucidates the computational framework for LEE degradation and turbine operation simulation, while the second one delves into the decision-making framework for the optimisation of O&M costs.

6.2.1 Computational framework

This subsection provides a description of the *environment* and the computational framework that defines the dynamics of the degradation of the system.

LEE is a degradation phenomenon that affects wind turbine blades in several aspects (acoustic, aerodynamic and structural). The relations between the parameters

affecting this problem is shown in Figure 6.1. This phenomenon is caused by fatigue degradation through a repeated number of impacts of airborne particles (rain, insects and other airborne particles) onto the outermost layers of the blade. The dynamics of this process are affected by a number of parameters such as the impact energy, coating material parameters and weather conditions. The present computational framework provides a method to consider uncertainty in the abovementioned parameters. This computational framework is presented in [240] and depicted in Figure 6.2. To account for the uncertainty in climatic, material and aerodynamic parameters, the techniques described below can be used.

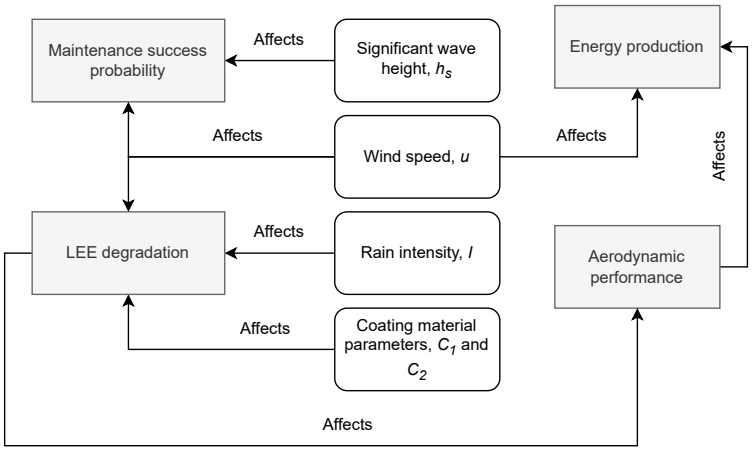

Figure 6.1: Relations between parameters

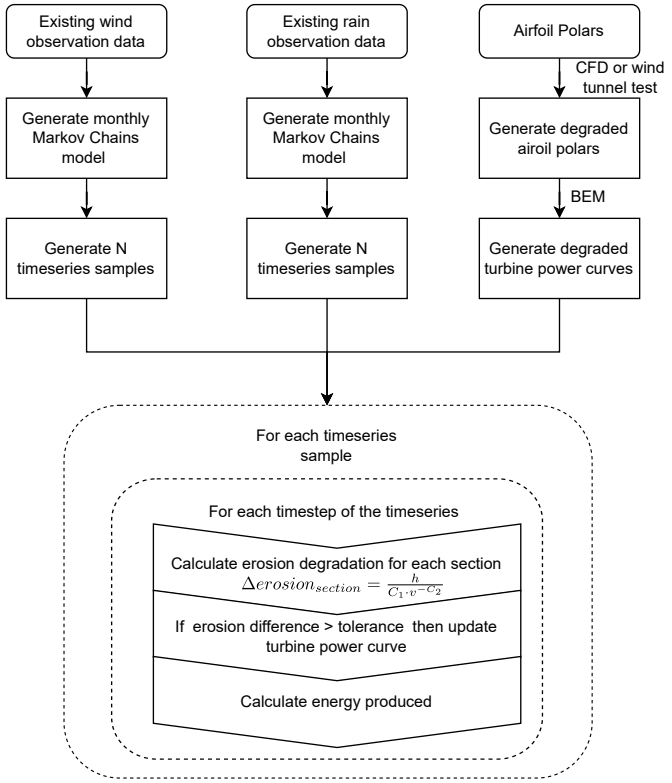

Figure 6.2: LEE calculation framework. Source: [240]

First, synthetic weather data needs to be generated for the location of the turbine. Rain intensity, wind speed and significant wave height time series should be generated in order to compute damage degradation and maintenance success rates. Depending on the availability of data for the project's location, various approaches can be considered. If a considerable amount of observations is not available, data can then be obtained from the ERA5 reanalysis data [174]. A Markov chains model [293] can then be used to generate synthetic wind series as shown in [240]. Significant wave height is an important parameter to account for the limitations in the logistics for offshore wind turbine maintenance activities. The generation of significant wave height series should be dependent on wind speed. Different approaches can be used to achieve this conditioned on data availability. In this case, an Artificial Neural Network (ANN) was used to mimic the significant wave height, h_s, patterns registered by the FINO1 platform. The parameters of the neural network used are the significant wave height of the two previous time steps, the wind speed of the current and two previous time steps and

the calendar month (to account for seasonality). The proposed ANN is composed of a hidden layer of 4 neurons using the sigmoid activation function and an output layer with the significant wave height value.

LEE is known to cause effects on the aerodynamic performance of wind turbine blades [173, 214, 270, 341], resulting in reduced lift and increased drag forces. These effects lead to a decrease in the power generated by the turbine. The estimated annual energy production losses can range from 1.5% to 10%, depending on the turbine's characteristics and site-specific climatic conditions [57, 112, 301, 341, 351]. Estimating changes in aerodynamic performance is a non-trivial task, often requiring the application of 2D and 3D Computational Fluid Dynamics (CFD) numerical models due to the limited availability of observational data [55, 252, 270, 303]. Once the blade's performance at various levels of LEE degradation is determined, the degraded power curves of the turbine can be constructed. These curves are used to assess the energy losses of the turbine. The energy produced at each time step, ΔE_i, is calculated using Equation 6.1, where $P(u, d)$ represents the power obtained from the degraded power curves, and Δt is the computational time step. Energy losses due to LEE degradation are then estimated as the difference between the pristine and degraded power curves.

$$\Delta E_i = P(u, d) \cdot \Delta t \tag{6.1}$$

Considering the high uncertainty in the behaviour of various coating materials is essential because the agent needs to account for uncertain degradation dynamics. To address this, the proposed method leverages the inherent uncertainty found in the Whirling Arm Rain Erosion test Rig (WARER) results, as shown in Figure 6.3. In these tests, leading edge protection coatings are subjected to water droplet impacts until they reach their final degradation. By analysing the evolution of the coating's degradation, the accumulated volume of water impacting the blade, and the velocity of the section being tested, curves showing the coating's failure can be obtained, as illustrated in Figure 6.3. The curve fitting used in this case follows Equation 6.2.

$$H = C_1 \cdot v(r)^{-C_2} \tag{6.2}$$

being H, the accumulated rain impingement to erosion failure and C_1, C_2 material parameters calibrated using experimental WARER test data for a specific protection system. For this study, damage evolution is assumed to be linear and damage accumulation calculated using the Palmgren-Miner rule:

$$\Delta d = \frac{h_i}{C_1 \cdot v(r)^{-C_2}} \tag{6.3}$$

with h being the accumulated rain impingement and $v(r)$ the local rotor speed during time-step i.

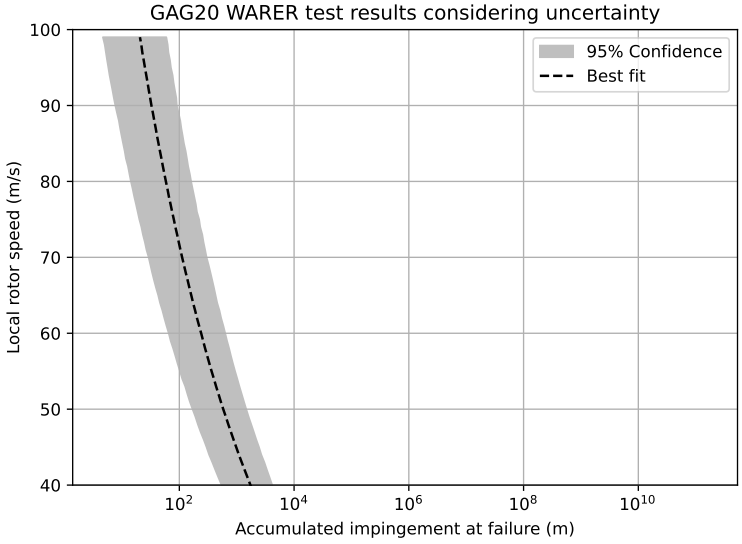

Figure 6.3: Accumulated impingement at failure for the GAG20 coating

In the literature, the evolution of LEE damage is typically described using a five-stage framework, which includes the following stages: incubation (stage 0), formation of minor pits (stage 1), formation of pits (stage 2), partial removal of topcoat (stage 3), and total removal of topcoat with delaminations (stage 4). In this study, a continuous damage parameter, denoted as d, is defined within the interval [0,1], allowing for the representation of the damage severity across these stages. Figure 6.4 illustrates the mapping of these stages to the damage levels within the [0,1] range, providing a clear visualisation of how different damage severity levels are associated with the stages of LEE damage evolution.

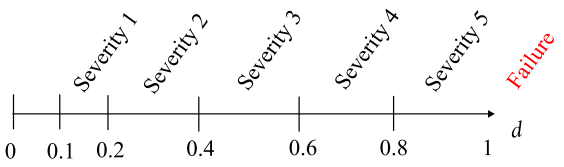

Figure 6.4: Damage, d, assigned to different damage severity categories

The proposed framework operates on two different timescales: one for computational modeling (computational time step) and another for decision-making (decision time step). In this study, the computational time step is set to 10 minutes, while the decision time-step is 1 calendar month. To mimic real-world conditions, the agent operates without prior knowledge of the model but relies on observations. The agent's state representation at each time step includes:

1. Time from last maintenance, t_{lm}: represents the last time a successful maintenance was performed.

2. Time until decommissioning, t_{td}: remaining time of the life of the turbine.

3. Estimated maximum damage D_{max}: represents the maximum level of damage of the turbine as estimated through the model and updated through inspection data when available.

4. Current calendar month.

5. Average annual erosion rate, a_d: this is the prognostic feature for the agent representing the average annual erosion rate expected for the turbine given the information available.

At each decision step, the RL agent is presented with three possible actions: continue operating normally with no maintenance activities, attempt inspection, and attempt repair. The variable D_{max} is updated at each decision time step using the average annual erosion rate, unless new maintenance information is acquired. When new maintenance data, denoted as D_{ins}, becomes available, D_{max} is updated using the equation below:

$$D_{max} \rightarrow \frac{D_{max} + D_{ins}}{2} \tag{6.4}$$

The average annual erosion rate is initially set at 0.3, representing the average rate for the coating and the specific study site. Whenever new inspection data becomes available, a_d is updated using a weighted average, where the weights are proportional to the time between inspections. Greater weight is assigned to inspection data collected over longer intervals.

6.2.2 Decision-making framework

The decision-making process is executed by an agent trained using Reinforcement Learning. In this context, the agent is trained by interacting with the *environment*, receiving rewards and penalties to maximise a *reward* signal R. The problem is framed as a Markov Decision Process (MDP). Using this formalism, at each time step t, the agent receives some representation of the environment's *state*, $S_t \in \mathcal{S}$, and selects an *action*, $A_t \in \mathcal{A}(s)$. In the subsequent time step, the agent receives a numerical *reward*, $R_{t+1} \in \mathcal{R} \subset \mathbb{R}$ and receives the representation of the new state of the environment, S_{t+1}. In an MDP, the dynamics of the *environment* (S_t, R_t) are entirely characterised by the dynamics function $p(S, A)$ that depends only on the immediately preceding state and action (S_{t-1}, A_{t-1}).

$$p(s', r \mid s, a) \doteq \Pr\{S_t = s', R_t = r \mid S_{t-1} = s, A_{t-1} = a\}$$

Therefore, the interaction between agent and environment in a finite MDP gives rise to a trajectory $\{S_0, A_0\}, \{R_1, S_1, A_1\}, \ldots, \{R_T, S_T, A_T\}$ being T the termination state. The flexibility of the MDP framework makes it ideal for modeling O&M tasks, including the one addressed in this work. The final goal of the agent in RL is the maximisation of the cumulative sum of rewards, referred to as *return* G_t, following an action:

$$G_t = R_{t+1} + \gamma R_{t+2} + \gamma^2 R_{t+3} + \cdots = \sum_{k=t+1}^{T} \gamma^{k-t-1} R_k$$

being $\gamma \in [0, 1]$ the discount factor used in continuous task problems, where $T = \infty$, to avoid the potential issue of G_t approaching infinity. For finite episodic tasks, γ shall be

taken as 1 to avoid suboptimal solutions in the optimisation of G. However, reducing γ can aid in stabilising the training process and encourage riskier decision-making [132]. To assess the preference for different actions in a given state, the agent utilises *value functions* or *action-value functions*. The *action-value function* of a state s under a policy π, denoted $q_\pi(s, a)$, is defined as follows:

$$q_\pi(s, a) \doteq \mathbb{E}_\pi[G_t \mid S_t = s, A_t = a]$$

The optimal value function $q^*(s, a)$ provides the maximum values in all states and can be determined by solving the Bellman equation:

$$q^*(s, a) = \mathbb{E}[R(s, a) + \gamma \sum_{s'} P(s' \mid s, a) \max_{a'} q^*(s', a')] \tag{6.5}$$

the optimal policy π^* is then constructed by following:

$$\pi^*(s) = \arg\max_a q^*(s, a)$$

To achieve the optimal policy, one of the strategies is to make use of the *ε-greedy* policy, which can be expressed as follows:

$$A_t = \begin{cases} \arg\max_a q^*(s, a) & \text{with probability } 1 - \varepsilon \\ A \in \mathcal{A}(S_t) & \text{with probability } \varepsilon \end{cases} \tag{6.6}$$

where the agent balances the exploration, $\arg\max_a q^*(s, a)$ with the exploration, *random* action, by utilising the exploration rate, $\varepsilon \in [0, 1]$. Typical approaches consider a decaying exploration rate over time to explore more intensively the state space frequented by the best-known policy to the agent. In this case, the update rule for the exploration is as follows:

$$\varepsilon_i = \varepsilon_0 + (\varepsilon_f - \varepsilon_0) \cdot \frac{\min(i, f)}{f} \tag{6.7}$$

where i is the step, ε_0 the initial learning rate, and ε_f the final learning rate. The

values used were 0.6, 0.03 and 10^5 for ε_0 , ε_f and f, respectively.

Given the nature of the problem at hand, Temporal Difference (TD) learning methods, in which the values are updated online based on the difference of temporally successive estimates, can be beneficial. In this case, the method chosen to solve the problem is *Q-learning* [433]. *Q-learning* is an off-policy TD method used to find the action-value function of the states to find the optimal or nearly optimal policy. To address this problem, Deep Q Networks (DQN) are used for function approximation. The value $q(s, a)$ is approximated as $\hat{q}_\pi(s, a, w) \approx q_\pi(s, a)$, where w represents the set of weights for the DQN. This approach was chosen to improve the generalisation of the agent and better approach different regions of the state space given the continuous value of the damage state and the large state-action space of the problem. To use this method, two separate networks need to be kept, one called the online or behaviour network with weights w, which is the one being updated every step, and the target network, which shares architecture with the first but has a different weight vector w^- that is updated less frequently. In the agent's design, the weight vector update frequency C is set to 10^4 steps (months). The adoption of this approach, along with the use of the experience replay buffer M, help break the correlation of the sequence and stabilise the training of the agent. Throughout the learning process, Q-learning updates are applied to minibatches extracted from the experience replay, following the equation below:

$$w_{t+1} \leftarrow w_t + \alpha \frac{1}{N} \sum_{i=1}^{N} [R_i + \gamma \arg\max_{a_i} \hat{q}(s'_i, a'_i; w_t^-) - \hat{q}(s_i, a_i; w_t)] \cdot \nabla_w \hat{q}(s_i, a_i; w_t) \quad (6.8)$$

where the subindex i is used to denote the sample in the batch, and t is the time index at which the weights are updated. Here, α represents the learning rate, and N is the number of samples in the minibatch. The chosen size of the minibatch for the RL agent solving the LEE degradation O&M optimisation problem is 128. The weights learnt by the agent approximate the optimal state-action function $q^*(s, a)$ regardless of the followed policy. Then, the agent can approximate the optimal policy π^* by choosing the action with the greatest state-action value:

$$\widehat{\pi^*} = \arg\max_a \hat{q}^*(s, a; w) \approx \pi^* \tag{6.9}$$

The experiences from the replay buffer are not sampled uniformly but by a priority, P, assigned on its importance, using what is termed as prioritised replay buffer [346]. When stored in the replay buffer, each experience is assigned a priority based on its TD-error, creating what is termed a *prioritised replay buffer* [346]. These priorities are then used to calculate a probability distribution for sampling, which has been calculated as:

$$p_k = \frac{P(k)^\alpha}{\sum_{j=1}^{N} P(j)^\alpha} \tag{6.10}$$

With α as a parameter emphasising higher probabilities, p as the sampling probability of experience k, and N as the size of the experience replay buffer, sampling weights, denoted as w_s, are used to compensate for the bias introduced by the sampling probability distribution. These weights are calculated using the following expression:

$$w_{s_k} = \left(\frac{1}{N} \cdot \frac{1}{P(k)}\right)^\beta \tag{6.11}$$

During the training of the agent, the loss calculated for each experience is weighted by w_s to increase the importance of experiences with higher priorities. In this case, values of 0.6 and 0.4 were used for the parameters α and β, respectively.

The Deep Neural Network used is a fully connected network composed of three hidden layers with 300, 600, and 150 units, respectively, and it employs the $ReLU$ activation function. The output layer provides the state-action value, $\hat{q}(s, a; w)$, for each of the actions available for the agent. The activation function for the output layer is linear, allowing the network to provide negative q-values, as expected for the rewards of the environment. The optimisation algorithm chosen for training the network is ADAM [201], using a fixed learning rate, α, of 0.0001. The reward function defined for this problem is shown in Equation 6.12. The reward is composed of 3 terms, the aerodynamic losses, C_{aero}, the maintenance costs, C_{om}, and the downtime costs, C_{dt}. C_{aero} is computed as the difference in production between the original and the eroded power curves of the turbine, C_{om} using the costs provided in Table 6.2 and C_{dt} as

energy lost during downtime. Maintenance costs are obtained following the procedure depicted in Figure 6.5. This function is defined to produce rewards ≤ 0 for which a zero initialisation of Q-values will encourage exploration. The algorithm outlining the training of the RL agent is provided in Algorithm 1.

$$R_i = C_{aero} - C_{om} - C_{dt} \tag{6.12}$$

Algorithm 1 Deep Q-learning for wind turbine blade LEE O&M optimisation with experience replay buffer

Initialise priority replay buffer M to capacity N
Initialise action-value function $\hat{q}$ with random weights w
Initialise action-value function $\hat{q}$ for target network with weights $w^- = w$
Environment initialisation ▷ Wind turbine definition, Blade degradation power curves, weather data, maintenance success probabilities
Generate k transitions to pre-fill M using a random policy
for episode = 1, m **do**
    Reset environment, $s = s_0$
    Generate random material coating parameters C_1, C_2 and weather scenarios $I(t), u(t)$.
    for decision step $t_d = 1$,T **do**
        With probability ε select a random action a_t
        otherwise select $a_{t_d} = \arg\max_a \hat{q}^*(s, a; w)$
        execute action a_{t_d}
        while computation time $t_c \leq t_d$ **do**
            Accumulate impacted rain.
            Calculate real erosion degradation accrued, Δd.
            if $\Delta d \geq tol$ **then**
                Update turbine power curve due to erosion degradation.
            Accumulate energy production, ΔE.
            Calculate downtime and maintenance costs C_{dt} and C_{om}.
            Calculate erosion energy losses.
        Estimate blade damage state, D_{max}
        Generate reward r_{t_d+1} and next state s_{t_d+1}
        Observe r_{t_d+1} and s_{t_d+1}
        Store transition $(s_{t_d}, a_{t_d}, r_{t_d+1}, s_{t_d+1})$ in M
        Sample minibatch of transitions $(s_j, a_j, r_{j+1}, s_{j+1})$ from M
        Calculate average loss of transitions
        Perform training step with respect to network parameters w
        Every C steps reset $w^- = w$

6.3 O&M considerations

For the O&M simulations, the following assumptions were considered:

- Only the O&M costs related to blade damage due to LEE are considered in this study; no other failure modes are taken into account.
- Turbine operation is assumed to commence at the beginning of January.
- Imperfect repairs are considered, where the true damage state of each calculation point, denoted as d, is set to a value drawn from a Gaussian distribution with $d \sim \mathcal{N}(\mu, \sigma^2)$, where $\mu = 0.05$ and $\sigma = 0.001$, and truncated at the interval $[0, 1]$.
- Imperfect inspections are also considered, with inspected damage denoted as D_{ins}. Inspected damage follows a Gaussian distribution with parameters $\mu = d$ and $\sigma = 0.1$, truncated within the interval $[0, 1]$.
- If any real damage calculation point on the blade reaches $d = 1$, the turbine will be preventively stopped until it undergoes repair or replacement. This study assumes that when the blade reaches this degradation level, alarms from other systems such as SCADA will trigger the preventive shutdown.
- An energy cost of 50 GBP/MWh is considered, in line with the Contracts for Difference (CfD) strike price signed for CfD4 in the UK in 2022.
- Probabilistic definitions of repair success are discredited by month to mimic real O&M scheduling. The associated cost of a repair is a function of the damage and the month when the repair is attempted.
- For condition-based maintenance strategies, referred to as AC, repairs are attempted upon reaching an estimated damage, D, above a specified damage threshold.
- Energy production losses resulting from reduced aerodynamic performance of the blade due to erosion are considered, following the calculation framework outlined in [240] and summarised in this study.

- Energy production losses stemming from downtime and preventive stops are also taken into account.
- Maintenance costs are as specified in Table 6.2.
- Inspections are mandated for all maintenance strategies during the early operation phase of the turbine, specifically during months 3 to 6, to ensure more stable results that closely resemble real-life operations.

Table 6.1: Weather repair constraints.

Damage category	Logistic requirements	Duration (h)	Max. significant wave height (m)	Max 10-min avg. wind speed (m/s)
1: LE discoloration, paint or bugs	CTV, rope access	6	1.5	11
2: Coat/paint damage, surface: Missing less than 10 cm^2	CTV, rope access	15	1.5	11
3: Coat/paint damage, surface: Missing more than 10 cm^2 Damaged leading edge protection Damaged leading edge tape LE erosion, down to laminate	CTV, rope access	18	1.5	11
4: LE erosion, down to laminate and first layer laminate	CTV, crawler platform	40	1.5	12
5: LE erosion, through laminate / Open LE	HLV, blade dissassembly	72	1.8	10
6: LE erosion, blade failure	HLV, blade disassembly	72	1.8	10

Table 6.2: Repair costs per damage severity - 3 blades. Data obtained from [288] and [446]. m_b, m_a and m_e are the booking, access and execution costs, respectively.

Damage severity	m_b(£)	m_a(£)	m_e(£)
0 (Inspection)	1,600	1,000	3,200
1	2,000	1,000	4,000
2	2,000	1,000	4,000
3	3,000	1,000	6,000
4	5,000	1,000	36,000
5	0	250,000	3,500,000
6	0	250,000	5,000,000

This study models the maintenance success rate for a maintenance mission in three sequential steps as shown in Figure 6.5. First, it considers the probability of a given month to have wind and significant wave height values below the threshold, denoted as P_1. Second, it evaluates the probability of the forecasted weather complying with a

required weather window, known as P_2. Finally, it assesses the probability of the actual weather matching the weather predictions, labelled as P_3. The weather constraints for different maintenance methods and the required weather windows are provided in Tables 6.1 and 6.2. Synthetic weather data generation techniques, as described earlier, are used to obtain values for P_1 and P_2. In the absence of data, real weather is assumed to deviate from the forecast with increasing uncertainty. For the calculation of P_3 values, a Gaussian distribution is employed, centred on the forecast value, with a standard deviation increasing by 4% daily.

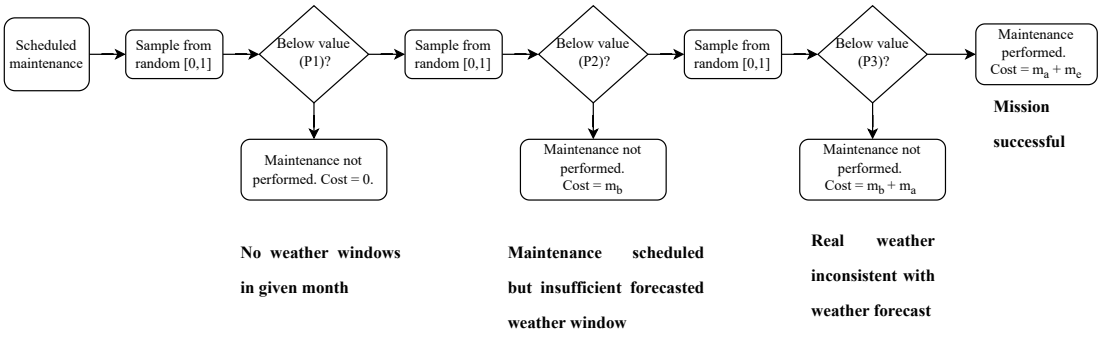

Figure 6.5: Repair modelling.

6.4 Case studies

To assess the effectiveness of the proposed framework, two case studies were conducted. Both cases share the same location and turbine model but differ in terms of maintenance success probabilities. In Case 2, there is a lower maintenance success rate and a more pronounced seasonal influence, resulting in a higher difference between the success rates during spring-summer and autumn-winter months. These probabilities are presented in Section D.1.

For these cases, the O&M costs related to leading-edge erosion were analysed under condition-based maintenance policies, AC, and the policies generated by the RL agents. Two AC policies were selected as baselines for comparison with the performance of RL agents: *AC 0.4* and *AC 0.3*. These AC policies initiate maintenance when the blade reaches 0.4 and 0.3 D_{max}, respectively. The results are analysed and compared in terms

of several aspects, including the average estimated damage throughout the turbine's lifetime, the estimated damage when maintenance is attempted, the evolution of the frequency of maintenance activities over time, the average time between maintenance actions in relation to the estimated annual damage rate, repair frequency per calendar month and the percentage of O&M actions taken. Finally, a thorough cost analysis based on a number of cost metrics is shown to compare the analysed policies.

Both case studies are situated at the FINO1 platform, located 45 km off the coast of Germany. The 5MW NREL offshore wind turbine serves as the model for simulating these scenarios, with its characteristics detailed in Table 6.3.

Table 6.3: 5 MW NREL Turbine data. Data extracted from [193]

Property	Value
Rated power	5 MW
Control	Variable speed, collective pitch
Drivetrain	High speed, multiple-stage gearbox
Rotor diameter	126 m
Hub height	90 m
Cut-In / Rated / Cut-out wind speed	3 m/s / 11.4 m/s / 25 m/s
Cut-in / Rated rotor speed	6.9 rpm, 12.1 rpm
Rated tip speed	80 m/s

For these case studies, a training period of 10^6 months was employed for training the RL agents. Simulations were conducted using γ values ranging from 0.95 to 1 at intervals of 0.01. The two best-performing agents are compared with condition-based maintenance strategies featuring damage repair thresholds of 0.3 and 0.4.

Both condition-based and RL maintenance strategies utilised updates in the estimated maximum damage, D_{max}, and the average annual erosion rate, a_d, to estimate the blade's condition. To evaluate the results of the various O&M strategies, 5,000 simulations spanning 25 years each were performed.

When assessing risk, the expected O&M cost value must be supplemented with additional metrics. Therefore, the policies will be compared based on the following metrics: Conditional Value at Risk ($CVaR_{0.95}$), which represents the average of values above the 95th percentile; the median; the expected cost (mean); and Value at Risk

($VaR_{0.95}$).

6.4.1 Case study 1

In this subsection, we present and analyse the results of Case Study 1. Figure 6.6 provides a summary of the most relevant aspects of the different policies. Figure 6.6a illustrates the evolution of the average maximum blade LEE damage over time. At the start of the operation, the 90^{th} percentile damage approaches the damage threshold of AC strategies. The periodic waviness in the data series is attributed to the seasonality of maintenance success probability, with a period of 12 months, and the distinct strategies employed for maintenance scheduling. AC strategies exhibit a more regular damage pattern compared to RL strategies. It's worth noting that RL strategies tend to utilise most of the LEE's lifespan before decommissioning. This tendency is more pronounced in the case of the *RL CS1* $\gamma = 0.98$ RL agent.

Figure 6.6b displays the distribution of D_{max} for the maintenance attempts of the different strategies. AC strategies follow an exponential-like distribution with peaks at their respective damage thresholds (0.3 and 0.4), which decrease with the success of maintenance activities. Conversely, the RL agents employ different strategies. *RL CS1* $\gamma = 1$ demonstrates a Gaussian distribution with a mean of 0.3, while *RL CS1* $\gamma = 0.98$ shows a wider Gaussian-like distribution with a mean around 0.35.

The frequency of attempted repair activities over the turbine's service life is presented in Figure 6.6c. AC strategies maintain a constant maintenance rate throughout the turbine's life, whereas RL strategies tend to accumulate more maintenance activities at the beginning of their service life and reduce them as decommissioning approaches. This trend is more pronounced in the *RL CS1* $\gamma = 0.98$ policy but is also evident in the *RL CS1* $\gamma = 1$ policy.

Figure 6.6d illustrates the average time between maintenance actions for the different policies analysed. *AC 0.4* shows the longest time between maintenance actions for all values of a_d. As expected, the time between maintenance actions for this policy is greater than *AC 0.3*. RL agents adopt different approaches, with *RL CS1* $\gamma = 0.98$ being closer to *AC 0.3*, while *RL CS1* $\gamma = 1$ follows a safer strategy for $a_d \leq 0.4$.

Figure 6.6e provides insights into the planning of maintenance activities by calendar month. It's important to note that this graph displays all maintenance attempts, not just the successful ones. *AC* policies show a curve with lower values in the months of April to October, with similar shapes and values. This is because maintenance success probabilities are higher during those months, reducing the need for maintenance actions in the coming months. In contrast, *RL* policies exhibit a different behavior, with a significant increase in maintenance planning intentions for the period from October to February. RL agents have learned the benefit of anticipating maintenance, as failure to do so would lead to an increase in the blade's damage state and higher maintenance costs. RL policies adopt a more conservative approach in this regard compared to *AC* policies.

Finally, Figure 6.6f presents the percentage of different actions taken. Given that *AC 0.4* has a higher damage repair threshold, it's expected that the 'operate' action is more frequent (85.29% of months) compared to *AC 0.3* (82.77%). The fixed inspections scheduled for all policies remain at 1.34%, with RL agents showing a marginal increase in the use of inspections (2.00% and 2.22% for *RL CS1* $\gamma = 1$ and *RL CS1* $\gamma = 0.98$, respectively). *RL CS1* $\gamma = 1$ employs the highest maintenance intention rate (16.98%), while *RL CS1* $\gamma = 0.98$ adopts a rate of 14.98%, falling between *AC 0.3* and *AC 0.4*.

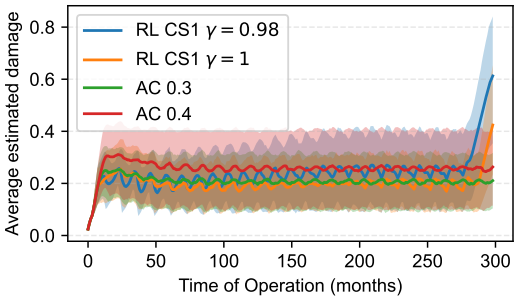

(a) Evolution of maximum estimated damage, D_{max} vs time of operation. The shadowed regions represent the 10-90 percentile band

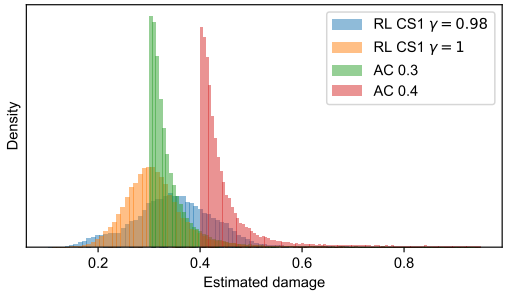

(b) Distribution of attempted repairs by estimated damage. *AC* policies have a fixed threshold while *RL* policies are left free to modify it to optimise expected O&M costs

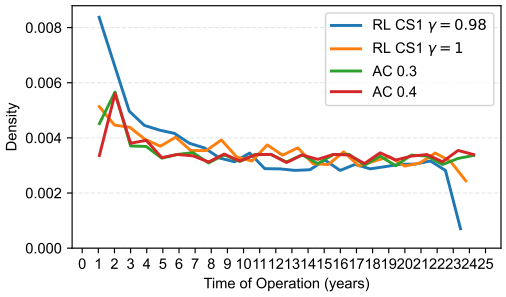

(c) Evolution of attempted repairs over the years of operation. *AC* policies have a fixed policy with forced inspections at the beginning of operation

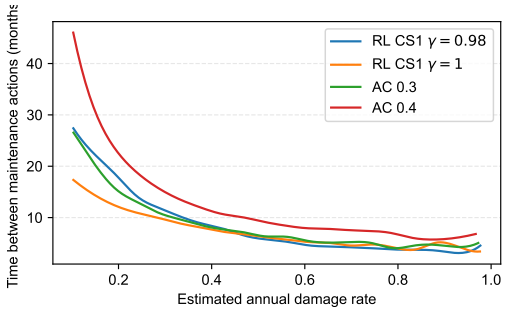

(d) Average time between maintenance actions vs estimated annual damage rate, a_d

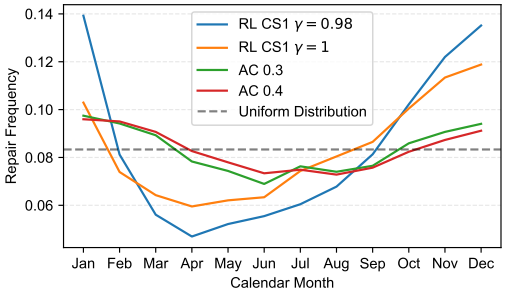

(e) Repair attempt frequency over calendar months. The dashed line represents the uniform maintenance planning distribution

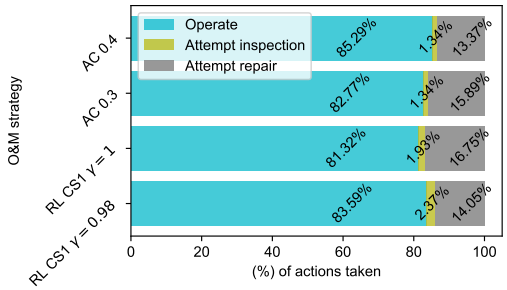

(f) O&M actions taken by the policies

Figure 6.6: Case study 1 O&M policy analysis

Figures 6.7 and 6.8 display the distribution of the O&M cost for the evaluated O&M maintenance policies, while Table 6.4 presents various cost metrics compared to the baseline policy *AC 0.3*. Concerning cost distribution, *AC 0.4* exhibits a higher

number of values at the lower end of the cost spectrum. This can be attributed to the fixed policy of *AC 0.4*, which entails some risk to the blade's condition but proves effective for scenarios involving slow damage growth.

In contrast, both *AC 0.3* and *RL CS1* $\gamma = 0.98$ show similar cost distributions, with a slight advantage in median values observed for *RL CS1* $\gamma = 0.98$. On the other hand, *RL CS1* $\gamma = 1$ outperforms in terms of the average, $CVaR_{0.95}$, and $VaR_{0.95}$ values. It presents reductions of 23.4%, 46.1%, and 8.7%, respectively, when compared to the *AC 0.3* policy, along with a marginal increase in the median value (8.5%).

RL CS1 $\gamma = 0.98$ closely resembles the behavior of *AC 0.3* by achieving a 5% reduction in median cost, with slight increases observed in the $CVaR_{0.95}$ and $VaR_{0.95}$ values. Conversely, *AC 0.4* displays a 12.1% reduction in the median value but experiences significant increases in the remaining metrics.

Table 6.4: Cost metrics for Case study 1

Label	Median	Average	$CVaR_{0.95}$	$VaR_{0.95}$
RL CS1 $\gamma = 0.98$	95.0%	100.7%	102.4%	105.4%
RL CS1 $\gamma = 1$	108.5%	78.6%	53.9%	91.3%
AC 0.3	100.0%	100.0%	100.0%	100.0%
AC 0.4	87.9%	192.0%	273.2%	432.8%

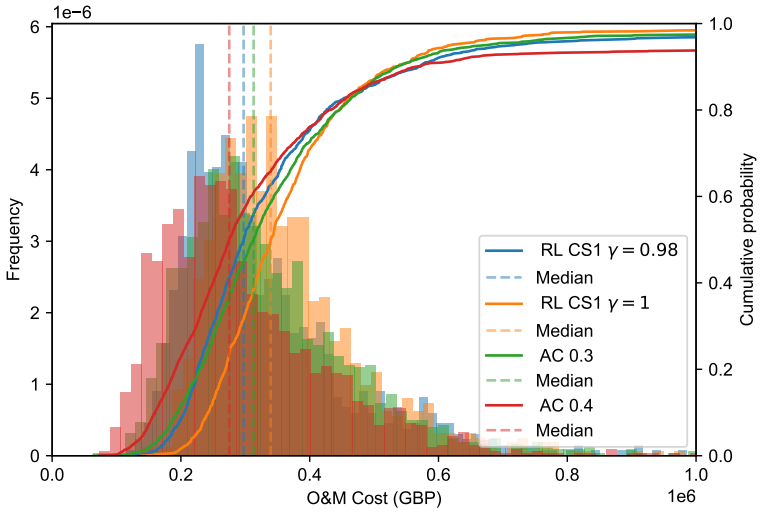

Figure 6.7: O&M cost distribution of the CS1 policies analysed. The dashed lines represent the median of the distribution. The right axis shows the cumulative probability of the distribution

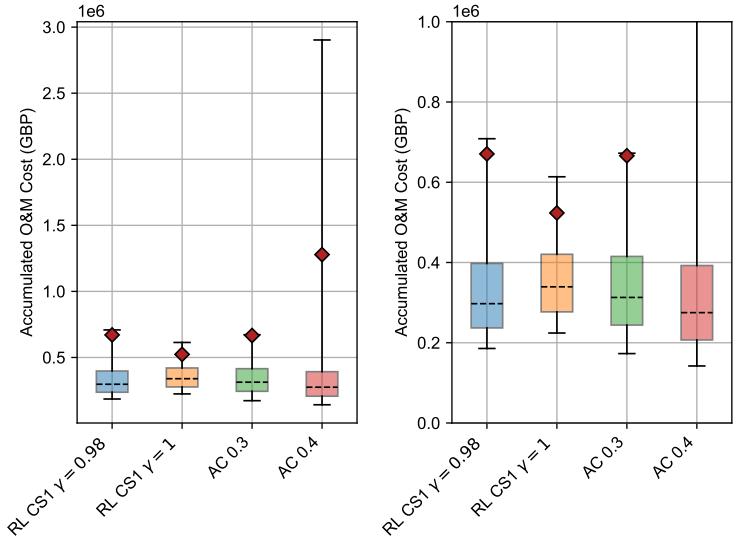

Figure 6.8: Cost distribution of CS1 O&M policies. The minimum and maximum values of the whiskers repesent P_5 and P_{95}, respectively and the red marker the average cost

6.4.2 Case study 2

In this subsection, we present and analyse the results of case study 2. Figure 6.9 summarises the most relevant aspects of the different policies. Figure 6.9a illustrates the

evolution of the average maximum blade LEE damage over the turbine's operational period. During the turbine's operation, the 90th percentile damage increases above the thresholds of the *AC* strategies, reaching 0.47 for *AC 0.4* and 0.39 for *AC 0.3*. The wavy pattern in the data series is attributed to the seasonality of maintenance success probability, exhibiting a periodic behaviour with a 12-month cycle, and the distinct strategies in maintenance scheduling. While *AC* strategies demonstrate a similar regularity in the damage pattern compared to RL strategies, the last 50 months of operation show a noticeable difference. RL strategies tend to make more extensive use of the blade's leading-edge erosion resistance before decommissioning. This trend is managed differently by *RL CS2* $\gamma = 0.98$ and *RL CS2* $\gamma = 0.99$, with the agent having $\gamma = 0.98$ progressively reducing the average damage.

Figure 6.9b presents the distribution of D_{max} for the maintenance attempts of various strategies. *AC* strategies exhibit an exponential-like distribution with peaks at their respective damage thresholds (0.3 and 0.4), which decrease with the success of maintenance activities. In contrast, the RL agents adopt different strategies. *RL CS2* $\gamma = 0.99$ showcases a Gaussian-shaped distribution with a mean around 0.3, while *RL CS2* $\gamma = 0.98$ displays a more skewed distribution, peaking around 0.4.

The frequency of attempted repair activities over the turbine's service life is shown in Figure 6.9c. *AC* strategies maintain a consistent maintenance rate throughout the turbine's life, whereas RL strategies aim to reduce repair activities as the turbine approaches the end of its operational life. Both RL strategies exhibit a peak in maintenance activities during the final years, with year 23 for *RL CS2* $\gamma = 0.99$ and years 20-21 for *RL CS2* $\gamma = 0.98$.

Figure 6.9d displays the average time between maintenance actions for the different policies analysed. *AC 0.4* shows the longest intervals between maintenance actions for all a_d. As expected, the time between maintenance actions in this policy is greater than that of *AC 0.3*. RL agents follow distinct policies, with *RL CS2* $\gamma = 0.98$ resembling the approach of *AC 0.3*, while *RL CS2* $\gamma = 0.99$ adopts a more cautious strategy for $a_d \leq 0.4$. However, *RL CS2* $\gamma = 0.99$ appears to face generalisation issues for $0.8 \leq a_d \leq 1.0$.

Figure 6.9e provides insight into maintenance planning by calendar month. Notably, this graph illustrates all maintenance attempts, not just the successful ones. *AC* policies and *RL CS2* $\gamma = 0.99$ exhibit a similar curve with lower values during the months from April to October. This behaviour aligns with higher maintenance success probabilities in those months, reducing the need for maintenance actions in the coming months. In contrast, the *RL CS2* $\gamma = 0.98$ policy deviates from this pattern, displaying a pronounced increase in maintenance planning from October to December.

Lastly, Figure 6.9f presents the percentage of different actions taken. As *AC 0.4* has a higher damage repair threshold, it is unsurprising that the "operate" action is more prevalent (77.37% of months) compared to *AC 0.3* (73.23%). Fixed inspections are scheduled for all policies at a rate of 1.34%, with RL agents demonstrating an increase in inspection usage, particularly *RL CS2* $\gamma = 0.98$ (13.3%) compared to *RL CS2* $\gamma = 0.99$ (5.61%). Furthermore, *RL CS2* $\gamma = 0.99$ exhibits a slightly higher repair intention rate than *AC 0.3* (25.95% vs. 25.44%), and *RL CS2* $\gamma = 0.98$ adopts a repair attempt rate of 23.12%, positioning it between *AC 0.3* and *AC 0.4*.

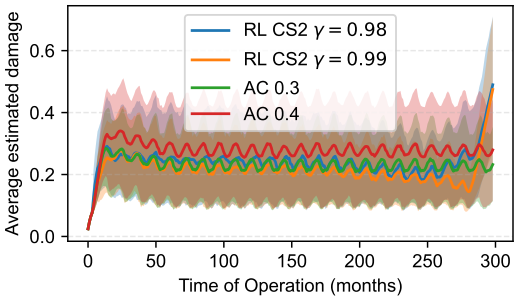

(a) Evolution of maximum estimated damage, D_{max} vs time of operation. The shadowed regions represent the 10-90 percentile band

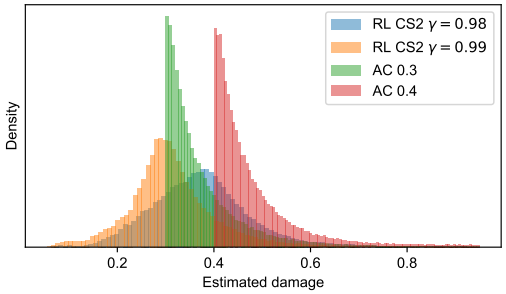

(b) Distribution of attempted repairs by estimated damage. *AC* policies have a fixed threshold while RL policies are left free to modify it to optimise expected O&M costs

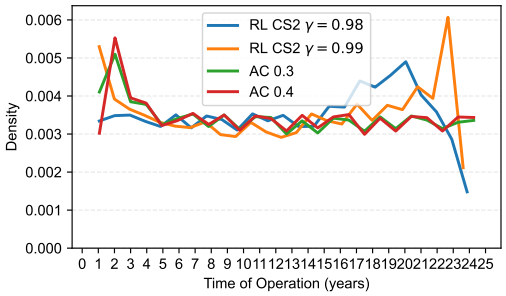

(c) Evolution of attempted repairs over the years of operation. *AC* policies have a fixed policy with forced inspections at the beginning of operation

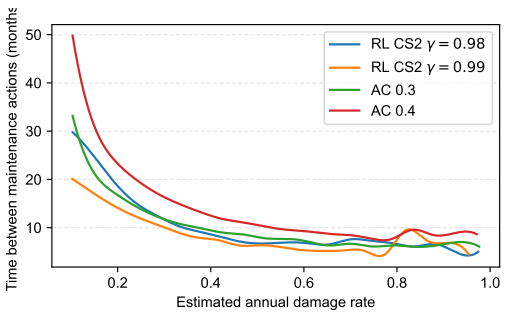

(d) Average time between maintenance actions vs estimated annual damage rate, a_d

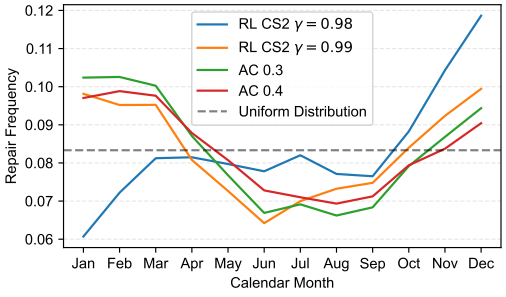

(e) Repair attempt frequency over calendar months. The dashed line represents the uniform maintenance planning distribution

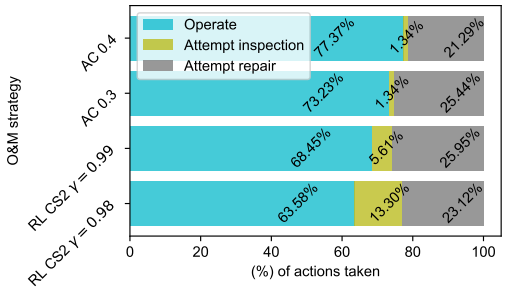

(f) O&M actions taken by the policies

Figure 6.9: Case study 2 O&M policy analysis

Figures 6.10 and 6.11 display the distribution of O&M costs for the evaluated O&M maintenance policies, and Table 6.5 presents various cost metrics compared to the baseline policy, *AC 0.3*. Regarding cost distribution, *AC 0.4* has more values in the

lower end, which can be attributed to the fixed policy of *AC 0.4* taking risks with the blade's condition and being successful for slowly growing damage cases. *AC 0.3* reaches a higher cumulative probability (0.91) at £1.5 million than *AC 0.4* (0.88), while higher values are achieved by RL policies, specifically *RL CS2* $\gamma = 0.98$ (0.948) and $\gamma = 0.99$ (0.95). In terms of cost metrics, *RL CS2* $\gamma = 0.98$ and $\gamma = 0.99$ outperform *AC 0.3*, with reductions in the range of 12-13%, 16-19%, and 73-78% for Average, $CVaR_{0.95}$, and $VaR_{0.95}$, respectively. They also exhibit a slight increase in the median value (11.5% and 6.2%, respectively). In contrast, *AC 0.4* shows a 6.2% reduction in the median value but experiences significant increases in the other metrics.

Table 6.5: Cost metrics for Case study 2

Label	Median	Average	$CVaR_{0.95}$	$VaR_{0.95}$
RL CS2 $\gamma = 0.98$	111.5%	86.8%	80.9%	26.9%
RL CS2 $\gamma = 0.99$	106.2%	87.3%	84.0%	21.7%
AC 0.3	100.0%	100.0%	100.0%	100.0%
AC 0.4	93.8%	159.4%	154.4%	308.5%

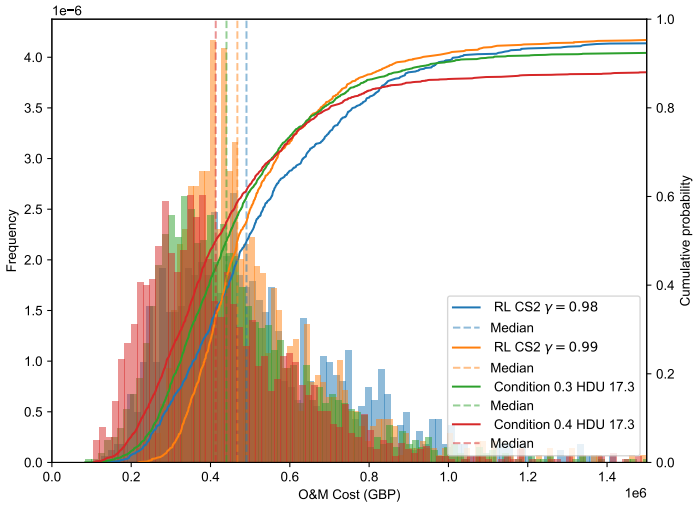

Figure 6.10: O&M cost distribution of the CS2 policies analysed. The dashed lines represent the median of the distribution. The right axis shows the cummulative probability of the distribution

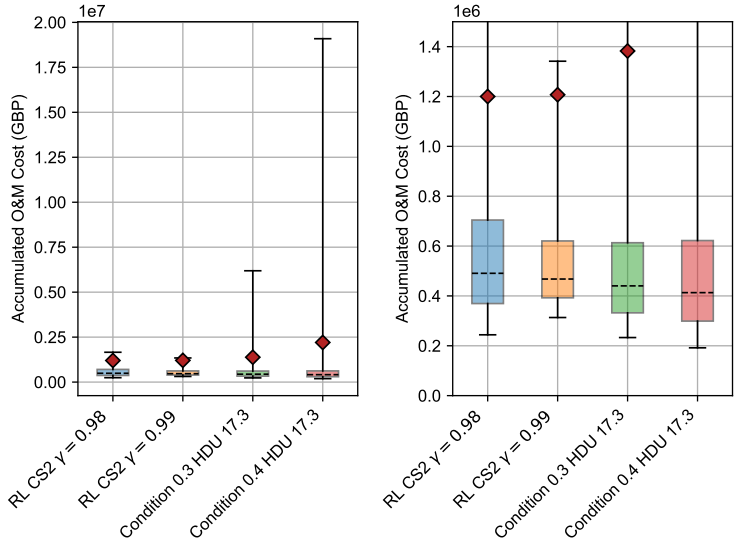

Figure 6.11: Cost distribution of CS2 O&M policies. The minimum and maximum values of the whiskers represent P_5 and P_{95}, respectively. The right plot is a zoomed in version of the left one

6.5 Discussion

The analysis of both case studies has led us to the conclusion that RL agents have been able to improve the target metric of the optimization, which is the expected value of the O&M cost, within a certain range. Additionally, γ values between 0.98 and 1.0 have proven to be the most effective in achieving this reduction. Alongside the reduction in average costs, there was also a decrease in several relevant cost metrics related to risk-based decision-making, such as $CVaR_{0.95}$ and $VaR_{0.95}$. This reduction comes with an increase in the median cost, making the condition-based policies (AC) more cost-efficient in some cases. Overall, RL agents have successfully identified a cost advantage by reducing maintenance activities towards the end of the turbines' operational life. The use of inspections by RL agents has increased as maintenance success rates decreased; the inspection intention rate grew from 2.0% in CS1 to a range of 5-13% in CS2, explaining the importance of a reduced uncertainty of the damage state for low accessibility sites. Regarding maintenance planning by calendar month, RL agents did not provide a clear indication of a single planning strategy.

The presented framework has proven to be effective in high-uncertainty scenarios, with the material parameters C_1 and C_2 having the greatest influence on the degradation dynamics. This information is valuable for the initial planning of the O&M of the turbine. To reduce the uncertainty in the degradation dynamics, the probabilistic description of the abovementioned parameters can be modified once real operation data becomes available to improve the performance of the agent. Unfortunately, the modification of the description of the stochastic variables requires the retraining of the agent, which can be time-consuming.

This framework can be used by operators at the early O&M design stage at the wind farm level. By analysing the behavior of the best agents, important qualitative metrics can be extracted to define global policies such as the damage threshold for optimal maintenance scheduling for a particular failure mode if considered alone. If combined with additional components and failure modes, this framework can provide O&M policies at the wind turbine level. In this study, only the leading-edge erosion failure mode of the blade was considered. Nevertheless, it can be extended to accommodate different failure modes as long as a degradation function can be defined. This would require the inclusion of, at least, two parameters for the DQN per failure mode. One of the parameters would be the estimation of the state of the component and failure mode, and the other a prognostic parameter to improve the O&M planning of the agent. The selection of the failure modes to consider should be based on risk priority to provide efficiency to the framework.

In this study, material parameters C_1 and C_2 have been assumed to remain constant throughout the life of the turbine. It is important to note that there are many types of repair available (protection tapes, protective coatings, and epoxy or polyurethane fillers) the durability of which is not well known yet. An interesting opportunity to overcome this issue would be the inclusion of SHM in the turbine to provide timely inspection data. Moreover, this would reduce the cost of inspection data for low-accessibility sites, which has proven to be determinant for O&M for cost reduction. Also, there is potential for improvement in the quantification of uncertainty in the damage state and prognostic features of the agent. In the proposed definition of the RL agent, there is

no quantification of the uncertainty about $D_{\max}$ and a_d made by the agent, which can be bypassed by the usage of the parameters t_{tm} and t_{td}. Another interesting direction of providing additional functionality to this framework would be the inclusion of opportunistic maintenance as an action for the agent. It would be interesting to explore the damage level at which opportunistic maintenance becomes attractive, as this is sometimes the case when unexpected failures of different components of the turbines occur.

6.6 Conclusions and further remarks

In this chapter, a comprehensive framework designed for the development of an autonomous decision-making agent has been presented. The proposed framework is grounded in the RL paradigm, training the agent to make independent decisions for O&M activities. It specifically addresses uncertainties inherent in damage evolution, climatic conditions, and repair success rates.The proposed O&M blade LEE maintenance optimisation based on RL is able to produce an improvement in average costs in the range 12-21% and a reduction in risk of failure of the blades under this failure mode against condition-based policies. This framework has proven to be robust as to produce consistent improvements in different settings. Besides, the provided framework has the option to be re-trained with real data of different turbines of a site during operation to reduce the uncertainty in the material parameters and approximate better the degradation dynamics of this failure mode.

The versatility of this framework extends to various applications, notably serving as a tool for online O&M decision support and facilitating the early-stage design of O&M strategies, particularly in the context of the identified failure mode. Furthermore, this framework lays the groundwork for a more sophisticated O&M representation that encompasses all components of a wind turbine or extends to the entire wind farm.

Notwithstanding, the high uncertainty underlying this problem sets a difficult scenario for decision-making in which the interpretability of the recommendations and the models used is key for practitioners to modify their current way of operating. Also, the need to incorporate the risk-critical failure modes to produce a common mainte-

nance strategy calls for computationally efficient frameworks in which the logistics of the whole wind farm is considered and the opportunities for maintenance actions when not strictly required can be studied. In order to reduce the complexity of the models, a thorough understanding of the problem at hand is required, and this is why frameworks such as the proposed are required. Once there is a more profound knowledge about the dynamics of the failure mode and the relevance of different parameters modifying them, computationally efficient reduced-order models can be built for strategic wind farm decision-making. Techniques such as intelligent PN [337, 338] are promising for this last step in which the maintenance optimisation of assets in similar conditions can be jointly considered.

Beyond its immediate applications, this tool has the potential to establish a foundation for a higher-level O&M approach, accommodating additional failure modes. This flexibility becomes evident when incorporating degradation functions and prognostic features, thus enabling a more comprehensive consideration of diverse failure scenarios.

In essence, the designed framework not only addresses the intricacies of the identified failure mode but also sets the stage for a broader and more advanced O&M decision-making system that can adapt to evolving conditions and encompass a wider array of potential failure modes across wind turbine components and wind farm levels.

Chapter 7

Discussion

Reinforcement learning stands out as a potent method for crafting autonomous decision-making systems, offering diverse techniques adaptable to various problem domains and input natures, be they data-based, physics-based, or hybrid. The primary challenge in employing models, as proposed in this thesis, lies in striking a delicate balance between accuracy and computational demands, particularly when confronted with constraints in dimensionality. Models developed herein can incur substantial computational expenses, escalating with the addition of numerous failure modes and degradation functions. Acquiring sufficient data representing a diverse array of failure modes proves challenging, especially considering the variety of systems available in the market. This underscores the pressing need for detailed knowledge on different failure modes to construct surrogate models that are both robust and computationally efficient. Additionally, strategic maintenance planning necessitates varying levels of representation, prompting the careful selection of the level of detail in system modeling.

The framework presented herein finds practical application for operators in the early Operations and Maintenance (O&M) design phase at the wind farm level. Through an analysis of optimal agent behavior, qualitative metrics emerge, facilitating the establishment of overarching policies, such as defining damage thresholds for efficient maintenance scheduling in isolation for a specific failure mode. When integrated with additional components and failure modes, the framework's adaptability extends to formulating O&M policies at the wind turbine level. Although the study exclusively

focused on the leading-edge erosion failure mode of the blade, its versatility allows the incorporation of various failure modes, contingent upon the definition of a degradation function. This extension requires at least two parameters for the Deep Q-Network (DQN) per failure mode—one for estimating the state of the component and failure mode and another as a prognostic parameter to enhance the O&M planning of the agent. The choice of which failure modes to consider should prioritise risk, optimising the framework's efficiency. Once trained for a specific site, the model is poised to provide real-time recommendations based on the current condition of the blade.

Integrating additional failure modes into the proposed agent mandates defining the degradation model of the failure mode and prognostic features for the agent to consider. While the method can be retrained with real data to enhance performance, its computational expense and the necessity for multiple iterations to find an optimal policy candidate pose challenges. Tuning hyperparameters is non-trivial, requiring problem-specific knowledge and iterative adjustments to establish a feasible range. Moreover, modifying the problem by adding failure modes or altering climatic parameters for a different site may necessitate a reevaluation of hyperparameters, incurring additional computational costs.

The proposed model has effectively reduced Operations and Maintenance (O&M) costs and mitigated failure risks associated with offshore wind turbine blades under Leading Edge Erosion (LEE). However, the results lack contrast with real operational data due to accessibility challenges. Given the high uncertainty in coating behavior compared to WARER test data, it is anticipated that the model's accuracy will improve with the inclusion of real operational data.

7.1 Contribution

This section aims to consolidate the findings and substantiate the contribution of the thesis and the approach followed to fulfill the objectives. The overall contribution The overall contribution of this work is analysed from the perspectives of novelty, scientific soundness and value to the different stakeholders.

Table 7.1 presents a summary of the objectives of the research project, how they are

addressed through the research performed, along with the contribution of each objective in terms of novelty, scientific soundness and value to the different stakeholders.

The first objective was addressed through a literature review of the maintenance practices used for wind turbine blades and other safety-critical composite structures. Furthermore, the benefits and limitations in the use of composite structures for this kind of applications in different sectors (Aerospace, Civil, Naval and Wind) was analysed. This review provides an overview of the current state of the art of the maintenance models applied to wind turbines along with the limitations experienced in the current market. This review can be valuable primarily to researchers and academics in O&M problems, listing latest applications of different maintenance methods and highlighting benefits and limitations of each method.

Chapter 3 provided an FMECA to identify the most risk-critical failure modes and subcomponents of the wind turbine blade. Leading edge erosion, root-hub connection damage, spar caps and web damage, lightning strike damage, and the debonding of leading and trailing edges were identified as the most critical failure modes of the blade. Potential SHM technologies were also proposed for the failure modes identified. Furthermore, the spar and the leading edge were highlighted as the most critical subcomponents of the blade. This study can be useful for O&M wind industry practitioners that need to stablish a maintenance policy for a wind farm.

Table 7.1: Contribution of research analysed by means of novelty, scientific soundness and value per each set objective

Set objective	**Novelty** *What is new?*	**Scientific Soundness** *What methods have been used and how have they been validated?*	**Value to different stakeholders** *Who will benefit from this part of the work?*
Assemble a state-of-the-art literature review of current maintenance methods for wind turbine blades	The produced literature review responds to a unique research question: What are the current maintenance methods applied to wind turbine blades?	The most relevant papers regarding maintenance of safety-critical composite structures of 4 different sectors (Civil, Wind, Naval and Aerospace) have been reviewed.	This review can be valuable primarily to researchers and academics in O&M problems, listing latest applications of different maintenance methods and highlighting benefits and limitations of each method.
Identify the most critical failure modes of a wind turbine blade	The chapter produced offers a view of the most critical failure modes and subcomponents of a generic wind turbine blade along with potential monitoring techniques.	The work was performed following a systematic FMECA analysis to rank the criticality of the different failure modes and subcomponents.	This work can be useful for O&M wind industry practitioners that need to stablish a maintenance policy for a wind farm.
Provide a degradation function to evaluate O&M policies	The work that has been presented in this thesis proposes a degradation computational framework for LEE considering aerodynamic efficiency losses of the blade.	CFD simulations were performed to estimate erosion-related aerodynamic properties modifications. The AEP losses and coating service lifetimes resulting from the simulations using the proposed framework are in line with those reported in other works.	The proposed framework can be valuable for researchers and O&M practitioners to evaluate the service life and estimated AEP losses for different LEP coatings.
Provide a risk-based tool to evaluate baseline calendar-based LEE maintenance scheduling policies	This work provides a tool to evaluate the cost-benefit of different candidates calendar-based maintenance policies to stablish a baseline policy at wind farm level.	The computational framework presented in chapter 4 was used to provide the degradation function of the blade and a reliability analysis was perform on the LEE failure. A reliability function for LEE damage was proposed. Unfortunately, no validation against real operation data has been able to be performed, but the results align with the data expected from the literature in terms of service life of coatings.	This tool can be of use for wind farm operators to compare candidate calendar-based LEE maintenance policies at wind farm level.
Design an autonomous decision-making system for blade's O&M.	The work presented in chapter 5 provides the definition of an autonomous RL-based agent for O&M decision making for offshore wind turbine blades under LEE damage.	Deep Q networks have been used alongside RL to provide the basis for the decision-making. The agent has been trained to optimise the expected O&M costs considering uncertainty in weather, damage evolution and maintenance success.	This tool can be of use for wind farm operators as an online decision-support tool for LEE maintenance at wind turbine level and to extract knowledge from it.

Following on from the failure mode identification, Chapter 4 focuses on providing a degradation function for LEE, one of the most risk critical failure modes. The proposed framework provides the estimated service life of a protection coating and expected AEP reduction considering weather uncertainty. This can be a useful tool when performing life cycle cost comparisons of different coatings and O&M simulations considering this failure mode.

Making use of the proposed degradation function, a risk-based maintenance selection tool for calendar-based LEE maintenance policies was presented in Chapter 5. This tool considers the uncertainty in coating behaviour, weather and repair success. This tool can be useful for O&M practitioners when designing preliminary policies, given that it provides a direct way to compare candidate policies and find a good balance between PoF and cost for this failure mode.

Finally, Chapter 6 provides the definition of an autonomous decision-making agent for wind turbine blade O&M optimisation. This agent is based on Reinforcement learning and provides the approximation of the action-value function by means of Deep Q Networks. Combining this agent with the proposed degradation function from Chapter 4, the maintenance lifecycle costs of this failure mode can be optimised. This work provides a valuable framework for prognostics-based O&M optimisation of wind turbine blades that can accommodate additional failure modes by including degradation function, required state parameters describing the damage and a useful prognostic feature.

Chapter 8

Overall conclusions and future work

The aim of the research presented in this Thesis is to provide insight into the following research question:

"How an autonomous decision-making system to support O&M for wind turbine blades based on prognostics can be designed?"

Each of the chapters has presented research to build up the steps to provide insight into the primary research question, however it is now important to discuss these findings in its context. The conclusions below will attempt to bring out the pertinent findings of each chapter, however full detail along with all uncertainties, assumptions and discussion can be found in each individual chapter. This chapter will conclude by outlining future work, and provide an overview of how the research and conclusions presented will contribute to the wind industry.

8.1 Conclusions

Chapter 2 has presented an overview of the current landscape of maintenance practices in the wind industry, specifically focusing on turbine blades and the challenges associated with applying Prognostics and Health Management practices to safety-critical composite structures. The utilisation of composite materials in the wind sector intro-

duces various challenges, including uncertainties related to failure modes, difficulties in monitoring damage progression during operational use, and reliability issues in manufacturing large composite components.

While monitoring systems for drive train and gearbox components, leveraging data from SCADA and other vibration control systems, have been successfully implemented, blade monitoring remains in its early stages. Despite an expanding body of research offering promising solutions, existing SHM systems for wind turbine blades provide data under controlled conditions, yielding meaningful damage indicators. However, there is insufficient substantiated evidence regarding the performance of these systems over extended durations and in challenging environmental conditions, raising concerns about the potential drawbacks of non-durable SHM systems, such as increased maintenance costs and downtime.

Currently, the dominant approach to wind turbine maintenance relies on visual and tap test inspections, often supplemented by calendar-based campaigns. As discussed in this chapter, this method has limitations, particularly in detecting subtle impact damage that may go unnoticed. The implementation of SHM or CBM systems for continuous structural assessment proves to be an effective strategy for extending the service life of wind turbines. This approach is most advantageous when combined with an analysis of factors influencing Operations and Maintenance (O&M) costs and critical failure modes of the system.

In the realm of offshore wind farms, where operation and maintenance costs are projected to constitute approximately 30% of the total life cycle costs, integrating SHM technology and adopting a predictive maintenance approach through PHM can significantly contribute to cost reduction by considering the structural condition. Furthermore, this approach has the potential to enhance overall profitability and turbine availability, aligning with the overarching goal of this thesis.

In order to offer a comprehensive understanding of the system and address its most crucial failure modes, it is essential to adopt a systematic approach for identifying these modes at the component level. Chapter 3 takes on this task by conducting an FMECA specifically for the wind turbine blade. This analysis meticulously pinpoints

the most critical subcomponents and failure modes inherent to the wind turbine blade. The study illuminates that among the identified failure modes, leading edge erosion, damage to the root-hub connection, issues with spar caps and web integrity, lightning strike damage, and the debonding of both leading and trailing edges stand out as the most critical. Furthermore, the analysis singles out the spar and leading edge as the most critical subcomponents within the wind turbine blade system. This FMECA, thus, provides valuable insights into the vulnerabilities of the system, facilitating a more targeted and informed approach to addressing potential failures.

Armed with this information, the next step involves establishing degradation functions for the most critical failure modes and identifying prognostic features to address the assessment of damage progression. Chapter 4 takes on this task by outlining a computational framework specifically for Leading Edge Erosion (LEE) degradation. Within this framework, an estimation of the aerodynamic consequences of leading edge erosion is also presented, shedding light on its impact on the Annual Energy Production (AEP) reduction.

This computational framework is adept at generating the anticipated degradation state of a blade affected by LEE, taking into account data from the Wind Turbine Blade Erosion (WARER) test and site-specific climatic parameters. Furthermore, it offers insights into the power degradation of the wind turbine, taking into consideration the compromised state of the blade.

Upon establishing a degradation function for a specific failure mode, the optimisation of O&M activities becomes viable. Chapter 5 initiates this process by focusing on calendar-based optimisation at the wind farm level for the identified failure mode. While this approach may yield suboptimal policies when applied at the individual wind turbine level, it serves as a foundational reference point for crafting maintenance policies during the early stages. Additionally, it offers an anticipated cost for the O&M of the blade.

This chapter equips O&M practitioners with a valuable tool for evaluating potential maintenance strategies, allowing them to analyse cost-benefit relationships through metrics related to risk and expenditure. By providing insights into the expected costs

associated with various maintenance approaches, it facilitates informed decision-making in optimising O&M practices for enhanced efficiency and effectiveness.

Having established the initial framework for O&M optimisation, the opportunity arises to explore a condition-based approach. Chapter 6 delves into the depiction of an autonomous RL-based agent designed to optimise O&M costs. Employing Deep Q-Networks, this agent focuses on refining O&M decisions concerning LEE, accounting for uncertainties in climatic parameters, dynamics of damage evolution, and the efficacy of maintenance activities. The approach introduces a fundamental prognostic feature—the average degradation rate—to address the problem.

In the presented case study, the prevailing scenario, where the blade's state is typically revealed through inspections, is taken into account. This method has demonstrated its effectiveness in reducing expected O&M costs compared to basic CBM approaches. Moreover, it has proven successful in minimising catastrophic failures associated with blade deterioration.

8.2 Future Work

Neural networks, offering complex function approximations, often yield challenging-to-interpret weights, necessitating exploration into enhancing the interpretability of decision support systems. Extracting knowledge from system recommendations holds the potential to provide valuable insights for optimising efficiency and reducing the expansive search space inherent to these systems. Moreover, garnering knowledge from system outputs can contribute to a more accurate high-level representation for strategic decisions.

Reducing the training time of the agent represents a promising avenue for future work. Injecting expert knowledge or leveraging transfer learning from agents in similar environments could expedite training by allowing the agent to focus on critical regions. However, caution is warranted to avoid overly constraining the agent's freedom to explore, preventing it from inadvertently settling into suboptimal regions.

Addressing the challenges of high-level representations for Operations and Maintenance (O&M) optimisation at the wind farm level requires careful consideration.

Given the complexities of managing numerous turbines, their diverse components, failure modes, and logistical constraints, an intriguing approach involves the utilisation of intelligent Petri Nets (PNs) [338]. These PNs efficiently represent damage states across different components and turbines, making them well-suited for integration with Reinforcement Learning (RL)-based agents.

The exploration of smart operation modes for fatigue and Leading Edge Erosion (LEE) damage reductions presents an interesting avenue for preventing damage progression. Investigating the cost-effectiveness of damage arrest or prevention and identifying optimal scenarios for their implementation could provide valuable insights. Additionally, incorporating additional actions into O&M models offers a promising direction for enhancing the existing framework. Analysing the implications of various actions, such as curtailment, and exploring how they can mitigate turbine downtime losses during maintenance tasks would contribute to a more comprehensive understanding of the system dynamics.

Appendix A

Sustainable Development Goals

A.1 Sustainable Development Goals

Appendix A. Sustainable Development Goals

Table A.1: The 17 Sustainable Development Goals (SDGs). Source [418].

Sustainable Development Goals
Goal 1: No poverty *End poverty in all its forms everywhere.*
Goal 2: Zero hunger *End hunger, achieve food security and improved nutrition and promote sustainable agriculture.*
Goal 3: Good health and well-being *Ensure healthy lives and promote well-being for all at all ages.*
Goal 4: Quality education *Ensure inclusive and equitable quality education and promote lifelong learning opportunities for all.*
Goal 5: Gender equality *Achieve gender equality and empower all women and girls.*
Goal 6: Clean water and sanitation *Ensure availability and sustainable management of water and sanitation for all.*
Goal 7: Affordable and clean energy *Ensure access to affordable, reliable, sustainable and modern energy for all.*
Goal 8: Decent work and economic growth *Promote sustained, inclusive and sustainable economic growth, full and productive employment and decent work for all.*
Goal 9: Industry, innovation and infrastructure *Build resilient infrastructure, promote inclusive and sustainable industrialization and foster innovation.*
Goal 10: Reduced inequalities *Reduce inequality within and among countries.*
Goal 11: Sustainable cities and communities *Make cities and human settlements inclusive, safe, resilient and sustainable.*
Goal 12: Responsible consumption and production *Ensure sustainable consumption and production patterns.*
Goal 13: Climate action *Take urgent action to combat climate change and its impacts.*
Goal 14: Life below water *Conserve and sustainably use the oceans, seas and marine resources for sustainable development.*
Goal 15: Life on land *Protect, restore and promote sustainable use of terrestrial ecosystems, sustainably manage forests, combat desertification, and halt and reverse land degradation and halt biodiversity loss.*
Goal 16: Peace, justice and strong institutions *Promote peaceful and inclusive societies for sustainable development, provide access to justice for all and build effective, accountable and inclusive institutions at all levels.*
Goal 17: Partnerships for the goals *Strengthen the means of implementation and revitalize the global partnership for sustainable development.*

Table A.2: Boolean indicators of contribution of composite materials to SDGs 1 to 8, as per considered industries.

Target	Aerospace	Civil	Wind	Naval
1.1	0	0	0	0
1.2	0	0	0	0
1.3	0	0	0	0
1.4	0	0	0	0
1.5	0	0	0	0
1.A	0	0	0	0
1.B	0	0	0	0
Total	**0/7**	**0/7**	**0/7**	**0/7**

(a) SDG 1

Target	Aerospace	Civil	Wind	Naval
2.1	0	0	0	0
2.2	0	0	0	0
2.3	0	1	1	0
2.4	0	0	1	0
2.5	0	0	0	0
2.A	0	0	0	0
2.B	0	0	0	0
2.C	0	0	0	0
Total	**0/8**	**1/8**	**2/8**	**0/8**

(b) SDG 2

Target	Aerospace	Civil	Wind	Naval
3.1	0	0	0	0
3.2	0	0	0	0
3.3	0	0	0	0
3.4	0	0	0	0
3.5	0	0	0	0
3.6	0	0	0	0
3.7	0	0	0	0
3.8	0	0	0	0
3.9	1	0	1	1
3.A	0	0	0	0
3.B	0	0	0	0
3.C	0	0	0	0
3.D	0	0	0	0
Total	**1/13**	**0/13**	**1/13**	**1/13**

(c) SDG 3

Target	Aerospace	Civil	Wind	Naval
4.1	0	0	0	0
4.2	0	0	0	0
4.3	0	0	0	0
4.4	0	0	0	0
4.5	0	0	0	0
4.6	0	0	0	0
4.7	0	0	0	0
4.A	0	0	0	0
4.B	0	0	0	0
4.C	0	0	0	0
Total	**0/10**	**0/10**	**0/10**	**0/10**

(d) SDG 4

Target	Aerospace	Civil	Wind	Naval
5.1	0	0	0	0
5.2	0	0	0	0
5.3	0	0	0	0
5.4	0	0	0	0
5.5	0	0	0	0
5.6	0	0	0	0
5.A	0	0	0	0
5.B	0	0	0	0
5.C	0	0	0	0
Total	**0/9**	**0/9**	**0/9**	**0/9**

(e) SDG 5

Target	Aerospace	Civil	Wind	Naval
6.1	0	0	1	0
6.2	0	0	0	0
6.3	1	1	1	1
6.4	0	1	0	0
6.5	0	0	0	0
6.6	0	0	0	0
6.A	0	0	0	0
6.B	0	0	0	0
Total	**1/8**	**2/8**	**1/8**	**1/8**

(f) SDG 6

Target	Aerospace	Civil	Wind	Naval
7.1	0	0	1	0
7.2	0	0	1	0
7.3	1	1	1	1
7.A	0	1	1	0
7.B	0	1	1	0
Total	**1/5**	**3/5**	**5/5**	**1/5**

(g) SDG 7

Target	Aerospace	Civil	Wind	Naval
8.1	0	0	0	0
8.2	1	1	1	1
8.3	0	0	0	0
8.4	1	1	1	1
8.5	0	0	0	0
8.6	0	0	0	0
8.7	0	0	0	0
8.8	0	0	0	0
8.9	0	0	0	0
8.A	0	0	0	0
8.B	0	0	0	0
Total	**2/11**	**2/11**	**2/11**	**2/11**

(h) SDG 8

Table A.3: Boolean indicators of contribution of composite materials to SDGs 9 to 16, as per considered industries.

Target	Aerospace	Civil	Wind	Naval
9.1	0	1	1	0
9.2	1	1	1	1
9.3	0	0	0	0
9.4	1	1	1	1
9.5	1	1	1	1
9.A	0	1	1	1
9.B	1	1	1	1
9.C	0	0	0	0
Total	**4/8**	**6/8**	**6/8**	**5/8**

(a) SDG 9

Target	Aerospace	Civil	Wind	Naval
10.1	0	0	0	0
10.2	0	0	0	0
10.3	0	0	0	0
10.4	0	0	0	0
10.5	0	0	0	0
10.6	0	0	0	0
10.7	0	0	0	0
10.A	0	0	0	0
10.B	0	0	0	0
10.C	0	0	0	0
Total	**0/10**	**0/10**	**0/10**	**0/10**

(b) SDG 10

Target	Aerospace	Civil	Wind	Naval
11.1	0	1	0	0
11.2	1	1	1	1
11.3	0	0	0	0
11.4	0	0	0	0
11.5	0	0	0	0
11.6	0	1	1	0
11.7	0	0	0	0
11.A	0	0	0	0
11.B	0	1	1	0
11.C	0	1	0	0
Total	**1/10**	**5/10**	**3/10**	**1/10**

(c) SDG 11

Target	Aerospace	Civil	Wind	Naval
12.1	0	0	0	0
12.2	1	1	1	1
12.3	0	0	0	0
12.4	0	0	0	0
12.5	1	1	1	1
12.6	1	1	1	0
12.7	0	0	0	0
12.8	0	0	0	0
12.A	0	0	0	0
12.B	0	0	0	0
12.C	0	0	0	0
Total	**3/11**	**3/11**	**3/11**	**2/11**

(d) SDG 12

Target	Aerospace	Civil	Wind	Naval
13.1	0	0	0	0
13.2	0	0	0	0
13.3	0	0	0	0
13.A	0	0	0	0
13.B	0	0	0	0
Total	**0/5**	**0/5**	**0/5**	**0/5**

(e) SDG 13

Target	Aerospace	Civil	Wind	Naval
14.1	0	0	0	1
14.2	0	0	0	0
14.3	0	0	0	0
14.4	0	0	0	0
14.5	0	0	0	0
14.6	0	0	0	0
14.7	0	0	0	0
14.A	0	0	0	0
14.B	0	0	0	0
14.C	0	0	0	0
Total	**0/10**	**0/10**	**0/10**	**1/10**

(f) SDG 14

Target	Aerospace	Civil	Wind	Naval
15.1	0	0	0	0
15.2	0	0	0	0
15.3	0	0	0	0
15.4	0	0	0	0
15.5	0	0	0	0
15.6	0	0	0	0
15.7	0	0	0	0
15.8	0	0	0	0
15.9	0	0	0	0
15.A	0	0	0	0
15.B	0	0	0	0
15.C	0	0	0	0
Total	**0/12**	**0/12**	**0/12**	**0/12**

(g) SDG 15

Target	Aerospace	Civil	Wind	Naval
16.1	0	0	0	0
16.2	0	0	0	0
16.3	0	0	0	0
16.4	0	0	0	0
16.5	0	0	0	0
16.6	0	0	0	0
16.7	0	0	0	0
16.8	0	0	0	0
16.9	0	0	0	0
16.10	0	0	0	0
16.A	0	0	0	0
16.B	0	0	0	0
Total	**0/12**	**0/12**	**0/12**	**0/12**

(h) SDG 16

Table A.4: Boolean indicators of contribution of composite materials to SDG 17, as per considered industries.

Target	**Aerospace**	**Civil**	**Wind**	**Naval**
17.1	0	0	0	0
17.2	0	0	0	0
17.3	0	0	0	0
17.4	0	0	0	0
17.5	0	0	0	0
17.6	1	1	1	1
17.7	1	1	1	1
17.8	0	0	0	0
17.9	0	0	0	0
17.10	0	0	0	0
17.11	1	0	0	1
17.12	0	0	0	0
17.13	0	0	0	0
17.14	0	0	0	0
17.15	0	0	0	0
17.16	0	0	0	0
17.17	0	0	0	0
17.18	0	0	0	0
17.19	0	0	0	0
Total	**3/19**	**2/19**	**2/19**	**3/19**

Appendix B

FMECA Tables

Table B.1: FMECA analysis (Failure modes 1 to 31).

ID	Subcomponent Level 1	Subcomponent Level 2	Subcomponent Level 3	Failure mode	CN	Criticality level	Failure mechanism	Associated Monitoring Feature	Associated References	CMS	RMS
LE1	Leading edge	Bondline		Adhesive joint failure (Debonding)	4	Moderate	Overstress of the interphase (peeling stresses), separation of shells	Temperature distribution, strain fields, standing wave energy, FBG reflectivity - strain, AE power and spectral features, strain and displacement fields	[69, 160, 170, 211, 305, 310]	Regular inspections	Regular inspections
LE2	Leading edge	Bondline		Adhesive joint failure (Debonding)	8	High	Overstress of the interphase (peeling stresses), separation of shells	Temperature distribution, strain fields, standing wave energy, FBG reflectivity - strain, AE power and spectral features, strain and displacement fields	[69, 160, 170, 211, 305, 310]	Regular inspections	Regular inspections
LE3	Leading edge	Bondline		Adhesive joint failure (Debonding)	4	Moderate	Overstress of the interphase (peeling stresses), separation of shells	Temperature distribution, strain fields, standing wave energy, FBG reflectivity - strain, AE power and spectral features, strain and displacement fields	[69, 160, 170, 211, 305, 310]	Regular inspections	Regular inspections
LE4	Leading edge	Skin		Erosion of LEP	12	High	Wear of coating, loss of mass of the blade	Temperature distribution, image analysis aided by deep-learning	[181, 339, 361, 430]	Regular inspections	Continuous monitoring
LE5	Leading edge	Skin		Erosion of LEP	12	High	Wear of coating, loss of mass of the blade	Temperature distribution, image analysis aided by deep-learning	[181, 339, 361, 430]	Regular inspections	Continuous monitoring
LE6	Leading edge	Skin		Erosion of LEP	9	High	Wear of coating, loss of mass of the blade	Temperature distribution, image analysis aided by deep-learning	[181, 339, 361, 430]	Regular inspections	Continuous monitoring
LE7	Leading edge			Cracks	3	Low	Degradation and overstress of laminates	Temperature distribution, strain fields, sound signal amplitude, strain and displacement fields, FBG reflectivity - strain, AE power and amplitude, image analysis aided by deep-learning, statistical vibration features	[106, 135, 181, 222, 310, 339, 361, 381, 417, 430, 438, 453]	Regular inspections	Regular inspections
LE8	Leading edge			Ice accumulation	2	Low	Accumulation of ice	Power curve, tower lateral oscillation acceleration, natural frequency, damping ratio, peak magnitude, group phase velocity, amplitude, group phase velocity	[364, 372, 413, 428]	Continuous monitoring	Continuous monitoring
TE9	Trailing edge	Bondline		Adhesive joint failure (Debonding)	4	Moderate	Overstress of adhesive	Temperature distribution, standing wave energy, FBG reflectivity - strain, AE power and spectral features, strain and displacement fields, modal shape, frequencies, AE power and amplitude	[69, 156, 160, 170, 211, 305, 310, 453]	Regular inspections	Regular inspections
TE10	Trailing edge	Bondline		Adhesive joint failure (Debonding)	8	High	Overstress of the interphase (peeling stresses)	Temperature distribution, strain fields, standing wave energy, FBG reflectivity - strain, AE power and spectral features, strain and displacement fields, modal shape, frequencies	[69, 156, 160, 170, 211, 305, 310]	Regular inspections	Regular inspections
TE11	Trailing edge	Bondline		Adhesive joint failure (Debonding)	8	High	Overstress of adhesive	Temperature distribution, standing wave energy, FBG reflectivity - strain, AE power and spectral features, strain and displacement fields, modal shape, frequencies	[69, 156, 160, 170, 211, 305, 310]	Regular inspections	Regular inspections
TE12	Trailing edge			Buckling	5	Moderate	Overstress of laminate in compression causing buckling instabilities	Temperature distribution, strain and displacement fields	[69, 170]	None	None
TE13	Trailing edge			Cracks	6	Moderate	Degradation and overstress of laminates	Temperature distribution, sound signal amplitude, strain and displacement fields, FBG reflectivity - strain, AE power and amplitude, image analysis aided by deep-learning, statistical vibration features	[106, 135, 181, 222, 310, 339, 361, 381, 417, 430, 438, 453]	Regular inspections	Regular inspections
T14	Tip			Blade rupturing, blade burnout, wire melting (lightning)	5	Moderate	Strike of lightning	Wind speed - rotational speed, wind speed - power, image analysis aided by deep-learning, current	[207, 259, 361, 430]	Regular inspections	Continuous monitoring
T15	Tip			Surface cracking, Surface tearing (lightning)	8	High	Strike of lightning	Temperature distribution, strain fields, sound signal amplitude, AE power and amplitude, wind speed - rotational speed, wind speed - power, image analysis aided by deep-learning, current	[106, 135, 181, 207, 259, 339, 361, 381, 430, 453]	Regular inspections	Continuous monitoring
T16	Tip			Surface stripping, receptor loss (lightning)	9	High	Strike of lightning	Temperature distribution, wind speed - rotational speed, wind speed - power, image analysis aided by deep-learning, current	[135, 181, 207, 259, 361, 430]	Regular inspections	Continuous monitoring
T17	Tip			Receptor vaporization, surface scorching, surface blotching surface delamination (Lightning)	8	High	Strike of lightning	Strain, time of flight, wind speed - rotational speed, wind speed - power, image analysis aided by deep-learning, current, frequency response functions, time of flight	[160, 207, 259, 306, 307, 332, 361, 430]	Regular inspections	Continuous monitoring
R18	Root	Root-hub connection		Failure of root-hub connection	5	Moderate	Interlaminar failure, fatigue failure during operation, detachment of the blade	Strain and displacement fields	[222]	Regular inspections	Regular inspections
R19	Root	Root-hub connection		Failure of root-hub connection	5	Moderate	Interlaminar failure, fatigue failure during operation, detachment of the blade	Strain and displacement fields	[222]	Regular inspections	Regular inspections
R20	Root	Root-hub connection		Failure of root-hub connection	10	High	Damage progression in the surroundings of the bolts until critical damage of the blade	Strain and displacement fields	[222]	Regular inspections	Continuous monitoring
US21	Upper shell	Skin	Gelcoat	Cracks	1	Low	Crack initiation due to degradation of properties (UV, impacts), exposing internal layers	Temperature distribution, strain and displacement fields, AE energy, AE amplitude, image analysis aided by deep-learning	[106, 181, 222, 361, 402, 430, 438]	Regular inspections	Regular inspections
US22	Upper shell	Skin	Skin-laminate interphase	Skin/adhesive debonding	2	Low	Initiation of debonding during operation	Strain and displacement fields, AE power and spectral features	[160, 211, 222, 438]	Corrective maintenance	Corrective maintenance
US23	Upper shell	Sandwich	Core	Water ingress	2	Low	Moisture ingressing slowly and increasing the weight of the blade			Corrective maintenance	Corrective maintenance
US24	Upper shell	Sandwich	Laminate-core interphase	Debonding (Laminate to core)	4	Moderate	Overstress of the interphase (peeling stresses) and fatigue, breathing effects	Temperature distribution, standing wave energy, strain and displacement fields, AE power and spectral features, group wave propagation velocity, energy and amplitude of the wave	[69, 160, 211, 222, 305, 345, 438]	Corrective maintenance	Corrective maintenance
US25	Upper shell	Sandwich	Laminate	Delamination	4	Moderate	Delamination will progress until cracks join and the cross section cannot withstand existing loads	Temperature distribution, guided wave amplitude, sound signal amplitude, standing wave energy, strain and displacement fields, time of flight, frequency response functions	[69, 135, 148, 160, 181, 222, 305–307, 332, 381, 438]	Corrective maintenance	Corrective maintenance
US26	Upper shell	Sandwich	Laminate	Delamination	4	Moderate	Intralaminar fractures progressing and evolving into delamination, damage propagation until failure	Temperature distribution, guided wave amplitude, sound signal amplitude, standing wave energy, strain and displacement fields, time of flight, frequency response functions	[69, 135, 148, 160, 181, 222, 305–307, 332, 381, 438]	Corrective maintenance	Corrective maintenance
US27	Upper shell	Sandwich	Laminate	Intralaminar fracture (matrix cracking - microcracks)	3	Low	Reduced strength, static or fatigue damage progression	AE energy, AE amplitude, decay, energy, peak frequency	[402, 439]	Corrective maintenance	Corrective maintenance
US28	Upper shell	Sandwich	Laminate	Intralaminar fracture (matrix cracking - microcracks)	3	Low	Reduced strength, static or fatigue damage progression	AE energy, AE amplitude, decay, energy, peak frequency	[402, 439]	Corrective maintenance	Corrective maintenance
US29	Upper shell	Sandwich	Laminate	Intralaminar fracture (matrix cracking - microcracks)	3	Low	Reduced strength, static or fatigue damage progression	AE energy, AE amplitude, decay, energy, peak frequency	[402, 439]	Corrective maintenance	Corrective maintenance
US30	Upper shell	Sandwich	Laminate	Cracks	2	Low	Static and/or fatigue loading	Temperature distribution, sound signal amplitude, strain and displacement fields, FBG reflectivity - strain, AE power and amplitude, image analysis aided by deep-learning	[106, 135, 181, 222, 310, 339, 361, 381, 430, 438, 453]	Corrective maintenance	Corrective maintenance
US31	Upper shell	Sandwich	Laminate	Cracks	2	Low	Static and/or fatigue loading	Temperature distribution, sound signal amplitude, strain and displacement fields, FBG reflectivity - strain, AE power and amplitude, image analysis aided by deep-learning	[106, 135, 181, 222, 310, 339, 361, 381, 430, 438, 453]	Corrective maintenance	Corrective maintenance

CN: Criticality number LEP: Leading edge protection AE: Acoustic emission FBG: Fibre Bragg grating

Table B.2: FMECA analysis (Failure modes 32 to 62).

ID	Subcomponent Level 1	Subcomponent Level 2	Subcomponent Level 3	Failure mode	Effects	Cause	Cause detail	O	S	CN	Criticality level
LS32	Lower shell	Skin	Gelcoat	Cracks in the gelcoat	Increase of water ingress to sandwich and laminates, degradation of properties, loss of stiffness and strength	Design	Insufficient environmental and impact protection	3	1	3	Low
LS33	Lower shell	Skin	Skin-laminate interphase	Skin/adhesive debonding	Exposure of laminates to environment, increase of degradation of sandwich composites, reduction of aerodynamic efficiency	Manufacturing	Incorrect application of adhesive	1	2	2	Low
LS34	Lower shell	Sandwich	Core	Water ingress	Increase of weight, degradation of stiffness and strength	Operation	Degradation of gelcoat, penetration of water	2	1	2	Low
LS35	Lower shell	Sandwich	Laminate-core interphase	Debonding (Laminate to core)	Increase of stress, reduction of stiffness of the sandwich	Manufacturing	Incorrect application of adhesive	2	2	4	Moderate
LS36	Lower shell	Sandwich	Laminate	Delamination	Increase of stress concentration, reduction of stiffness, reduction of power	Manufacturing	Voids during manufacturing	2	2	4	Moderate
LS37	Lower shell	Sandwich	Laminate	Delamination	Increase of stress concentration, reduction of stiffness, reduction of power	Design	Failure in the design, underestimation of loads	2	2	4	Moderate
LS38	Lower shell	Sandwich	Laminate	Intralaminar fracture (matrix cracking - microcracks)	Increase of stress concentration, reduction of stiffness, damage progress to delamination	Manufacturing	Voids in the laminate, fibre misalignment, wrinkles in the fibres	3	1	3	Low
LS39	Lower shell	Sandwich	Laminate	Intralaminar fracture (matrix cracking - microcracks)	Increase of stress concentration, reduction of stiffness, damage progress to delamination	Installation	Damage in coating with tools, transportation, and assembly	3	1	3	Low
LS40	Lower shell	Sandwich	Laminate	Intralaminar fracture (matrix cracking - microcracks)	Increase of stress concentration, reduction of stiffness, damage progress to delamination	Operation	Incorrect operation	3	1	3	Low
LS41	Lower shell	Sandwich	Laminate	Cracks	Increase of stress concentration, reduction of stiffness, reduction of power	Design	Underestimation of loads	1	2	2	Low
LS42	Lower shell	Sandwich	Laminate	Cracks	Increase of stress concentration, reduction of stiffness, reduction of power	Manufacturing	Voids during manufacturing	1	2	2	Low
S43	Spar	Spar-shell connection		Debonding	Increase of blade deformations, increase of stress in shell sandwich members, failure of the blade	Manufacturing	Poor quality or insufficient adhesive bonding between the parts	2	3	6	Moderate
S44	Spar	Spar-shell connection		Debonding	Increase of blade deformations, increase of stress in shell sandwich members, failure of the blade	Operation	Fatigue damage of bonding due to gravitational loads during operation	2	3	6	Moderate
S45	Spar	Caps	Laminate	Delamination	Increase of stress concentration, reduction of stiffness, progress to crack formation	Manufacturing	Voids during manufacturing	2	4	8	High
S46	Spar	Caps	Laminate	Delamination	Increase of stress concentration, reduction of stiffness, progress to crack formation	Design	Failure in the design, underestimation of loads	2	4	8	High
S47	Spar	Caps	Laminate	Delamination	Increase of stress concentration, reduction of stiffness, progress to crack formation	Operation	Incorrect operation, increase of loads	2	4	8	High
S48	Spar	Caps	Laminate	Intralaminar fracture (matrix cracking - microcracks)	Increase of stress concentration, reduction of stiffness, damage progression to delamination	Design	Failure in the design, underestimation of loads	3	2	6	Moderate
S49	Spar	Caps	Laminate	Intralaminar fracture (matrix cracking - microcracks)	Increase of stress concentration, reduction of stiffness, damage progression to delamination	Manufacturing	Voids in the laminate, fibre misalignment, wrinkles in the fibres	3	2	6	Moderate
S50	Spar	Caps	Laminate	Intralaminar fracture (matrix cracking - microcracks)	Increase of stress concentration, reduction of stiffness, damage progression to delamination	Operation	Incorrect operation resulting in loads not covered by design	3	2	6	Moderate
S51	Spar	Caps	Laminate	Cracks	Increase of stress concentration, reduction of stiffness, failure of the blade	Operation	Misoperation, increase of loads	2	5	10	High
S52	Spar	Caps	Laminate	Cracks	Increase of stress concentration, reduction of stiffness, failure of the blade	Design	Underestimation of loads	2	5	10	High
S53	Spar	Caps	Laminate	Cracks	Increase of stress concentration, reduction of stiffness, failure of the blade	Manufacturing	Voids during manufacturing	2	5	10	High
S54	Spar	Sandwich shear webs	Laminate	Delamination	Increase of stress concentration, reduction of stiffness, progress to crack formation	Manufacturing	Voids during manufacturing	2	4	8	High
S55	Spar	Sandwich shear webs	Laminate	Delamination	Increase of stress concentration, reduction of stiffness, progress to crack formation	Design	Failure in the design, underestimation of loads	2	4	8	High
S56	Spar	Sandwich shear webs	Laminate	Intralaminar fracture (matrix cracking - microcracks)	Increase of stress concentration, reduction of stiffness, damage progress to delamination	Manufacturing	Voids in the laminate, fibre misalignment, wrinkles in the fibres	2	1	2	Low
S57	Spar	Sandwich shear webs	Laminate	Intralaminar fracture (matrix cracking - microcracks)	Increase of stress concentration, reduction of stiffness, damage progress to delamination	Installation	Damage in coating with tools, transportation, and assembly	2	1	2	Low
S58	Spar	Sandwich shear webs	Laminate	Intralaminar fracture (matrix cracking - microcracks)	Increase of stress concentration, reduction of stiffness, damage progress to delamination	Operation	Incorrect operation	2	1	2	Low
S59	Spar	Sandwich shear webs	Laminate	Cracks	Increase of stress concentration, reduction of stiffness, failure of the blade	Design	Underestimation of loads	1	5	5	Moderate
S60	Spar	Sandwich shear webs	Laminate	Cracks	Increase of stress concentration, reduction of stiffness, failure of the blade	Manufacturing	Voids during manufacturing	1	5	5	Moderate
S61	Spar	Sandwich shear webs	Core	Water ingress	Increase of weight, degradation of stiffness and strength	Design	Insufficient environmental and impact protection	1	1	1	Low
S62	Spar	Sandwich shear webs	Laminate-core interphase	Debonding (Laminate to core)	Increase of stress, reduction of stiffness of the sandwich, buckling of the blade	Manufacturing	Incorrect application of adhesive	1	5	5	Moderate

O:Occurrence S:Severity CN:Criticality number LEP: Leading edge protection AE: Acoustic emission FBG: Fibre Bragg grating

Table B.3: FMECA analysis (Failure modes 32 to 62).

ID	Subcomponent Level 1	Subcomponent Level 2	Subcomponent Level 3	Failure mode	CN	Criticality level	Failure mechanism	Associated Monitoring Feature	Associated References	CMS	RMS
LS32	Lower shell	Skin	Gelcoat	Cracks in the gelcoat	3	Low	Crack initiation due to degradation of properties (UV, impacts), exposing internal layers	Temperature distribution, strain and displacement fields, AE energy, AE amplitude, image analysis aided by deep-learning	[106, 181, 222, 361, 402, 430, 438]	Corrective maintenance	Corrective maintenance
LS33	Lower shell	Skin	Skin-laminate interphase	Skin/adhesive debonding	2	Low	Initiation of debonding during operation	Strain and displacement fields, AE power and spectral features	[160, 211, 222, 438]	Corrective maintenance	Corrective maintenance
LS34	Lower shell	Sandwich	Core	Water ingress	2	Low	Moisture ingressing slowly and increasing the weight of the blade			Corrective maintenance	Corrective maintenance
LS35	Lower shell	Sandwich	Laminate-core interphase	Debonding (Laminate to core)	4	Moderate	Overstress of the interphase (peeling stresses) and fatigue, breathing effects	Temperature distribution, standing wave energy, strain and displacement fields, AE power and spectral features, group wave propagation velocity, energy and amplitude of the wave	[69, 160, 211, 222, 305, 345, 438]	Corrective maintenance	Corrective maintenance
LS36	Lower shell	Sandwich	Laminate	Delamination	4	Moderate	Delamination will progress until cracks join and the cross section cannot withstand existing loads	Temperature distribution, guided wave amplitude, sound signal amplitude, standing wave energy, strain and displacement fields, time of flight, frequency response functions	[69, 135, 148, 160, 181, 222, 305–307, 332, 381, 438]	Corrective maintenance	Corrective maintenance
LS37	Lower shell	Sandwich	Laminate	Delamination	4	Moderate	Intralaminar fractures progressing and evolving into delamination, damage propagation until failure	Temperature distribution, guided wave amplitude, sound signal amplitude, standing wave energy, strain and displacement fields, time of flight, frequency response functions	[69, 135, 148, 160, 181, 222, 305–307, 332, 381, 438]	Corrective maintenance	Corrective maintenance
LS38	Lower shell	Sandwich	Laminate	Intralaminar fracture (matrix cracking - microcracks)	3	Low	Reduced strength, static or fatigue damage progression	AE energy, AE amplitude, decay, energy, peak frequency	[402, 439]	Corrective maintenance	Corrective maintenance
LS39	Lower shell	Sandwich	Laminate	Intralaminar fracture (matrix cracking - microcracks)	3	Low	Reduced strength, static or fatigue damage progression	AE energy, AE amplitude, decay, energy, peak frequency	[402, 439]	Corrective maintenance	Corrective maintenance
LS40	Lower shell	Sandwich	Laminate	Intralaminar fracture (matrix cracking - microcracks)	3	Low	Reduced strength, static or fatigue damage progression	AE energy, AE amplitude, decay, energy, peak frequency	[402, 439]	Corrective maintenance	Corrective maintenance
LS41	Lower shell	Sandwich	Laminate	Cracks	2	Low	Crack formation, failure of the blade	Temperature distribution, sound signal amplitude, strain and displacement fields, FBG reflectivity - strain, strain and displacement fields, AE power and amplitude, image analysis aided by deep-learning	[106, 135, 181, 222, 310, 361, 381, 430, 438, 453]	Corrective maintenance	Corrective maintenance
LS42	Lower shell	Sandwich	Laminate	Cracks	2	Low	Crack formation, failure of the blade	Temperature distribution, sound signal amplitude, strain and displacement fields, FBG reflectivity - strain, strain and displacement fields, AE power and amplitude, image analysis aided by deep-learning	[106, 135, 181, 222, 310, 361, 381, 430, 438, 453]	Corrective maintenance	Corrective maintenance
S43	Spar	Spar-shell connection		Debonding	6	Moderate	Separation of the spar from the shell, overstress of the interphase (peeling stresses) and fatigue, breathing effects	Temperature distribution, standing wave energy, strain and displacement fields, AE power and spectral features, group wave propagation velocity, energy and amplitude of the wave	[69, 160, 211, 222, 305, 345, 438]	Corrective maintenance	Continuous monitoring
S44	Spar	Spar-shell connection		Debonding	6	Moderate	Separation of the spar from the shell, overstress of the interphase (peeling stresses) and fatigue, breathing effects	Temperature distribution, standing wave energy, strain and displacement fields, AE power and spectral features, group wave propagation velocity, energy and amplitude of the wave	[69, 160, 211, 222, 305, 345, 438]	Corrective maintenance	Continuous monitoring
S45	Spar	Caps	Laminate	Delamination	8	High	Delamination will progress until cracks join and the cross section cannot withstand existing loads	Temperature distribution, guided wave amplitude, sound signal amplitude, standing wave energy, strain and displacement fields, time of flight, frequency response functions	[69, 135, 148, 160, 181, 222, 305–307, 332, 381, 438]	Corrective maintenance	Corrective maintenance
S46	Spar	Caps	Laminate	Delamination	8	High	Intralaminar fractures progressing and evolving into delamination and damage propagation until failure	Temperature distribution, guided wave amplitude, sound signal amplitude, standing wave energy, strain and displacement fields, time of flight, frequency response functions	[69, 135, 148, 160, 181, 222, 305–307, 332, 381, 438]	Corrective maintenance	Corrective maintenance
S47	Spar	Caps	Laminate	Delamination	8	High	Intralaminar fractures progressing and evolving into delamination and damage propagation until failure	Temperature distribution, guided wave amplitude, sound signal amplitude, standing wave energy, strain and displacement fields, time of flight, frequency response functions	[69, 135, 148, 160, 181, 222, 305–307, 332, 381, 438]	Corrective maintenance	Corrective maintenance
S48	Spar	Caps	Laminate	Intralaminar fracture (matrix cracking - microcracks)	6	Moderate	Reduced strength and static or fatigue damage progression	AE energy, AE amplitude, decay, energy, peak frequency	[402, 439]	Corrective maintenance	Corrective maintenance
S49	Spar	Caps	Laminate	Intralaminar fracture (matrix cracking - microcracks)	6	Moderate	Reduced strength and static or fatigue damage progression	AE energy, AE amplitude, decay, energy, peak frequency	[402, 439]	Corrective maintenance	Corrective maintenance
S50	Spar	Caps	Laminate	Intralaminar fracture (matrix cracking - microcracks)	6	Moderate	Reduced strength and static or fatigue damage progression	AE energy, AE amplitude, decay, energy, peak frequency	[402, 439]	Corrective maintenance	Corrective maintenance
S51	Spar	Caps	Laminate	Cracks	10	High	Crack formation, failure of the blade	Temperature distribution, Temperature distribution, Strain fields, Sound signal amplitude, Strain and displacement fields, FBG reflectivity - strain, Strain and displacement fields, Natural frequency, damping ratio, mode shapes and curvatures, accelerations, AE power and amplitude	[106, 135, 181, 222, 296, 310, 381, 438, 453]	Corrective maintenance	Continuous monitoring
S52	Spar	Caps	Laminate	Cracks	10	High	Crack formation, failure of the blade	Temperature distribution, strain fields, sound signal amplitude, strain and displacement fields, FBG reflectivity - strain, natural frequency, damping ratio, mode shape and curvatures, accelerations, AE power and amplitude	[106, 135, 181, 222, 296, 310, 381, 438, 453]	Corrective maintenance	Continuous monitoring
S53	Spar	Caps	Laminate	Cracks	10	High	Crack formation, failure of the blade	Temperature distribution, strain fields, sound signal amplitude, strain and displacement fields, FBG reflectivity - strain, natural frequency, damping ratio, mode shape and curvatures, accelerations, AE power and amplitude	[106, 135, 181, 222, 296, 310, 381, 438, 453]	Corrective maintenance	Continuous monitoring
S54	Spar	Sandwich shear webs	Laminate	Delamination	8	High	Delamination will progress until cracks join and the cross section cannot withstand existing loads	Guided wave amplitude, sound signal amplitude, temperature distribution, standing wave energy, strain and displacement fields, time of flight, frequency response functions	[69, 148, 160, 222, 305–307, 332, 381, 438]	Corrective maintenance	Corrective maintenance
S55	Spar	Sandwich shear webs	Laminate	Delamination	8	High	Intralaminar fractures progressing and evolving into delamination and damage propagation until failure	Guided wave amplitude, sound signal amplitude, temperature distribution, standing wave energy, strain and displacement fields, time of flight, frequency response functions	[69, 148, 160, 222, 305–307, 332, 381, 438]	Corrective maintenance	Corrective maintenance
S56	Spar	Sandwich shear webs	Laminate	Intralaminar fracture (matrix cracking - microcracks)	2	Low	Reduced strength and static or fatigue damage progression	AE energy, AE amplitude, decay, energy, peak frequency	[402, 439]	Corrective maintenance	Corrective maintenance
S57	Spar	Sandwich shear webs	Laminate	Intralaminar fracture (matrix cracking - microcracks)	2	Low	Reduced strength and static or fatigue damage progression	AE energy, AE amplitude, decay, energy, peak frequency	[402, 439]	Corrective maintenance	Corrective maintenance
S58	Spar	Sandwich shear webs	Laminate	Intralaminar fracture (matrix cracking - microcracks)	2	Low	Reduced strength and static or fatigue damage progression	AE energy, AE amplitude, decay, energy, peak frequency	[402, 439]	Corrective maintenance	Corrective maintenance
S59	Spar	Sandwich shear webs	Laminate	Cracks	5	Moderate	Crack formation, failure of the blade	Sound signal amplitude, strain and displacement fields, FBG reflectivity - strain, natural frequency, damping ratio, mode shape and curvatures, accelerations, AE power and amplitude	[106, 222, 296, 310, 381, 438, 453]	Corrective maintenance	Corrective maintenance
S60	Spar	Sandwich shear webs	Laminate	Cracks	5	Moderate	Crack formation, failure of the blade	Sound signal amplitude, strain and displacement fields, FBG reflectivity - strain, natural frequency, damping ratio, mode shape and curvatures, accelerations, AE power and amplitude	[106, 222, 296, 310, 381, 438, 453]	Corrective maintenance	Corrective maintenance
S61	Spar	Sandwich shear webs	Core	Water ingress	1	Low	Moisture ingressing slowly and increasing the weight of the blade			Corrective maintenance	Corrective maintenance
S62	Spar	Sandwich shear webs	Laminate-core interphase	Debonding (Laminate to core)	5	Moderate	Overstress of the interphase (peeling stresses) and fatigue, breathing effects	Group wave propagation velocity, energy and amplitude of the wave	[345]	Corrective maintenance	Corrective maintenance

CN: Criticality number LEP: Leading edge protection AE: Acoustic emission FBG: Fibre Bragg grating

Appendix B. FMECA Tables

Appendix C

Repair success probabilities (Chapter 5)

C.1 Repair success probabilities

Table C.1: P_1 probabilities.

	0 (Inspection)	1	2	3	4	5	6
Jan	0.6614	0.6614	0.6614	0.6614	0.6614	0.3665	0.3665
Feb	0.7075	0.7075	0.7075	0.7075	0.7075	0.4052	0.4052
Mar	0.7194	0.7194	0.7194	0.7194	0.7194	0.4138	0.4138
Apr	0.8004	0.8004	0.8004	0.8004	0.8004	0.4807	0.4807
May	0.8138	0.8138	0.8138	0.8138	0.8138	0.4812	0.4812
Jun	0.8533	0.8533	0.8533	0.8533	0.8533	0.5326	0.5326
Jul	0.8663	0.8663	0.8663	0.8663	0.8663	0.5356	0.5356
Aug	0.8388	0.8388	0.8388	0.8388	0.8388	0.5083	0.5083
Sep	0.7908	0.7908	0.7908	0.7908	0.7908	0.4722	0.4722
Oct	0.7169	0.7169	0.7169	0.7169	0.7169	0.3162	0.3162
Nov	0.6880	0.6880	0.6880	0.6880	0.6880	0.3813	0.3813
Dec	0.6605	0.6605	0.6605	0.6605	0.6605	0.3841	0.3841

Table C.2: P_2 probabilities.

	0 (Inspection)	1	2	3	4	5	6
Jan	0.8444	0.7615	0.7243	0.6891	0.4624	0.1000	0.1000
Feb	0.8653	0.7925	0.7595	0.7281	0.5264	0.1000	0.1000
Mar	0.8832	0.8186	0.7892	0.7611	0.5715	0.1000	0.1000
Apr	0.9071	0.8544	0.8298	0.8062	0.6418	0.1000	0.1000
May	0.9070	0.8556	0.8317	0.8088	0.6483	0.1000	0.1000
Jun	0.9191	0.8728	0.8514	0.8307	0.6846	0.1000	0.1000
Jul	0.9221	0.8772	0.8514	0.8356	0.6921	0.1000	0.1000
Aug	0.8945	0.8369	0.8103	0.7849	0.6118	0.1000	0.1000
Sep	0.8912	0.8314	0.8037	0.7772	0.5964	0.1000	0.1000
Oct	0.8442	0.7597	0.7216	0.6856	0.4571	0.1000	0.1000
Nov	0.8303	0.7409	0.7006	0.6624	0.4264	0.1000	0.1000
Dec	0.8412	0.7576	0.7198	0.6840	0.4567	0.1000	0.1000

Table C.3: P_3 probabilities.

	0 (Inspection)	1	2	3	4	5	6
Jan	0.9614	0.9414	0.9309	0.9191	0.8066	0.1000	0.1000
Feb	0.9613	0.9409	0.9302	0.9196	0.8124	0.3930	0.3779
Mar	0.9680	0.9510	0.9417	0.9321	0.8387	0.1000	0.1000
Apr	0.9703	0.9538	0.9449	0.9352	0.8432	0.4560	0.4560
May	0.9708	0.9550	0.9463	0.9374	0.8502	0.4124	0.4124
Jun	0.9666	0.9481	0.9383	0.9281	0.8320	0.2432	0.2571
Jul	0.9751	0.9606	0.9383	0.9446	0.8645	0.3236	0.2991
Aug	0.9689	0.9521	0.9433	0.9342	0.8447	0.6747	0.6898
Sep	0.9703	0.9545	0.9459	0.9369	0.8510	0.2917	0.2917
Oct	0.9590	0.9353	0.9223	0.9095	0.7857	0.1000	0.1000
Nov	0.9630	0.9425	0.9316	0.9199	0.8057	0.1000	0.1000
Dec	0.9690	0.9534	0.9447	0.9359	0.8492	0.1000	0.1000

Appendix D

Repair success probabilities (Chapter 6)

D.1 Repair success probabilities

Table D.1: CS1 P_1 probabilities. The first row represents the damage severity

	0 (Inspection)	1	2	3	4	5	6
Jan	0.6614	0.6614	0.6614	0.6614	0.6614	0.3665	0.3665
Feb	0.7075	0.7075	0.7075	0.7075	0.7075	0.4052	0.4052
Mar	0.7194	0.7194	0.7194	0.7194	0.7194	0.4138	0.4138
Apr	0.8004	0.8004	0.8004	0.8004	0.8004	0.4807	0.4807
May	0.8138	0.8138	0.8138	0.8138	0.8138	0.4812	0.4812
Jun	0.8533	0.8533	0.8533	0.8533	0.8533	0.5326	0.5326
Jul	0.8663	0.8663	0.8663	0.8663	0.8663	0.5356	0.5356
Aug	0.8388	0.8388	0.8388	0.8388	0.8388	0.5083	0.5083
Sep	0.7908	0.7908	0.7908	0.7908	0.7908	0.4722	0.4722
Oct	0.7169	0.7169	0.7169	0.7169	0.7169	0.3162	0.3162
Nov	0.6880	0.6880	0.6880	0.6880	0.6880	0.3813	0.3813
Dec	0.6605	0.6605	0.6605	0.6605	0.6605	0.3841	0.3841

Table D.2: CS1 P_2 probabilities. The first row represents the damage severity

	0 (Inspection)	1	2	3	4	5	6
Jan	0.8444	0.7615	0.7243	0.6891	0.4624	0.1000	0.1000
Feb	0.8653	0.7925	0.7595	0.7281	0.5264	0.1000	0.1000
Mar	0.8832	0.8186	0.7892	0.7611	0.5715	0.1000	0.1000
Apr	0.9071	0.8544	0.8298	0.8062	0.6418	0.1000	0.1000
May	0.9070	0.8556	0.8317	0.8088	0.6483	0.1000	0.1000
Jun	0.9191	0.8728	0.8514	0.8307	0.6846	0.1000	0.1000
Jul	0.9221	0.8772	0.8514	0.8356	0.6921	0.1000	0.1000
Aug	0.8945	0.8369	0.8103	0.7849	0.6118	0.1000	0.1000
Sep	0.8912	0.8314	0.8037	0.7772	0.5964	0.1000	0.1000
Oct	0.8442	0.7597	0.7216	0.6856	0.4571	0.1000	0.1000
Nov	0.8303	0.7409	0.7006	0.6624	0.4264	0.1000	0.1000
Dec	0.8412	0.7576	0.7198	0.6840	0.4567	0.1000	0.1000

Table D.3: CS1 P_3 probabilities. The first row represents the damage severity

	0 (Inspection)	1	2	3	4	5	6
Jan	0.9614	0.9414	0.9309	0.9191	0.8066	0.1000	0.1000
Feb	0.9613	0.9409	0.9302	0.9196	0.8124	0.3930	0.3779
Mar	0.9680	0.9510	0.9417	0.9321	0.8387	0.1000	0.1000
Apr	0.9703	0.9538	0.9449	0.9352	0.8432	0.4560	0.4560
May	0.9708	0.9550	0.9463	0.9374	0.8502	0.4124	0.4124
Jun	0.9666	0.9481	0.9383	0.9281	0.8320	0.2432	0.2571
Jul	0.9751	0.9606	0.9383	0.9446	0.8645	0.3236	0.2991
Aug	0.9689	0.9521	0.9433	0.9342	0.8447	0.6747	0.6898
Sep	0.9703	0.9545	0.9459	0.9369	0.8510	0.2917	0.2917
Oct	0.9590	0.9353	0.9223	0.9095	0.7857	0.1000	0.1000
Nov	0.9630	0.9425	0.9316	0.9199	0.8057	0.1000	0.1000
Dec	0.9690	0.9534	0.9447	0.9359	0.8492	0.1000	0.1000

Table D.4: CS2 P_1 probabilities. The first row represents the damage severity

	0 (Inspection)	1	2	3	4	5	6
Jan	0.4374	0.4374	0.4374	0.4374	0.6614	0.3665	0.3665
Feb	0.5006	0.5006	0.5006	0.5006	0.7075	0.4052	0.4052
Mar	0.5175	0.5175	0.5175	0.5175	0.7194	0.4138	0.4138
Apr	0.6406	0.6406	0.6406	0.6406	0.8004	0.4807	0.4807
May	0.6622	0.6622	0.6622	0.6622	0.8138	0.4812	0.4812
Jun	0.7282	0.7282	0.7282	0.7282	0.8533	0.5326	0.5326
Jul	0.7504	0.7504	0.7504	0.7504	0.8663	0.5356	0.5356
Aug	0.7036	0.7036	0.7036	0.7036	0.8388	0.5083	0.5083
Sep	0.6253	0.6253	0.6253	0.6253	0.7908	0.4722	0.4722
Oct	0.5140	0.5140	0.5140	0.5140	0.7169	0.3162	0.3162
Nov	0.4733	0.4733	0.4733	0.4733	0.6880	0.3813	0.3813
Dec	0.4362	0.4362	0.4362	0.4362	0.6605	0.3841	0.3841

Table D.5: CS2 P_2 probabilities. The first row represents the damage severity

	0 (Inspection)	1	2	3	4	5	6
Jan	0.7130	0.5799	0.5246	0.4748	0.4624	0.1000	0.1000
Feb	0.7488	0.6280	0.5768	0.5302	0.5264	0.1000	0.1000
Mar	0.7800	0.6701	0.6228	0.5793	0.5715	0.1000	0.1000
Apr	0.8229	0.7300	0.6885	0.6500	0.6418	0.1000	0.1000
May	0.8226	0.7320	0.6917	0.6541	0.6483	0.1000	0.1000
Jun	0.8448	0.7618	0.7248	0.6900	0.6846	0.1000	0.1000
Jul	0.8502	0.7694	0.4790	0.6983	0.6921	0.1000	0.1000
Aug	0.8001	0.7004	0.6566	0.6160	0.6118	0.1000	0.1000
Sep	0.7943	0.6912	0.6459	0.6041	0.5964	0.1000	0.1000
Oct	0.7126	0.5771	0.5207	0.4700	0.4571	0.1000	0.1000
Nov	0.6894	0.5489	0.4908	0.4388	0.4264	0.1000	0.1000
Dec	0.7077	0.5740	0.5181	0.4678	0.4567	0.1000	0.1000

Table D.6: CS2 P_3 probabilities. The first row represents the damage severity

	0 (Inspection)	1	2	3	4	5	6
Jan	0.9243	0.8862	0.8666	0.8447	0.8066	0.1000	0.1000
Feb	0.9241	0.8853	0.8653	0.8457	0.8124	0.3930	0.3779
Mar	0.9370	0.9044	0.8868	0.8688	0.8387	0.0940	0.0880
Apr	0.9415	0.9097	0.8928	0.8746	0.8432	0.4560	0.4560
May	0.9425	0.9120	0.8955	0.8787	0.8502	0.4124	0.4124
Jun	0.9343	0.8989	0.8804	0.8614	0.8320	0.2432	0.2571
Jul	0.9508	0.9228	0.7474	0.8923	0.8645	0.3236	0.2991
Aug	0.9388	0.9065	0.8898	0.8727	0.8447	0.6747	0.6898
Sep	0.9415	0.9111	0.8947	0.8778	0.8510	0.2917	0.2917
Oct	0.9197	0.8748	0.8506	0.8272	0.7857	0.1000	0.1000
Nov	0.9274	0.8883	0.8679	0.8462	0.8057	0.1000	0.1000
Dec	0.9390	0.9090	0.8925	0.8759	0.8492	0.1000	0.1000

Bibliography

[1] OpenFAST. `https://github.com/OpenFAST/openfast`, 2017. Accessed: 2021-12-20.

[2] 3M. A 3m study is the first to show the effects of erosion on wind turbine efficiency. Technical report, 3M, 2011.

[3] Yazid Aafif, Anis Chelbi, Lahcen Mifdal, Sofiene Dellagi, and Ilias Majdouline. Optimal preventive maintenance strategies for a wind turbine gearbox. *Energy Reports*, 8:803–814, 2022.

[4] Hojjat Adeli and Kaveripatnam V Balasubramanyam. *Expert systems for structural design: A new generation*. Prentice Hall, Hoboken, 1988.

[5] A Agusta, BJ Leira, and Sebastian Thöns. Value of information-based risk and fatigue management for offshore structures. *Journal of Structural Integrity and Maintenance*, 5(2):127–141, 2020.

[6] Nihad Tareq Khshain Al-Saadi, Alyaa Mohammed, Riadh Al-Mahaidi, and Jay Sanjayan. A state-of-the-art review: Near-surface mounted FRP composites for reinforced concrete structures. *Construction and Building Materials*, 209:748–769, 2019.

[7] R. C. Alderliesten and R. Benedictus. Fiber/Metal Composite Technology for Future Primary Aircraft Structures. *Journal of Aircraft*, 45(4):1182–1189, 2008.

[8] Belal Alemour, Omar Badran, and Mohd Roshdi Hassan. A Review of Using Conductive Composite Materials in Solving Lightening Strike and Ice Accumulation Problems in Aviation. *Journal of Aerospace Technology and Management*, 11, 2019.

[9] Hafiz Tauqeer Ali, Roya Akrami, Sakineh Fotouhi, Mahdi Bodaghi, Milad Saeedifar, Mohammad Yusuf, and Mohamad Fotouhi. Fiber reinforced polymer composites in bridge industry. *Structures*, 30:774–785, 2021.

[10] Allianz. Safety and Shipping Review 2020. Technical report, Allianz, 2020.

[11] Mar Alonso-Martinez, José M Adam, Felipe P Alvarez-Rabanal, and Juan J del Coz Díaz. Wind turbine tower collapse due to flange failure: FEM and DOE analyses. *Engineering Failure Analysis*, 104:932–949, 2019.

[12] Joham Alvarez-Montoya, Alejandro Carvajal-Castrillón, and Julián Sierra-Pérez. In-flight and wireless damage detection in a UAV composite wing using fiber optic sensors and strain field pattern recognition. *Mechanical Systems and Signal Processing*, 136, 2020.

[13] Louis Anthony (Tony) Cox Jr. What's wrong with risk matrices? *Risk Analysis: An International Journal*, 28(2):497–512, 2008.

[14] Hooman Arabian-Hoseynabadi, Hashem Oraee, and PJ Tavner. Failure modes and effects analysis (FMEA) for wind turbines. *International Journal of Electrical Power & Energy Systems*, 32(7):817–824, 2010.

[15] Maurizio Arena and Massimo Viscardi. Strain state detection in composite structures: Review and new challenges. *Journal of Composites Science*, 4(2):60, 2020.

[16] Muhammad Arshad and Brendan C O'Kelly. Offshore wind-turbine structures: a review. *Proceedings of the Institution of Civil Engineers-Energy*, 166(4):139–152, 2013.

[17] Luigi Ascione, Jean-François Caron, Patrice Godonou, Kees van IJselmuijden, Jan Knippers, Toby Mottram, Matthias Oppe, Morten Gantriis Sorensen, Jon Taby, and Liesbeth Tromp. *Prospect for New Guidance in the Design of FRP: Support to the Implementation, Harmonization and Further Development of the Eurocodes*. Publications Office of the European Union, Luxembourg, 2016.

[18] Behnam Ashrafi, Jingwen Guan, Vahid Mirjalili, Pascal Hubert, Benoit Simard, and Andrew Johnston. Correlation between Young's modulus and impregnation quality of epoxy-impregnated SWCNT buckypaper. *Composites Part A: Applied Science and Manufacturing*, 41(9):1184–1191, 2010.

[19] ASTM. Standard Test Method for Liquid Impingement Erosion Using Rotating Apparatus. Standard, ASTM, December 2021.

[20] Hakan Aydemir, Ugur Zengin, and Umut Durak. The Digital Twin Paradigm for Aircraft Review and Outlook. In *AIAA Scitech 2020 Forum*, page 0553, 2020.

[21] Jens Bachmann, Carme Hidalgo, and Stéphanie Bricout. Environmental analysis of innovative sustainable composites with potential use in aviation sector—a life cycle assessment review. *Science China Technological Sciences*, 60(9):1301–1317, 2017.

[22] Jiping Bai. *Advanced Fibre-Reinforced Polymer (FRP) Composites for Structural Applications*. Elsevier, Amsterdam, 2013.

[23] AE Baidin. The reliability of condition-based maintenance. In *3rd EFNMS Congress, Stockholm*, 1976.

[24] AE Baidin and L Furlanetto. Condition-based maintenance implementation and experiences. In *VI AI Man Congress, Trieste*, 1973.

[25] AE Baldin. Condition based maintenance in chemical and chemical fibre industries. In *Monitoring Diagnostics in the Industry Congress, Prague*, 1975.

[26] AE Baldin. Technical diagnostic-and condition-based maintenance for better plant availability. *Measurement*, 4(1):7–22, 1986.

[27] Asturio E Baldin. Condition based maintenance: A powerful tool for modern plant management. *Terotechnica*, 1(2):119–129, 1979.

[28] Lawrence C Bank. *Composites for Construction: Structural Design with FRP Materials*. John Wiley & Sons, Hoboken, 2006.

[29] Jakob Ilsted Bech, Charlotte Bay Hasager, and Christian Bak. Extending the life of wind turbine blade leading edges by reducing the tip speed during extreme precipitation events. *Wind Energy Science*, 3(2):729–748, 2018.

[30] Jakob Ilsted Bech, Nicolai Frost-Jensen Johansen, Martin Bonde Madsen, Ásta Hannesdóttir, and Charlotte Bay Hasager. Experimental study on the effect of drop size in rain erosion test and on lifetime prediction of wind turbine blades. *Renewable Energy*, 197:776–789, 2022.

[31] François Besnard and Lina Bertling. An approach for condition-based maintenance optimization applied to wind turbine blades. *IEEE Transactions on Sustainable Energy*, 1(2):77–83, 2010.

[32] AC Best. The size distribution of raindrops. *Quarterly journal of the royal meteorological society*, 76(327):16–36, 1950.

[33] Ebrahim Zamani Beydokhti and Hashem Shariatmadar. Strengthening and rehabilitation of exterior RC beam–column joints using carbon-FRP jacketing. *Materials and Structures*, 49(12):5067–5083, 2016.

[34] Kedar Bharadwaj, Azadeh Sheidaei, Arash Afshar, and Javad Baqersad. Full-field strain prediction using mode shapes measured with digital image correlation. *Measurement*, 139:326–333, 2019.

[35] Innes Murdo Black, Mark Richmond, and Athanasios Kolios. Condition monitoring systems: a systematic literature review on machine-learning methods improving offshore-wind turbine operational management. *International Journal of Sustainable Energy*, pages 1–24, 2021.

[36] Bladena, Vattenfall, EON, Statkraft, Engie, and Kirt x Thomsen. Instruction: Blade inspections. Technical report, Bladena, 2016.

[37] Bladena, Vattenfall, EON, Statkraft, Engie, and Kirt x Thomsen. The blade handbook. Technical report, Bladena, 2021.

[38] Arielle Blonder and Yasha Jacob Grobman. Design and fabrication with fibre-reinforced polymers in architecture: a case for complex geometry. *Architectural Science Review*, 59(4):257–268, 2016.

[39] Boeing. Boeing 787 from the Ground Up. Technical report, Boeing, 2006.

[40] Christian Boller, Fu-Kuo Chang, and Yozo Fujino. *Encyclopedia of Structural Health Monitoring*. Wiley, Hoboken, 2009.

[41] Pietro Bortolotti, Carlo L Bottasso, Alessandro Croce, and Luca Sartori. Integration of multiple passive load mitigation technologies by automated design optimization—the case study of a medium-size onshore wind turbine. *Wind Energy*, 22(1):65–79, 2019.

[42] Ervin A Bossanyi. Individual blade pitch control for load reduction. *Wind Energy: An International Journal for Progress and Applications in Wind Power Conversion Technology*, 6(2):119–128, 2003.

[43] Clemens Brand and Christian Boller. Identification of Life Cycle Cost Reductions in Structures with Self-Diagnostic Devices. Technical report, Daimler Chrisler Aerospace AG Munchen (Germany) Military Aircraft Division, 2000.

[44] Povl Brondsted and Rogier PL Nijssen. *Advances in Wind Turbine Blade Design and Materials*. Woodhead Publishing, Cambridge, 2013.

[45] A Bussiba, M Kupiec, S Ifergane, R Piat, and T Böhlke. Damage evolution and fracture events sequence in various composites by acoustic emission technique. *Composites Science and Technology*, 68(5):1144–1155, 2008.

[46] Paul Cahill, Budhaditya Hazra, Raid Karoumi, Alan Mathewson, and Vikram Pakrashi. Vibration energy harvesting based monitoring of an operational bridge undergoing forced vibration and train passage. *Mechanical Systems and Signal Processing*, 106:265–283, 2018.

[47] Elcin Aleixo Calado, Marco Leite, and Arlindo Silva. Selecting composite materials considering cost and environmental impact in the early phases of aircraft structure design. *Journal of Cleaner Production*, 186:113–122, 2018.

[48] Luis Pablo Canal, Carlos González, Jon M Molina-Aldareguía, Javier Segurado, and Javier LLorca. Application of digital image correlation at the microscale in fiber-reinforced composites. *Composites Part A: Applied Science and Manufacturing*, 43(10):1630–1638, 2012.

[49] RV Canfield. Cost optimization of periodic preventive maintenance. *IEEE Transactions on Reliability*, 35(1):78–81, 1986.

[50] Daniel Veira Canle, Ari Salmi, and Edward Hæggström. Non-contact damage detection on a rotating blade by Lamb wave analysis. *NDT & E International*, 92:159–166, 2017.

[51] Lee Canning. Performance and 8-year load test on West Mill FRP bridge. *Proceedings of CICE 2012, Rome, Italy*, 2012.

[52] Giovanni Capellari, Eleni Chatzi, and Stefano Mariani. Cost–benefit optimization of structural health monitoring sensor networks. *Sensors*, 18(7), 2018.

[53] Lorenzo Cappugi, Alessio Castorrini, Aldo Bonfiglioli, Edmondo Minisci, and M Sergio Campobasso. Machine learning-enabled prediction of wind turbine energy yield losses due to general blade leading edge erosion. *Energy Conversion and Management*, 245:114567, 2021.

[54] J. Cardoso, R. Valette, and D. Dubois. Possibilistic Petri nets. *IEEE Transactions on Systems, Man, and Cybernetics, Part B: Cybernetics*, 29(5):573–582, 1999.

[55] Michael Carraro, Francesco De Vanna, Feras Zweiri, Ernesto Benini, Ali Heidari, and Homayoun Hadavinia. Cfd modeling of wind turbine blades with eroded leading edge. *Fluids*, 7(9):302, 2022.

[56] Michel Castaings, Dilbag Singh, and Philippe Viot. Sizing of impact damages in composite materials using ultrasonic guided waves. *NDT & E International*, 46:22–31, 2012.

[57] Alessio Castorrini, Alessandro Corsini, Franco Rispoli, Paolo Venturini, Kenji Takizawa, and Tayfun E Tezduyar. Computational analysis of performance deterioration of a wind turbine blade strip subjected to environmental erosion. *Computational Mechanics*, 64(4):1133–1153, 2019.

[58] G Catalanotti, PP Camanho, J Xavier, CG Dávila, and AT Marques. Measurement of resistance curves in the longitudinal failure of composites using digital image correlation. *Composites Science and Technology*, 70(13):1986–1993, 2010.

[59] Peter Cawley. Structural health monitoring: Closing the gap between research and industrial deployment. *Structural Health Monitoring*, 17(5):1225–1244, 2018.

[60] D Cevasco, S Koukoura, and AJ Kolios. Reliability, availability, maintainability data review for the identification of trends in offshore wind energy applications. *Renewable and Sustainable Energy Reviews*, 136:110414, 2021.

[61] D. W. Chalmers. The potential for the use of composite materials in marine structures. *Marine Structures*, 7(2-5):441–456, 1994.

[62] Kartik Chandrasekhar, Nevena Stevanovic, Elizabeth J Cross, Nikolaos Dervilis, and Keith Worden. Damage detection in operational wind turbine blades using a new approach based on machine learning. *Renewable Energy*, 168:1249–1264, 2021.

[63] Rabia Charef, Eshmaiel Ganjian, and Stephen Emmitt. Socio-economic and environmental barriers for a holistic asset lifecycle approach to achieve circular economy: A pattern-matching method. *Technological Forecasting and Social Change*, 170:120798, 2021.

[64] Bindi Chen, Peter C Matthews, and Peter J Tavner. Automated on-line fault prognosis for wind turbine pitch systems using supervisory control and data acquisition. *IET Renewable Power Generation*, 9(5):503–513, 2015.

[65] Jinge Chen, Xin Shen, Xiaocheng Zhu, and Zhaohui Du. Study on composite bend-twist coupled wind turbine blade for passive load mitigation. *Composite Structures*, 213:173–189, 2019.

[66] Junlei Chen, Jihui Wang, and Aiqing Ni. A review on rain erosion protection of wind turbine blades. *Journal of Coatings Technology and Research*, 16(1):15–24, 2019.

[67] S.-M. Chen, J.-S. Ke, and J.-F. Chang. Knowledge representation using fuzzy Petri nets. *IEEE Transactions on Knowledge and Data Engineering*, 2(3):311–319, 1990.

[68] Xi Chen, Cees Bil, and He Ren. Influence of SHM Techniques on Scheduled Maintenance for Aircraft Composite Structures. In *14th AIAA Aviation Technology, Integration, and Operations Conference*, 2014.

[69] Xiao Chen, Sergei Semenov, Malcolm McGugan, Steen Hjelm Madsen, Süleyman Cem Yeniceli, Peter Berring, and Kim Branner. Fatigue testing of a 14.3 m composite blade embedded with artificial defects–damage growth and structural health monitoring. *Composites Part A: Applied Science and Manufacturing*, 140:106189, 2021.

[70] Zukun Chen. Structural health monitoring for ship structures. In *Proceedings of the 10th Biennial Conference on Engineering Systems Design and Analysis ESDA 10 July 12-14, 2010, Istanbul, Turkey ESDA2010-24598*, volume 836, pages 1–4, 2001.

[71] Juan Chiachío, Manuel Chiachío, Shankar Sankararaman, Abhinav Saxena, and Kai Goebel. Condition-based prediction of time-dependent reliability in composites. *Reliability Engineering & System Safety*, 142:134–147, 2015.

[72] Juan Chiachio, Maria L Jalon, Manuel Chiachio, and Athanasios Kolios. A Markov chains prognostics framework for complex degradation processes. *Reliability Engineering & System Safety*, 195:106621, 2020.

[73] Manuel Chiachío, Juan Chiachío, Darren Prescott, and John Andrews. Plausible Petri nets as self-adaptive expert systems: A tool for infrastructure asset monitoring. *Computer-Aided Civil and Infrastructure Engineering*, 34(4):281–298, 2019.

[74] Manuel Chiachio, Juan Chiachio, and Guillermo Rus. Reliability in composites–a selective review and survey of current development. *Composites Part B: Engineering*, 43(3):902–913, 2012.

[75] Manuel Chiachío, Juan Chiachío, Shankar Sankararaman, Kai Goebel, and John Andrews. A new algorithm for prognostics using subset simulation. *Reliability Engineering & System Safety*, 168:189–199, 2017.

[76] DE Chimenti. Guided waves in plates and their use in materials characterization. 1997.

[77] Yunshil Choi, Syed Haider Abbas, and Jung-Ryul Lee. Aircraft integrated structural health monitoring using lasers, piezoelectricity, and fiber optics. *Measurement*, 125:294–302, 2018.

[78] Alan Kim Wing Chong, Abdul Hakim Mohammed, Mat Naim Abdullah, and Mohd Shahril Abdul Rahman. Maintenance prioritization–a review on factors and methods. *Journal of Facilities Management*, 17:18–39, 2019.

[79] Zafer Civelek, Murat Lüy, Ertuğrul Çam, and Hayati Mamur. A new fuzzy logic proportional controller approach applied to individual pitch angle for wind turbine load mitigation. *Renewable Energy*, 111:708–717, 2017.

[80] John L Clarke. *Structural Design of Polymer Composites: EUROCOMP Design Code and Background Document*. CRC Press, London, 2003.

[81] International Electrotechnical Commission et al. IEC 60812: 2018–Failure modes and effects analysis (FMEA and FMECA), 3rd edn.,(International Standard. IEC, Geneva, Switzerland, August 10, 2018).

[82] Javier Contreras and Athanasios Kolios. Risk-based maintenance strategy selection for wind turbine composite blades. *Energy Reports*, pages (on–line), 2022.

[83] Javier Contreras Lopez, Juan Chiachío, Ali Saleh, Manuel Chiachío, and Athanasios Kolios. A cross-sectoral review of the current and potential maintenance strategies for composite structures. *SN Applied Sciences*, 4(6):180, 2022.

[84] Andrew J Cook, Graham Tanner, and Stephen Anderson. Evaluating the true cost to airlines of one minute of airborne or ground delay. 2004.

[85] G Corbetta, A Ho, I Pineda, K Ruby, L Van de Velde, and J Bickley. Wind energy scenarios for 2030 Report European Wind Energy Association. Technical report, The European Wind Energy Association, 2015.

[86] Matteo Corbetta, Claudio Sbarufatti, Marco Giglio, Abhinav Saxena, and Kai Goebel. A Bayesian framework for fatigue life prediction of composite laminates under co-existing matrix cracks and delamination. *Composite Structures*, 187:58–70, 2018.

[87] Matteo Corbetta, Claudio Sbarufatti, Andrea Manes, and Marco Giglio. Real-time prognosis of random loaded structures via bayesian filtering: A preliminary discussion. *Engineering Fracture Mechanics*, 145:143–160, 2015.

[88] Enrique Cortés, Fernando Sánchez, Anthony O'Carroll, Borja Madramany, Mark Hardiman, and Trevor M Young. On the material characterisation of wind turbine blade coatings: the effect of interphase coating–laminate adhesion on rain erosion performance. *Materials*, 10(10):1146, 2017.

[89] Global Wind Energy Council. Global Wind Report: Annual market update 2018. Technical report, Global Wind Energy Council, 2018.

[90] Ricardo Coutinho, Bastien Fernandez, Ricardo Lima, and Arnaud Meyroneinc. Discrete time piecewise affine models of genetic regulatory networks. *Journal of Mathematical Biology*, 52(4):524–570, 2006.

[91] Corina Covaci and Aurel Gontean. Piezoelectric energy harvesting solutions: A review. *Sensors*, 20(12):3512, 2020.

[92] C.J. Crabtree, D. Zappala, and P.J. Tavner. Survey of Commercially Available Condition Monitoring Systems for Wind Turbines. Technical report, DU, May 2014.

[93] Demetrio Cristiani, Claudio Sbarufatti, and Marco Giglio. Damage diagnosis and prognosis in composite double cantilever beam coupons by particle filtering and surrogate modelling. *Structural Health Monitoring*, 2020.

[94] Alireza Daneshkhah, Nigel G Stocks, and Paul Jeffrey. Probabilistic sensitivity analysis of optimised preventive maintenance strategies for deteriorating infrastructure assets. *Reliability Engineering & System Safety*, 163:33–45, 2017.

[95] Milton Kumar Das, Subhash Chandra Panja, Sunetra Chowdhury, Shyamapada P Chowdhury, and Andreas I Elombo. Expert-based FMEA of wind turbine system. In *2011 IEEE International Conference on Industrial Engineering and Engineering Management*, pages 1582–1585. IEEE, 2011.

[96] Peter Davies and Yapa DS Rajapakse. *Durability of Composites in a Marine Environment*, volume 208. Springer, New York, 2014.

[97] Ives De Baere, Geert Luyckx, Eli Voet, Wim Van Paepegem, and Joris Degrieck. On the feasibility of optical fibre sensors for strain monitoring in thermoplastic composites under fatigue loading conditions. *Optics and Lasers in Engineering*, 47(3-4):403–411, 2009.

[98] Peter J De Groot, Peter AM Wijnen, and Roger BF Janssen. Real-time frequency determination of acoustic emission for different fracture mechanisms in carbon/epoxy composites. *Composites Science and Technology*, 55(4):405–412, 1995.

[99] N Dervilis, M Choi, SG Taylor, RJ Barthorpe, G Park, CR Farrar, and K Worden. On damage diagnosis for a wind turbine blade using pattern recognition. *Journal of sound and vibration*, 333(6):1833–1850, 2014.

[100] Palash Dewangan, Anand Parey, Ahmed Hammami, Fakher Chaari, and Mohamed Haddar. Damage detection in wind turbine gearbox using modal strain energy. *Engineering Failure Analysis*, 107:104228, 2020.

[101] Nikolay Dimitrov. Risk-based approach for rational categorization of damage observations from wind turbine blade inspections. In *Journal of Physics: Conference Series*, volume 1037, page 042021. IOP Publishing, 2018.

[102] Fateme Dinmohammadi and Mahmood Shafiee. A fuzzy-FMEA risk assessment approach for offshore wind turbines. *International Journal of Prognostics and Health Management*, 4(13):59–68, 2013.

[103] Ting Dong and Nam H. Kim. Cost-effectiveness of structural health monitoring in fuselage maintenance of the civil aviation industry. *Aerospace*, 5(3), 2018.

[104] Xinghui Dong, Di Gao, Jia Li, Zhang Jincao, and Kai Zheng. Blades icing identification model of wind turbines based on SCADA data. *Renewable Energy*, 162:575–586, 2020.

[105] You Dong and Dan M Frangopol. Risk-informed life-cycle optimum inspection and maintenance of ship structures considering corrosion and fatigue. *Ocean Engineering*, 101:161–171, 2015.

[106] Austin Downey, Simon Laflamme, and Filippo Ubertini. Experimental wind tunnel study of a smart sensing skin for condition evaluation of a wind turbine blade. *Smart Materials and Structures*, 26(12):125005, 2017.

[107] Shanyi Du. Advanced composite materials and aerospace engineering. *Acta Materiae Compositae Sinica*, 24(1):1–12, 2007.

[108] Ying Du, Shengxi Zhou, Xingjian Jing, Yeping Peng, Hongkun Wu, and Ngaiming Kwok. Damage detection techniques for wind turbine blades: A review. *Mechanical Systems and Signal Processing*, 141:106445, 2020.

[109] S Durgadevi, S Karthikeyan, N Lavanya, and C Kavitha. A review on retrofitting of reinforced concrete elements using FRP. *Materials Today: Proceedings*, 45:1050–1054, 2021.

[110] EASA. AMC 20-29: Composite Aircraft Structure. Technical report, EASA, 2010.

[111] Ottmar Edenhofer, Ramon Pichs-Madruga, Youba Sokona, Kristin Seyboth, Patrick Matschoss, Susanne Kadner, Timm Zwickel, Patrick Eickemeier, Gerrit Hansen, Steffen Schlömer, et al. IPCC special report on renewable energy sources and climate change mitigation. Technical report, Working Group III of the Intergovernmental Panel on Climate Change, Cambridge University Press, Cambridge, UK, 2011.

[112] Drew Eisenberg, Steffen Laustsen, and Jason Stege. Wind turbine blade coating leading edge rain erosion model: Development and validation. *Wind Energy*, 21(10):942–951, 2018.

[113] MH El-Hofy and H El-Hofy. Laser beam machining of carbon fiber reinforced composites: a review. *The International Journal of Advanced Manufacturing Technology*, 101(9):2965–2975, 2019.

[114] Nick Eleftheroglou, Dimitrios Zarouchas, Theodoros Loutas, Rene Alderliesten, and Rinze Benedictus. Structural health monitoring data fusion for in-situ life prognosis of composite structures. *Reliability Engineering & System Safety*, 178:40–54, 2018.

[115] Mohamed Elhadi Ibrahim and Mamoun Medraj. Water droplet erosion of wind turbine blades: Mechanics, testing, modeling and future perspectives. *Materials*, 13(1):157, 2020.

[116] Tobi Elusakin, Mahmood Shafiee, Tosin Adedipe, and Fateme Dinmohammadi. A stochastic petri net model for o&m planning of floating offshore wind turbines. *Energies*, 14(4):1134, 2021.

[117] Brandon Lee Ennis, Christopher Lee Kelley, Brian Thomas Naughton, Bob Norris, Sujit Das, Dominic Lee, and Dave Miller. Optimized Carbon Fiber Composites in Wind Turbine Blade Design. Technical report, Sandia National Lab.(SNL-NM), Albuquerque, NM (United States), 2019.

[118] Alper Erturk, WGR Vieira, C De Marqui Jr, and Daniel J Inman. On the energy harvesting potential of piezoaeroelastic systems. *Applied Physics Letters*, 96(18):184103, 2010.

[119] Eurofighter. Eurofighter typhoon. https://www.eurofighter.com/the-aircraft, 2020. Last accessed 08 March 2021.

[120] TW Evans, RF Swann, and MA Troffer. The submarine perspective. In *Proceedings of the National Conference on the Use of Composite Materials in Load-Bearing Marine Structures, National Academy Press, Washington, DC*, pages 11–17, 1991.

[121] Charles R Farrar and Nick AJ Lieven. Damage prognosis: The future of structural health monitoring. *Philosophical Transactions of the Royal Society A: Mathematical, Physical and Engineering Sciences*, 365(1851):623–632, 2007.

[122] Charles R Farrar, Gyuhae Park, Marian Anghel, Matthew T Bement, and Liming Salvino. Structural health monitoring for ship structures. Technical report, Los Alamos National Lab.(LANL), Los Alamos, NM (United States), 2009.

[123] Fawcet, A. J. , Oakes, G. D. Boeing composite airframe damage tolerance and service experience. Technical report, Boeing, 2006.

[124] Benedikt Fengler, Marielouise Schäferling, Bastian Schäfer, Lucas Bretz, Gisela Lanza, Benjamin Häfner, Andrew Hrymak, and Luise Kärger. Manufacturing uncertainties and resulting robustness of optimized patch positions on continuous-discontinuous fiber reinforced polymer structures. *Composite Structures*, 213:47–57, 2019.

[125] Fiberline. The fiberline bridge in kolding, bridges. Available at `https://fiberline.com/cases-construction/bridges/the-fiberline-bridge-in-kolding/` (2021/2/11), 1997.

[126] Fiberline. Germany's first road bridge of GFRP. Available at `https://fiberline.com/cases-construction/bridges/germany-s-first-road-bridge-of-grp/`, 2005.

[127] Fiberline. Crumbling concrete bridge replaced by GRP composite, Bridges. Available at `https://fiberline.com/cases-construction/bridges/crumbling-concrete-bridge-replaced-by-grp-composite/` (2021/2/11), 2008.

[128] Giovanni Fiore and Michael S Selig. Simulation of damage for wind turbine blades due to airborne particles. *Wind Engineering*, 39(4):399–418, 2015.

[129] Katharina Fischer, Francois Besnard, and Lina Bertling. Reliability-centered maintenance for wind turbines based on statistical analysis and practical experience. *IEEE Transactions on Energy Conversion*, 27(1):184–195, 2011.

[130] Mihai Florian and John Dalsgaard Sørensen. Wind turbine blade life-time assessment model for preventive planning of operation and maintenance. *Journal of Marine Science and Engineering*, 3(3):1027–1040, 2015.

[131] Forschungs- und Entwicklungszentrum Fachhochschule Kiel GmbH. Forschungsplattformen in nordund ostsee nr. 1, 2, 3., 2022. data retrieved from FINO1 Database, `https://www.fino-offshore.de/de/index.html`.

[132] Vincent François-Lavet, Raphael Fonteneau, and Damien Ernst. How to discount deep reinforcement learning: Towards new dynamic strategies. *arXiv preprint arXiv:1512.02011*, 2015.

[133] M Froese. 3m to launch wind protection tape 2.0 at windenergy hamburg. *Wind power engineering*, 9, 2016.

[134] Martin Gagné and Daniel Therriault. Lightning strike protection of composites. *Progress in Aerospace Sciences*, 64:1–16, 2014.

[135] C Galleguillos, A Zorrilla, A Jimenez, L Diaz, ÁL Montiano, M Barroso, A Viguria, and F Lasagni. Thermographic non-destructive inspection of wind turbine blades using unmanned aerial systems. *Plastics, Rubber and Composites*, 44(3):98–103, 2015.

[136] Y Garbatov, F Sisci, and M Ventura. Risk-based framework for ship and structural design accounting for maintenance planning. *Ocean Engineering*, 166:12–25, 2018.

[137] Ginger Gardiner. Removing the barriers to lightweighting ships with composites, 2019.

[138] Geoff Garfield. Material advantage: Seeking alternatives to reliance on steel, 2018.

[139] N Gaudern. A practical study of the aerodynamic impact of wind turbine blade leading edge erosion. In *Journal of Physics: Conference Series*, volume 524, page 012031. IOP Publishing, 2014.

[140] Xiaolin Ge, Quan Chen, Yang Fu, CY Chung, and Yang Mi. Optimization of maintenance scheduling for offshore wind turbines considering the wake effect of arbitrary wind direction. *Electric Power Systems Research*, 184:106298, 2020.

[141] Gardiner Ginger. The Markets: Civil Infrastructure (2021), 2020.

[142] M Giordano, A Calabro, C Esposito, A D'amore, and L Nicolais. An acoustic-emission characterization of the failure modes in polymer-composite materials. *Composites Science and Technology*, 58(12):1923–1928, 1998.

[143] Victor Giurgiutiu. Structural Health Monitoring (SHM) of aerospace composites. In Philip Irving and Constantinos Soutis, editors, *Polymer Composites in the Aerospace Industry*, chapter 17, pages 491–558. Woodhead Publishing, Cambridge, 2020.

[144] Branko Glisic and Daniele Inaudi. *Fibre Optic Methods for Structural Health Monitoring*. John Wiley & Sons, Hoboken, 2008.

[145] Maurizio Gobbato, Joel P Conte, John B Kosmatka, and Charles R Farrar. A reliability-based framework for fatigue damage prognosis of composite aircraft structures. *Probabilistic Engineering Mechanics*, 29:176–188, 2012.

[146] Kai Goebel, Matthew John Daigle, Abhinav Saxena, Indranil Roychoudhury, Shankar Sankararaman, and José R Celaya. *Prognostics: The Science of Making Predictions*. 2017.

[147] Guilherme Ferreira Gomes, Yohan Alí Diaz Mendéz, Patrícia da Silva Lopes Alexandrino, Sebastião Simões da Cunha Jr, and Antonio Carlos Ancelotti Jr. The use of intelligent computational tools for damage detection and identification with an emphasis on composites–a review. *Composite Structures*, 196:44–54, 2018.

[148] Carlos Quiterio Gómez Muñoz, Fausto Pedro García Márquez, Borja Hernández Crespo, and Kena Makaya. Structural health monitoring for delamination detection and location in wind turbine blades employing guided waves. *Wind Energy*, 22(5):698–711, 2019.

[149] Sankar Karuppannan Gopalraj and Timo Kärki. A review on the recycling of waste carbon fibre/glass fibre-reinforced composites: Fibre recovery, properties and life-cycle analysis. *SN Applied Sciences*, 2(433), 2020.

[150] Ivan Grabovac and David Whittaker. Application of bonded composites in the repair of ships structures–a 15-year service experience. *Composites Part A: applied science and manufacturing*, 40(9):1381–1398, 2009.

[151] Matthieu Gresil, Lingyu Yu, Victor Giurgiutiu, and Michael Sutton. Predictive modeling of electromechanical impedance spectroscopy for composite materials. *Structural Health Monitoring*, 11(6):671–683, 2012.

[152] Michael Grieves and John Vickers. Digital twin: Mitigating unpredictable, undesirable emergent behavior in complex systems. In *Transdisciplinary perspectives on complex systems*, pages 85–113. Springer, New York, 2017.

[153] D Todd Griffith. Structural Health and Prognostics Management for Offshore Wind Plants : Final Report of Sandia R & D Activities. Technical Report March, Sandia National Laboratories, 2015.

[154] D Todd Griffith, Nathanael Yoder, Brian Resor, Jonathan White, Joshua Paquette, Alistair Ogilvie, and Valerie Peters. Prognostic control to enhance offshore wind turbine operations and maintenance strategies. *management*, 5:8–10, 2012.

[155] D Todd Griffith, Nathanael C Yoder, Brian Resor, Jonathan White, and Joshua Paquette. Structural Health and Prognostics Management for the Enhancement of Offshore Wind Turbine Operations and Maintenance Strategies. *Wind Energy*, 17(11):1737–1751, 2014.

[156] Daniel Griffith. Sensing in renewable energy systems: Modal testing and structural health & prognostics management. Technical report, Sandia National Lab.(SNL-NM), Albuquerque, NM (United States), 2015.

[157] Ernesto Guades, Thiru Aravinthan, Mainul Islam, and Allan Manalo. A review on the driving performance of FRP composite piles. *Composite Structures*, 94(6):1932–1942, 2012.

[158] Hong Guan, Vistasp M Karbhari, and Charles S Sikorsky. Web-based structural health monitoring of an FRP composite bridge. *Computer-Aided Civil and Infrastructure Engineering*, 21(1):39–56, 2006.

[159] Hong Guan, Vistasp M Karbhari, and Charles S Sikorsky. Long-term structural health monitoring system for a FRP composite highway bridge structure. *Journal of Intelligent Material Systems and Structures*, 18(8):809–823, 2007.

[160] Alfredo Güemes, Antonio Fernández-López, Patricia F Díaz-Maroto, Angel Lozano, and Julian Sierra-Perez. Structural health monitoring in composite structures by fiber-optic sensors. *Sensors*, 18(4):1094, 2018.

[161] Alfredo Güemes, Antonio Fernandez-Lopez, Angel Renato Pozo, and Julián Sierra-Pérez. Structural Health Monitoring for Advanced Composite Structures: A Review. *Journal of Composites Science*, 4(1):13, 2020.

[162] Honglei Guo, Gaozhi Xiao, Nezih Mrad, and Jianping Yao. Fiber optic sensors for structural health monitoring of air platforms. *Sensors*, 11(4):3687–3705, 2011.

[163] Jihong Guo, Chao Liu, Jinfeng Cao, and Dongxiang Jiang. Damage identification of wind turbine blades with deep convolutional neural networks. *Renewable Energy*, 174:122–133, 2021.

[164] Yanzhen Guo, Liangfeng Yu, Xiuting Wei, Weisheng Liu, Xuemei Huang, et al. Structural collapse characteristics of a 48.8 m wind turbine blade under ultimate bending loading. *Engineering Failure Analysis*, 106:104150, 2019.

[165] Reza Haghani, Jincheng Yang, Rami Hawileh, Jamal Abdullah, Karrar Al-Lami, Pierluigi Colombi, and Tommaso D'Antino. Adhesively bonded frp composites for strengthening of rc structures: Recent advances. In *International Conference on Fibre-Reinforced Polymer (FRP) Composites in Civil Engineering*, pages 1373–1384. Springer, 2021.

[166] Woobeom Han, Jonghwa Kim, and Bumsuk Kim. Effects of contamination and erosion at the leading edge of blade tip airfoils on the annual energy production of wind turbines. *Renewable Energy*, 115:817–823, 2018.

[167] C Hasager, F Vejen, JI Bech, WR Skrzypiński, A-M Tilg, and M Nielsen. Assessment of the rain and wind climate with focus on wind turbine blade leading edge erosion rate and expected lifetime in danish seas. *Renewable Energy*, 149:91–102, 2020.

[168] Charlotte Hasager, Leon Mishnaevsky Jr, Christian Bak, Jakob Ilsted Bech, Søren Fæster, and Nicolai Frost-Jensen Johansen. How can we combat leading-edge erosion on wind turbine blades? *Danmarks Tekniske Universitet, Institut for Vindenergi, Risø Campus*, 4000, 2021.

[169] Charlotte Bay Hasager, Flemming Vejen, Witold Robert Skrzypiński, and Anna-Maria Tilg. Rain erosion load and its effect on leading-edge lifetime and potential of erosion-safe mode at wind turbines in the north sea and baltic sea. *Energies*, 14(7):1959, 2021.

[170] Philipp Ulrich Haselbach, Martin Alexander Eder, and Federico Belloni. A comprehensive investigation of trailing edge damage in a wind turbine rotor blade. *Wind Energy*, 19(10):1871–1888, 2016.

[171] M H Hassan, A R Othman, and S Kamaruddin. A review on the manufacturing defects of complex-shaped laminate in aircraft composite structures. *The International Journal of Advanced Manufacturing Technology*, 91(9):4081–4094, 2017.

[172] WPMH Heemels and B De Schutter. On the equivalence of classes of hybrid systems: Mixed logical dynamical and complementarity systems. *Measurement and Control Systems*, 2000.

[173] Robbie Herring, Kirsten Dyer, Ffion Martin, and Carwyn Ward. The increasing importance of leading edge erosion and a review of existing protection solutions. *Renewable and Sustainable Energy Reviews*, 115:109382, 2019.

[174] Hans Hersbach, Bill Bell, Paul Berrisford, Shoji Hirahara, András Horányi, Joaquín Muñoz-Sabater, Julien Nicolas, Carole Peubey, Raluca Radu, Dinand Schepers, et al. The era5 global reanalysis. *Quarterly Journal of the Royal Meteorological Society*, 146(730):1999–2049, 2020.

[175] I Herszberg, HCH Li, F Dharmawan, AP Mouritz, M Nguyen, and J Bayandor. Damage assessment and monitoring of composite ship joints. *Composite structures*, 67(2):205–216, 2005.

[176] Valerie Ann-Peters Hines, Alistair B Ogilvie, and Cody R Bond. Continuous Reliability Enhancement for Wind (CREW) Database. Technical report, Sandia National Lab.(SNL-NM), Albuquerque, NM (United States), 2013.

[177] Matthias Hofmann and Iver Bakken Sperstad. Nowicob–a tool for reducing the maintenance costs of offshore wind farms. *Energy Procedia*, 35:177–186, 2013.

[178] Leonard C Hollaway and Jin-Guang Teng. *Strengthening and Rehabilitation of Civil Infrastructures using Fibre-Reinforced Polymer (FRP) Composites*. Elsevier, Amsterdam, 2008.

[179] R. A. Howard. Information value theory. *IEEE Transactions on Systems Science and Cybernetics*, 2(1):22–26, 1966.

[180] Soonkyu Hwang, Yun-Kyu An, and Hoon Sohn. Continuous-wave line laser thermography for monitoring of rotating wind turbine blades. *Structural Health Monitoring*, 18(4):1010–1021, 2019.

[181] Soonkyu Hwang, Yun-Kyu An, Jinyeol Yang, and Hoon Sohn. Remote inspection of internal delamination in wind turbine blades using continuous line laser scanning thermography. *International Journal of Precision Engineering and Manufacturing-Green Technology*, pages 1–14, 2020.

[182] Fadzidah Mohd Idris, Mansor Hashim, Zulkifly Abbas, Ismayadi Ismail, Rodziah Nazlan, and Idza Riati Ibrahim. Recent developments of smart electromagnetic absorbers based polymer-composites at gigahertz frequencies. *Journal of Magnetism and Magnetic Materials*, 405:197–208, 2016.

[183] IEA. Projected Costs of Generating Electricity 2020. Technical report, IEA, 2020.

[184] Frits Immers. Movares designs the world's first steel/fibre-reinforced plastic bridge. Available at `https://movares.nl/europe/projecten/steel-bridges/`, 2012.

[185] International Renewable Energy Agency (IRENA). Renewable capacity statistics 2021. Technical report, IRENA, Abu Dhabi, 2021.

[186] AM Jadali, Anastasia Ioannou, Konstantinos Salonitis, and A Kolios. Decommissioning vs. repowering of offshore wind farms—a techno-economic assessment. *The International Journal of Advanced Manufacturing Technology*, 112(9):2519–2532, 2021.

[187] Ravi Jain and Luke Lee. *Fiber Reinforced Polymer (FRP) Composites for Infraestructure Applications*, volume 9. Routledge, Abingdon-on-Thames, 2013.

[188] Rims Janeliukstis and Xiao Chen. Review of digital image correlation application to large-scale composite structure testing. *Composite Structures*, 271:114143, 2021.

[189] S Jayaram, K Sivaprasad, and CG Nandakumar. Recycling of FRP boats. *International Journal of Advanced Research in Science, Engineering and Technology*, 9(3):244–252, 2018.

[190] Jonas Pagh Jensen and Kristen Skelton. Wind turbine blade recycling: Experiences, challenges and possibilities in a circular economy. *Renewable and Sustainable Energy Reviews*, 97:165–176, 2018.

[191] CAI Jing and DAI Dingqiang. Inspection interval optimization for aircraft composite structures with dent and delamination damage. *Journal of Systems Engineering and Electronics*, 32(1):252–260, 2021.

[192] Nicolai Frost-Jensen Johansen. *Test Methods for Evaluating Rain Erosion Performance of Wind Turbine Blade Leading Edge Protection Systems*. PhD thesis, Technical University of Denmark, 2020.

[193] Jason Jonkman, Sandy Butterfield, Walter Musial, and George Scott. Definition of a 5-mw reference wind turbine for offshore system development. Technical report, National Renewable Energy Lab.(NREL), Golden, CO (United States), 2009.

[194] A Joshuva and V Sugumaran. Wind turbine blade fault diagnosis using vibration signals through decision tree algorithm. *Indian Journal of Science and Technology*, 9(48):1–7, 2016.

[195] Petros Karvelis, George Georgoulas, Vassilios Kappatos, and Chrysostomos Stylios. Deep machine learning for structural health monitoring on ship hulls using acoustic emission method. *Ships and Offshore Structures*, 16(4):440–448, 2021.

[196] Mark Hugh Keegan, DH Nash, and MM Stack. On erosion issues associated with the leading edge of wind turbine blades. *Journal of Physics D: Applied Physics*, 46(38):383001, 2013.

[197] Adnan Kefal, Olgun Hizir, and Erkan Oterkus. A smart system to determine sensor locations for structural health monitoring of ship structures. *International Workshop on Ship and Marine Hydrodynamics*, (January 2016):26–28, 2015.

[198] TH Keller, J De Castro, S Dooley, and Veronique Dubois. Use of Fibre Reinforced Polymers in Bridge Construction. Technical report, Bundesamt Fuer Strassenbau (ASTRA) / Office Federal Des Routes (OFROU), 2001.

[199] Sang-Woo Kim, Eun-Ho Kim, Min-Soo Jeong, and In Lee. Damage evaluation and strain monitoring for composite cylinders using tin-coated FBG sensors under low-velocity impacts. *Composites Part B: Engineering*, 74:13–22, 2015.

[200] Yail J Kim. State of the practice of FRP composites in highway bridges. *Engineering Structures*, 179:1–8, 2019.

[201] Diederik P Kingma and Jimmy Ba. Adam: A method for stochastic optimization. *arXiv preprint arXiv:1412.6980*, 2014.

[202] Athanasios Kolios and María Martínez-Luengo. The end of the line for today's wind turbines. *Renewable Energy Focus*, 17(3):109–111, 2016.

[203] Athanasios J Kolios. Risk-based maintenance strategies for offshore wind energy assets, 2020.

[204] Jung S Kong and Dan M Frangopol. Life-cycle reliability-based maintenance cost optimization of deteriorating structures with emphasis on bridges. *Journal of Structural Engineering*, 129(6):818–828, 2003.

[205] Sofia Koukoura, Matti Niclas Scheu, and Athanasios Kolios. Influence of extended potential-to-functional failure intervals through condition monitoring systems on offshore wind turbine availability. *Reliability Engineering & System Safety*, 208:107404, 2021.

[206] Christoph Kralovec and Martin Schagerl. Review of structural health monitoring methods regarding a multi-sensor approach for damage assessment of metal and composite structures. *Sensors*, 20(3):826, 2020.

[207] Sebastian GM Kramer, Fernando Puente Leon, and Benoit Appert. Fiber optic sensor network for lightning impact localization and classification in wind turbines. In *2006 IEEE International Conference on Multisensor Fusion and Integration for Intelligent Systems*, pages 173–178, 2006.

[208] Andrey E Krauklis, Christian W Karl, Abedin I Gagani, and Jens K Jørgensen. Composite Material Recycling Technology–State-of-the-Art and Sustainable Development for the 2020s. *Journal of Composites Science*, 5(1):28, 2021.

[209] Andreas Krause, Carlos Guestrin, Anupam Gupta, and Jon Kleinberg. Near-optimal sensor placements: Maximizing information while minimizing communication cost. In *Proceedings of the 5th international conference on Information processing in sensor networks*, pages 2–10, 2006.

[210] Matthias Krause, Frank Roland, and Carlo Cau. RAMSSES – Realisation and Demonstration of Advanced Material Solutions for Sustainable and Efficient Ships. *Transport Research Arena TRA 2018*, 2018.

[211] Thomas Krause and Jörn Ostermann. Damage detection for wind turbine rotor blades using airborne sound. *Structural Control and Health Monitoring*, 27(5), 2020.

[212] Christian Krupitzer, Felix Maximilian Roth, Sebastian VanSyckel, Gregor Schiele, and Christian Becker. A survey on engineering approaches for self-adaptive systems. *Pervasive and Mobile Computing*, 17:184–206, 2015.

[213] Emil Krog Kruse. *A Method for Quantifying Wind Turbine Leading Edge Roughness and its Influence on Energy Production*. DTU Vindenergi, 2019.

[214] Ryan Kyle, Fan Wang, and Brian Forbes. The effect of a leading edge erosion shield on the aerodynamic performance of a wind turbine blade. *Wind Energy*, 23(4):953–966, 2020.

[215] P Labossière and JP Newhook. Will sustainable development objectives increase the need for structural health monitoring in civil engineering? 2005.

[216] Pou-Man Lam, Kin-Tak Lau, Hang-Yin Ling, Zhongqing Su, and Hwa-Yaw Tam. Acousto-ultrasonic sensing for delaminated GFRP composites using an embedded FBG sensor. *Optics and Lasers in Engineering*, 47(10):1049–1055, 2009.

[217] Kari Larsen. Recycling wind turbine blades. *Renewable Energy Focus*, 9(7):70–73, 2009.

[218] Kostas Latoufis, Vasilis Riziotis, Spyros Voutsinas, and Nikos Hatziargyriou. Effects of leading edge erosion on the power performance and acoustic noise emissions of locally manufactured small wind turbine blades. In *Journal of Physics: Conference Series*, volume 1222, page 012010. IOP Publishing, 2019.

[219] Castro-Santos Laura and Diaz-Casas Vicente. Life-cycle cost analysis of floating offshore wind farms. *Renewable Energy*, 66:41–48, 2014.

[220] Hamish Law and Vasileios Koutsos. Leading edge erosion of wind turbines: Effect of solid airborne particles and rain on operational wind farms. *Wind Energy*, 23(10):1955–1965, 2020.

[221] John Leahy. Global Market Forecast 2015-2034. Technical report, Airbus, 2015.

[222] Bruce LeBlanc, Christopher Niezrecki, Peter Avitabile, Julie Chen, and James Sherwood. Damage detection and full surface characterization of a wind turbine blade using three-dimensional digital image correlation. *Structural Health Monitoring*, 12(5-6):430–439, 2013.

[223] J. Lee, K.F.R. Liu, and W. Chiang. Modeling uncertainty reasoning with possibilistic Petri nets. *IEEE Transactions on Systems, Man, and Cybernetics, Part B: Cybernetics*, 33(2):214–224, 2003.

[224] Anaële Lefeuvre, Sébastien Garnier, Leslie Jacquemin, Baptiste Pillain, and Guido Sonnemann. Anticipating in-use stocks of carbon fibre reinforced polymers and related waste generated by the wind power sector until 2050. *Resources, Conservation and Recycling*, 141:30–39, 2019.

[225] Mareike Leimeister and Athanasios Kolios. A review of reliability-based methods for risk analysis and their application in the offshore wind industry. *Renewable and Sustainable Energy Reviews*, 91:1065–1076, 2018.

[226] Gustavo de Novaes Pires Leite, Alex Maurício Araújo, and Pedro André Carvalho Rosas. Prognostic techniques applied to maintenance of wind turbines: a concise and specific review. *Renewable and Sustainable Energy Reviews*, 81:1917–1925, 2018.

[227] Dongsheng Li, Junlong Zhou, and Jinping Ou. Damage, nondestructive evaluation and rehabilitation of FRP composite-RC structure: A review. *Construction and Building Materials*, 271, 2020.

[228] HCH Li, I Herszberg, CE Davis, AP Mouritz, and SC Galea. Health monitoring of marine composite structural joints using fibre optic sensors. *Composite Structures*, 75(1-4):321–327, 2006.

[229] He Li, Angelo P. Teixeira, and C. Guedes Soares. A two-stage failure mode and effect analysis of offshore wind turbines. *Renewable Energy*, 162:1438–1461, 12 2020.

[230] Hong-Nan Li, Dong-Sheng Li, Liang Ren, Ting-Hua Yi, Zi-Guang Jia, and LI Kun-Peng. Structural health monitoring of innovative civil engineering structures in Mainland China. *Structural Monitoring and Maintenance*, 3(1):1, 2016.

[231] Hong-Nan Li, Dong-Sheng Li, and Gang-Bing Song. Recent applications of fiber optic sensors to health monitoring in civil engineering. *Engineering structures*, 26(11):1647–1657, 2004.

[232] Mingxin Li, Xiaoli Jiang, James Carroll, and Rudy R Negenborn. A multi-objective maintenance strategy optimization framework for offshore wind farms considering uncertainty. *Applied Energy*, 321:119284, 2022.

[233] Qiang Li, Mandar T Naik, Hao-Sheng Lin, Cheng Hu, Wilson K Serem, Li Liu, Pravat Karki, Fujie Zhou, and Joshua S Yuan. Tuning hydroxyl groups for quality carbon fiber of lignin. *Carbon*, 139:500–511, 2018.

[234] Yao Li, Caichao Zhu, Chaosheng Song, and Jianjun Tan. Research and development of the wind turbine reliability. *International Journal of Mechanical Engineering and Applications*, 6(2):35–45, 2018.

[235] Yingguang Li, Nanya Li, and James Gao. Tooling design and microwave curing technologies for the manufacturing of fiber-reinforced polymer composites in aerospace applications. *The International Journal of Advanced Manufacturing Technology*, 70(1):591–606, 2014.

[236] Wenyi Liu, Baoping Tang, and Yonghua Jiang. Status and problems of wind turbine structural health monitoring techniques in China. *Renewable Energy*, 35(7):1414–1418, 2010.

[237] Yan Liu, Dan M Frangopol, and Minghui Cheng. Risk-informed structural repair decision making for service life extension of ageing naval ships. *Marine Structures*, 64:305–321, 2019.

[238] Carl G Looney. Fuzzy Petri nets for rule-based decision-making. *IEEE Transactions on Systems, Man, and Cybernetics*, 18(1):178–183, 1988.

[239] Javier Contreras Lopez and Athanasios Kolios. Risk-based maintenance strategy selection for wind turbine composite blades. *Energy Reports*, 8:5541–5561, 2022.

[240] Javier Contreras López, Athanasios Kolios, Lin Wang, and Manuel Chiachio. A wind turbine blade leading edge rain erosion computational framework. *Renewable Energy*, 203:131–141, 2023.

[241] Roberto A Lopez-Anido and Tarun R Naik. *Emerging Materials for Civil Infrastructure: State of the Art*. ASCE Publications, Virginia, 2000.

[242] Theodoros Loutas, Nick Eleftheroglou, and Dimitrios Zarouchas. A data-driven probabilistic framework towards the in-situ prognostics of fatigue life of composites based on acoustic emission data. *Composite Structures*, 161:522–529, 2017.

[243] Theodoros Loutas, Nick Eleftheroglou, and Dimitrios Zarouchas. A data-driven probabilistic framework towards the in-situ prognostics of fatigue life of composites based on acoustic emission data. *Composite Structures*, 161:522–529, 2017.

[244] Estivaliz Lozano-Minguez, Athanasios J Kolios, and Feargal P Brennan. Multi-criteria assessment of offshore wind turbine support structures. *Renewable Energy*, 36(11):2831–2837, 2011.

[245] Maria Martinez Luengo and Athanasios Kolios. Failure mode identification and end of life scenarios of offshore wind turbines: A review. *Energies*, 8(8):8339–8354, 2015.

[246] Nancy Lynch, Roberto Segala, Frits Vaandrager, and Henri B Weinberg. Hybrid I/O automata. In *International Hybrid Systems Workshop*, pages 496–510. Springer, 1995.

[247] I. A. Magomedov, V. S. Magomadov, A. A. Rahimov, S. Kh Alikhadzhiev, and M. A.A. Gudaev. FMMA and FMECA for analysis of reliability of a wind turbine. volume 1399. Institute of Physics Publishing, 12 2019.

[248] C Maienza, AM Avossa, F Ricciardelli, D Coiro, G Troise, and Christos Thomas Georgakis. A life cycle cost model for floating offshore wind farms. *Applied Energy*, 266:114716, 2020.

[249] John F Mandell, Daniel D Samborsky, Pancasatya Agastra, Aaron T Sears, and Timothy J Wilson. Analysis of SNL/MSU/DOE Fatigue Database Trends for Wind Turbine Blade Materials. Technical report, Sandia Contractor Report), 2010.

[250] John F Mandell, Daniel D Samborsky, David A Miller, Pancasatya Agastra, and Aaron T Sears. Analysis of SNL/MSU/DOE Fatigue Database Trends for Wind Turbine Blade Materials 2010-2015. Technical report, Sandia National Lab.(SNL-NM), Albuquerque, NM (United States), 2016.

[251] P. D. Mangalgiri. Composite materials for aerospace applications. *Bulletin of Materials Science*, 22(3):657–664, 1999.

[252] David C Maniaci, Edward B White, Benjamin Wilcox, Christopher M Langel, CP van Dam, and Joshua A Paquette. Experimental measurement and cfd model development of thick wind turbine airfoils with leading edge erosion. In *Journal of Physics: Conference Series*, volume 753, page 022013. IOP Publishing, 2016.

[253] JC Marin, A Barroso, F Paris, and J Canas. Study of fatigue damage in wind turbine blades. *Engineering Failure Analysis*, 16(2):656–668, 2009.

[254] Fausto Pedro García Márquez and Ana María Peco Chacón. A review of non-destructive testing on wind turbines blades. *Renewable Energy*, 161:998–1010, 2020.

[255] George Marsh. 50 years of reinforced plastic boats. *Reinforced Plastics*, 50(9):16–19, 2006.

[256] Rebecca Martin, Iraklis Lazakis, Sami Barbouchi, and Lars Johanning. Sensitivity analysis of offshore wind farm operation and maintenance cost and availability. *Renewable Energy*, 85:1226–1236, 2016.

[257] Maria Martinez-Luengo, Athanasios Kolios, and Lin Wang. Structural health monitoring of offshore wind turbines: A review through the Statistical Pattern Recognition Paradigm. *Renewable and Sustainable Energy Reviews*, 64:91–105, 2016.

[258] Maria Martinez-Luengo, Mahmood Shafiee, and Athanasios Kolios. Data management for structural integrity assessment of offshore wind turbine support structures: data cleansing and missing data imputation. *Ocean Engineering*, 173:867–883, 2019.

[259] Takuto Matsui, Kazuo Yamamoto, Shinichi Sumi, and Nawakun Triruttanapiruk. Detection of lightning damage on wind turbine blades using the scada system. *IEEE Transactions on Power Delivery*, 36(2):777–784, 2020.

[260] John J McCall. Maintenance policies for stochastically failing equipment: A survey. *Management Science*, 11(5):493–524, 1965.

[261] Fred C McCormick. Why not plastics bridges? *Journal of the Structural Division*, 98(8):1757–1767, 1972.

[262] Malcolm McGugan, Gunner Chr Larsen, Bent F Sørensen, Kaj Kvisgård Borum, and Jonas Engelhardt. Fundamentals for Remote Condition Monitoring of Offshore Wind Turbines. Technical report, Danmarks Tekniske Universitet, Risø Nationallaboratoriet for Bæredygtig Energi, 2008.

[263] Florianr Menter. Zonal two equation kw turbulence models for aerodynamic flows. In *23rd fluid dynamics, plasmadynamics, and lasers conference*, page 2906, 1993.

[264] Magdalena Mieloszyk, Katarzyna Majewska, and Wieslaw Ostachowicz. Application of embedded fibre Bragg grating sensors for structural health monitoring of complex composite structures for marine applications. *Marine Structures*, 76, 2021.

[265] Lennart Mischnaewski III and Leon Mishnaevsky Jr. Structural repair of wind turbine blades: Computational model for the evaluation of the effect of adhesive properties. *Wind Energy*, 24(4):402–408, 2021.

[266] Leon Mishnaevsky, Kim Branner, Helga Nørgaard Petersen, Justine Beauson, Malcolm McGugan, and Bent F. Sørensen. Materials for wind turbine blades: An overview. *Materials*, 10(11):1–24, 2017.

[267] Leon Mishnaevsky, Kim Branner, Helga Nørgaard Petersen, Justine Beauson, Malcolm McGugan, and Bent F Sørensen. Materials for wind turbine blades: an overview. *Materials*, 10(11):1285, 2017.

[268] L Mishnaevsky Jr, Povl Brøndsted, Rogier Nijssen, DJ Lekou, and TP Philippidis. Materials of large wind turbine blades: recent results in testing and modeling. *Wind Energy*, 15(1):83–97, 2012.

[269] Leon Mishnaevsky Jr. Toolbox for optimizing anti-erosion protective coatings of wind turbine blades: overview of mechanisms and technical solutions. *Wind Energy*, 22(11):1636–1653, 2019.

[270] Leon Mishnaevsky Jr, Charlotte Bay Hasager, Christian Bak, Anna-Maria Tilg, Jakob I Bech, Saeed Doagou Rad, and Søren Fæster. Leading edge erosion of wind turbine blades: Understanding, prevention and protection. *Renewable Energy*, 169:953–969, 2021.

[271] Mikołaj Miśkiewicz, Łukasz Pyrzowski, and Bartosz Sobczyk. Short and long term measurements in assessment of FRP composite footbridge behavior. *Materials*, 13(3):525, 2020.

[272] Ali A Mohammed, Allan C Manalo, Wahid Ferdous, Yan Zhuge, PV Vijay, Ashraf Q Alkinani, and Amir Fam. State-of-the-art of prefabricated FRP composite jackets for structural repair. *Engineering Science and Technology, an International Journal*, 2020.

[273] Jochen Moll, Philip Arnold, Moritz Mälzer, Viktor Krozer, Dimitry Pozdniakov, Rahmi Salman, Stephan Rediske, Markus Scholz, Herbert Friedmann, and Andreas Nuber. Radar-based structural health monitoring of wind turbine blades: The case of damage detection. *Structural Health Monitoring*, 17(4):815–822, 2018.

[274] Alysson Mondoro, Mohamed Soliman, and Dan M. Frangopol. Prediction of structural response of naval vessels based on available structural health monitoring data. *Ocean Engineering*, 125:295–307, 2016.

[275] Diogo Montalvao, Nuno Manuel Mendes Maia, and António Manuel Relógio Ribeiro. A review of vibration-based structural health monitoring with special emphasis on composite materials. *Shock and Vibration Digest*, 38(4):295–324, 2006.

[276] Rosana Monte Soldado, Iván Palomares, Eugenio Martinez-Camara, Pablo Garcia-Moral, Manuel Chiachio, Juan Chiachio, Sergio Alonso, F. Javier Melero, Daniel Molina, Barbara Fernandez, Cristina Moral, Rosario Marchena, Javier Perez de Vargas, and Francisco Herrera. A panoramic view and swot analysis of artificial intelligence for achieving the sustainable development goals by 2030: Progress and prospects. *Applied Intelligence*, 51:6497–6527, 2021.

[277] SM Moon, KL Jerina, and HT Hahn. Acousto-ultrasonic wave propagation in composite laminates. In *Acousto-Ultrasonics*, pages 111–125. Springer, New York, 1988.

[278] Pablo G Morato, KG Papakonstantinou, CP Andriotis, Jannie Sønderkær Nielsen, and Philippe Rigo. Optimal inspection and maintenance planning for deteriorating structural components through dynamic bayesian networks and markov decision processes. *Structural Safety*, 94:102140, 2022.

[279] A. P. Mouritz, E. Gellert, P. Burchill, and K. Challis. Review of advanced composite structures for naval ships and submarines. *Composite Structures*, 53(1):21–42, 2001.

[280] Nezih Mrad. Potential of Bragg grating sensors for aircraft health monitoring. *Transactions of the Canadian Society for Mechanical Engineering*, 31(1):1–17, 2007.

[281] Maria Mrazova. Advanced composite materials of the future in aerospace industry. *Incas bulletin*, 5(3):139, 2013.

[282] Aftab A Mufti and Kenneth W Neale. State-of-the-art of FRP and SHM applications in bridge structures in Canada. *Composites & Polycon, The American Composites Manufacturers Association, Tampa, FL USA*, 2007.

[283] T Munk, D Kane, and DM Yebra. The effects of corrosion and fouling on the performance of ocean-going vessels: a naval architectural perspective. In *Advances in marine antifouling coatings and technologies*, pages 148–176. Elsevier, Amsterdam, 2009.

[284] W Musial and B Ram. Large-scale offshore wind energy for the united state: Assessment of opportunities and barriers. *CO, Golden: National Renewable Energy Laboratory*, 2010.

[285] MZ Naser, RA Hawileh, and JA Abdalla. Fiber-reinforced polymer composites in strengthening reinforced concrete structures: A critical review. *Engineering Structures*, 198:109542, 2019.

[286] Amir Rasekhi Nejad, Peter Fogh Odgaard, Zhen Gao, and Torgeir Moan. A prognostic method for fault detection in wind turbine drivetrains. *Engineering Failure Analysis*, 42:324–336, 2014.

[287] Jannie Jessen Nielsen and John Dalsgaard Sørensen. On risk-based operation and maintenance of offshore wind turbine components. *Reliability engineering & system safety*, 96(1):218–229, 2011.

[288] Jannie S Nielsen, Dmitri Tcherniak, and Martin D Ulriksen. A case study on risk-based maintenance of wind turbine blades with structural health monitoring. *Structure and Infrastructure Engineering*, 17(3):302–318, 2021.

[289] Jannie Sønderkær Nielsen and John Dalsgaard Sørensen. Methods for risk-based planning of o&m of wind turbines. *Energies*, 7(10):6645–6664, 2014.

[290] Jannie Sønderkær Nielsen and John Dalsgaard Sørensen. Framework for risk-based optimal planning of o&m and inspections: Work package 4–deliverable 4.5. Technical report, European Commission, 2017.

[291] Jannie Sonderkaer Nielsen, John Dalsgaard Sørensen, Iver Bakken Sperstad, and Thomas Michael Welte. A bayesian network based approach for integration of condition-based maintenance in strategic offshore wind farm o&m simulation models. *Life-Cycle Analysis and Assessment in Civil Engineering: Towards an Integrated Vision*, 2018.

[292] LI Ningbo, YAN Tao, LI Naipeng, KONG Detong, LIU Qingchao, and LEI Yaguo. Ice Detection Method by Using SCADA Data on Wind Turbine Blades. *Power Generation Technology*, 39(1):58–62, 2018.

[293] James R Norris and James Robert Norris. *Markov chains*. Number 2 in 1. Cambridge university press, 1998.

[294] Andre D Orcesi and Dan M Frangopol. Optimization of bridge maintenance strategies based on structural health monitoring information. *Structural Safety*, 33(1):26–41, 2011.

[295] Wieslaw Ostachowicz, Rohan Soman, and Pawel Malinowski. Optimization of sensor placement for structural health monitoring: A review. *Structural Health Monitoring*, 18(3):963–988, 2019.

[296] Yaowen Ou, Eleni N Chatzi, Vasilis K Dertimanis, and Minas D Spiridonakos. Vibration-based experimental damage detection of a small-scale wind turbine blade. *Structural Health Monitoring*, 16(1):79–96, 2017.

[297] Yaowen Ou, Konstantinos E Tatsis, Vasilis K Dertimanis, Minas D Spiridonakos, and Eleni N Chatzi. Vibration-based monitoring of a small-scale wind turbine blade under varying climate conditions. Part I: An experimental benchmark. *Structural Control and Health Monitoring*, 28(6):e2660, 2021.

[298] Samet Ozturk, Vasilis Fthenakis, and Stefan Faulstich. Failure modes, effects and criticality analysis for wind turbines considering climatic regions and comparing geared and direct drive wind turbines. *Energies*, 11(9):2317, 2018.

[299] Fernando Pacheco-Torgal, Luisa F Cabeza, João Labrincha, and Aldo Giuntini De Magalhaes. *Eco-efficient Construction and Building Materials: Life Cycle Assessment (LCA), Eco-Labelling and Case Studies*. Woodhead Publishing, Cambridge, 2014.

[300] Y Paek and H Adeli. Structural design language for coupled knowledge-based systems. *Advances in Engineering Software (1978)*, 12(4):154–166, 1990.

[301] F Papi, G Ferrara, and A Bianchini. Practical considerations on wind turbine blade leading edge erosion modelling and its impact on performance and loads. In *Journal of Physics: Conference Series*, volume 1618, page 052005. IOP Publishing, 2020.

[302] Francesco Papi, Francesco Balduzzi, Giovanni Ferrara, and Alessandro Bianchini. Uncertainty quantification on the effects of rain-induced erosion on annual energy production and performance of a multi-mw wind turbine. *Renewable Energy*, 165:701–715, 2021.

[303] Francesco Papi, Lorenzo Cappugi, Sebastian Perez-Becker, and Alessandro Bianchini. Numerical modeling of the effects of leading-edge erosion and trailing-edge damage on wind turbine loads and performance. *Journal of Engineering for Gas Turbines and Power*, 142(11):111005, 2020.

[304] Francesco Papi, Lorenzo Cappugi, Simone Salvadori, Mauro Carnevale, and Alessandro Bianchini. Uncertainty Quantification of the Effects of Blade Damage on the Actual Energy Production of Modern Wind Turbines. *Energies*, 13(15):3785, 2020.

[305] Byeongjin Park, Yun-Kyu An, and Hoon Sohn. Visualization of hidden delamination and debonding in composites through noncontact laser ultrasonic scanning. *Composites Science and Technology*, 100:10–18, 2014.

[306] Byeongjin Park, Hoon Sohn, Pawel Malinowski, and Wieslaw Ostachowicz. Delamination localization in wind turbine blades based on adaptive time-of-flight analysis of noncontact laser ultrasonic signals. *Nondestructive Testing and Evaluation*, 32(1):1–20, 2017.

[307] Gyuhae Park, Stuart G Taylor, Kevin M Farinholt, and Charles R Farrar. SHM of Wind Turbine Blades Using Piezoelectric Active-Sensors. Technical report, Los Alamos National Lab.(LANL), Los Alamos, NM (United States), 2010.

[308] Tishun Peng, Yongming Liu, Abhinav Saxena, and Kai Goebel. In-situ fatigue life prognosis for composite laminates based on stiffness degradation. *Composite Structures*, 132:155–165, 2015.

[309] Ying Peng, Ming Dong, and Ming Jian Zuo. Current status of machine prognostics in condition-based maintenance: A review. *The International Journal of Advanced Manufacturing Technology*, 50(1-4):297–313, 2010.

[310] G Pereira, Lars Pilgaard Mikkelsen, and Malcolm McGugan. Damage tolerant design and condition monitoring of composite material and bondlines in wind turbine blades: Failure and crack propagation. In *EWEA Offshore 2015 Conference*. European Wind Energy Association (EWEA), 2015.

[311] Marco A Perez, Lluís Gil, and Sergio Oller. Impact damage identification in composite laminates using vibration testing. *Composite Structures*, 108:267–276, 2014.

[312] Jean-Noël Périé, Sylvain Calloch, Christophe Cluzel, and François Hild. Analysis of a multiaxial test on a C/C composite by using digital image correlation and a damage model. *Experimental Mechanics*, 42(3):318–328, 2002.

[313] Carl Adam Petri. Fundamentals of a theory of asynchronous information flow. In *IFIP congress*, volume 62, pages 386–390, 1962.

[314] Carl Adam Petri. *Kommunikation mit Automaten*. PhD thesis, Institut für Instrumentelle Mathematik an der Universität Bonn, 1962.

[315] Jürgen Pohl, Sven Herold, Gerhard Mook, and Fritz Michel. Damage detection in smart CFRP composites using impedance spectroscopy. *Smart Materials and Structures*, 10(4):834, 2001.

[316] Daniel A Pohoryles, Jose Melo, Tiziana Rossetto, Humberto Varum, and Luke Bisby. Seismic retrofit schemes with FRP for deficient RC beam-column joints: State-of-the-art review. *Journal of Composites for Construction*, 23(4), 2019.

[317] Richard L Puthoff. *Fabrication and Assembly of the ERDA/NASA 100-Kilowatt Experimental Wind Turbine*, volume 3390. US National Aeronautics and Space Administration, Lewis Research Center, Cleveland, 1976.

[318] F Michael Raj, VA Nagarajan, and KP Vinod Kumar. Evaluation of mechanical behavior of multifilament waste fish net/glass fiber in polyester matrix for the application of mechanized boat deckhouse in marine composites. In *Applied Mechanics and Materials*, volume 592, pages 2639–2644. Trans Tech Publ, 2014.

[319] Alan Ramírez-Noriega, Reyes Juárez-Ramírez, Samantha Jiménez, and Yobani Martínez-Ramírez. Knowledge representation in intelligent tutoring system. In *International Conference on Advanced Intelligent Systems and Informatics*, pages 12–21. Springer, 2016.

[320] Akshay Koodly Ravishankara, Huseyin Özdemir, and Edwin van der Weide. Analysis of leading edge erosion effects on turbulent flow over airfoils. *Renewable energy*, 172:765–779, 2021.

[321] Yoram Reich. Artificial intelligence in bridge engineering: Towards matching practical needs with technology. *Microcomputers in Civil Engineering*, pages 1–25, 1995.

[322] Yoram Reich and Steven J Fenves. The potential of machine learning techniques for expert systems. *AI EDAM*, 3(3):175–193, 1989.

[323] Zhengru Ren, Amrit Shankar Verma, Ye Li, Julie JE Teuwen, and Zhiyu Jiang. Offshore wind turbine operations and maintenance: A state-of-the-art review. *Renewable and Sustainable Energy Reviews*, 144, 2021.

[324] Francisco J Rescalvo, María Rodríguez, Rafael Bravo, Chihab Abarkane, and Antolino Gallego. Acoustic emission and numerical analysis of pine beams retrofitted with FRP and poplar wood. *Materials*, 13(2):435, 2020.

[325] Mohammad M Rezaei, Mehdi Behzad, Hamed Moradi, and Hassan Haddadpour. Modal-based damage identification for the nonlinear model of modern wind turbine blade. *Renewable Energy*, 94:391–409, 2016.

[326] Phillip W Richards, D Todd Griffth, and Dewey H Hodges. Smart loads management for damaged offshore wind turbine blades. *Wind Engineering*, 39(4):419–436, 2015.

[327] P. Rizzo. NDE/SHM of underwater structures: A review. *Advances in Science and Technology*, 83:208–216, 2012.

[328] Helena Rocha, Christopher Semprimoschnig, and João P Nunes. Sensors for process and structural health monitoring of aerospace composites: A review. *Engineering Structures*, 237:112231, 2021.

[329] F. Romano, A. Sorrentino, L. Pellone, U. Mercurio, and L. Notarnicola. New design paradigms and approaches for aircraft composite structures. *Multiscale and Multidisciplinary Modeling, Experiments and Design*, 2(2):75–87, 2019.

[330] Mário F Sá, João Pacheco, João R Correia, Nuno Silvestre, and John D Sørensen. Structural safety of pultruded FRP profiles for global buckling. Part 1: Approach to material uncertainty, resistance models, and model uncertainties. *Composite Structures*, 257:113304, 2021.

[331] Karim G. Sabra and Steven Huston. Passive structural health monitoring of a high-speed naval ship from ambient vibrations. *The Journal of the Acoustical Society of America*, 129(5):2991–2999, 2011.

[332] Milad Saeedifar, Mehdi Ahmadi Najafabadi, Jalal Yousefi, Reza Mohammadi, Hossein Hosseini Toudeshky, and Giangiacomo Minak. Delamination analysis in composite laminates by means of acoustic emission and bi-linear/tri-linear cohesive zone modeling. *Composite Structures*, 161:505–512, 2017.

[333] Milad Saeedifar and Dimitrios Zarouchas. Damage characterization of laminated composites using acoustic emission: A review. *Composites Part B: Engineering*, 195:108039, 2020.

[334] Milad Saeedifar and Dimitrios Zarouchas. Damage characterization of laminated composites using acoustic emission: A review. *Composites Part B: Engineering*, page 108039, 2020.

[335] SK Sahoo, RN Rao, Srinivas Kuchipudi, and MK Buragohain. Application of Single-Sided NMR and Acousto-Ultrasonic Methods for NDE of Composite Structures. In *Advances in Applied Mechanical Engineering*, pages 547–555. Springer, New York, 2020.

[336] M Sakr, MH El Naggar, and M Nehdi. Interface characteristics and laboratory constructability tests of novel fiber-reinforced polymer/concrete piles. *Journal of Composites for Construction*, 9(3):274–283, 2005.

[337] Ali Saleh, Manuel Chiachío, Juan Fernández Salas, and Athanasios Kolios. Self-adaptive optimized maintenance of offshore wind turbines by intelligent petri nets. *Reliability Engineering & System Safety*, 231:109013, 2023.

[338] Ali Saleh, Rasa Remenyte-Prescott, Darren Prescott, and Manuel Chiachío. Intelligent and adaptive asset management model for railway sections using the ipn method. *Reliability Engineering & System Safety*, page 109687, 2023.

[339] Hadi Sanati, David Wood, and Qiao Sun. Condition monitoring of wind turbine blades using active and passive thermography. *Applied Sciences*, 8(10):2004, 2018.

[340] Mauricio Sánchez-Silva, Dan M Frangopol, Jamie Padgett, and Mohamed Soliman. Maintenance and operation of infrastructure systems. *Journal of Structural Engineering*, 142(9):F4016004, 2016.

[341] Agrim Sareen, Chinmay A Sapre, and Michael S Selig. Effects of leading edge erosion on wind turbine blade performance. *Wind Energy*, 17(10):1531–1542, 2014.

[342] Jabran Saroia, Yanen Wang, Qinghua Wei, Mingju Lei, Xinpei Li, Ying Guo, and Kun Zhang. A review on 3d printed matrix polymer composites: its potential and future challenges. *The International Journal of Advanced Manufacturing Technology*, 106(5):1695–1721, 2020.

[343] Aral Sarrafi, Zhu Mao, Christopher Niezrecki, and Peyman Poozesh. Vibration-based damage detection in wind turbine blades using phase-based motion estimation and motion magnification. *Journal of Sound and Vibration*, 421:300–318, 2018.

[344] L. Scelsi, M. Bonner, A. Hodzic, C. Soutis, C. Wilson, R. Scaife, and K. Ridgway. Potential emissions savings of lightweight composite aircraft components evaluated through life cycle assessment. *Express Polymer Letters*, 5(3):209–217, 2011.

[345] Christoph Schaal and Ajit Mal. Core-skin disbond detection in a composite sandwich panel using guided ultrasonic waves. *Journal of Nondestructive Evaluation, Diagnostics and Prognostics of Engineering Systems*, 1(1), 2018.

[346] Tom Schaul, John Quan, Ioannis Antonoglou, and David Silver. Prioritized experience replay. *arXiv preprint arXiv:1511.05952*, 2015.

[347] Matti Niclas Scheu, Lorena Tremps, Ursula Smolka, Athanasios Kolios, and Feargal Brennan. A systematic failure mode effects and criticality analysis for offshore wind turbine systems towards integrated condition based maintenance strategies. *Ocean Engineering*, 176:118–133, 3 2019.

[348] Matti Niclas Scheu, Lorena Tremps, Ursula Smolka, Athanasios Kolios, and Feargal Brennan. A systematic failure mode effects and criticality analysis for offshore wind turbine systems towards integrated condition based maintenance strategies. *Ocean Engineering*, 176:118–133, 2019.

[349] Robert Schlaifer and Howard Raiffa. *Applied Statistical Decision Theory*. 1961.

[350] Thijs Nicolaas Schouten, Rommert Dekker, Mustafa Hekimoğlu, and Ayse Sena Eruguz. Maintenance optimization for a single wind turbine component under time-varying costs. *European Journal of Operational Research*, 300(3):979–991, 2022.

[351] Matthias Schramm, Hamid Rahimi, Bernhard Stoevesandt, and Kim Tangager. The influence of eroded blades on wind turbine performance using numerical simulations. *Energies*, 10(9):1420, 2017.

[352] PJ Schubel, RJ Crossley, EKG Boateng, and JR Hutchinson. Review of structural health and cure monitoring techniques for large wind turbine blades. *Renewable Energy*, 51:113–123, 2013.

[353] Pierre Selva, Olivier Cherrier, Valérie Budinger, Frédéric Lachaud, and Joseph Morlier. Smart monitoring of aeronautical composites plates based on electromechanical impedance measurements and artificial neural networks. *Engineering Structures*, 56:794–804, 2013.

[354] S Selvaraju and S Ilaiyavel. Applications of composites in marine industry. *Journal of Engineering Research and Studies*, 2(II):89–91, 2011.

[355] Mahmood Shafiee. Maintenance logistics organization for offshore wind energy: Current progress and future perspectives. *Renewable energy*, 77:182–193, 2015.

[356] Mahmood Shafiee and Fateme Dinmohammadi. An FMEA-based risk assessment approach for wind turbine systems: a comparative study of onshore and offshore. *Energies*, 7(2):619–642, 2014.

[357] Mahmood Shafiee and Fateme Dinmohammadi. An FMEA-based risk assessment approach for wind turbine systems: A comparative study of onshore and offshore. *Energies*, 7:619–642, 2014.

[358] Faisal Karim Shaikh and Sherali Zeadally. Energy harvesting in wireless sensor networks: A comprehensive review. *Renewable and Sustainable Energy Reviews*, 55:1041–1054, 2016.

[359] Gang Shen, Dong Xiang, Kan Zhu, Li Jiang, Yinhua Shen, and Yanlin Li. Fatigue failure mechanism of planetary gear train for wind turbine gearbox. *Engineering Failure Analysis*, 87:96–110, 2018.

[360] Richard J Sheridan, Jeffrey W Gilman, John Busel, David Hartman, Gale A Holmes, Daniel Coughlin, Paul Kelley, Dustin Troutman, Jim Gutierrez, Charles Bakis, et al. Road Mapping Workshop Report on Overcoming Barriers to Adoption of Composites in Sustainable Infrastructure. Technical report, National Institute of Standards and Technology, 2017.

[361] ASM Shihavuddin, Xiao Chen, Vladimir Fedorov, Anders Nymark Christensen, Nicolai Andre Brogaard Riis, Kim Branner, Anders Bjorholm Dahl, and Rasmus Reinhold Paulsen. Wind turbine surface damage detection by deep learning aided drone inspection analysis. *Energies*, 12(4):676, 2019.

[362] Hye-Jin Shin, Jung-Ryul Lee, Chen-Ciang Chia, and Dong-Jin Yoon. Ultrasonic propagation imaging for in-situ wind turbine blade damage visualization. In *10th European Conference on Non-Destructive Testing*, 2010.

[363] Md Abu S Shohag, Emily C Hammel, David O Olawale, and Okenwa I Okoli. Damage mitigation techniques in wind turbine blades: A review. *Wind Engineering*, 41(3):185–210, 2017.

[364] Siavash Shoja, Viktor Berbyuk, and Anders Boström. Guided wave–based approach for ice detection on wind turbine blades. *Wind Engineering*, 42(5):483–495, 2018.

[365] Mahmood M Shokrieh and Roham Rafiee. Simulation of fatigue failure in a full composite wind turbine blade. *Composite structures*, 74(3):332–342, 2006.

[366] Alireza Shourangiz-Haghighi, Mohammad Amin Haghnegahdar, Lin Wang, Marco Mussetta, Athanasios Kolios, and Martin Lander. State of the art in the optimisation of wind turbine performance using CFD. *Archives of Computational Methods in Engineering*, 27(2):413–431, 2020.

[367] Sasan Siavashi, Christopher D Eamon, Abdel A Makkawy, and Hwai-Chung Wu. Long-term durability of FRP bond in the midwest United States for externally strengthened bridge components. *Journal of Composites for Construction*, 23(2):05019001, 2019.

[368] Robert A. Sielski. Ship structural health monitoring research at the office of naval research. *JOM*, 64(7):823–827, 2012.

[369] Georgios Sieros, Panagiotis Chaviaropoulos, John Dalsgaard Sørensen, Bernard H Bulder, and Peter Jamieson. Upscaling wind turbines: Theoretical and practical aspects and their impact on the cost of energy. *Wind energy*, 15(1):3–17, 2012.

[370] Shirsendu Sikdar, Abhishek Kundu, Michał Jurek, and Wiesław Ostachowicz. Nondestructive analysis of debonds in a composite structure under variable temperature conditions. *Sensors*, 19(16):3454, 2019.

[371] Tomasz Siwowski, Damian Kaleta, and Mateusz Rajchel. Structural behaviour of an all-composite road bridge. *Composite Structures*, 192:555–567, 2018.

[372] Georgios Alexandros Skrimpas, Karolina Kleani, Nenad Mijatovic, Christian Walsted Sweeney, Bogi Bech Jensen, and Joachim Holboell. Detection of icing on wind turbine blades by means of vibration and power curve analysis. *Wind Energy*, 19(10):1819–1832, 2016.

[373] H.M. Slot, E.R.M. Gelinck, C. Rentrop, and E. van der Heide. Leading edge erosion of coated wind turbine blades: Review of coating life models. *Renewable Energy*, 80:837–848, 2015.

[374] HM Slot, ERM Gelinck, C Rentrop, and Emile Van Der Heide. Leading edge erosion of coated wind turbine blades: Review of coating life models. *Renewable Energy*, 80:837–848, 2015.

[375] CS Smith. Design of submersible pressure hulls in composite materials. *Marine Structures*, 4(2):141–182, 1991.

[376] Faye Smith. The use of composites in aerospace: Past, present and future challenges. *Avalon Consultancy Services LTD*, pages 1–40, 2013.

[377] Brian Snyder and Mark J Kaiser. Ecological and economic cost-benefit analysis of offshore wind energy. *Renewable Energy*, 34(6):1567–1578, 2009.

[378] C Guedes Soares, Yordan Garbatov, A Zayed, and G Wang. Influence of environmental factors on corrosion of ship structures in marine atmosphere. *Corrosion Science*, 51(9):2014–2026, 2009.

[379] Hoon Sohn, D Dutta, Jin-Yeol Yang, Hyun-Jun Park, M DeSimio, S Olson, and E Swenson. Delamination detection in composites through guided wave field image processing. *Composites Science and Technology*, 71(9):1250–1256, 2011.

[380] MS Sohn, XZ Hu, Jang Kyo Kim, and L Walker. Impact damage characterisation of carbon fibre/epoxy composites with multi-layer reinforcement. *Composites Part B: Engineering*, 31(8):681–691, 2000.

[381] Jaclyn Solimine, Christopher Niezrecki, and Murat Inalpolat. An experimental investigation into passive acoustic damage detection for structural health monitoring of wind turbine blades. *Structural Health Monitoring*, 19(6):1711–1725, 2020.

[382] Rohan N Soman, Katarzyna Majewska, Magdalena Mieloszyk, and Wieslaw Ostachowicz. Damage assessment in composite beam using infrared thermography, optical sensors, and terahertz technique. *Journal of Nondestructive Evaluation, Diagnostics and Prognostics of Engineering Systems*, 1(3), 2018.

[383] Gangbing Song, Hui Li, Bosko Gajic, Wensong Zhou, Peng Chen, and Haichang Gu. Wind turbine blade health monitoring with piezoceramic-based wireless sensor network. *International Journal of Smart and Nano Materials*, 4(3):150–166, 2013.

[384] Bent F Sørensen, E Jørgensen, CP Debel, FM Jensen, HM Jensen, TK Jacobsen, and K Halling. Improved design of large wind turbine blade of fibre composites based on studies of scale effects (Phase 1). Summary Report. *Riso-R1390 (EN), Risø National Laboratory, Denmark*, 2004.

[385] G S Springer. Erosion by liquid impact. *Osti*, 1 1976.

[386] British Standard and New Zealand Standard. ISO 31010: Risk management–Risk assessment techniques. *BS ISO*, 31010, 2009.

[387] British Standard and New Zealand Standard. Risk management-principles and guidelines. *BS ISO*, 31000:2009, 2009.

[388] British Standard and New Zealand Standard. ISO 2394:2015 General principles on reliability for structures. *BS ISO*, 2015.

[389] Norsok Standard. Criticality analysis for maintenance purposes. *Z-008, Rev*, 2, 2001.

[390] B Stankiewicz. Composite GFRP deck for bridge structures. *Procedia Engineering*, 40:423–427, 2012.

[391] Trevor Starr. *Pultrusion for Engineers*. CRC Press, Cambridge, 2000.

[392] Tyler Stehly and Patrick Duffy. 2021 cost of wind energy review. Technical report, National Renewable Energy Lab.(NREL), Golden, CO (United States), 2022.

[393] Tyler J Stehly and Philipp C Beiter. 2018 Cost of Wind Energy Review. Technical report, National Renewable Energy Lab.(NREL), Golden, CO (United States), 2020.

[394] H Stehmeier and H Speckmann. Comparative vacuum monitoring (CVM). In *Proceedings of the 2nd European Workshop on Structural Health Monitoring, Munich, Germany*, pages 7–9. Citeseer, 2004.

[395] DM Steinweg, M Hornung, and Willy Bauhaus Luftfahrt eV. Methods evaluating the impact of structural health monitoring on aircraft lifecycle costs. *Deutsche Gesellschaft für Luft-und Raumfahrt-Lilienthal-Oberth eV*, 2019.

[396] Christopher J. Stull, Christopher J. Earls, and Phaedon Stelios Koutsourelakis. Model-based structural health monitoring of naval ship hulls. *Computer Methods in Applied Mechanics and Engineering*, 200(9-12):1137–1149, 2011.

[397] Dabiao Sun, Xinyu Xue, and Qiang Wang. Lamb wave and GA-BP neural network based damage identification for wind turbine blade. In *2018 5th IEEE International Conference on Cloud Computing and Intelligence Systems (CCIS)*, pages 767–771. IEEE, 2018.

[398] Svendborg. Svendborg pedestrian and bicycle bridge. Available at `https://dissingweitling.com/en/project/svendborg-gang-og-cykelbro` (2021/2/11), 2008.

[399] Ramesh Talreja. Damage and fatigue in composites–a personal account. *Composites Science and Technology*, 68(13):2585–2591, 2008.

[400] Ramesh Talreja and Chandra Veer Singh. *Damage and failure of composite materials*. Cambridge University Press, Cambridge, 2012.

[401] ASB Tam, Weng Meng Chan, and John William Howard Price. Optimal maintenance intervals for a multi-component system. *Production Planning and Control*, 17(8):769–779, 2006.

[402] Jialin Tang, Slim Soua, Cristinel Mares, and Tat-Hean Gan. An experimental study of acoustic emission methodology for in service condition monitoring of wind turbine blades. *Renewable Energy*, 99:170–179, 2016.

[403] Lin Tang, Junliang Zhang, Yusheng Tang, Jie Kong, Tianxi Liu, and Junwei Gu. Polymer matrix wave-transparent composites: A review. *Journal of Materials Science & Technology*, 75:225–251, 2020.

[404] Fei Tao, Meng Zhang, Yushan Liu, and AYC Nee. Digital twin driven prognostics and health management for complex equipment. *CIRP Annals*, 67(1):169–172, 2018.

[405] Jannis Tautz-Weinert and Simon J Watson. Using SCADA data for wind turbine condition monitoring–A review. *IET Renewable Power Generation*, 11(4):382–394, 2016.

[406] D Tcherniak and Lasse Lohilahti Mølgaard. Vibration-based SHM system: application to wind turbine blades. In *Journal of Physics: Conference Series*, volume 628, page 012072. IOP Publishing, 2015.

[407] Dmitri Tcherniak and Lasse L Mølgaard. Active vibration-based structural health monitoring system for wind turbine blade: Demonstration on an operating Vestas V27 wind turbine. *Structural Health Monitoring*, 16(5):536–550, 2017.

[408] Jens Telgkamp. *Encyclopedia of Structural Health Monitoring*. Wiley, Hoboken, 2009.

[409] W Timmer. An overview of naca 6-digit airfoil series characteristics with reference to airfoils for large wind turbine blades. In *47th AIAA aerospace sciences meeting including the new horizons forum and aerospace exposition*, page 268, 2009.

[410] Damage Tolerance and Maintenance Workshop. Damage Tolerance and Maintenance. *Composites*, 2006.

[411] Zaigham Saeed Toor. Space applications of composite materials. *Journal of Space Technology*, 8(1):65–70, 2018.

[412] Hossein Towsyfyan, Ander Biguri, Richard Boardman, and Thomas Blumensath. Successes and challenges in non-destructive testing of aircraft composite structures. *Chinese Journal of Aeronautics*, 33(3):771–791, 2020.

[413] Stavroula Tsiapoki, Moritz W Häckell, Tanja Grießmann, and Raimund Rolfes. Damage and ice detection on wind turbine rotor blades using a three-tier modular structural health monitoring framework. *Structural Health Monitoring*, 17(5):1289–1312, 2018.

[414] C Tuloup, W Harizi, Zoheir Aboura, Yann Meyer, Kamel Khellil, and R Lachat. On the use of in-situ piezoelectric sensors for the manufacturing and structural health monitoring of polymer-matrix composites: A literature review. *Composite Structures*, 215:127–149, 2019.

[415] Chhugani Tushar, Routray Ralish, M Rajesh, M Manikandan, R Rajapandi, VR Kar, and Kandasamy Jayakrishna. Maintenance and monitoring of composites. In *Structural Health Monitoring of Biocomposites, Fibre-Reinforced Composites and Hybrid Composites*, pages 129–151. Elsevier, Amsterdam, 2019.

[416] Martin D Ulriksen, Dmitri Tcherniak, Poul H Kirkegaard, and Lars Damkilde. Operational modal analysis and wavelet transformation for damage identification in wind turbine blades. *Structural Health Monitoring*, 15(4):381–388, 2016.

[417] Martin Dalgaard Ulriksen, Dmitri Tcherniak, and Lars Damkilde. Vibration-based damage identification in wind turbine blades. 2015.

[418] United Nations. United Nations. transforming our world: the 2030 Agenda for Sustainable Development. UN General Assembly, New York: United Nations, 2015.

[419] Jordi Uyttersprot, Wouter De Corte, and Robert Somers. FRP bridges in the Flanders region: Experiences from the C-bridge project. In *Proceeding of the 10th International Conference on Fibre-Reinforced Polymer (FRP) Composites in Civil Engineering*, 2020.

[420] Lelli Van Den Einde, Lei Zhao, and Frieder Seible. Use of FRP composites in civil structural applications. *Construction and Building Materials*, 17(6-7):389–403, 2003.

[421] Alex Vary. Acousto-ultrasonic characterization of fiber reinforced composites. 1981.

[422] Martijn Veltkamp et al. Eurocode and the Design, Manufacture and Installation of 62 Clear Span FRP Bridges to the City of Rotterdam (NL). In *Australian Small Bridges Conference, 9th, 2019, Surfers Paradise, Queensland, Australia*, 2019.

[423] Amrit Shankar Verma, Zhiyu Jiang, Marco Caboni, Hans Verhoef, Harald van der Mijle Meijer, Saullo GP Castro, and Julie JE Teuwen. A probabilistic rainfall model to estimate the leading-edge lifetime of wind turbine blade coating system. *Renewable Energy*, 178:1435–1455, 2021.

[424] Larry A Viterna and Robert D Corrigan. Fixed pitch rotor performance of large horizontal axis wind turbines. *NASA*, 1982.

[425] DJ Wagg, Keith Worden, RJ Barthorpe, and Paul Gardner. Digital twins: State-of-the-art and future directions for modeling and simulation in engineering dynamics applications. *ASCE-ASME J Risk and Uncertainty in Engineering Systems Part B: Mechanical Enineering*, 6(3), 2020.

[426] Julia Walgern, Katharina Fischer, Paul Hentschel, and Athanasios Kolios. Reliability of electrical and hydraulic pitch systems in wind turbines based on field-data analysis. *Energy Reports*, 9:3273–3281, 2023.

[427] L Wang, A Kolios, X Liu, D Venetsanos, and Rui Cai. Reliability of offshore wind turbine support structures: A state-of-the-art review. *Renewable and Sustainable Energy Reviews*, 161:112250, 2022.

[428] Peng Wang, Wensong Zhou, Yuequan Bao, and Hui Li. Ice monitoring of a full-scale wind turbine blade using ultrasonic guided waves under varying temperature conditions. *Structural Control and Health Monitoring*, 25(4):e2138, 2018.

[429] Xiaojun Wang and DDL Chung. Real-time monitoring of fatigue damage and dynamic strain in carbon fiber polymer-matrix composite by electrical resistance measurement. *Smart Materials and Structures*, 6(4):504, 1997.

[430] Yinan Wang, Ryota Yoshihashi, Rei Kawakami, Shaodi You, Tohru Harano, Masahiko Ito, Katsura Komagome, Makoto Iida, and Takeshi Naemura. Unsupervised anomaly detection with compact deep features for wind turbine blade images taken by a drone. *IPSJ Transactions on Computer Vision and Applications*, 11(1):1–7, 2019.

[431] Yiwei Wang. *Development of Predictive Structural Maintenance Strategies for Aircraft Using Model-based Prognostics*. PhD thesis, Institut Clément Ader, 2017.

[432] Yong Wang and Qirong Deng. Optimization of maintenance scheme for offshore wind turbines considering time windows based on hybrid ant colony algorithm. *Ocean Engineering*, 263:112357, 2022.

[433] Christopher John Cornish Hellaby Watkins. Learning from delayed rewards. 1989.

[434] Bin Wei, Hailin Cao, and Shenhua Song. Degradation of basalt fibre and glass fibre/epoxy resin composites in seawater. *Corrosion Science*, 53(1):426–431, 2011.

[435] David R Wilburn. *Wind energy in the United States and materials required for the land-based wind turbine industry from 2010 through 2030*. US Department of the Interior, US Geological Survey, Washington, 2011.

[436] Cecilia Larrosa Wilson and Fu Kuo Chang. Monitoring fatigue-induced transverse matrix cracks in laminated composites using built-in acousto-ultrasonic techniques. *Structural Health Monitoring*, 15(3):335–350, 2016.

[437] Chengke Wu, Peng Wu, Jun Wang, Rui Jiang, Mengcheng Chen, and Xiangyu Wang. Critical review of data-driven decision-making in bridge operation and maintenance. *Structure and Infrastructure Engineering*, pages 1–24, 2020.

[438] Rong Wu, Dongsheng Zhang, Qifeng Yu, Yuxi Jiang, and Dwayne Arola. Health monitoring of wind turbine blades in operation using three-dimensional digital image correlation. *Mechanical Systems and Signal Processing*, 130:470–483, 2019.

[439] D Xu, PF Liu, and ZP Chen. Damage mode identification and singular signal detection of composite wind turbine blade using acoustic emission. *Composite Structures*, 255:112954, 2021.

[440] Rundong Yan and Sarah Dunnett. Improving the strategy of maintaining offshore wind turbines through petri net modelling. *Applied Sciences*, 11(2):574, 2021.

[441] Wei Yan and WQ Chen. Structural health monitoring using high-frequency electromechanical impedance signatures. *Advances in Civil Engineering*, 2010, 2010.

[442] Wenxian Yang, Zhike Peng, Kexiang Wei, and Wenye Tian. Structural health monitoring of composite wind turbine blades: challenges, issues and potential solutions. *IET Renewable Power Generation*, 11(4):411–416, 2016.

[443] Yang Yi and Sørensen, John Dalsgaard. Reduction of Operation and Maintenance Cost for Wind Turbine Blades – Cost Model and Decision Making. Technical Report 261, Aalborg Universitet, 2019. Project No. 871062.

[444] Junjie Ye, Chenchen Chu, Heng Cai, Xiaonan Hou, Baoquan Shi, Shaohua Tian, Xuefeng Chen, and Jianqiao Ye. A multi-scale model for studying failure mechanisms of composite wind turbine blades. *Composite Structures*, 212:220–229, 2019.

[445] Yu-Yi Ye, Sheng-Da Liang, Peng Feng, and Jun-Jie Zeng. Recyclable LRS FRP composites for engineering structures: Current status and future opportunities. *Composites Part B: Engineering*, 2021.

[446] Yang Yi and John Dalsgaard Sørensen. Reduction of operation and maintenance cost for wind turbine blades–reliability model. *Department of Civil Engineering, Aalborg University*, 2019.

[447] A Zayed, Y Garbatov, and C Guedes Soares. Corrosion degradation of ship hull steel plates accounting for local environmental conditions. *Ocean engineering*, 163:299–306, 2018.

[448] C Zhang and HP Chen. Optimum maintenance strategy for fatigue damaged composite blades of offshore wind turbines using stochastic modelling. In *2016 World Congress on The Structures Congress (Structures16)*, page 575, 2016.

[449] Chizhi Zhang, Hua-Peng Chen, Kong Fah Tee, and Dongfang Liang. Reliability-Based Lifetime Fatigue Damage Assessment of Offshore Composite Wind Turbine Blades. *Journal of Aerospace Engineering*, 34(3):04021019, 2021.

[450] Jin Zhang, Venkata S Chevali, Hao Wang, and Chun-Hui Wang. Current status of carbon fibre and carbon fibre composites recycling. *Composites Part B: Engineering*, 193:108053, 2020.

[451] Lijun Zhang, Kai Liu, Yufeng Wang, and Zachary Omariba. Ice detection model of wind turbine blades based on random forest classifier. *Energies*, 11(10):2548, Sep 2018.

[452] Shizhong Zhang, Kim Dam-Johansen, Sten Nørkjær, Pablo L Bernad Jr, and Søren Kiil. Erosion of wind turbine blade coatings–design and analysis of jet-based laboratory equipment for performance evaluation. *Progress in Organic Coatings*, 78:103–115, 2015.

[453] Yang Zhang, Yuanzhen Cui, Yu Xue, and Yan Liu. Modeling and measurement study for wind turbine blade trailing edge cracking acoustical detection. *IEEE Access*, 8:105094–105103, 2020.

[454] Menghan Zhao, You Dong, and Hongyuan Guo. Comparative life cycle assessment of composite structures incorporating uncertainty and global sensitivity analysis. *Engineering Structures*, 242, 2021.

[455] Jianjian Zhu, Xinlin Qing, Xiao Liu, and Yishou Wang. Electromechanical impedance-based damage localization with novel signatures extraction methodology and modified probability-weighted algorithm. *Mechanical Systems and Signal Processing*, 146, 2021.

[456] Wenjin Zhu, Mitra Fouladirad, and Christophe Bérenguer. A predictive maintenance policy based on the blade of offshore wind turbine. In *2013 Proceedings Annual Reliability and Maintainability Symposium (RAMS)*, pages 1–6. IEEE, 2013.

[457] Yue-ting Zhuang, Fei Wu, Chun Chen, and Yun-he Pan. Challenges and opportunities: from big data to knowledge in AI 2.0. *Frontiers of Information Technology & Electronic Engineering*, 18(1):3–14, 2017.

[458] Lisa Ziegler, Nicolai Cosack, Athanasios Kolios, and Michael Muskulus. Structural monitoring for lifetime extension of offshore wind monopiles: Verification of strain-based load extrapolation algorithm. *Marine Structures*, 66:154–163, 2019.

[459] Enrico Zio. The future of risk assessment. *Reliability Engineering & System Safety*, 177:176–190, 2018.

[460] ZJA. Sint sebastiaansbrug bridge. Available at `https://www.zja.nl/en/Sint-Sebastiaansbrug-Delft`, 2020.

[461] H Zobel and W Karwowski. Polkaczenia kompozytowych elementów konstrukcji mostowych. *Archiwum Instytutu Inzynierii Lkadowej*, (2):187–199, 2007.

[462] Tiago Zonta, Cristiano André da Costa, Rodrigo da Rosa Righi, Miromar José de Lima, Eduardo Silveira da Trindade, and Guann Pyng Li. Predictive maintenance in the Industry 4.0: A systematic literature review. *Computers & Industrial Engineering*, 2020.

[463] Guang Zou and Athanasios Kolios. Quantifying the value of negative inspection outcomes in fatigue maintenance planning: Cost reduction, risk mitigation and reliability growth. *Reliability Engineering & System Safety*, 226:108668, 2022.

[464] Hong-Xiang Zou, Lin-Chuan Zhao, Qiu-Hua Gao, Lei Zuo, Feng-Rui Liu, Ting Tan, Ke-Xiang Wei, and Wen-Ming Zhang. Mechanical modulations for enhancing energy harvesting: Principles, methods and applications. *Applied Energy*, 255:113871, 2019.

[465] Yi Zou, LPSG Tong, and Grant P Steven. Vibration-based model-dependent damage (delamination) identification and health monitoring for composite structures—a review. *Journal of Sound and vibration*, 230(2):357–378, 2000.